

# PATHOPHYSIOLOGY OF RARE HEMOLYTIC ANEMIAS

EDITED BY: Richard Van Wijk and Paola Bianchi  
PUBLISHED IN: Frontiers in Physiology



# frontiers

## Frontiers eBook Copyright Statement

The copyright in the text of individual articles in this eBook is the property of their respective authors or their respective institutions or funders. The copyright in graphics and images within each article may be subject to copyright of other parties. In both cases this is subject to a license granted to Frontiers.

The compilation of articles constituting this eBook is the property of Frontiers.

Each article within this eBook, and the eBook itself, are published under the most recent version of the Creative Commons CC-BY licence.

The version current at the date of publication of this eBook is CC-BY 4.0. If the CC-BY licence is updated, the licence granted by Frontiers is automatically updated to the new version.

When exercising any right under the CC-BY licence, Frontiers must be attributed as the original publisher of the article or eBook, as applicable.

Authors have the responsibility of ensuring that any graphics or other materials which are the property of others may be included in the CC-BY licence, but this should be checked before relying on the CC-BY licence to reproduce those materials. Any copyright notices relating to those materials must be complied with.

Copyright and source acknowledgement notices may not be removed and must be displayed in any copy, derivative work or partial copy which includes the elements in question.

All copyright, and all rights therein, are protected by national and international copyright laws. The above represents a summary only. For further information please read Frontiers' Conditions for Website Use and Copyright Statement, and the applicable CC-BY licence.

ISSN 1664-8714

ISBN 978-2-88966-270-8

DOI 10.3389/978-2-88966-270-8

## About Frontiers

Frontiers is more than just an open-access publisher of scholarly articles: it is a pioneering approach to the world of academia, radically improving the way scholarly research is managed. The grand vision of Frontiers is a world where all people have an equal opportunity to seek, share and generate knowledge. Frontiers provides immediate and permanent online open access to all its publications, but this alone is not enough to realize our grand goals.

## Frontiers Journal Series

The Frontiers Journal Series is a multi-tier and interdisciplinary set of open-access, online journals, promising a paradigm shift from the current review, selection and dissemination processes in academic publishing. All Frontiers journals are driven by researchers for researchers; therefore, they constitute a service to the scholarly community. At the same time, the Frontiers Journal Series operates on a revolutionary invention, the tiered publishing system, initially addressing specific communities of scholars, and gradually climbing up to broader public understanding, thus serving the interests of the lay society, too.

## Dedication to Quality

Each Frontiers article is a landmark of the highest quality, thanks to genuinely collaborative interactions between authors and review editors, who include some of the world's best academicians. Research must be certified by peers before entering a stream of knowledge that may eventually reach the public - and shape society; therefore, Frontiers only applies the most rigorous and unbiased reviews.

Frontiers revolutionizes research publishing by freely delivering the most outstanding research, evaluated with no bias from both the academic and social point of view. By applying the most advanced information technologies, Frontiers is catapulting scholarly publishing into a new generation.

## What are Frontiers Research Topics?

Frontiers Research Topics are very popular trademarks of the Frontiers Journals Series: they are collections of at least ten articles, all centered on a particular subject. With their unique mix of varied contributions from Original Research to Review Articles, Frontiers Research Topics unify the most influential researchers, the latest key findings and historical advances in a hot research area! Find out more on how to host your own Frontiers Research Topic or contribute to one as an author by contacting the Frontiers Editorial Office: [researchtopics@frontiersin.org](mailto:researchtopics@frontiersin.org)

# PATHOPHYSIOLOGY OF RARE HEMOLYTIC ANEMIAS

Topic Editors:

**Richard Van Wijk**, Utrecht University, Netherlands

**Paola Bianchi**, IRCCS Ca 'Granda Foundation Maggiore Policlinico Hospital, Italy

**Citation:** Van Wijk, R., Bianchi, P., eds. (2020). Pathophysiology of Rare Hemolytic Anemias. Lausanne: Frontiers Media SA. doi: 10.3389/978-2-88966-270-8

# Table of Contents

- 05 Editorial: Pathophysiology of Rare Hemolytic Anemias**  
Richard van Wijk and Paola Bianchi
- 08 The Pleiotropic Effects of GATA1 and KLF1 in Physiological Erythropoiesis and in Dyserythropoietic Disorders**  
Gloria Barbarani, Cristina Fugazza, John Strouboulis and Antonella E. Ronchi
- 19 PIEZO1 Hypomorphic Variants in Congenital Lymphatic Dysplasia Cause Shape and Hydration Alterations of Red Blood Cells**  
Immacolata Andolfo, Gianluca De Rosa, Edoardo Errichiello, Francesco Manna, Barbara Eleni Rosato, Antonella Gambale, Annalisa Vetro, Valeria Calcaterra, Gloria Pelizzo, Lucia De Franceschi, Orsetta Zuffardi, Roberta Russo and Achille Iolascon
- 26 The EPO-FGF23 Signaling Pathway in Erythroid Progenitor Cells: Opening a New Area of Research**  
Annelies J. van Vuren, Carlo A. J. M. Gaillard, Michele F. Eisenga, Richard van Wijk and Eduard J. van Beers
- 42 Red Blood Cell Membrane Conductance in Hereditary Haemolytic Anaemias**  
Polina Petkova-Kirova, Laura Hertz, Jens Danielczok, Rick Huisjes, Asya Makhro, Anna Bogdanova, Maria del Mar Mañú-Pereira, Joan-Lluis Vives Corrons, Richard van Wijk and Lars Kaestner
- 59 Clinical and Molecular Spectrum of Glucose-6-Phosphate Isomerase Deficiency. Report of 12 New Cases**  
Elisa Fermo, Cristina Vercellati, Anna Paola Marcello, Anna Zaninoni, Selin Aytac, Mualla Cetin, Ilaria Capolsini, Maddalena Casale, Sabrina Paci, Alberto Zanella, Wilma Barcellini and Paola Bianchi
- 68 Glutaraldehyde – A Subtle Tool in the Investigation of Healthy and Pathologic Red Blood Cells**  
Asena Abay, Greta Simionato, Revaz Chachanidze, Anna Bogdanova, Laura Hertz, Paola Bianchi, Emile van den Akker, Marieke von Lindern, Marc Leonetti, Giampaolo Minetti, Christian Wagner and Lars Kaestner
- 82 Red Blood Cell Homeostasis and Altered Vesicle Formation in Patients With Paroxysmal Nocturnal Hemoglobinuria**  
Joames K. Freitas Leal, Frank Preijers, Roland Brock, Merel Adjobo-Hermans and Giel Bosman
- 92 Characterization of Two Cases of Congenital Dyserythropoietic Anemia Type I Shed Light on the Uncharacterized C15orf41 Protein**  
Roberta Russo, Roberta Marra, Immacolata Andolfo, Gianluca De Rosa, Barbara Eleni Rosato, Francesco Manna, Antonella Gambale, Maddalena Raia, Sule Unal, Susanna Barella and Achille Iolascon
- 102 Corrigendum: Characterization of Two Cases of Congenital Dyserythropoietic Anemia Type I Shed Light on the Uncharacterized C15orf41 Protein**  
Roberta Russo, Roberta Marra, Immacolata Andolfo, Gianluca De Rosa, Barbara Eleni Rosato, Francesco Manna, Antonella Gambale, Maddalena Raia, Sule Unal, Susanna Barella and Achille Iolascon



- 103 The Spectrum of SPTA1-Associated Hereditary Spherocytosis**  
Satheesh Chonat, Mary Risinger, Haripriya Sakthivel, Omar Niss, Jennifer A. Rothman, Loan Hsieh, Stella T. Chou, Janet L. Kwiatkowski, Eugene Khandros, Matthew F. Gorman, Donald T. Wells, Tamara Maghathe, Neha Dagaonkar, Katie G. Seu, Kejian Zhang, Wenying Zhang and Theodosia A. Kalfa
- 110 Corrigendum: The Spectrum of SPTA1-Associated Hereditary Spherocytosis**  
Satheesh Chonat, Mary Risinger, Haripriya Sakthivel, Omar Niss, Jennifer A. Rothman, Loan Hsieh, Stella T. Chou, Janet L. Kwiatkowski, Eugene Khandros, Matthew F. Gorman, Donald T. Wells, Tamara Maghathe, Neha Dagaonkar, Katie G. Seu, Kejian Zhang, Wenying Zhang and Theodosia A. Kalfa
- 112 Receptor for Advanced Glycation End Products Antagonism Blunts Kidney Damage in Transgenic Townes Sickle Mice**  
Emmanuelle Charrin, Camille Faes, Amandine Sotiaux, Sarah Skinner, Vincent Pialoux, Philippe Joly, Philippe Connes and Cyril Martin
- 122 CoDysAn: A Telemedicine Tool to Improve Awareness and Diagnosis for Patients With Congenital Dyserythropoietic Anemia**  
Cristian Tornador, Edgar Sánchez-Prados, Beatriz Cadenas, Roberta Russo, Veronica Venturi, Immacolata Andolfo, Ines Hernández-Rodríguez, Achille Iolascon and Mayka Sánchez
- 128 Clinical Diagnosis of Red Cell Membrane Disorders: Comparison of Osmotic Gradient Ektacytometry and Eosin Maleimide (EMA) Fluorescence Test for Red Cell Band 3 (AE1, SLC4A1) Content for Clinical Diagnosis**  
Ahmar Urooj Zaidi, Steven Buck, Manisha Gadageel, Miguel Herrera-Martinez, Araathi Mohan, Kenya Johnson, Shruti Bagla, Robert M. Johnson and Yaddanapudi Ravindranath



# Editorial: Pathophysiology of Rare Hemolytic Anemias

Richard van Wijk<sup>1\*</sup> and Paola Bianchi<sup>2</sup>

<sup>1</sup> Central Diagnostic Laboratory - Research, University Medical Center Utrecht, Utrecht University, Utrecht, Netherlands,

<sup>2</sup> Hematology Unit, Pathophysiology of Anemias Unit, Fondazione IRCCS Ca' Granda Ospedale Maggiore Policlinico, Milan, Italy

**Keywords:** red blood cell, hemolytic anemia, enzymopathies, membranopathies, congenital dyserythropoetic anemia

## Editorial on the Research Topic

### Pathophysiology of Rare Hemolytic Anemias

The current Research Topic focuses on rare hereditary hemolytic anemias, and arises from the need to increase awareness for this heterogeneous group of disorders. Rare hereditary hemolytic anemias can be roughly categorized into hemoglobinopathies, membrane- and hydration disorders, metabolic disorders (all hyper-regenerative anemias), or defects of red blood cell production (hypo-regenerative anemias). In many cases, disease pathophysiology and genotype-to-phenotype correlations is poorly understood, complicating recognition and diagnosis, as well as development of effective treatment. This Research Topic brings together a number of studies that contribute to increasing our knowledge on the pathophysiology of red blood cell disorders, and that may raise an interest of pharmaceutical companies and device manufacturers in developing specific drugs and technological devices.

Red blood cell membrane- and hydration defects generally associated with morphological changes. However, more definitive diagnosis requires the use of additional diagnostic tests. Zaidi et al. report on their many years of experience using osmotic gradient ektacytometry, a highly specialized technique, in comparison with the eosin maleimide (EMA) binding test. The former technique provides a fluid, physiological and hence functional test of red blood cell deformability whereas the EMA binding test is a static test that provides a quantifiable measurement of the major red blood cell membrane protein band 3. Using patients with various disorders of the red cell membrane, such as hereditary spherocytosis (HS), hereditary elliptocytosis, and south-east asian ovalocytosis the authors describe the key differences between the two tests. They outline a number of pitfalls of in particular the EMA binding test but conclude that when combined both rapid tests are complimentary, and therefore worthwhile in the diagnosis of red blood cell membrane- and hydration disorders (Zaidi et al.).

Analysis of peripheral blood film is also an essential tool to evaluate red blood cell morphology. It needs to be evaluated on fresh blood. The conservation of original red blood cell shapes, obtained following glutaraldehyde fixation for imaging and in particular 3D-analysis, is a common desire. In a very punctual analysis, Abay et al. investigated and documents the subtle use of glutaraldehyde on healthy and pathologic red blood cells, and how to deal with or circumvent pitfalls.

Most red blood cell membrane disorders are inherited in an autosomal dominant manner. However, an important subgroup is autosomal recessive HS. This disease is mainly caused by bi-allelic mutations of *SPTA1*, the gene that codes for  $\alpha$ -spectrin. Chonat et al. focus on this specific patient category and systematically compare genetic, rheological, and protein data to the clinical presentation of patients. They show that  $\alpha$ -spectrin levels correlate to disease severity and, importantly, the obtained genetic and phenotypic data they collected shows differences in response

## OPEN ACCESS

### Edited and reviewed by:

Lars Kaestner,  
Saarland University, Germany

### \*Correspondence:

Richard van Wijk  
R.vanWijk@umcutrecht.nl

### Specialty section:

This article was submitted to  
Red Blood Cell Physiology,  
a section of the journal  
Frontiers in Physiology

**Received:** 01 September 2020

**Accepted:** 30 September 2020

**Published:** 22 October 2020

### Citation:

van Wijk R and Bianchi P (2020)  
Editorial: Pathophysiology of Rare  
Hemolytic Anemias.  
Front. Physiol. 11:601746.  
doi: 10.3389/fphys.2020.601746

to splenectomy, a commonly used procedure to treat patients with HS. Although the number of patients in this study was limited such results will be of importance for clinical decision making.

With specific focus on deciphering disease pathophysiology of rare hereditary hemolytic anemias in general Petkova-Kirova et al. investigated if changes in membrane conductance could be a factor contributing to phenotypic expression by means of altering cation content and subsequent disrupting volume homeostasis. They performed whole-cell patch-clamp measurements on red blood cells from patients with a variety of different rare hereditary anemias. They show that red blood cells from patients with specific molecular defects causing HS or hereditary xerocytosis (HX) show altered membrane conductance. At the same time such changes were not detected in  $\beta$ -thalassemia patients and patients with enzyme deficiencies such as glucose-6-phosphate dehydrogenase deficiency. Their results open up an exciting new area of research to identify the channel(s) underlying the observed changes conductances.

One red blood cell ion channel that is currently the topic of intensive investigation is *PIEZO1*. Upon mutation this mechanosensitive cation channel is associated with distinct abnormalities, either autosomal dominant HX (a rare red cell hydration disorder) due to gain of function mutations in *PIEZO1* or autosomal recessive lymphatic dysplasia with non-immune hydrops fetalis due to loss of function mutations. Andolfo et al. now for the first time report on the red blood cell changes of a case of lymphatic dysplasia. Red blood cells from this patient showed altered hydration and intracellular loss of potassium, as well as structural abnormalities such as spherocytes and stomatocytes, indicating shared features of both HS and HX. Thus, their findings complement the clinical features of mutant *PIEZO1*-mediated lymphatic dysplasia.

Apart from glucose-6-phosphate dehydrogenase-deficiency, enzyme deficiencies of the red blood cell are very rare metabolic disorders. Fermo et al. report here on a relatively large cohort of 12 patients with chronic hemolytic anemia due to glucose-6-phosphate isomerase (GPI) deficiency, a glycolytic enzymopathy. They describe the clinical, hematological and molecular characteristics of these patients whom they had the unique opportunity to follow from infancy to adulthood. This allowed them to report three features associated with GPI-deficiency not previously reported: (1) increased susceptibility to infections; (2) poor response to splenectomy; (3) a tendency for reticulocyte numbers to increase post-splenectomy. In addition, they show that GPI-deficient red blood cells behave differently when analyzed with osmotic gradient ektacytometry. Altogether, these findings contribute to a better understanding of disease pathophysiology and diagnosis of this rare red blood cell enzymopathy.

Sickle cell disease (SCA) is a hemoglobinopathy and a relatively simple monogenetic disorder. Yet, its pathophysiology is highly complex and the disease truly is a multi-system disorder. Using a mouse model of SCA Charrin et al. have investigated the contribution of advanced glycation end products (AGE) and their receptor (RAGE) in the development of kidney complications, one of many complications associated

with SCA. They particularly focused on the effects of RAGE inhibition by a specific RAGE-antagonist (RAP). They show that specific inhibition of RAGE blunts anemia-related markers. In addition, RAP-treatment reduced glomerular hypertrophy, interstitial fibrosis, and tubular iron deposits, possibly mediated by reduced oxidative stress markers and decreased pro-inflammatory molecule expression. Thus, this work provides proof for RAGE as an important pathogenic factor in the development of renal changes in SCA.

Another very heterogeneous group of rare disorders includes congenital dyserythropoietic anemias (CDA), that are characterized by ineffective erythropoiesis, moderate to severe anemia, distinct morphological features in bone marrow late erythroblasts, and development of secondary iron overload. The prevalence of these disorders is still not well-defined. The morphological classification, initially proposed, is now supported by the identification of the molecular lesions. Most of the causative genes involved in the pathogenesis of CDAs (*CDAN1*, and *C15orf41* for CDA-I, *SEC23B* for CDA-II or *KIF23* responsible for CDA-III) seems to be directly or indirectly involved in the erythroid maturation process or a mitotic kinesin crucial for cytokinesis.

One of the clear advantages of next generation sequencing technologies is the availability of molecular testing for rare diseases in many laboratories, resulting in the increased awareness of rare congenital conditions. On the other hand, the huge amount of data obtained should be always supported by functional studies. This is illustrated by two new variants that Russo et al. detected in the *C15orf41* gene (p. (His230Pro) and p. (Glu94Ser)) that cause a reduction of gene expression and protein production, both resulting in impaired erythroid maturation and suggesting a block of cell cycle dynamics as a putative pathogenic mechanism for *C15orf41*-related CDA-I. More recently, mutations in genes codifying for erythroid-specific transcription factors (*GATA1* and *KLF1*) have been also described in patients with dyserythropoietic anemia.

To support the clinical management and diagnostic iter of these disorders a new telemedicine tool was developed by Tornador et al., hosted on a webpage named CoDysAn and available at <http://www.codysan.eu>. CoDysAn algorithm was validated on 24 patients genetically diagnosed of different types of CDA and with a set of 19 hemolytic patients non-CDA-I.

The advent of new technological approaches also enabled a better knowledge of the ontogeny of erythropoiesis supporting the concept that hematopoietic stem cell themselves are highly heterogeneous and lineages separate earlier than previously thought. The coordination of these events is orchestrated by transcription factors that work in a combinatorial manner to activate and/or repress their target genes as reviewed by Barbarani et al.. The examples of *GATA1* and *KLF1* presented in this review suggest that in the next few years the number of mutations identified in transcription factors associated with diserythropoietic disorders will further increase.

Other less known signaling pathways seem to influence the erythroid progenitor cells in the bone marrow. Fibroblast Growth Factor 23 (FGF23) is a hormone involved in phosphate, vitamin D metabolism and has been recognized as an important regulator

of bone mineralization. Erythroid progenitors highly express FGF23 protein and carry the FGF23 receptor. van Vuren et al. describe how the EPO-FGF23 pathway seems to interact with red blood cell production and the responses to endogenous erythropoietin in rare hereditary anemias, thereby providing a novel pathophysiological feature that may be common to many different forms of (rare) anemia.

Among the group of acquired hemolytic anemias paroxysmal nocturnal hemoglobinuria definitely represents a fascinating model among red blood cell diseases. Due to the lack of membrane GPI-anchored proteins, complement is strongly activated causing complement-mediated lysis. This results not only in anemia, but also in the release of free hemoglobin and iron, which catalyze the generation of reactive oxygen species and subsequent NO depletion and vasoconstriction. For untreated patients, thrombosis is the most common cause of death. To further investigate these aspects, microvesicles formation was considered by Freitas Leal et al.. The absence of GPI-anchored membrane proteins seems to both strongly increase microvesicle formation and to affects the composition of red blood cell-derived as well as platelet-derived vesicles. These data open the way to new aspect in pathophysiological mechanism of paroxysmal nocturnal hemoglobinuria, and possibly contribute to the development of new treatment strategies.

The articles collected in the present Research Topic reflect current and future directions of research, development of diagnostic tools and therapies for red blood cell related diseases. Given the rarity and the heterogeneity of this group of disorders, research, and diagnostics often merge into each other, especially for rare or undiagnosed cases. It is also evident that increasing awareness, developing of new diagnostic devices and networking activities to join expertise is crucial in this field, as highlighted recently by Kaestner and Bianchi.

## AUTHOR CONTRIBUTIONS

RW and PB wrote the manuscript. All authors contributed to the article and approved the submitted version.

**Conflict of Interest:** The authors declare that the research was conducted in the absence of any commercial or financial relationships that could be construed as a potential conflict of interest.

*Copyright © 2020 van Wijk and Bianchi. This is an open-access article distributed under the terms of the Creative Commons Attribution License (CC BY). The use, distribution or reproduction in other forums is permitted, provided the original author(s) and the copyright owner(s) are credited and that the original publication in this journal is cited, in accordance with accepted academic practice. No use, distribution or reproduction is permitted which does not comply with these terms.*



# The Pleiotropic Effects of GATA1 and KLF1 in Physiological Erythropoiesis and in Dyserythropoietic Disorders

Gloria Barbarani<sup>1</sup>, Cristina Fugazza<sup>1</sup>, John Strouboulis<sup>2</sup> and Antonella E. Ronchi<sup>1\*</sup>

<sup>1</sup> Dipartimento di Biotecnologie e Bioscienze, Università degli Studi Milano-Bicocca, Milan, Italy, <sup>2</sup> School of Cancer & Pharmaceutical Sciences, Faculty of Life Sciences & Medicine, King's College London, London, United Kingdom

## OPEN ACCESS

### Edited by:

Richard Van Wijk,  
Utrecht University, Netherlands

### Reviewed by:

Andrew Charles Perkins,  
Monash University, Australia  
Patrick G. Gallagher,  
Yale University, United States  
Marije Bartels,  
University Medical Center Utrecht,  
Netherlands

### \*Correspondence:

Antonella E. Ronchi  
antonella.ronchi@unimib.it

### Specialty section:

This article was submitted to  
Red Blood Cell Physiology,  
a section of the journal  
Frontiers in Physiology

Received: 21 November 2018

Accepted: 25 January 2019

Published: 12 February 2019

### Citation:

Barbarani G, Fugazza C,  
Strouboulis J and Ronchi AE (2019)  
The Pleiotropic Effects of GATA1  
and KLF1 in Physiological  
Erythropoiesis  
and in Dyserythropoietic Disorders.  
Front. Physiol. 10:91.  
doi: 10.3389/fphys.2019.00091

In the last few years, the advent of new technological approaches has led to a better knowledge of the ontogeny of erythropoiesis during development and of the journey leading from hematopoietic stem cells (HSCs) to mature red blood cells (RBCs). Our view of a well-defined hierarchical model of hematopoiesis with a near-homogeneous HSC population residing at the apex has been progressively challenged in favor of a landscape where HSCs themselves are highly heterogeneous and lineages separate earlier than previously thought. The coordination of these events is orchestrated by transcription factors (TFs) that work in a combinatorial manner to activate and/or repress their target genes. The development of next generation sequencing (NGS) has facilitated the identification of pathological mutations involving TFs underlying hematological defects. The examples of GATA1 and KLF1 presented in this review suggest that in the next few years the number of TF mutations associated with dyserythropoietic disorders will further increase.

**Keywords:** erythropoiesis, dyserythropoiesis, transcription factors, GATA1, KLF1

## INTRODUCTION

Erythropoiesis leads to the production of the proper number of RBCs required by the body under homeostatic and stress conditions. In healthy adults, erythropoiesis ensures the release in the blood stream of  $2 \times 10^6$  RBCs/second, but this number dramatically increases to respond to inadequate tissue oxygenation (Tsiftoglou et al., 2009; Dzierzak and Philipsen, 2013; Nandakumar et al., 2016).

Insufficient quantitative or qualitative production of fully functional RBCs, whether acquired or inherited, results in a wide spectrum of diseases generally defined as anemias.

The causes of anemias are variable and reflect the complexity of the differentiation and maturation of erythrocytes. In some cases, the number of RBCs is extremely low because of the failure to produce erythroid progenitors, as in Diamond-Blackfan Anemia (DBA) (Da Costa et al., 2018). In other cases, impaired differentiation leads to the accumulation of erythroid precursors in the bone marrow [ $\beta$ -thalassemia (Rivella, 2015), congenital dyserythropoietic anemia, CDA (Iolascon et al., 2011)] or to the unbalanced production of different blood cell types [myelodysplastic syndromes, MDS (Levine et al., 2007; Lefevre et al., 2017)], resulting in insufficient RBC numbers in the bloodstream.



In other forms of anemias, RBCs are produced but defects in some crucial gene products [typically specific enzymes (Koralkova et al., 2014; Grace et al., 2018), membrane proteins or cytoskeletal components (Mohandas and Gallagher, 2008; Perrotta et al., 2008), sickle globin chains (Rees et al., 2010), channel proteins (Glogowska and Gallagher, 2015), specific pathways (Bianchi et al., 2009; Schwarz et al., 2009)] result in RBCs with decreased oxygen delivery capacity and/or shortened lifespan. Very often, different diseases share common features: for example imbalanced globin chains in  $\beta$ -thalassemia is accompanied by the accumulation of defective precursors in the bone marrow and by ineffective erythropoiesis (IE), as is also observed in CDA (Libani et al., 2008; Iolascon et al., 2011; Ribeil et al., 2013; Rivella, 2015).

Recently, thanks to the advent of new technologies, including NGS using small pools of cells or single cells (Nestorowa et al., 2016; Paul et al., 2016; Ye et al., 2017; Giladi et al., 2018), the development of improved panels of surface markers (Guo et al., 2013; Notta et al., 2016) and the design of *in vivo* cell tracing systems (Dykstra and Bystrykh, 2014; Perie et al., 2014; Pei et al., 2017; Rodriguez-Fraticelli et al., 2018; Upadhaya et al., 2018), our understanding of hematopoiesis -and erythropoiesis- has greatly expanded. In parallel, genome wide association approaches (GWAS) (Menzel et al., 2007; Sankaran et al., 2008; Uda et al., 2008; Soranzo et al., 2009; van der Harst et al., 2012), massive genome and exome sequencing (Chami et al., 2016) led to the identification of new variant/modifier alleles influencing erythropoiesis associated with TFs.

In this scenario, TFs not only control lineage commitment transitions but are emerging as key-players underpinning, so far unexplained erythroid diseases. Here, we consider GATA1 and KLF1 as paradigmatic TFs. By focusing on these examples, we aim to provide evidence of their pleiotropic effects rather than to give a complete list of GATA1 or KLF1 mutations identified so far.

## ERYTHROPOIESIS

### Erythropoiesis During Development

The first wave of erythropoiesis originates in the yolk sac, where Primitive Erythroid Cells (EryPs) sustain the oxygenation demand of the growing embryo (Dzierzak and Philipsen, 2013). EryPs are large in size and still nucleated when released in the circulation, where they later enucleate (Isern et al., 2011; Dzierzak and Philipsen, 2013; Palis, 2014). In mouse, at E8.25 a second wave of erythro-myelo-precursors (EMPs) originates in the yolk sac and colonizes the fetal liver, generating the first definitive RBCs (Palis, 2016). Finally, around E10.5, hematopoietic stem cells (HSCs) from aorta-gonad-mesonephros (AGM), placenta and possibly other yet unknown sites, colonize the fetal liver. These cells will sustain definitive hematopoiesis for the remainder of gestation and, around birth, will migrate to the bone marrow, the site of adult hematopoiesis (Dzierzak and Philipsen, 2013).

### From HSC to RBC

Until recently, the “classical model” of hematopoiesis was considered a paradigm of a stepwise, hierarchical cellular

specification system, whereby HSCs generated multipotent progenitors with progressively restricted lineage potential through a sequence of binary choices. The grand entrance of new single-cell separation technologies, *in vivo* lineage tracing systems and single-cell analysis, provided novel and surprising insights, prompting the idea that early transcriptional priming develops into the acquisition of specific lineage programs (Cabezas-Wallscheid et al., 2014; Haas et al., 2018). In this context, erythroid cells would originate early in the hematopoietic hierarchy, i.e., from stem/multipotent progenitor stages (Guo et al., 2013; Notta et al., 2016; Tusi et al., 2018), soon after the emergence of the megakaryocytic lineage (Upadhaya et al., 2018).

The first clearly recognizable unipotent erythroid progenitor, identified decades ago in *in vitro* clonogenic assays, is the BFU-E (burst-forming unit-erythroid), that differentiate into rapidly dividing colony-forming-unit erythroid (CFU-E) (Hattangadi et al., 2011; Koury, 2016; Dulmovits et al., 2017). The entry of CFU-Es into erythroid terminal differentiation marks the transition into final maturation (Hwang et al., 2017; Tusi et al., 2018).

## EXTRACELLULAR AND INTRACELLULAR SIGNALS

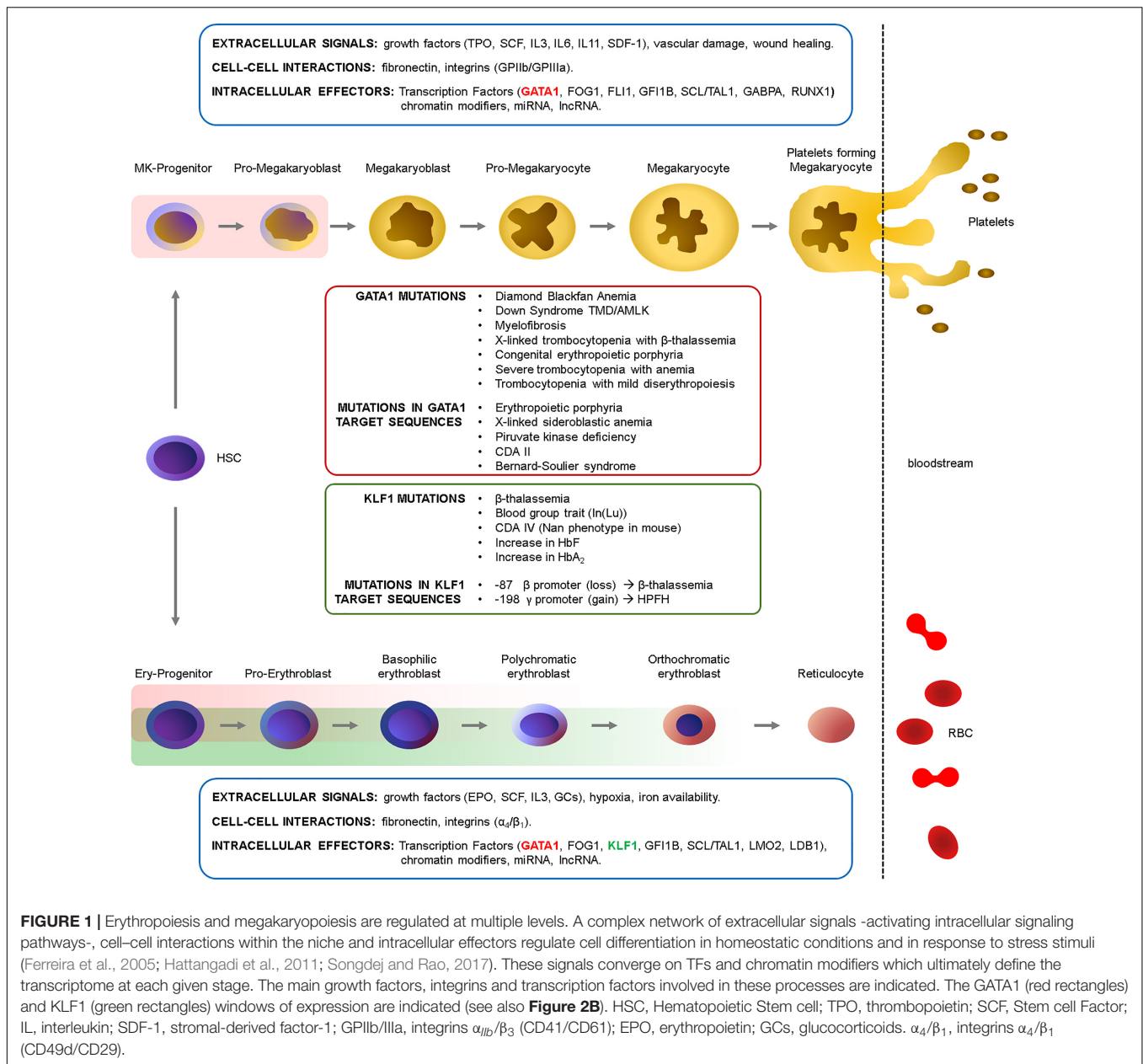
Red blood cell differentiation, their production in homeostatic and stress condition, is governed by an integrated complex interplay of extracellular and cell-cell signals within the microenvironment that activate the appropriate downstream intracellular signals, ultimately converging on key TFs. Although these aspects are beyond the scope of this review, we give a glimpse of the major players in these regulatory networks in **Figure 1**.

## THE ROLE OF TRANSCRIPTION FACTORS

Transcription factors, together with cofactors and chromatin modifiers, dictate the lineage-specific, stage-specific transcriptional programs by coordinately activating and/or repressing their targets through their binding to DNA (Portela and Esteller, 2010; Dore and Crispino, 2011; Love et al., 2014). The advent of NGS has rapidly expanded our understanding of TFs functions in physiological erythropoiesis, discovering TF mutations as cause of yet unexplained hematological -and dyserythropoietic- defects. Here, we focus on the key examples of GATA1 and KLF1 and their mutations to provide a glimpse of the complexity of their actions (**Figure 2**).

### The Example of the “Master Regulator” GATA1

The X-linked *GATA1* gene encodes a zinc finger TF expressed in the hematopoietic system in erythroid, megakaryocytic and, at lower levels, in eosinophilic, dendritic, and mast cells (Yu et al., 2002a; Ferreira et al., 2005; Gutierrez et al., 2007; Kozma et al., 2010).



GATA1 has three main functional domains: an N-terminal activation domain (N-TAD) and two homologous zinc (Zn) finger domains in the C-terminal half of the protein. The N-terminal Zn finger binds to the GATA1 main cofactor FOG1 (Friend-of-GATA) and modulates the affinity of GATA1 for binding to complex sites *in vitro* (Trainor et al., 1996; Newton et al., 2001; Yu et al., 2002b). The C-terminal Zn finger (C-ZnF) binds to DNA (WGATAR motif).

GATA1 produces two isoforms: the full length protein (GATA1-FL, 47 kDa) and a shorter variant (GATA1s, 40 kDa), translated from codon 84 within the third exon. GATA1s lacks the N-TAD and results in a protein with a reduced transactivation activity (Calligaris et al., 1995). *Gata1* knockout in mice (Pevny et al., 1991) results in embryonic lethality around E10.5–E11.5

due to severe anemia, with GATA1-null cells undergoing massive apoptosis at the proerythroblastic stage (Pevny et al., 1995; Fujiwara et al., 1996). The conditional erythroid knockout in adult mice causes aplastic anemia, revealing its essential role in both steady-state and stress erythropoiesis (Gutierrez et al., 2008).

By contrast, megakaryoblasts lacking GATA1 proliferate abnormally but fail to undergo terminal differentiation (Shivdasani et al., 1997; Vyas et al., 1999). Since these first studies, many other reports revealed the many roles of GATA1 in the erythro/megakaryocytic differentiation (Ferreira et al., 2005). *GATA1* mutations identified in patients underscore this pleiotropy: mutations altering the quantity or quality of GATA1 can lead to a variety of phenotypes. Depending on the type of mutation and whether germline or somatic, the severity

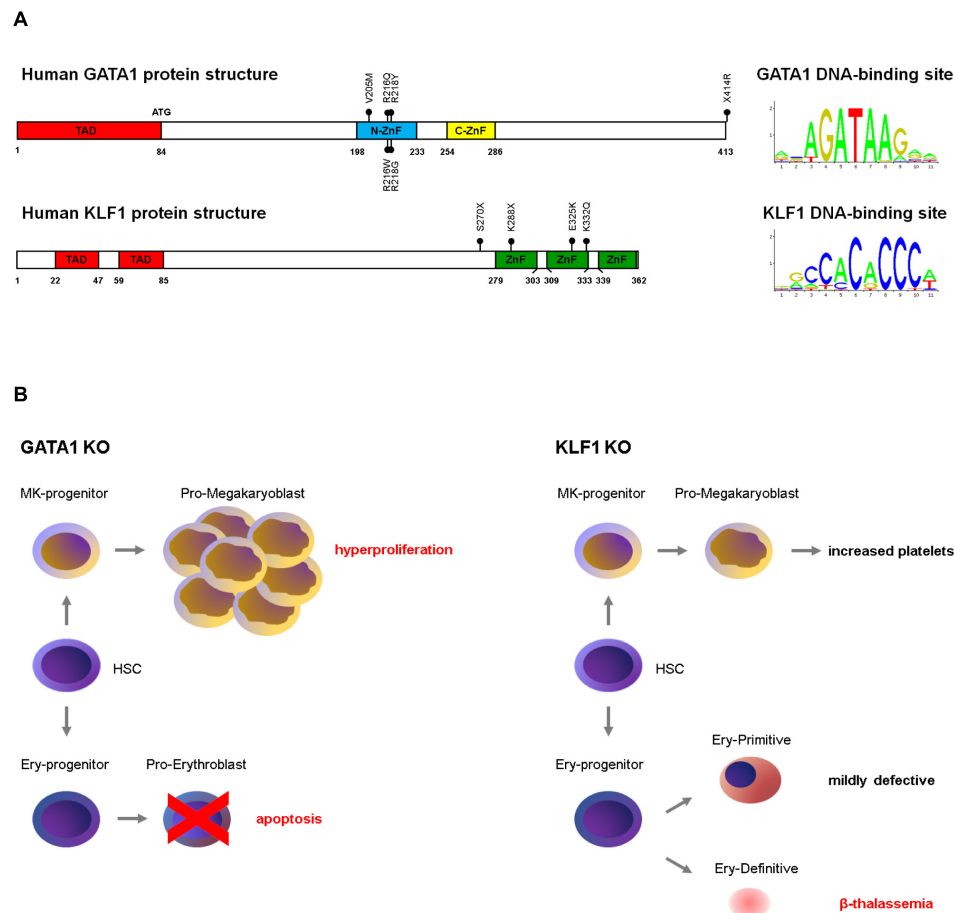


**FIGURE 2 | (A)** Schematic structure of GATA1 and KLF1 proteins and of their DNA-binding motifs. The position of the mutations discussed in this review are indicated. ZnF, zinc fingers; TAD, transactivation domains. The DNA consensus are from the JASPAR database (<http://jaspar2016.genereg.net/>). **(B)** Phenotype of *GATA1* (Pevny et al., 1991, 1995; Fujiwara et al., 1996; Shivdasani et al., 1997; Gutierrez et al., 2008) and *KLF1* (Nuez et al., 1995; Perkins et al., 1995; Hodge et al., 2006; Nilsson et al., 2006; Frontelo et al., 2007; Tallack and Perkins, 2010) gene knockouts in mouse.

of the disease and the involvement of the erythroid and/or megakaryocytic compartments greatly varies.

## “QUANTITATIVE MUTATIONS”: GENE DOSAGE AND BACKGROUND EFFECTS AT WORK

### Mutations Causing GATA1-FL Loss: Inherited

Diamond-Blackfan anemia (DBA) is an inherited bone marrow failure syndrome characterized by severe anemia due to a great reduction in BFU-Es, without involvement of other hematopoietic lineages. Heterozygous mutations in ribosomal proteins account for about 65% of DBA cases. In 2012 an exome sequencing approach discovered the first *GATA1* mutation in a DBA patient (Sankaran et al., 2012). This mutation (c.220G > C transversion) causes the skipping of exon 2, determining GATA1-FL loss, while retaining GATA1s. Unrelated

DBA patients were reported to carry the same mutation (Klar et al., 2014), or mutations in the ATG of GATA1-FL (Ludwig et al., 2014; Parrella et al., 2014). Of interest, in a family reported by Hollanda et al. (2006) the inherited loss of GATA1-FL results in macrocytic anemia of various severity in the different patients (with variable involvement of megakaryocytes and neutrophils).

### Mutations Causing GATA1-FL Loss: Acquired

Somatic mutations in *GATA1*, preventing the synthesis of GATA1-FL, predispose newborn Down Syndrome (DS) patients to develop (in 10–20% of cases) transient myeloproliferative disease (TMD) (Wechsler et al., 2002; Xu et al., 2003; Hitzler and Zipursky, 2005). This pre-leukemic condition often spontaneously resolves. However, in about 30% of TMD cases, it develops into acute pediatric megakaryoblastic leukemia (AMKL) (Wechsler et al., 2002; Magalhaes et al., 2006). All the DS-TMD *GATA1* mutations identified so far, map in exon 2 and either introduce a STOP codon or alter splicing



such that only GATA1s is translated (Mundschau et al., 2003; Rainis et al., 2003). The loss of GATA1-FL in pre-malignant cells characterizes virtually all cases of DS-TMD. The detection of clone-specific *GATA1* mutations in DS-TMD and AMKL proves that AMKL derive from the TMD clone (Rainis et al., 2003; Ahmed et al., 2004; Hitzler and Zipursky, 2005). Moreover, *GATA1* mutations are extremely rare in AMKL blasts of non-DS patients, clearly indicating a specific cooperation of *GATA1* mutations with trisomy 21 (Gruber and Downing, 2015). The restoration of GATA1-FL expression in DS-AMKL-derived cells partially restores erythroid differentiation, further supporting the notion that the loss of GATA1-FL is essential for leukemogenesis (Xu et al., 2003). Importantly, DS-AMKL *GATA1* mutations have very little effect on erythropoiesis, suggesting that the co-occurrence trisomy 21 confers the property of specific targeting megakaryoblasts in DS patients.

Various evidences suggest that TMD likely emerges in a yolk sac/fetal liver progenitor *in utero* (Shimada et al., 2004). In agreement with this hypothesis, in mouse, a knockin allele abolishing GATA1-FL (and leaving GATA1s intact) results in a transient reduction of erythroid cells accompanied by increased megakaryopoiesis that resolves around E14.5 (Li et al., 2005). Despite these observations, the fetal cell type originating TMD and molecular mechanisms by which *GATA1* mutations specifically synergizes with trisomy 21 are still unclear (Crispino, 2005).

## GATA1 Low Levels and Disease

The notion that low levels of GATA1 lead to the development of myelofibrosis comes from studies in the GATA1-low mouse model, that also develops anemia with age (Vannucchi et al., 2002). In line with this first observation, the majority of patients with primary myelofibrosis (PMF) have GATA1-deficient megakaryocytes (Migliaccio et al., 2005). Of interest, in PMF patients, the reduced level of GATA1 is due to its impaired translation secondary to RPS14 deficiency (Gilles et al., 2017). The connection between GATA1 levels and RP proteins hinges on additional observations: indeed, in cells from DBA patients who are haploinsufficient for RPS19, GATA1 translation is greatly reduced (Ludwig et al., 2014; O'Brien et al., 2017; Khajuria et al., 2018).

Together, these examples again point toward the importance of the correct GATA1 protein dosage and indicates *GATA1* post-transcriptional regulation as an important determinant of GATA1 protein level.

## “QUALITATIVE MUTATIONS”: THE IMPORTANCE OF PROTEIN-PROTEIN INTERACTIONS AND MORE

### Mutations Abolishing the Interaction With FOG1

In Tsang et al. (1997) identified by yeast two-hybrid a novel zinc finger protein, named FOG1, binding to the

N-ZnF of GATA1. GATA1 mutants unable to bind FOG1 (but still retaining DNA binding) do not rescue the severe block in terminal erythroid maturation of GATA1-deficient cells (Tsang et al., 1997). Instead, a compensatory FOG1 mutation restoring the interaction, rescues the GATA1<sup>−</sup> phenotype, demonstrating that the interaction between the two proteins is essential for erythroid and megakaryocytic differentiation (Crispino et al., 1999; Chang et al., 2002). In Nichols et al. (2000) described a family with dyserythropoietic anemia and thrombocytopenia caused by a GATA1 (V205M) mutation abolishing the GATA1:FOG1 interaction.

## Other Allelic Variants, Other Interactions, Other Phenotypes

Remarkably, distinct substitutions at a single residue lead to very different outcomes, underlying the complexity of the GATA1 networks. The R216Q substitution causes X-linked thrombocytopenia with  $\beta$ -Thalassemia (Yu et al., 2002b; Balduini et al., 2004), whereas R216W patients also show features of congenital erythropoietic porphyria (CEP) (Phillips et al., 2007; Di Pierro et al., 2015). The D218Y mutation causes severe thrombocytopenia with anemia (Freson et al., 2002), whereas the D218G substitution causes macrothrombocytopenia with mild dyserythropoiesis and no anemia (Freson et al., 2001; Mehaffey et al., 2001).

Notably, whereas the D218Y diminishes the FOG1:GATA1 interaction, the D218G and R216Q do not, but they rather impair GATA1 ability to recruit the TAL1 cofactor complex (Campbell et al., 2013).

## MUTATIONS IN THE GATA1 DNA TARGET SEQUENCES AS A CAUSE OF HUMAN ERYTHROID DISORDERS

Ultimately, TFs elicit their function by binding to DNA motifs on their target genes. Thus, it is expected that mutations creating new -or disrupting- specific binding sites could have phenotypic consequences. Although these mutations remain very elusive, over the years an increasing number of cases has accumulated, implicating these polymorphisms as a source of disease. Such mutations have been associated with congenital erythropoietic porphyria (Solis et al., 2001), X-linked sideroblastic anemia (Campagna et al., 2014; Kaneko et al., 2014), pyruvate kinase deficiency (Manco et al., 2000), CD41 (Russo et al., 2017), Bernard-Soulier syndrome (Ludlow et al., 1996) or linked to erythroid trait variants such as  $\delta$ -thalassemia (Matsuda et al., 1992) and blood groups (Tournamille et al., 1995; Nakajima et al., 2013; Oda et al., 2015; Moller et al., 2018). Interestingly, a mutation abolishing a GATA1 consensus in the *KLF1* promoter (see below), causes a reduction of KLF1, which in turn results in reduced transcription of the *KLF1* target genes more sensitive to KLF1 levels, such as *BCAM*, encoding for the Lutheran (Lu) antigen (Singleton et al., 2008).

## E/KLF1: An Unsuspected Key-Player in Various Types of Dyserythropoiesis

*KLF1* gene, located on chromosome 19, encodes for a proline-rich protein containing three zinc fingers (Bieker, 1996; Mas et al., 2011; **Figure 1B**), expressed in the bone marrow and in the erythroid lineage. KLF1 mainly acts by recruiting coactivators and chromatin remodelers, thus contributing to the large epigenetics changes which shape erythroid maturation (Shyu et al., 2014).

As for GATA1, the first evidence for an essential role in erythropoiesis came from the observation that *KLF1* knockout mice die *in utero* around E15 due to fatal anemia (Nuez et al., 1995; Perkins et al., 1995). Given that KLF1 is an important activator of  $\beta$ -globin, lethality was first attributed to  $\beta$ -thalassemia. However, this is not the sole explanation for the defect: the rescue of the  $\alpha/\beta$  imbalance obtained by the transgenic expression of  $\gamma$ -globin is not sufficient to rescue hemolysis, thus pointing to additional roles for KLF1 (Perkins et al., 2000). In 2015, the first case of severe neonatal anemia with kernicterus due to *KLF1* compound heterozygosis was described in man (Magor et al., 2015), with an erythroid phenotype largely mirroring that observed in mice: hydrops fetalis, hemolytic anemia, jaundice, hepatosplenomegaly, marked erythroblastosis and high levels of HbF. Another report confirms that in humans, although compatible with life, the loss of KLF1 severely impairs erythropoiesis (Lee et al., 2016).

## QUANTITATIVE MUTATIONS OF KLF1: HAPLOINSUFFICIENCY/HYPOMORPHIC ALLELES

*KLF1* is haplosufficient. The loss of one allele is asymptomatic and only genes particularly sensitive to *KLF1* gene dosage are affected. This is observed in the Lutheran In(Lu) Blood group, where either frameshift mutations, introducing premature termination, or amino acids substitutions in the zinc binding domain, lead to reduced or ineffective KLF1 production (Singleton et al., 2008; Helias et al., 2013). Interestingly, the search for possible mutations in an erythroid TF -that turned out to be KLF1- as a cause of the In(Lu) phenotype came from transcriptomic analyses showing that In(Lu) cells express reduced levels of many erythroid-specific genes associated with red cell maturation, including *BCAM* (encoding for the Lu antigen), *ALAS2*, *HBB*, *SLC4A1*, and *CD44* (Singleton et al., 2008). More recently, extended serological and FACS analysis of In(Lu) samples also revealed a reduced expression of *CD35*, *ICAM4*, and *CD147* (Fraser et al., 2018). Interestingly, in one single case the In(Lu) phenotype has been associated with a GATA1 mutation (X414R) (Singleton et al., 2013).

It is now clear that different KLF1 target genes are differentially sensitive not only to KLF1 levels (when one allele carries an inactivating mutation), but also to the type of KLF1 mutation, making it difficult to clearly separate “quantitative” from “qualitative” effects of KLF1 mutations.

Indeed, KLF1 coordinately regulates the expression of a multitude of red cell specific genes including heme biosynthesis genes [*ALAS2*, *HMBS*, *TFR2* (Singleton et al., 2008)], red cell enzymes [such as pyruvate kinase genes -*PKLR* (Viprakasit et al., 2014)], globins (see below) or cell cycle proteins (Hodge et al., 2006; Pilon et al., 2008; Tallack et al., 2009; Gnanapragasam et al., 2016). Thus, depending on the type of mutation, a specific subset of targets can be affected, leading to a broad spectrum of phenotypes (Perkins et al., 2016).

## The Semi-Dominant Phenotype in Nan (Neonatal Anemia) Mouse and in Human CDAIV

This is particularly evident in the case of the neonatal anemia (Nan) semi-dominant (Nan/+) mouse phenotype (Heruth et al., 2010; Siatecka et al., 2010) and in the phenotype observed in human Congenital dyserythropoietic anemia type IV (CDA IV) (Wickramasinghe et al., 1991; Arnaud et al., 2010; Jaffray et al., 2013; Ravindranath et al., 2018). In the Nan mouse model, the E339D substitution in the second ZnF within the Nan allele, alters Nan-KLF1 binding specificity, resulting in an aberrant transcriptome (Gillinder et al., 2017). The homologous E325K heterozygous mutation in CDA IV patients causes the reduced expression of a subset of KLF1 targets (such as *AQP1* and *CD44*), whereas other targets are normally expressed (such as *BCAM*) (Singleton et al., 2011). In analogy with the Nan mouse mutation, it is likely that also in man the E325K mutation could alter the mutant-KLF1 DNA-binding specificity, resulting in detrimental gain of function effects. On the basis of the different charge of the variant residues (Aspartic Acid or Lysine) it is possible to speculate that subsets of targets can be differentially affected by the different mutant proteins, likely explaining the distinct human and mice pathologies (Arnaud et al., 2010; Siatecka et al., 2010). On the other hand, traits common to mouse and human phenotypes could likely result from the reduced (50%) WT-KLF1.

## The Intricate Link Between KLF1, Globin Expression and the Hemoglobin Switching: Direct and Indirect Effects

KLF1 was originally identified by its ability to bind to the  $\beta$ -globin promoter (Miller and Bieker, 1993) and the connection between KLF1 and  $\beta$ -thalassemia is demonstrated by the paradigmatic -87 mutation in the  $\beta$ -globin promoter CACC box (Feng et al., 1994).

Accordingly, the more evident phenotype of *KLF1* knockout mice is a marked  $\beta$ -thalassemia associated with increased *HBG1/HBG2*, suggesting that KLF1 interferes at different levels with globin genes expression. Indeed, the ablation of KLF1 perturbs the 3-dimensional conformation of the  $\beta$ -globin locus (Noordermeer and de Laat, 2008; Schoenfelder et al., 2010). Moreover, mutations creating *de novo* KLF1 motifs can also alter the relative expression within the  $\beta$ -locus: this is the case of the -198 mutation in the  $\gamma$ -promoter that introduces a new KLF1 binding site, generating the British type HFPH (Wienert et al., 2017). Besides these direct effects of loss or gain of KLF1 binding, an intricate network of indirect effects

downstream to KLF1 haploinsufficiency/mutations must be considered. Borg et al. (2010) reported a Maltese family with HPFH and mild hypochromatic microcytic RBCs, caused by the KLF1 K288X non-sense mutation, ablating the DNA binding domain. Transcription profiling and functional studies in cells from these subjects revealed low levels of BCL11a, the most important known *HBG1/HBG2* repressor, suggesting that failure to properly activate BCL11a is the major cause of the observed HPFH (Borg et al., 2011). This was proven true also in the KLF1-deficient mouse model (Zhou et al., 2010). However, the situation is far more complicated: in another family described shortly thereafter, KLF1 haploinsufficiency did not result in HPFH (Satta et al., 2011). Instead, in this family, HPFH was observed only in compound heterozygotes (non-sense S270X and K332Q missense mutations) together with increased red cell protoporphyrin, a trait observed in the Nan mouse phenotype. Large-scale screening of patients with hemoglobinopathies of different ethnic origin supported the association of *KLF1* mutations with elevated HbF, thus confirming that KLF1 variants are an important source of HbF variation (Gallienne et al., 2012). Finally, more subtle effects of *KLF1* polymorphisms also account for an appreciable proportion of cases with borderline elevated HbA<sub>2</sub> (Perseu et al., 2011). Thus, again, the pleiotropic effects of KLF1 are the sum of quantitative and qualitative effects, possibly in combination with other genetic modifiers.

## CONCLUSION AND PERSPECTIVES

The recent identification of mutations/variants alleles associated with RBC traits involving TFs has greatly increased thanks

to new technologies and is expected to further increase in the next few years. This will help not only to explain so far unexplained diseases -and possibly to envisage new therapeutic strategies-, but also to better understand the structure and function of TFs themselves and their involvement in the different gene regulatory networks. This, in turn, will shed light on the contribution of TFs and their target sequences as a source of genetic variability underlying the wide spectrum of the observed erythroid phenotypes.

## AUTHOR CONTRIBUTIONS

AR conceived and wrote the manuscript. GB, CF, and JS contributed with ideas and discussion. CF created figures.

## FUNDING

This work was supported by the People Programme (Marie Curie Actions) of the European Union's Seventh Framework Programme FP7/2007-2013/ under REA grant agreement no. 289611 (HEM\_ID Project) to AR and JS and by Fondazione Cariplo grant no. 2012.0517 to AR and JS.

## ACKNOWLEDGMENTS

We thank Dr. Stephan Menzel for critical reading of the manuscript.

## REFERENCES

- Ahmed, M., Sternberg, A., Hall, G., Thomas, A., Smith, O., O'Marcaigh, A., et al. (2004). Natural history of GATA1 mutations in Down syndrome. *Blood* 103, 2480–2489. doi: 10.1182/blood-2003-10-3383
- Arnaud, L., Saison, C., Helias, V., Lucien, N., Steschenko, D., Giarratana, M. C., et al. (2010). A dominant mutation in the gene encoding the erythroid transcription factor KLF1 causes a congenital dyserythropoietic anemia. *Am. J. Hum. Genet.* 87, 721–727. doi: 10.1016/j.ajhg.2010.10.010
- Balduini, C. L., Pecci, A., Loffredo, G., Izzo, P., Noris, P., Grosso, M., et al. (2004). Effects of the R216Q mutation of GATA-1 on erythropoiesis and megakaryocytopoiesis. *Thromb. Haemost.* 91, 129–140. doi: 10.1160/TH03-05-0290
- Bianchi, P., Fermo, E., Vercellati, C., Boschetti, C., Barcellini, W., Iurlo, A., et al. (2009). Congenital dyserythropoietic anemia type II (CDAAII) is caused by mutations in the SEC23B gene. *Hum. Mutat.* 30, 1292–1298. doi: 10.1002/humu.21077
- Bieker, J. J. (1996). Isolation, genomic structure, and expression of human erythroid Kruppel-like factor (EKLF). *DNA Cell Biol.* 15, 347–352. doi: 10.1089/dna.1996.15.347
- Borg, J., Papadopoulos, P., Georgitsi, M., Gutierrez, L., Grech, G., Fanis, P., et al. (2010). Haploinsufficiency for the erythroid transcription factor KLF1 causes hereditary persistence of fetal hemoglobin. *Nat. Genet.* 42, 801–805. doi: 10.1038/ng.630
- Borg, J., Patrinos, G. P., Felice, A. E., and Philipson, S. (2011). Erythroid phenotypes associated with KLF1 mutations. *Haematologica* 96, 635–638. doi: 10.3324/haematol.2011.043265
- Cabezas-Wallscheid, N., Klimmeck, D., Hansson, J., Lipka, D. B., Reyes, A., Wang, Q., et al. (2014). Identification of regulatory networks in HSCs and their immediate progeny via integrated proteome, transcriptome, and DNA methylome analysis. *Cell Stem Cell* 15, 507–522. doi: 10.1016/j.stem.2014.07.005
- Calligaris, R., Bottardi, S., Cogoi, S., Apezteguia, I., and Santoro, C. (1995). Alternative translation initiation site usage results in two functionally distinct forms of the GATA-1 transcription factor. *Proc. Natl. Acad. Sci. U.S.A.* 92, 11598–11602. doi: 10.1073/pnas.92.25.11598
- Campagna, D. R., de Bie, C. I., Schmitz-Abe, K., Sweeney, M., Sendamarai, A. K., Schmidt, P. J., et al. (2014). X-linked sideroblastic anemia due to ALAS2 intron 1 enhancer element GATA-binding site mutations. *Am. J. Hematol.* 89, 315–319. doi: 10.1002/ajh.23616
- Campbell, A. E., Wilkinson-White, L., Mackay, J. P., Matthews, J. M., and Blobel, G. A. (2013). Analysis of disease-causing GATA1 mutations in murine gene complementation systems. *Blood* 121, 5218–5227. doi: 10.1182/blood-2013-03-488080
- Chami, N., Chen, M. H., Slater, A. J., Eicher, J. D., Evangelou, E., Tajuddin, S. M., et al. (2016). Exome genotyping identifies pleiotropic variants associated with red blood cell traits. *Am. J. Hum. Genet.* 99, 8–21. doi: 10.1016/j.ajhg.2016.05.007
- Chang, A. N., Cantor, A. B., Fujiwara, Y., Lodish, M. B., Droho, S., Crispino, J. D., et al. (2002). GATA-factor dependence of the multitype zinc-finger protein FOG-1 for its essential role in megakaryopoiesis. *Proc. Natl. Acad. Sci. U.S.A.* 99, 9237–9242. doi: 10.1073/pnas.142302099
- Crispino, J. D. (2005). GATA1 mutations in Down syndrome: implications for biology and diagnosis of children with transient myeloproliferative disorder and acute megakaryoblastic leukemia. *Pediatr. Blood Cancer* 44, 40–44. doi: 10.1002/pbc.20066
- Crispino, J. D., Lodish, M. B., MacKay, J. P., and Orkin, S. H. (1999). Use of altered specificity mutants to probe a specific protein-protein interaction in



- differentiation: the GATA-1:FOG complex. *Mol. Cell* 3, 219–228. doi: 10.1016/S1097-2765(00)80312-3
- Da Costa, L., Narla, A., and Mohandas, N. (2018). An update on the pathogenesis and diagnosis of Diamond-Blackfan anemia. *F1000Res.* 7:F1000 Faculty Rev-1350. doi: 10.12688/f1000research.15542.1
- Di Pierro, E., Russo, R., Karakas, Z., Brancaloni, V., Gambale, A., Kurt, I., et al. (2015). Congenital erythropoietic porphyria linked to GATA1-R216W mutation: challenges for diagnosis. *Eur. J. Haematol.* 94, 491–497. doi: 10.1111/ejh.12452
- Dore, L. C., and Crispino, J. D. (2011). Transcription factor networks in erythroid cell and megakaryocyte development. *Blood* 118, 231–239. doi: 10.1182/blood-2011-04-285981
- Dulmovits, B. M., Hom, J., Narla, A., Mohandas, N., and Blanc, L. (2017). Characterization, regulation, and targeting of erythroid progenitors in normal and disordered human erythropoiesis. *Curr. Opin. Hematol.* 24, 159–166. doi: 10.1097/MOH.0000000000000328
- Dykstra, B., and Bystrykh, L. V. (2014). No monkeying around: clonal tracking of stem cells and progenitors in the macaque. *Cell Stem Cell* 14, 419–420. doi: 10.1016/j.stem.2014.03.006
- Dzierzak, E., and Philipsen, S. (2013). Erythropoiesis: development and differentiation. *Cold Spring Harb. Perspect. Med.* 3:a011601. doi: 10.1101/cshperspect.a011601
- Feng, W. C., Southwood, C. M., and Bieker, J. J. (1994). Analyses of beta-thalassemia mutant DNA interactions with erythroid Kruppel-like factor (EKLF), an erythroid cell-specific transcription factor. *J. Biol. Chem.* 269, 1493–1500.
- Ferreira, R., Ohneda, K., Yamamoto, M., and Philipsen, S. (2005). GATA1 function, a paradigm for transcription factors in hematopoiesis. *Mol. Cell Biol.* 25, 1215–1227. doi: 10.1128/MCB.25.4.1215-1227.2005
- Fraser, N. S., Knauth, C. M., Schoeman, E. M., Moussa, A., Perkins, A. C., Walsh, T., et al. (2018). Investigation of the variable In(Lu) phenotype caused by KLF1 variants. *Transfusion* 58, 2414–2420. doi: 10.1111/trf.14926
- Freson, K., Devriendt, K., Matthijs, G., Van Hoof, A., De Vos, R., Thys, C., et al. (2001). Platelet characteristics in patients with X-linked macrothrombocytopenia because of a novel GATA1 mutation. *Blood* 98, 85–92. doi: 10.1182/blood.V98.1.85
- Freson, K., Matthijs, G., Thys, C., Marien, P., Hoylaerts, M. F., Vermynen, J., et al. (2002). Different substitutions at residue D218 of the X-linked transcription factor GATA1 lead to altered clinical severity of macrothrombocytopenia and anemia and are associated with variable skewed X inactivation. *Hum. Mol. Genet.* 11, 147–152. doi: 10.1093/hmg/11.2.147
- Frontelo, P., Manwani, D., Galdass, M., Karsunky, H., Lohmann, F., Gallagher, P. G., et al. (2007). Novel role for EKLF in megakaryocyte lineage commitment. *Blood* 110, 3871–3880. doi: 10.1182/blood-2007-03-082065
- Fujiwara, Y., Browne, C. P., Cuniff, K., Goff, S. C., and Orkin, S. H. (1996). Arrested development of embryonic red cell precursors in mouse embryos lacking transcription factor GATA-1. *Proc. Natl. Acad. Sci. U.S.A.* 93, 12355–12358. doi: 10.1073/pnas.93.22.12355
- Gallienne, A. E., Dreau, H. M., Schuh, A., Old, J. M., and Henderson, S. (2012). Ten novel mutations in the erythroid transcription factor KLF1 gene associated with increased fetal hemoglobin levels in adults. *Haematologica* 97, 340–343. doi: 10.3324/haematol.2011.055442
- Giladi, A., Paul, F., Herzog, Y., Lubling, Y., Weiner, A., Yofe, I., et al. (2018). Single-cell characterization of haematopoietic progenitors and their trajectories in homeostasis and perturbed haematopoiesis. *Nat. Cell Biol.* 20, 836–846. doi: 10.1038/s41556-018-0121-4
- Gilles, L., Arslan, A. D., Marinaccio, C., Wen, Q. J., Arya, P., McNulty, M., et al. (2017). Downregulation of GATA1 drives impaired hematopoiesis in primary myelofibrosis. *J. Clin. Invest.* 127, 1316–1320. doi: 10.1172/JCI82905
- Gillinder, K. R., Ilsley, M. D., Nebor, D., Sachidanandam, R., Lajoie, M., Magor, G. W., et al. (2017). Promiscuous DNA-binding of a mutant zinc finger protein corrupts the transcriptome and diminishes cell viability. *Nucleic Acids Res.* 45, 1130–1143. doi: 10.1093/nar/gkw1014
- Glogowska, E., and Gallagher, P. G. (2015). Disorders of erythrocyte volume homeostasis. *Int. J. Lab. Hematol.* 37(Suppl. 1), 85–91. doi: 10.1111/ijlh.12357
- Gnanapragasam, M. N., McGrath, K. E., Catherman, S., Xue, L., Palis, J., and Bieker, J. J. (2016). EKLF/KLF1-regulated cell cycle exit is essential for erythroblast enucleation. *Blood* 128, 1631–1641. doi: 10.1182/blood-2016-03-706671
- Grace, R. F., Bianchi, P., van Beers, E. J., Eber, S. W., Glader, B., Yaish, H. M., et al. (2018). Clinical spectrum of pyruvate kinase deficiency: data from the Pyruvate Kinase Deficiency Natural History Study. *Blood* 131, 2183–2192. doi: 10.1182/blood-2017-10-810796
- Gruber, T. A., and Downing, J. R. (2015). The biology of pediatric acute megakaryoblastic leukemia. *Blood* 126, 943–949. doi: 10.1182/blood-2015-05-567859
- Guo, G., Luc, S., Marco, E., Lin, T. W., Peng, C., Kerenyi, M. A., et al. (2013). Mapping cellular hierarchy by single-cell analysis of the cell surface repertoire. *Cell Stem Cell* 13, 492–505. doi: 10.1016/j.stem.2013.07.017
- Gutierrez, L., Nikolic, T., van Dijk, T. B., Hammad, H., Vos, N., Willart, M., et al. (2007). Gata1 regulates dendritic-cell development and survival. *Blood* 110, 1933–1941. doi: 10.1182/blood-2006-09-048322
- Gutierrez, L., Tsukamoto, S., Suzuki, M., Yamamoto-Mukai, H., Yamamoto, M., Philipsen, S., et al. (2008). Ablation of Gata1 in adult mice results in aplastic crisis, revealing its essential role in steady-state and stress erythropoiesis. *Blood* 111, 4375–4385. doi: 10.1182/blood-2007-09-115121
- Haas, S., Trumpp, A., and Milsom, M. D. (2018). Causes and consequences of hematopoietic stem cell heterogeneity. *Cell Stem Cell* 22, 627–638. doi: 10.1016/j.stem.2018.04.003
- Hattangadi, S. M., Wong, P., Zhang, L., Flygare, J., and Lodish, H. F. (2011). From stem cell to red cell: regulation of erythropoiesis at multiple levels by multiple proteins, RNAs, and chromatin modifications. *Blood* 118, 6258–6268. doi: 10.1182/blood-2011-07-356006
- Helias, V., Saison, C., Peyrard, T., Vera, E., Prehu, C., Cartron, J. P., et al. (2013). Molecular analysis of the rare in(Lu) blood type: toward decoding the phenotypic outcome of haploinsufficiency for the transcription factor KLF1. *Hum. Mutat.* 34, 221–228. doi: 10.1002/humu.22218
- Heruth, D. P., Hawkins, T., Logsdon, D. P., Gibson, M. I., Sokolovsky, I. V., Nsumu, N. N., et al. (2010). Mutation in erythroid specific transcription factor KLF1 causes Hereditary Spherocytosis in the Nan hemolytic anemia mouse model. *Genomics* 96, 303–307. doi: 10.1016/j.ygeno.2010.07.009
- Hitzler, J. K., and Zipursky, A. (2005). Origins of leukaemia in children with Down syndrome. *Nat. Rev. Cancer* 5, 11–20. doi: 10.1038/nrc1525
- Hodge, D., Coghill, E., Keys, J., Maguire, T., Hartmann, B., McDowall, A., et al. (2006). A global role for EKLF in definitive and primitive erythropoiesis. *Blood* 107, 3359–3370. doi: 10.1182/blood-2005-07-2888
- Holland, L. M., Lima, C. S., Cunha, A. F., Albuquerque, D. M., Vassallo, J., Ozelo, M. C., et al. (2006). An inherited mutation leading to production of only the short isoform of GATA-1 is associated with impaired erythropoiesis. *Nat. Genet.* 38, 807–812. doi: 10.1038/ng1825
- Hwang, Y., Futran, M., Hidalgo, D., Pop, R., Iyer, D. R., Scully, R., et al. (2017). Global increase in replication fork speed during a p57(KIP2)-regulated erythroid cell fate switch. *Sci. Adv.* 3:e1700298. doi: 10.1126/sciadv.1700298
- Iolascon, A., Russo, R., and Delaunay, J. (2011). Congenital dyserythropoietic anemias. *Curr. Opin. Hematol.* 18, 146–151. doi: 10.1097/MOH.0b013e32834521b0
- Isern, J., He, Z., Fraser, S. T., Nowotschin, S., Ferrer-Vaquer, A., Moore, R., et al. (2011). Single-lineage transcriptome analysis reveals key regulatory pathways in primitive erythroid progenitors in the mouse embryo. *Blood* 117, 4924–4934. doi: 10.1182/blood-2010-10-313676
- Jaffray, J. A., Mitchell, W. B., Gnanapragasam, M. N., Seshan, S. V., Guo, X., Westhoff, C. M., et al. (2013). Erythroid transcription factor EKLF/KLF1 mutation causing congenital dyserythropoietic anemia type IV in a patient of Taiwanese origin: review of all reported cases and development of a clinical diagnostic paradigm. *Blood Cells Mol. Dis.* 51, 71–75. doi: 10.1016/j.bcmd.2013.02.006
- Kaneko, K., Furuyama, K., Fujiwara, T., Kobayashi, R., Ishida, H., Harigae, H., et al. (2014). Identification of a novel erythroid-specific enhancer for the ALAS2 gene and its loss-of-function mutation which is associated with congenital sideroblastic anemia. *Haematologica* 99, 252–261. doi: 10.3324/haematol.2013.085449
- Khajuria, R. K., Munschauer, M., Ulirsch, J. C., Fiorini, C., Ludwig, L. S., McFarland, S. K., et al. (2018). Ribosome levels selectively regulate translation and lineage commitment in human hematopoiesis. *Cell* 173, 90–103.e19. doi: 10.1016/j.cell.2018.02.036

- Klar, J., Khalfallah, A., Arzoo, P. S., Gazda, H. T., and Dahl, N. (2014). Recurrent GATA1 mutations in Diamond-Blackfan anaemia. *Br. J. Haematol.* 166, 949–951. doi: 10.1111/bjh.12919
- Koralkova, P., van Solinge, W. W., and van Wijk, R. (2014). Rare hereditary red blood cell enzymopathies associated with hemolytic anemia - pathophysiology, clinical aspects, and laboratory diagnosis. *Int. J. Lab. Hematol.* 36, 388–397. doi: 10.1111/ijlh.12223
- Koury, M. J. (2016). Tracking erythroid progenitor cells in times of need and times of plenty. *Exp. Hematol.* 44, 653–663. doi: 10.1016/j.exphem.2015.10.007
- Kozma, G. T., Martelli, F., Verrucci, M., Gutierrez, L., Migliaccio, G., Sanchez, M., et al. (2010). Dynamic regulation of Gata1 expression during the maturation of conventional dendritic cells. *Exp. Hematol.* 38, 489–503.e1. doi: 10.1016/j.exphem.2010.03.006
- Lee, H. H., Mak, A. S., Kou, K. O., Poon, C. F., Wong, W. S., Chiu, K. H., et al. (2016). An unusual hydrops fetalis associated with compound heterozygosity for kruppel-like factor 1 mutations. *Hemoglobin* 40, 431–434. doi: 10.1080/03630269.2016.1267017
- Lefevre, C., Bondu, S., Le Goff, S., Kosmider, O., and Fontenay, M. (2017). Dyserythropoiesis of myelodysplastic syndromes. *Curr. Opin. Hematol.* 24, 191–197. doi: 10.1097/MOH.0000000000000325
- Levine, R. L., Pardanani, A., Tefferi, A., and Gilliland, D. G. (2007). Role of JAK2 in the pathogenesis and therapy of myeloproliferative disorders. *Nat. Rev. Cancer* 7, 673–683. doi: 10.1038/nrc2210
- Li, Z., Godinho, F. J., Klusmann, J. H., Garriga-Canut, M., Yu, C., and Orkin, S. H. (2005). Developmental stage-selective effect of somatically mutated leukemogenic transcription factor GATA1. *Nat. Genet.* 37, 613–619. doi: 10.1038/ng1566
- Libani, I. V., Guy, E. C., Melchior, L., Schiro, R., Ramos, P., Breda, L., et al. (2008). Decreased differentiation of erythroid cells exacerbates ineffective erythropoiesis in beta-thalassemia. *Blood* 112, 875–885. doi: 10.1182/blood-2007-12-126938
- Love, P. E., Warzecha, C., and Li, L. (2014). Ldb1 complexes: the new master regulators of erythroid gene transcription. *Trends Genet.* 30, 1–9. doi: 10.1016/j.tig.2013.10.001
- Ludlow, L. B., Schick, B. P., Budarf, M. L., Driscoll, D. A., Zackai, E. H., Cohen, A., et al. (1996). Identification of a mutation in a GATA binding site of the platelet glycoprotein Ibbeta promoter resulting in the Bernard-Soulier syndrome. *J. Biol. Chem.* 271, 22076–22080. doi: 10.1074/jbc.271.36.22076
- Ludwig, L. S., Gazda, H. T., Eng, J. C., Eichhorn, S. W., Thiru, P., Ghazvinian, R., et al. (2014). Altered translation of GATA1 in diamond-Blackfan anemia. *Nat. Med.* 20, 748–753. doi: 10.1038/nm.3557
- Magalhaes, I. Q., Splendore, A., Emerenciano, M., Figueiredo, A., Ferrari, I., and Pombo-de-Oliveira, M. S. (2006). GATA1 mutations in acute leukemia in children with Down syndrome. *Cancer Genet. Cytogenet.* 166, 112–116. doi: 10.1016/j.cancergencyto.2005.10.008
- Magor, G. W., Tallack, M. R., Gillinder, K. R., Bell, C. C., McCallum, N., Williams, B., et al. (2015). KLF1-null neonates display hydrops fetalis and a deranged erythroid transcriptome. *Blood* 125, 2405–2417. doi: 10.1182/blood-2014-08-590968
- Manco, L., Ribeiro, M. L., Maximo, V., Almeida, H., Costa, A., Freitas, O., et al. (2000). A new PKLR gene mutation in the R-type promoter region affects the gene transcription causing pyruvate kinase deficiency. *Br. J. Haematol.* 110, 993–997. doi: 10.1046/j.1365-2141.2000.02283.x
- Mas, C., Lussier-Price, M., Soni, S., Morse, T., Arseneault, G., Di Lello, P., et al. (2011). Structural and functional characterization of an atypical activation domain in erythroid Kruppel-like factor (EKLf). *Proc. Natl. Acad. Sci. U.S.A.* 108, 10484–10489. doi: 10.1073/pnas.1017029108
- Matsuda, M., Sakamoto, N., and Fukumaki, Y. (1992). Delta-thalassemia caused by disruption of the site for an erythroid-specific transcription factor, GATA-1, in the delta-globin gene promoter. *Blood* 80, 1347–1351.
- Mehaffey, M. G., Newton, A. L., Gandhi, M. J., Crossley, M., and Drachman, J. G. (2001). X-linked thrombocytopenia caused by a novel mutation of GATA-1. *Blood* 98, 2681–2688. doi: 10.1182/blood.V98.9.2681
- Menzel, S., Garner, C., Gut, I., Matsuda, F., Yamaguchi, M., Heath, S., et al. (2007). A QTL influencing F cell production maps to a gene encoding a zinc-finger protein on chromosome 2p15. *Nat. Genet.* 39, 1197–1199. doi: 10.1038/ng2108
- Migliaccio, A. R., Rana, R. A., Vannucchi, A. M., and Manzoli, F. A. (2005). Role of GATA-1 in normal and neoplastic hemopoiesis. *Ann. N. Y. Acad. Sci.* 1044, 142–158. doi: 10.1196/annals.1349.019
- Miller, I. J., and Bieker, J. J. (1993). A novel, erythroid cell-specific murine transcription factor that binds to the CACCC element and is related to the Kruppel family of nuclear proteins. *Mol. Cell Biol.* 13, 2776–2786. doi: 10.1128/MCB.13.5.2776
- Mohandas, N., and Gallagher, P. G. (2008). Red cell membrane: past, present, and future. *Blood* 112, 3939–3948. doi: 10.1182/blood-2008-07-161166
- Moller, M., Lee, Y. Q., Vidovic, K., Kjellstrom, S., Bjorkman, L., Storry, J. R., et al. (2018). Disruption of a GATA1-binding motif upstream of XG/PBDX abolishes Xg(a) expression and resolves the Xg blood group system. *Blood* 132, 334–338. doi: 10.1182/blood-2018-03-842542
- Mundschaun, G., Gurbuxani, S., Gamis, A. S., Greene, M. E., Arcenci, R. J., and Crispino, J. D. (2003). Mutagenesis of GATA1 is an initiating event in Down syndrome leukemogenesis. *Blood* 101, 4298–4300. doi: 10.1182/blood-2002-12-3904
- Nakajima, T., Sano, R., Takahashi, Y., Kubo, R., Takahashi, K., Kominato, Y., et al. (2013). Mutation of the GATA site in the erythroid cell-specific regulatory element of the ABO gene in a Bm subgroup individual. *Transfusion* 53(11 Suppl. 2), 2917–2927. doi: 10.1111/trf.12181
- Nandakumar, S. K., Ulirsch, J. C., and Sankaran, V. G. (2016). Advances in understanding erythropoiesis: evolving perspectives. *Br. J. Haematol.* 173, 206–218. doi: 10.1111/bjh.13938
- Nestorowa, S., Hamey, F. K., Pijuan Sala, B., Diamanti, E., Shepherd, M., Laurenti, E., et al. (2016). A single-cell resolution map of mouse hematopoietic stem and progenitor cell differentiation. *Blood* 128, e20–e31. doi: 10.1182/blood-2016-05-716480
- Newton, A., Mackay, J., and Crossley, M. (2001). The N-terminal zinc finger of the erythroid transcription factor GATA-1 binds GATC motifs in DNA. *J. Biol. Chem.* 276, 35794–35801. doi: 10.1074/jbc.M106256200
- Nichols, K. E., Crispino, J. D., Poncz, M., White, J. G., Orkin, S. H., Maris, J. M., et al. (2000). Familial dyserythropoietic anaemia and thrombocytopenia due to an inherited mutation in GATA1. *Nat. Genet.* 24, 266–270. doi: 10.1038/73480
- Nilson, D. G., Sabatino, D. E., Bodine, D. M., and Gallagher, P. G. (2006). Major erythrocyte membrane protein genes in EKLf-deficient mice. *Exp. Hematol.* 34, 705–712. doi: 10.1016/j.exphem.2006.02.018
- Noordermeer, D., and de Laat, W. (2008). Joining the loops: beta-globin gene regulation. *IUBMB Life* 60, 824–833. doi: 10.1002/iub.129
- Notta, F., Zandi, S., Takayama, N., Dobson, S., Gan, O. I., Wilson, G., et al. (2016). Distinct routes of lineage development reshape the human blood hierarchy across ontogeny. *Science* 351:aab2116. doi: 10.1126/science.aab2116
- Nuez, B., Michalovich, D., Bygrave, A., Ploemacher, R., and Grosfeld, F. (1995). Defective haematopoiesis in fetal liver resulting from inactivation of the EKLf gene. *Nature* 375, 316–318. doi: 10.1038/375316a0
- O'Brien, K. A., Farrar, J. E., Vlachos, A., Anderson, S. M., Tsujiura, C. A., Lichtenberg, J., et al. (2017). Molecular convergence in ex vivo models of Diamond-Blackfan anemia. *Blood* 129, 3111–3120. doi: 10.1182/blood-2017-01-760462
- Oda, A., Isa, K., Ogasawara, K., Kameyama, K., Okuda, K., Hirashima, M., et al. (2015). A novel mutation of the GATA site in the erythroid cell-specific regulatory element of the ABO gene in a blood donor with the Am B phenotype. *Vox Sang.* 108, 425–427. doi: 10.1111/vox.12229
- Palis, J. (2014). Primitive and definitive erythropoiesis in mammals. *Front. Physiol.* 5:3. doi: 10.3389/fphys.2014.00003
- Palis, J. (2016). Hematopoietic stem cell-independent hematopoiesis: emergence of erythroid, megakaryocyte, and myeloid potential in the mammalian embryo. *FEBS Lett.* 590, 3965–3974. doi: 10.1002/1873-3468.12459
- Parrella, S., Aspesi, A., Quarello, P., Garelli, E., Pavesi, E., Carando, A., et al. (2014). Loss of GATA-1 full length as a cause of Diamond-Blackfan anemia phenotype. *Pediatr. Blood Cancer* 61, 1319–1321. doi: 10.1002/pbc.24944
- Paul, F., Arkin, Y., Giladi, A., Jaitin, D. A., Kenigsberg, E., Keren-Shaul, H., et al. (2016). Transcriptional heterogeneity and lineage commitment in myeloid progenitors. *Cell* 164, 325. doi: 10.1016/j.cell.2015.12.046
- Pei, W., Feyerabend, T. B., Rossler, J., Wang, X., Postrach, D., Busch, K., et al. (2017). Polylox barcoding reveals hematopoietic stem cell fates realized in vivo. *Nature* 548, 456–460. doi: 10.1038/nature23653

- Perie, L., Hodgkin, P. D., Naik, S. H., Schumacher, T. N., de Boer, R. J., and Duffy, K. R. (2014). Determining lineage pathways from cellular barcoding experiments. *Cell Rep.* 6, 617–624. doi: 10.1016/j.celrep.2014.01.016
- Perkins, A., Xu, X., Higgs, D. R., Patrinos, G. P., Arnaud, L., Bieker, J. J., et al. (2016). Kruppeling erythropoiesis: an unexpected broad spectrum of human red blood cell disorders due to KLF1 variants. *Blood* 127, 1856–1862. doi: 10.1182/blood-2016-01-694331
- Perkins, A. C., Peterson, K. R., Stamatoyanopoulos, G., Witkowska, H. E., and Orkin, S. H. (2000). Fetal expression of a human Agamma globin transgene rescues globin chain imbalance but not hemolysis in EKLF null mouse embryos. *Blood* 95, 1827–1833.
- Perkins, A. C., Sharpe, A. H., and Orkin, S. H. (1995). Lethal beta-thalassaemia in mice lacking the erythroid CACCC-transcription factor EKLF. *Nature* 375, 318–322. doi: 10.1038/375318a0
- Perrotta, S., Gallagher, P. G., and Mohandas, N. (2008). Hereditary spherocytosis. *Lancet* 372, 1411–1426. doi: 10.1016/S0140-6736(08)61588-3
- Perseu, L., Satta, S., Moi, P., Demartis, F. R., Manunza, L., Sollaino, M. C., et al. (2011). KLF1 gene mutations cause borderline HbA(2). *Blood* 118, 4454–4458. doi: 10.1182/blood-2011-04-345736
- Pevny, L., Lin, C. S., D'Agati, V., Simon, M. C., Orkin, S. H., and Costantini, F. (1995). Development of hematopoietic cells lacking transcription factor GATA-1. *Development* 121, 163–172.
- Pevny, L., Simon, M. C., Robertson, E., Klein, W. H., Tsai, S. F., D'Agati, V., et al. (1991). Erythroid differentiation in chimaeric mice blocked by a targeted mutation in the gene for transcription factor GATA-1. *Nature* 349, 257–260. doi: 10.1038/349257a0
- Phillips, J. D., Steensma, D. P., Pulsipher, M. A., Spangrude, G. J., and Kushner, J. P. (2007). Congenital erythropoietic porphyria due to a mutation in GATA1: the first trans-acting mutation causative for a human porphyria. *Blood* 109, 2618–2621. doi: 10.1182/blood-2006-06-022848
- Pilon, A. M., Arcasoy, M. O., Dressman, H. K., Vayda, S. E., Maksimova, Y. D., Sangerman, J. I., et al. (2008). Failure of terminal erythroid differentiation in EKLF-deficient mice is associated with cell cycle perturbation and reduced expression of E2F2. *Mol. Cell Biol.* 28, 7394–7401. doi: 10.1128/MCB.01087-08
- Portela, A., and Esteller, M. (2010). Epigenetic modifications and human disease. *Nat. Biotechnol.* 28, 1057–1068. doi: 10.1038/nbt.1685
- Rainis, L., Bercovich, D., Strehl, S., Teigler-Schlegel, A., Stark, B., Trka, J., et al. (2003). Mutations in exon 2 of GATA1 are early events in megakaryocytic malignancies associated with trisomy 21. *Blood* 102, 981–986. doi: 10.1182/blood-2002-11-3599
- Ravindranath, Y., Johnson, R. M., Goyette, G., Buck, S., Gadgil, M., and Gallagher, P. G. (2018). KLF1 E325K-associated congenital dyserythropoietic anemia type IV: insights into the variable clinical severity. *J. Pediatr. Hematol. Oncol.* 40, e405–e409. doi: 10.1097/MPH.0000000000001056
- Rees, D. C., Williams, T. N., and Gladwin, M. T. (2010). Sick cell disease. *Lancet* 376, 2018–2031. doi: 10.1016/S0140-6736(10)61029-X
- Ribeil, J. A., Arlet, J. B., Dussiot, M., Moura, I. C., Courtois, G., and Hermine, O. (2013). Ineffective erythropoiesis in beta-thalassemia. *ScientificWorldJournal*. 2013:394295. doi: 10.1155/2013/394295
- Rivella, S. (2015). beta-thalassemias: paradigmatic diseases for scientific discoveries and development of innovative therapies. *Haematologica* 100, 418–430. doi: 10.3324/haematol.2014.114827
- Rodriguez-Fraticelli, A. E., Wolock, S. L., Weinreb, C. S., Panero, R., Patel, S. H., Jankovic, M., et al. (2018). Clonal analysis of lineage fate in native haematopoiesis. *Nature* 553, 212–216. doi: 10.1038/nature25168
- Russo, R., Andolfo, I., Gambale, A., De Rosa, G., Manna, F., Arillo, A., et al. (2017). GATA1 erythroid-specific regulation of SEC23B expression and its implication in the pathogenesis of congenital dyserythropoietic anemia type II. *Haematologica* 102, e371–e374. doi: 10.3324/haematol.2016.162966
- Sankaran, V. G., Ghazvinian, R., Do, R., Thiru, P., Vergilio, J. A., Beggs, A. H., et al. (2012). Exome sequencing identifies GATA1 mutations resulting in Diamond-Blackfan anemia. *J. Clin. Invest.* 122, 2439–2443. doi: 10.1172/JCI63597
- Sankaran, V. G., Menne, T. F., Xu, J., Akie, T. E., Lettre, G., Van Handel, B., et al. (2008). Human fetal hemoglobin expression is regulated by the developmental stage-specific repressor BCL11A. *Science* 322, 1839–1842. doi: 10.1126/science.1165409
- Satta, S., Perseu, L., Moi, P., Asunis, I., Cabriolu, A., Maccioni, L., et al. (2011). Compound heterozygosity for KLF1 mutations associated with remarkable increase of fetal hemoglobin and red cell protoporphyrin. *Haematologica* 96, 767–770. doi: 10.3324/haematol.2010.037333
- Schoenfelder, S., Sexton, T., Chakalova, L., Cope, N. F., Horton, A., Andrews, S., et al. (2010). Preferential associations between co-regulated genes reveal a transcriptional interactome in erythroid cells. *Nat. Genet.* 42, 53–61. doi: 10.1038/ng.496
- Schwarz, K., Iolascon, A., Verissimo, F., Trede, N. S., Horsley, W., Chen, W., et al. (2009). Mutations affecting the secretory COPII coat component SEC23B cause congenital dyserythropoietic anemia type II. *Nat. Genet.* 41, 936–940. doi: 10.1038/ng.405
- Shimada, A., Xu, G., Toki, T., Kimura, H., Hayashi, Y., and Ito, E. (2004). Fetal origin of the GATA1 mutation in identical twins with transient myeloproliferative disorder and acute megakaryoblastic leukemia accompanying Down syndrome. *Blood* 103:366. doi: 10.1182/blood-2003-09-3219
- Shivdasani, R. A., Fujiwara, Y., McDevitt, M. A., and Orkin, S. H. (1997). A lineage-selective knockout establishes the critical role of transcription factor GATA-1 in megakaryocyte growth and platelet development. *EMBO J.* 16, 3965–3973. doi: 10.1093/emboj/16.13.3965
- Shyu, Y. C., Lee, T. L., Chen, X., Hsu, P. H., Wen, S. C., Liaw, Y. W., et al. (2014). Tight regulation of a timed nuclear import wave of EKLF by PKC $\theta$  and FOE during Pro-E to Baso-E transition. *Dev. Cell* 28, 409–422. doi: 10.1016/j.devcel.2014.01.007
- Siatecka, M., Sahr, K. E., Andersen, S. G., Mezei, M., Bieker, J. J., and Peters, L. L. (2010). Severe anemia in the Nan mutant mouse caused by sequence-selective disruption of erythroid Kruppel-like factor. *Proc. Natl. Acad. Sci. U.S.A.* 107, 15151–15156. doi: 10.1073/pnas.1004996107
- Singleton, B. K., Burton, N. M., Green, C., Brady, R. L., and Anstee, D. J. (2008). Mutations in EKLF/KLF1 form the molecular basis of the rare blood group In(Lu) phenotype. *Blood* 112, 2081–2088. doi: 10.1182/blood-2008-03-145672
- Singleton, B. K., Lau, W., Fairweather, V. S., Burton, N. M., Wilson, M. C., Parsons, S. F., et al. (2011). Mutations in the second zinc finger of human EKLF reduce promoter affinity but give rise to benign and disease phenotypes. *Blood* 118, 3137–3145. doi: 10.1182/blood-2011-04-349985
- Singleton, B. K., Roxby, D. J., Stirling, J. W., Spring, F. A., Wilson, C., Poole, J., et al. (2013). A novel GATA1 mutation (Stop414Arg) in a family with the rare X-linked blood group Lu(a-b-) phenotype and mild macrothrombocytic thrombocytopenia. *Br. J. Haematol.* 161, 139–142. doi: 10.1111/bjh.12184
- Solis, C., Aizencang, G. I., Astrin, K. H., Bishop, D. F., and Desnick, R. J. (2001). Uroporphyrinogen III synthase erythroid promoter mutations in adjacent GATA1 and CP2 elements cause congenital erythropoietic porphyria. *J. Clin. Invest.* 107, 753–762. doi: 10.1172/JCI10642
- Songdej, N., and Rao, A. K. (2017). Hematopoietic transcription factor mutations: important players in inherited platelet defects. *Blood* 129, 2873–2881. doi: 10.1182/blood-2016-11-709881
- Soranzo, N., Spector, T. D., Mangino, M., Kuhnel, B., Rendon, A., Teumer, A., et al. (2009). A genome-wide meta-analysis identifies 22 loci associated with eight hematological parameters in the HaemGen consortium. *Nat. Genet.* 41, 1182–1190. doi: 10.1038/ng.467
- Tallack, M. R., Keys, J. R., Humbert, P. O., and Perkins, A. C. (2009). EKLF/KLF1 controls cell cycle entry via direct regulation of E2f2. *J. Biol. Chem.* 284, 20966–20974. doi: 10.1074/jbc.M109.006346
- Tallack, M. R., and Perkins, A. C. (2010). Megakaryocyte-erythroid lineage promiscuity in EKLF null mouse blood. *Haematologica* 95, 144–147. doi: 10.3324/haematol.2009.010017
- Tournamille, C., Colin, Y., Cartron, J. P., and Le Van Kim, C. (1995). Disruption of a GATA motif in the Duffy gene promoter abolishes erythroid gene expression in Duffy-negative individuals. *Nat. Genet.* 10, 224–228. doi: 10.1038/ng0695-224
- Trainor, C. D., Omichinski, J. G., Vandergon, T. L., Gronenborn, A. M., Clore, G. M., and Felsenfeld, G. (1996). A palindromic regulatory site within vertebrate GATA-1 promoters requires both zinc fingers of the GATA-1 DNA-binding domain for high-affinity interaction. *Mol. Cell Biol.* 16, 2238–2247. doi: 10.1128/MCB.16.5.2238
- Tsang, A. P., Visvader, J. E., Turner, C. A., Fujiwara, Y., Yu, C., Weiss, M. J., et al. (1997). FOG, a multitype zinc finger protein, acts as a cofactor for transcription factor GATA-1 in erythroid and megakaryocytic differentiation. *Cell* 90, 109–119. doi: 10.1016/S0092-8674(00)80318-9

- Tsiftoglou, A. S., Vizirianakis, I. S., and Strouboulis, J. (2009). Erythropoiesis: model systems, molecular regulators, and developmental programs. *IUBMB Life* 61, 800–830. doi: 10.1002/iub.226
- Tusi, B. K., Wolock, S. L., Weinreb, C., Hwang, Y., Hidalgo, D., Zilionis, R., et al. (2018). Population snapshots predict early haematopoietic and erythroid hierarchies. *Nature* 555, 54–60. doi: 10.1038/nature25741
- Uda, M., Galanello, R., Sanna, S., Lettre, G., Sankaran, V. G., Chen, W., et al. (2008). Genome-wide association study shows BCL11A associated with persistent fetal hemoglobin and amelioration of the phenotype of beta-thalassemia. *Proc. Natl. Acad. Sci. U.S.A.* 105, 1620–1625. doi: 10.1073/pnas.0711566105
- Upadhyaya, S., Sawai, C. M., Papalexi, E., Rashidfarrokhi, A., Jang, G., Chattopadhyay, P., et al. (2018). Kinetics of adult hematopoietic stem cell differentiation in vivo. *J. Exp. Med.* 215:2815. doi: 10.1084/jem.20180136
- van der Harst, P., Zhang, W., Mateo Leach, I., Rendon, A., Verweij, N., Sehmi, J., et al. (2012). Seventy-five genetic loci influencing the human red blood cell. *Nature* 492, 369–375. doi: 10.1038/nature11677
- Vannucchi, A. M., Bianchi, L., Cellai, C., Paoletti, F., Rana, R. A., Lorenzini, R., et al. (2002). Development of myelofibrosis in mice genetically impaired for GATA-1 expression (GATA-1<sup>low</sup> mice). *Blood* 100, 1123–1132. doi: 10.1182/blood-2002-06-1913
- Viprakasit, V., Ekwattanakit, S., Rioueang, S., Chalaow, N., Fisher, C., Lower, K., et al. (2014). Mutations in Kruppel-like factor 1 cause transfusion-dependent hemolytic anemia and persistence of embryonic globin gene expression. *Blood* 123, 1586–1595. doi: 10.1182/blood-2013-09-526087
- Vyas, P., Ault, K., Jackson, C. W., Orkin, S. H., and Shivdasani, R. A. (1999). Consequences of GATA-1 deficiency in megakaryocytes and platelets. *Blood* 93, 2867–2875.
- Wechsler, J., Greene, M., McDevitt, M. A., Anastasi, J., Karp, J. E., Le Beau, M. M., et al. (2002). Acquired mutations in GATA1 in the megakaryoblastic leukemia of Down syndrome. *Nat. Genet.* 32, 148–152. doi: 10.1038/ng955
- Wickramasinghe, S. N., Illum, N., and Wimberley, P. D. (1991). Congenital dyserythropoietic anaemia with novel intra-erythroblastic and intra-erythrocytic inclusions. *Br. J. Haematol.* 79, 322–330. doi: 10.1111/j.1365-2141.1991.tb04541.x
- Wienert, B., Martyn, G. E., Kurita, R., Nakamura, Y., Quinlan, K. G. R., and Crossley, M. (2017). KLF1 drives the expression of fetal hemoglobin in British HPFH. *Blood* 130, 803–807. doi: 10.1182/blood-2017-02-767400
- Xu, G., Nagano, M., Kanazaki, R., Toki, T., Hayashi, Y., Taketani, T., et al. (2003). Frequent mutations in the GATA-1 gene in the transient myeloproliferative disorder of Down syndrome. *Blood* 102, 2960–2968. doi: 10.1182/blood-2003-02-0390
- Ye, F., Huang, W., and Guo, G. (2017). Studying hematopoiesis using single-cell technologies. *J. Hematol. Oncol.* 10:27. doi: 10.1186/s13045-017-0401-7
- Yu, C., Cantor, A. B., Yang, H., Browne, C., Wells, R. A., Fujiwara, Y., et al. (2002a). Targeted deletion of a high-affinity GATA-binding site in the GATA-1 promoter leads to selective loss of the eosinophil lineage in vivo. *J. Exp. Med.* 195, 1387–1395.
- Yu, C., Niakan, K. K., Matsushita, M., Stamatoyannopoulos, G., Orkin, S. H., and Raskind, W. H. (2002b). X-linked thrombocytopenia with thalassemia from a mutation in the amino finger of GATA-1 affecting DNA binding rather than FOG-1 interaction. *Blood* 100, 2040–2045.
- Zhou, D., Liu, K., Sun, C. W., Pawlik, K. M., and Townes, T. M. (2010). KLF1 regulates BCL11A expression and gamma- to beta-globin gene switching. *Nat. Genet.* 42, 742–744. doi: 10.1038/ng.637

**Conflict of Interest Statement:** The authors declare that the research was conducted in the absence of any commercial or financial relationships that could be construed as a potential conflict of interest.

Copyright © 2019 Barbarani, Fugazza, Strouboulis and Ronchi. This is an open-access article distributed under the terms of the Creative Commons Attribution License (CC BY). The use, distribution or reproduction in other forums is permitted, provided the original author(s) and the copyright owner(s) are credited and that the original publication in this journal is cited, in accordance with accepted academic practice. No use, distribution or reproduction is permitted which does not comply with these terms.





# PIEZO1 Hypomorphic Variants in Congenital Lymphatic Dysplasia Cause Shape and Hydration Alterations of Red Blood Cells

Immacolata Andolfo<sup>1,2\*</sup>, Gianluca De Rosa<sup>1,2</sup>, Edoardo Errichiello<sup>3</sup>, Francesco Manna<sup>1,2</sup>, Barbara Eleni Rosato<sup>1,2</sup>, Antonella Gambale<sup>1,2</sup>, Annalisa Vetro<sup>4</sup>, Valeria Calcaterra<sup>5</sup>, Gloria Pelizzo<sup>6</sup>, Lucia De Franceschi<sup>7</sup>, Orsetta Zuffardi<sup>3</sup>, Roberta Russo<sup>1,2</sup> and Achille Iolascon<sup>1,2</sup>

<sup>1</sup> Department of Molecular Medicine and Medical Biotechnologies, University of Naples Federico II, Naples, Italy, <sup>2</sup> CEINGE, Biotechnologie Avanzate, Naples, Italy, <sup>3</sup> Department of Molecular Medicine, University of Pavia, Pavia, Italy, <sup>4</sup> Pediatric Neurology, Neurogenetics and Neurobiology Unit and Laboratories, Department of Neuroscience, A. Meyer Children's Hospital, University of Florence, Florence, Italy, <sup>5</sup> Pediatric Unit, Department of Maternal and Children's Health, Fondazione IRCCS Policlinico San Matteo, University of Pavia, Pavia, Italy, <sup>6</sup> Department of Pediatric Surgery, Children's Hospital "G. Di Cristina", ARNAS Civico-Di Cristina-Benfratelli, Palermo, Italy, <sup>7</sup> Department of Medicine, University of Verona, Verona, Italy

## OPEN ACCESS

### Edited by:

Paola Bianchi,  
IRCCS Ca' Granda Foundation  
Maggiore Policlinico Hospital (IRCCS),  
Italy

### Reviewed by:

Loic Garçon,  
University Hospital Center (CHU)  
of Amiens, France  
Hitoshi Kanno,  
Tokyo Women's Medical University,  
Japan

### \*Correspondence:

Immacolata Andolfo  
andolfo@ceinge.unina.it

### Specialty section:

This article was submitted to  
Red Blood Cell Physiology,  
a section of the journal  
Frontiers in Physiology

**Received:** 03 December 2018

**Accepted:** 26 February 2019

**Published:** 15 March 2019

### Citation:

Andolfo I, De Rosa G, Errichiello E, Manna F, Rosato BE, Gambale A, Vetro A, Calcaterra V, Pelizzo G, De Franceschi L, Zuffardi O, Russo R and Iolascon A (2019) PIEZO1 Hypomorphic Variants in Congenital Lymphatic Dysplasia Cause Shape and Hydration Alterations of Red Blood Cells. *Front. Physiol.* 10:258. doi: 10.3389/fphys.2019.00258

PIEZO1 is a cation channel activated by mechanical force. It plays an important physiological role in several biological processes such as cardiovascular, renal, endothelial and hematopoietic systems. Two different diseases are associated with alteration in the DNA sequence of *PIEZO1*: (i) dehydrated hereditary stomatocytosis (DHS1, #194380), an autosomal dominant hemolytic anemia caused by gain-of-function mutations; (ii) lymphatic dysplasia with non-immune fetal hydrops (LMPH3, #616843), an autosomal recessive condition caused by biallelic loss-of-function mutations. We analyzed a 14-year-old boy affected by severe lymphatic dysplasia already present prenatally, with peripheral edema, hydrocele, and chylothoraces. By whole exome sequencing, we identified compound heterozygosity for *PIEZO1*, with one splicing and one deletion mutation, the latter causing the formation of a premature stop codon that leads to mRNA decay. The functional analysis of the erythrocytes of the patient highlighted altered hydration with the intracellular loss of the potassium content and structural abnormalities with anisopoikilocytosis and presence of both spherocytes and stomatocytes. This novel erythrocyte trait, sharing features with both hereditary spherocytosis and overhydrated hereditary stomatocytosis, complements the clinical features associated with loss-of-function mutations of *PIEZO1* in the context of the generalized lymphatic dysplasia of LMPH3 type.

**Keywords:** *PIEZO1*, lymphedema, red blood cell alterations, overhydration, stomatocytosis, spherocytosis

## BACKGROUND

*PIEZO1* gene encodes for the mechanoreceptor PIEZO1, a selective cation channel activated by mechanical force (Coste et al., 2010), with several different functions, such as regulation of urinary osmolarity (Martins et al., 2016), control of blood pressure (Wang et al., 2016), or sensor of epithelial cell crowding and stretching (Gudipaty et al., 2017). PIEZO1 is expressed in developing



blood and lymphatic vessels and plays a key role in blood vessel formation (Andolfo et al., 2013; Li et al., 2014; Ranade et al., 2014). Two different diseases are associated with *PIEZO1* mutations: (i) dehydrated hereditary stomatocytosis 1 (DHS1), hemolytic anemia caused by gain-of-function mutations (Zarychanski et al., 2012; Andolfo et al., 2013); (ii) autosomal recessive generalized lymphatic dysplasia with non-immune fetal hydrops (LMPH3) caused by biallelic, loss-of-function mutations (Fotiou et al., 2015; Lukacs et al., 2015). The two diseases are completely different: DHS1 affects red blood cells (RBCs) while LMPH3 is characterized by widespread lymphedema. The only shared phenotype is the presence of perinatal edema (Andolfo et al., 2016; Martin-Almedina et al., 2018).

Several animal models for *PIEZO1* were generated. *Piezo1*-deficient mice die in utero at mid-gestation due to defective vasculogenesis (Cahalan et al., 2015). Thus, another model was developed by a specific deletion in the hematopoietic system (Vav1-*P1cKO* mice). Interestingly, hematological analysis of Vav1-*P1cKO* mice revealed elevated MCV and MCH and reduced MCHC (Cahalan et al., 2015). RBCs exhibited increased osmotic fragility, suggesting that *Piezo1*-deficient erythrocytes were overhydrated. Recently, zebrafish models have also been created. Morpholino-knockdown of *Piezo1* expression in *Danio rerio* was reported to result in severe anemia (Faucherre et al., 2014; Shmukler et al., 2015). However, the phenotype observed in the morpholino-knockdown model was not present in an independent zebrafish model carrying a predicted truncated form of *Piezo1* (Shmukler et al., 2015). The debate on the phenotype observed in the two different models is still open (Shmukler et al., 2016).

Patients with homozygous loss-of-function mutations in human *PIEZO1* show lymphatic dysplasia and an asymptomatic, fully compensated, very mild hemolytic state (Fotiou et al., 2015; Lukacs et al., 2015). Of note, a comprehensible hematological characterization of the anemia carried by patients with *PIEZO1* loss-of-function mutations has not yet been performed. We herein characterized the hematological phenotype of a patient with *PIEZO1* biallelic mutations and lymphatic dysplasia, identifying a new nosological erythrocyte alteration.

## CASE PRESENTATION

Patient II.1 (Figure 1A) is a 17-years-old male child affected by non-immune hydrops fetalis and congenital lymphatic dysplasia. During pregnancy, a fetal pleural effusion (32 weeks) was observed. The proband was born at 38 weeks by cesarean section. Birth parameters showed a low Apgar score (5/8) with breathing difficulties treated by continuous positive airway pressure, axial hypotonia, peripheral edema, hydrocele, hypoglycemia, and normal auxologic parameters (weight 3.650 Kg; length 53 cm; and head circumference 36 cm). The hemogram resulted normal for age, and total hyperbilirubinemia was observed (13.2 mg/dL) treated by phototherapy. During childhood, a hydrocelectomy (2-years-old) and a scrotum reduction surgery (14-years-old) were performed. At 14 years, a lower limb lymphoscintigraphy was executed, showing distinctive changes of a severe bilateral

lymphovascular disease. Particularly, the patient highlighted poor asymmetrical uptake of tracer in the groin at 45 min (almost in the right limb) with evidence of rerouting in the scrotum at 2 h. At 15 years, a thoracentesis was performed to reduce the excess of fluid because of respiratory failure due to restrictive lung disease. The cytological analyses highlighted the presence of chylous fluid. After 1 week the chylous edema was re-observed at X-ray. Due to the worsening of respiratory disease at 16 years, magnetic resonance imaging was performed. The analysis showed an impairment of the chylothoraces and reoccurrence of the hydrocele (Figure 1B). Currently, the proband presents a progressive worsening of the respiratory function.

The other family members are healthy expect for the mother of the proband (I.2) that showed an iron deficiency anemia due to imbalanced diet supplies negative for hemoglobinopathies.

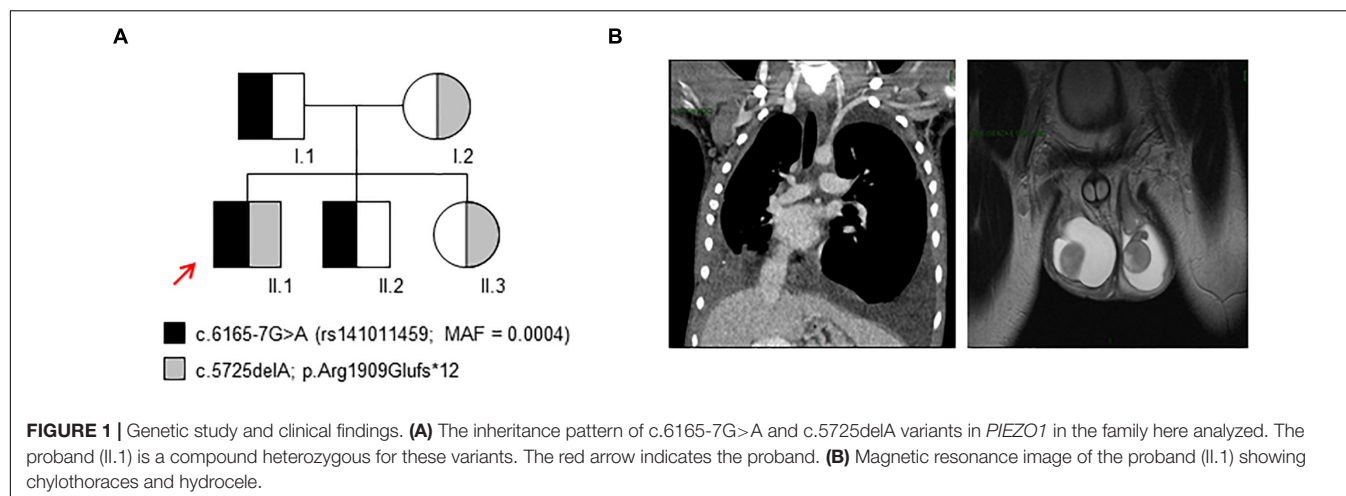
## PIEZO1 Mutational Analysis

We performed WES on the proband and the parents, highlighting the presence of two variants within *PIEZO1* gene: the nucleotide substitution c.6165-7G>A in the intron 42–43, annotated in 1000 Genomes database (rs141011459) with a minor allele frequency (MAF) = 0.0004; the novel nucleotide deletion c.5725delA that results in the frameshift variant p.Arg1909Glufs\*12 (Figure 1A). According to the recessive pattern of inheritance, the proband showed a compound heterozygous genotype. Indeed, the father, I.1, carried the variant c.6165-7G>A, while the mother, I.2, carried the variant c.5725delA. We also extended the analysis to additional unaffected subjects: the patient's brother, II.2, carried the variant c.6165-7G>A, while the sister, II.3, carried the variant c.5725delA.

To evaluate the possible effect of the frameshift variant on mRNA processing, we sequenced the *PIEZO1* cDNA of the proband. Amplification of the specific exon region, encompassing the mutation, of *PIEZO1* cDNA highlighted the selective expression of the wild-type allele, while the c.5725delA allele was not expressed, demonstrating its decay (Figure 2A). Human Splicing Finder web-tool predicted for the splicing variant c.6165-7G>A the creation of a new “branch point motif,” and two exon splicing enhancer (ESE) motifs for SRp40 protein. High sensitivity analysis of the exon regions encompassing the intronic variant (exons 42–44), using the Agilent 4200 TapeStation system (Supplementary Data Sheet S1), demonstrated that the proband and the father expressed about the 4 and 36%, respectively, of *PIEZO1* cDNA compared to the control (Figure 2B).

## Characterization of *PIEZO1* Expression

To further evaluate the role of *PIEZO1* variants, we assessed gene expression in all the family members, as well as in a subset of healthy controls (HCs). A significant decrease of *PIEZO1* expression in the proband compared to those revealed in the HCs was observed, and a minor decrease (about 50%) of mRNA levels in both parents was detected compared to HCs (Figure 2C). Nevertheless, immunoblot analysis on RBCs membranes highlighted a marked decrease of *PIEZO1* protein in the proband compared to the HCs expression with about 30% of expression (Figure 2D). The parents showed also a decrease of *PIEZO1* level with 47 and 65% of *PIEZO1* expression



for mother and father, respectively. Additionally, we evaluated the expression of other RBC membrane proteins, including Band 3 and Stomatin, altered in hereditary spherocytosis (HS) and overhydrated hereditary stomatocytosis (OHS). Proband showed a similar amount of both proteins compared to the HCs (**Figure 2E**).

### Osmotic Fragility Analysis

The ektacytometry analysis was performed for the proband and his parents. As shown in **Figure 3A**, the proband (II.1) exhibited an ektacytometry curve with right shift compared to the curve obtained from the HCs, indicating overhydration of the erythrocytes. The mother (I.2) showed a right shift of the osmolarity curve similar to those observed in the proband. Conversely, the osmolarity curve of the father I.1 was in the range of the controls with a slight right shift of the curve compared to both the proband II.1 and the subject I.2.

### Potassium Content Evaluation

We measured extracellular and intracellular potassium levels in fresh blood samples from all family members, and HCs. The proband (II.1) and his mother (I.2) showed a decrease of potassium content compared to the HC, while the father (I.1) showed intracellular [K<sup>+</sup>] comparable to HC (**Figure 3B**). The analysis of K<sup>+</sup> plasmatic levels showed increased levels in the proband and his parents compared to the HC.

### Peripheral Blood Smear Examination

The hemogram showed a slight reduction of the Hb content with normal MCV and decreased MCH and MCHC values (**Supplementary Table S1**). The RDW resulted increased while the reticulocytes count was normal (**Supplementary Table S1**). Accurate analysis of the peripheral blood (PB) smear of the proband revealed marked anisopoikilocytosis, hypochromia, several spherocytes, some stomatocytes, some mushroom-shaped RBCs, several RBCs fragmentation and debris (**Figure 3C**).

## DISCUSSION

*PIEZO1* gene encodes for the mechanoreceptor *PIEZO1*, a selective cation channel activated by mechanical force (Coste et al., 2010; Kim et al., 2012; Ge et al., 2015; Gnanasambandam et al., 2015; Andolfo et al., 2016; Dubin et al., 2017; Hyman et al., 2017; Zhao et al., 2017). In human, the first disease associated with mutations in *PIEZO1* was the DHS1 (Zarychanski et al., 2012; Andolfo et al., 2013). In erythrocytes, *PIEZO1* regulates cell volume homeostasis, and gain-of-function mutations in *DHS1* are causative of alterations of the RBC membrane permeability to monovalent cations Na<sup>+</sup> and K<sup>+</sup>, with consequent alterations of the intracellular cationic content and cell volume (Albuisson et al., 2013; Bae et al., 2013; Archer et al., 2014; Sandberg et al., 2014; Shmukler et al., 2014; Imashuku et al., 2016). Generally, *DHS1* patients show hemolytic anemia, with high reticulocyte count, the tendency to macrocytosis, and mild jaundice (Zarychanski et al., 2012; Andolfo et al., 2018b). The second condition associated with *PIEZO1* mutations is the lymphatic dysplasia. Two recent reports have described homozygous or compound heterozygous mutations in *PIEZO1* in families with LMPH3 (Fotiou et al., 2015; Lukacs et al., 2015). These cases exhibited full body edema and severe facial swelling. Most patients also presented intestinal lymphangiectasia, growth retardation, seizures, microcephaly, and intellectual disability. Loss-of-function mutations in *PIEZO1* also account for hydrops fetalis, chylothorax, and chronic pleural effusions with persistent lymphedema of legs, torso, and face. The cosegregating homozygous and compound heterozygous *PIEZO1* mutations in these families included non-sense, missense, and splice donor site mutations (Fotiou et al., 2015; Lukacs et al., 2015). Regarding the hematological framework, some of these patients were not anemic and exhibited normal hematological indices, including MCV (Lukacs et al., 2015).

The patient herein described shared some similar characteristics with the other LMPH3 patients until described such as hydrops fetalis, chylothorax, and chronic pleural effusions with persistent lymphedema. On the other hand, our patient showed peculiar characteristics: the hydrocele never

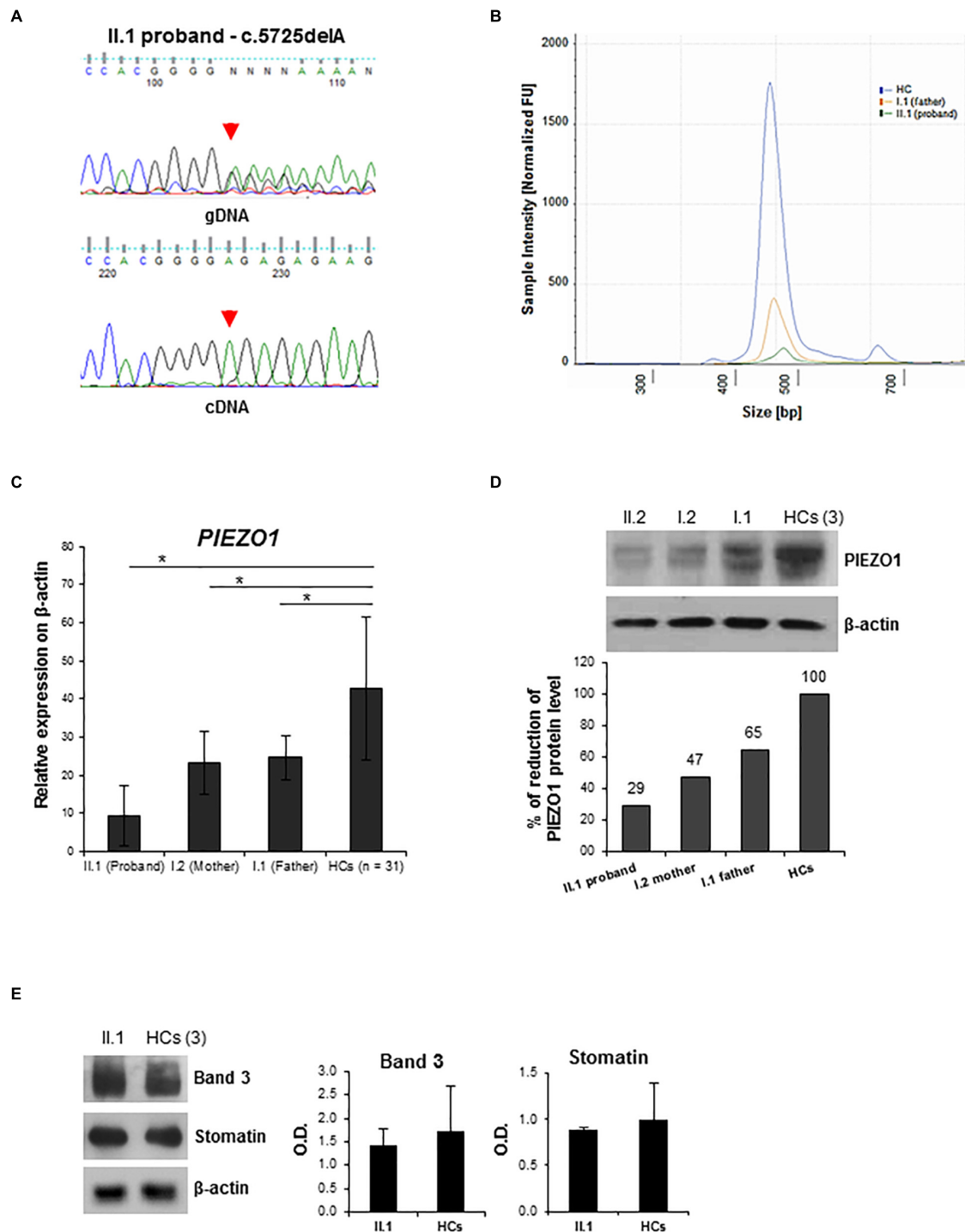
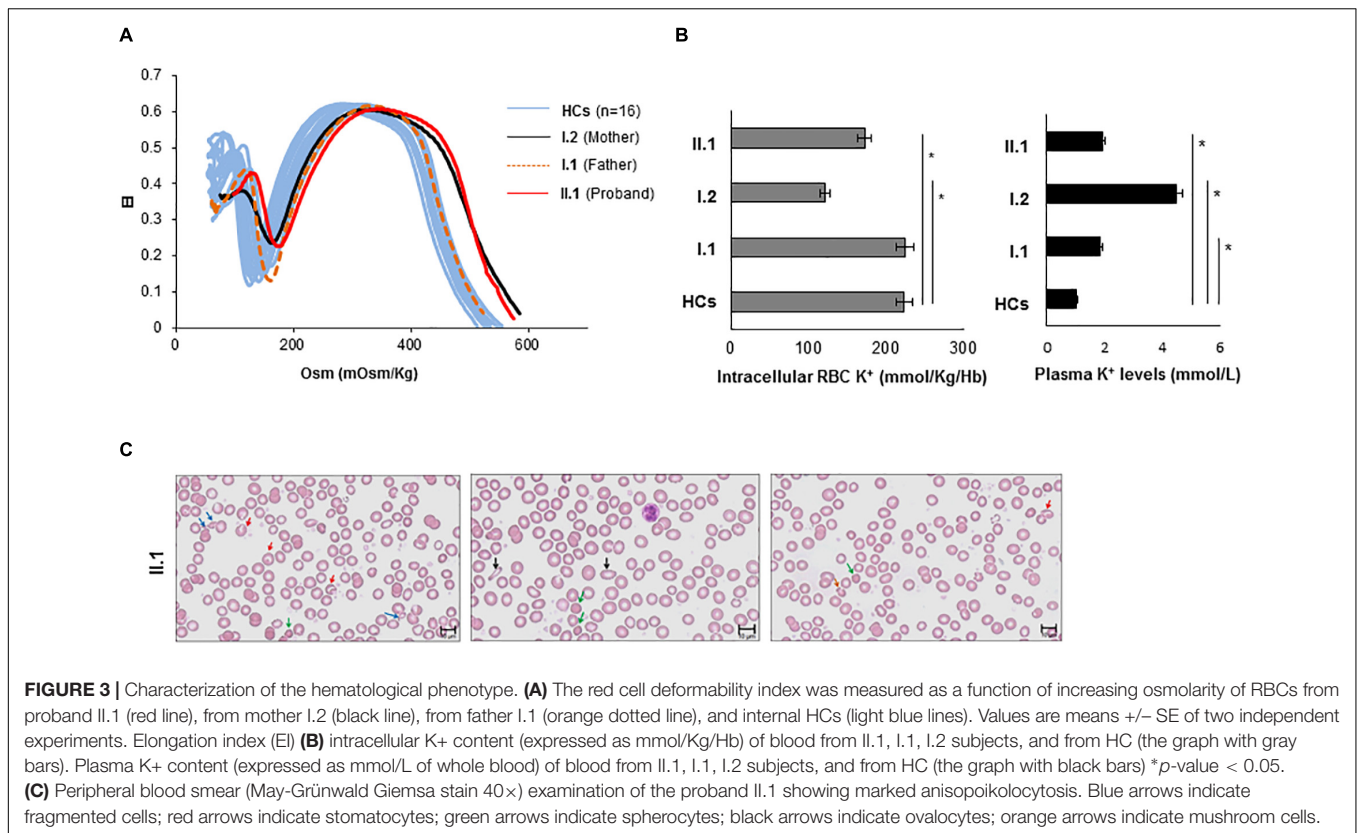


**FIGURE 2 |** Characterization of *PIEZO1* mutations: cDNA study and membrane proteins expression analysis. **(A)** Electropherograms showing sequencing analysis of the *PIEZO1* variant c.5725delA in the proband. Genomic DNA (gDNA) and cDNA sequences are shown. **(B)** DNA electrophoresis profile of the *PIEZO1* cDNA fragment encompassing exons 42–44 of the proband (green line), the father (orange line), and the control (blue line) by 4200 TapeStation system. The electropherogram shows the size distribution and the intensity of the detected bands of RT-PCR. **(C)** *PIEZO1* mRNA level normalized to *GAPDH* in the proband IL1 compared to his parents, I.1 and I.2 and the HCs ( $n = 30$ ). Data are presented as a mean  $\pm$  SD. \* $p$ -value  $< 0.05$ . **(D)** Immunoblot showing *PIEZO1* protein expression normalized to  $\beta$ -actin in the proband IL1 compared to his parents, I.1 and I.2 and the HCs (pool of  $n = 3$ ). Densitometric analysis of one representative western blotting is shown. **(E)** Immunoblot analysis of RBCs membrane proteins, Band 3 (Anion Exchanger 1) and Stomatin (Erythrocyte Membrane Protein 7.2), in the proband IL1 compared to the HCs (pool of  $n = 3$ ). Protein levels are normalized to  $\beta$ -actin. Densitometric analysis of two separate western blotting is shown. Data are presented as a mean  $\pm$  SD.



observed in the other *PIEZO1* loss-of-function patients, and the absence of facial swelling, lymphangiectasia, and intellectual disability. Of note, the proband is a compound heterozygous for a splicing variant and a coding deletion that causes a premature stop codon. We demonstrated the decay of the allele carrying the deletion variant, and the massive reduction of expression of the allele carrying the splicing variant. The combination of the two variants causes a substantial reduction of both mRNA and protein expression of *PIEZO1* in the proband.

*PIEZO1* is a highly polymorphic gene that has a very large tolerance for both missense and loss-of-function variants and has a lot of variations. The variable expressivity of both DHS1 and lymphatic dysplasia could be explained with the combination of multiple disease-causing alleles or their combination with polymorphic variants (Lupski, 2012; Lacroix et al., 2018). Indeed, we previously demonstrated that multiple modifier *PIEZO1* variants could account for highly variable clinical expressivity in DHS1, with subsequent difficulties in establishing the appropriate genotype/phenotype correlation (Andolfo et al., 2018a,b). Of note, the patient showed a peculiar phenotype characterized by peripheral edema, hydrocele, and chylothoraces. Furthermore, even if the blood count seems only slightly altered with a mild reduction of the Hb, and decreased MCH and MCHC values, the RDW resulted increased despite the reticulocytes count was normal. According to the increased RDW, the PB smear of the proband revealed anisopoikilocytosis, hypochromia, with the presence of some spherocytes, mushroom-shaped RBCs, stomatocytes, erythrocytes' fragmentation, and debris. Moreover,

the ektacytometry analysis revealed a right shift of the right arm of the osmolarity curve indicating mild overhydration of RBCs, without the decreased DIMax typical of HS. Finally, the ionic flux assay indicated increased plasma [K<sup>+</sup>] and decreased intracellular [K<sup>+</sup>] as in OHS. Thus, our patient seems to present pathological traits of the erythrocyte with some characteristics shared with hereditary spherocytosis as spherocytes at PB smear and normal MCV and several features of overhydrated hereditary stomatocytosis as stomatocytes at PB, decreased MCHC, normal DIMax, right shift of the osmolarity curve, and decreased intracellular potassium. The mother showed a similar, but less pronounced, right shift of the osmolarity curve. This finding could be caused by the iron deficiency anemia that is known to alter the deformability of RBCs (Vayá et al., 2005; Brandão et al., 2009).

Of note, Vav1-P1cKO mice with specific deletion of *Piezo1* in the hematopoietic system showed a slight increase of RDW and reduced MCHC confirming overhydration of RBCs as seen in our patient (Cahalan et al., 2015). Moreover, morpholino-knockdown of *Piezo1* in zebrafish showed the erythroid phenotype of fragile, spherocytic, dysmorphic cells also like our patient (Shmukler et al., 2015).

In conclusion, the proband presents an alteration of the structure and the ionic content of erythrocytes caused by the two hypomorphic variants in *PIEZO1*. We speculate that the substantial decreased expression of *PIEZO1* could be compensated by overactivation of other cation channels/pumps that act by compensating the hematological phenotype. Patients



affected by lymphedema caused by mutations in *PIEZO1* could benefit in future of therapy by Yoda1, a novel small synthetic molecule specific activator of *PIEZO1* (Cahalan et al., 2015; Lacroix et al., 2018), or by gene therapy by selective insertion of the gene in the lymphatic system, or by *in vivo* target gene activation via CRISPR/CAS9 mediated trans-epigenetic modulation.

## DATA AVAILABILITY

All datasets generated for this study are included in the manuscript and/or the **Supplementary Files**.

## ETHICS STATEMENT

Ethics Committee of University Federico II, number 197/18.

## AUTHOR CONTRIBUTIONS

IA, RR, and AI designed and conducted the study, and prepared the manuscript. GDR performed the western blotting analysis

and contributed to the preparation of the manuscript. EE and AV performed the preparation of the WES libraries and the NGS analysis. FM and BER performed the molecular analysis and collection of the samples. AG, VC, and GP contributed to take care of the patients. LDF performed the ionic flux data analysis. RR performed the mutational analysis. OZ designed and supervised the NGS analysis and also provided a critical evaluation of the study.

## FUNDING

This work was supported by Junior Research Grant 2018, 3978026 of European Hematology Association (EHA) to IA; from the Italian Ministry of University and Research (SIR to RR, RBSI144KXC).

## SUPPLEMENTARY MATERIAL

The Supplementary Material for this article can be found online at: <https://www.frontiersin.org/articles/10.3389/fphys.2019.00258/full#supplementary-material>

## REFERENCES

- Albuisson, J., Murthy, S. E., Bandell, M., Coste, B., Louis-Dit-Picard, H., Mathur, J., et al. (2013). Dehydrated hereditary stomatocytosis linked to gain-of-function mutations in mechanically activated piezo1 ion channels. *Nat. Commun.* 4:1884. doi: 10.1038/ncomms2899
- Andolfo, I., Alper, S. L., De Franceschi, L., Auriemma, C., Russo, R., De Falco, L., et al. (2013). Multiple clinical forms of dehydrated hereditary stomatocytosis arise from mutations in *PIEZO1*. *Blood* 121, 3925–3935. doi: 10.1182/blood-2013-02-482489
- Andolfo, I., Manna, F., De Rosa, G., Rosato, B. E., Gambale, A., Tomaiuolo, G., et al. (2018a). *PIEZO1*-R1864H rare variant accounts for a genetic phenotype-modifier role in dehydrated hereditary stomatocytosis. *Haematologica* 103, e94–e97. doi: 10.3324/haematol.2017.180687
- Andolfo, I., Russo, R., Rosato, B. E., Manna, F., Gambale, A., Brugnara, C., et al. (2018b). Genotype-phenotype correlation and risk stratification in a cohort of 123 hereditary stomatocytosis patients. *Am. J. Hematol.* 93, 1509–1517. doi: 10.1002/ajh.25276
- Andolfo, I., Russo, R., Gambale, A., and Iolascon, A. (2016). New insights on hereditary erythrocyte membrane defects. *Haematologica* 101, 1284–1294. doi: 10.3324/haematol.2016.142463
- Archer, N. M., Shmukler, B. E., Andolfo, I., Vidorpe, D. H., Gnanasambandam, R., Higgins, J. M., et al. (2014). Hereditary xerocytosis revisited. *Am. J. Hematol.* 89, 1142–1146. doi: 10.1002/ajh.23799
- Bae, C., Gnanasambandam, R., Nicolai, C., Sachs, F., and Gottlieb, P. A. (2013). Xerocytosis is caused by mutations that alter the kinetics of the mechanosensitive channel *PIEZO1*. *Proc. Natl. Acad. Sci. U.S.A.* 110, E1162–E1168. doi: 10.1073/pnas.1219777110
- Brandão, M. M., Castro Mde, L., Fontes, A., Cesar, C. L., Costa, F. F., and Saad, S. T. (2009). Impaired red cell deformability in iron deficient subjects. *Clin. Hemorheol. Microcirc.* 43, 217–221. doi: 10.3233/CH-2009-1211
- Cahalan, S. M., Lukacs, V., Ranade, S. S., Chien, S., Bandell, M., and Patapoutian, A. (2015). *Piezo1* links mechanical forces to red blood cell volume. *eLife* 22:4. doi: 10.7554/eLife.07370
- Coste, B., Mathur, J., Schmidt, M., Earley, T. J., Ranade, S., Petrus, M. J., et al. (2010). *Piezo1* and *Piezo2* are essential components of distinct mechanically activated cation channels. *Science* 330, 55–60. doi: 10.1126/science.1193270
- Dubin, A. E., Murthy, S., Lewis, A. H., Brosse, L., Cahalan, S. M., Grandl, J., et al. (2017). Endogenous *piezo1* can confound mechanically activated channel identification and characterization. *Neuron* 94, 266–270. doi: 10.1016/j.neuron.2017.03.039
- Faucherre, A., Kissa, K., Nargeot, J., Mangoni, M. E., and Jopling, C. (2014). *Piezo1* plays a role in erythrocyte volume homeostasis. *Haematologica* 99, 70–75. doi: 10.3324/haematol.2013.086090
- Fotiou, E., Martin-Almedina, S., Simpson, M. A., Lin, S., Gordon, K., Brice, G., et al. (2015). Novel mutations in *PIEZO1* cause an autosomal recessive generalized lymphatic dysplasia with non-immune hydrops fetalis. *Nat. Commun.* 6:8085. doi: 10.1038/ncomms9085
- Ge, J., Li, W., Zhao, Q., Li, N., Chen, M., Zhi, P., et al. (2015). Architecture of the mammalian mechanosensitive *Piezo1* channel. *Nature* 527, 64–69. doi: 10.1038/nature15247
- Gnanasambandam, R., Bae, C., Gottlieb, P. A., and Sachs, F. (2015). Ionic Selectivity and Permeation Properties of Human *PIEZO1* Channels. *PLoS One* 8:e0125503. doi: 10.1371/journal.pone.0125503
- Gudipaty, S. A., Lindblom, J., Loftus, P. D., Redd, M. J., Edes, K., Davey, C. F., et al. (2017). Mechanical stretch triggers rapid epithelial cell division through *Piezo1*. *Nature* 543, 118–121. doi: 10.1038/nature21407
- Hyman, A. J., Tumova, S., and Beech, D. J. (2017). *Piezo1* channels in vascular development and the sensing of shear stress. *Curr. Top. Membr.* 2017, 37–57. doi: 10.1016/bs.ctm.2016.11.001
- Imashuku, S., Muramatsu, H., Sugihara, T., Okuno, Y., Wang, X., Yoshida, K., et al. (2016). *PIEZO1* gene mutation in a Japanese family with hereditary high phosphatidylcholine hemolytic anemia and hemochromatosis-induced diabetes mellitus. *Int. J. Hematol.* 104, 125–129. doi: 10.1007/s12185-016-970-x
- Kim, S. E., Coste, B., Chadha, A., Cook, B., and Patapoutian, A. (2012). The role of *Drosophila piezo* in mechanical nociception. *Nature* 483, 209–212. doi: 10.1038/nature10801
- Lacroix, J. J., Botello-Smith, W. M., and Luo, Y. (2018). Probing the gating mechanism of the mechanosensitive channel *Piezo1* with the small molecule yoda1. *Nat. Commun.* 9:2029. doi: 10.1038/s41467-018-04405-3
- Li, J., Hou, B., Tumova, S., Muraki, K., Bruns, A., Ludlow, M. J., et al. (2014). *Piezo1* integration of vascular architecture with physiological force. *Nature* 515, 279–283. doi: 10.1038/nature13701
- Lukacs, V., Mathur, J., Mao, R., Bayrak-Toydemir, P., Procter, M., Cahalan, S. M., et al. (2015). Impaired *PIEZO1* function in patients with a novel autosomal

- recessive congenital lymphatic dysplasia. *Nat. Commun.* 6:8329. doi: 10.1038/ncomms9329
- Lupski, J. R. (2012). Digenic inheritance and mendelian disease. *Nat. Genet.* 44, 1291–1292. doi: 10.1038/ng.2479
- Martin-Almedina, S., Mansour, S., and Ostergaard, P. (2018). Human phenotypes caused by *piezo1* mutations one gene, two overlapping phenotypes? *J. Physiol.* 596, 985–992. doi: 10.1113/JP275718
- Martins, J. R., Penton, D., Peyronnet, R., Arhatte, M., Moro, C., Picard, N., et al. (2016). *Piezo1*-dependent regulation of urinary osmolarity. *Pflugers Arch.* 468, 1197–1206. doi: 10.1007/s00424-016-1811-z
- Ranade, S. S., Qiu, Z., Woo, S.-H., Hur, S. S., Murthy, S. E., Cahalan, S. M., et al. (2014). *Piezo1*, a mechanically activated ion channel, is required for vascular development in mice. *Proc. Natl. Acad. Sci. U.S.A.* 111, 10347–10352. doi: 10.1073/pnas.1409233111
- Sandberg, M. B., Nybo, M., Birgens, H., and Frederiksen, H. (2014). Hereditary xerocytosis and familial haemolysis due to mutation in the *piezo1* gene: a simple diagnostic approach. *Int. Jnl. Lab Hematol.* 36, e62–e65. doi: 10.1111/ijlh.12172
- Shmukler, B. E., Huston, N. C., Thon, J. N., Ni, C. W., Kourkoulis, G., Lawson, N. D., et al. (2015). Homozygous knockout of the *piezo1* gene in the zebrafish is not associated with anemia. *Haematologica* 100, e483–e485. doi: 10.3324/haematol.2015.132449
- Shmukler, B. E., Lawson, N. D., Paw, B. H., and Alper, S. L. (2016). Authors response to “comment on: homozygous knockout of the *piezo1* gene in the zebrafish is not associated with anemia”. *Haematologica* 101:e39. doi: 10.3324/haematol.2015.137810
- Shmukler, B. E., Vidorpe, D. H., Rivera, A., Auerbach, M., Brugnara, C., and Alper, S. L. (2014). Dehydrated stomatocytic anemia due to the heterozygous mutation R2456H in the mechanosensitive cation channel *PIEZO1*: a case report. *Blood Cells Mol. Dis.* 52, 53–54. doi: 10.1016/j.bcmd.2013.07.015
- Vayá, A., Simó, M., Santaolalla, M., Todolí, J., and Aznar, J. (2005). Red blood cell deformability in iron deficiency anaemia. *Clin. Hemorheol. Microcirc.* 33, 75–80.
- Wang, S., Chennupati, R., Kaur, H., Iring, A., Wettschureck, N., and Offermanns, S. (2016). Endothelial cation channel *PIEZO1* controls blood pressure by mediating flow-induced ATP release. *J. Clin. Invest.* 126, 4527–4536. doi: 10.1172/JCI87343
- Zarychanski, R., Schulz, V. P., Houston, B. L., Maksimova, Y., Houston, D. S., Smith, B., et al. (2012). Mutations in the mechanotransduction protein *piezo1* are associated with hereditary xerocytosis. *Blood* 120, 1908–1915. doi: 10.1182/blood-2012-04-422253
- Zhao, Q., Wu, K., Chi, S., Geng, J., and Xiao, B. (2017). Heterologous expression of the *Piezo1*-ASIC1 chimera induces mechanosensitive currents with properties distinct from *Piezo1*. *Neuron* 94, 274–277. doi: 10.1016/j.neuron.2017.03.040

**Conflict of Interest Statement:** The authors declare that the research was conducted in the absence of any commercial or financial relationships that could be construed as a potential conflict of interest.

Copyright © 2019 Andolfo, De Rosa, Errichiello, Manna, Rosato, Gambale, Vetro, Calcaterra, Pelizzo, De Franceschi, Zuffardi, Russo and Iolascon. This is an open-access article distributed under the terms of the Creative Commons Attribution License (CC BY). The use, distribution or reproduction in other forums is permitted, provided the original author(s) and the copyright owner(s) are credited and that the original publication in this journal is cited, in accordance with accepted academic practice. No use, distribution or reproduction is permitted which does not comply with these terms.



# The EPO-FGF23 Signaling Pathway in Erythroid Progenitor Cells: Opening a New Area of Research

Annelies J. van Vuren<sup>1\*</sup>, Carlo A. J. M. Gaillard<sup>2</sup>, Michele F. Eisenga<sup>3</sup>, Richard van Wijk<sup>4</sup> and Eduard J. van Beers<sup>1</sup>

<sup>1</sup> Van Creveldkliniek, Department of Internal Medicine and Dermatology, University Medical Center Utrecht, Utrecht University, Utrecht, Netherlands, <sup>2</sup> Department of Internal Medicine and Dermatology, University Medical Center Utrecht, Utrecht University, Utrecht, Netherlands, <sup>3</sup> Department of Internal Medicine, Division of Nephrology, University Medical Center Groningen, University of Groningen, Groningen, Netherlands, <sup>4</sup> Department of Clinical Chemistry and Haematology, University Medical Center Utrecht, Utrecht University, Utrecht, Netherlands

## OPEN ACCESS

### Edited by:

Lesley Jean Bruce,  
NHS Blood and Transplant,  
United Kingdom

### Reviewed by:

Anna Rita Migliaccio,  
Icahn School of Medicine at Mount  
Sinai, United States  
Angela Rizzo,  
University of Udine, Italy

### \*Correspondence:

Annelies J. van Vuren  
A.J.vanVuren@umcutrecht.nl

### Specialty section:

This article was submitted to  
Red Blood Cell Physiology,  
a section of the journal  
Frontiers in Physiology

**Received:** 10 December 2018

**Accepted:** 07 March 2019

**Published:** 26 March 2019

### Citation:

van Vuren AJ, Gaillard CAJM,  
Eisenga MF, van Wijk R and  
van Beers EJ (2019) The EPO-FGF23  
Signaling Pathway in Erythroid  
Progenitor Cells: Opening a New Area  
of Research. *Front. Physiol.* 10:304.  
doi: 10.3389/fphys.2019.00304

We provide an overview of the evidence for an erythropoietin-fibroblast growth factor 23 (FGF23) signaling pathway directly influencing erythroid cells in the bone marrow. We outline its importance for red blood cell production, which might add, among others, to the understanding of bone marrow responses to endogenous erythropoietin in rare hereditary anemias. FGF23 is a hormone that is mainly known as the core regulator of phosphate and vitamin D metabolism and it has been recognized as an important regulator of bone mineralization. Osseous tissue has been regarded as the major source of FGF23. Interestingly, erythroid progenitor cells highly express FGF23 protein and carry the FGF receptor. This implies that erythroid progenitor cells could be a prime target in FGF23 biology. FGF23 is formed as an intact, biologically active protein (iFGF23) and proteolytic cleavage results in the formation of the presumed inactive C-terminal tail of FGF23 (cFGF23). FGF23-knockout or injection of an iFGF23 blocking peptide in mice results in increased erythropoiesis, reduced erythroid cell apoptosis and elevated renal and bone marrow erythropoietin mRNA expression with increased levels of circulating erythropoietin. By competitive inhibition, a relative increase in cFGF23 compared to iFGF23 results in reduced FGF23 receptor signaling and mimics the positive effects of FGF23-knockout or iFGF23 blocking peptide. Injection of recombinant erythropoietin increases FGF23 mRNA expression in the bone marrow with a concomitant increase in circulating FGF23 protein. However, erythropoietin also augments iFGF23 cleavage, thereby decreasing the iFGF23 to cFGF23 ratio. Therefore, the net result of erythropoietin is a reduction of iFGF23 to cFGF23 ratio, which inhibits the effects of iFGF23 on erythropoiesis and erythropoietin production. Elucidation of the EPO-FGF23 signaling pathway and its downstream signaling in hereditary anemias with chronic hemolysis or ineffective erythropoiesis adds to the understanding of the pathophysiology of these diseases and its complications; in addition, it provides promising new targets for treatment downstream of erythropoietin in the signaling cascade.

**Keywords:** FGF23, erythropoietin, anemia, osteoporosis, red blood cells

## INTRODUCTION

At a concentration of 5 million red blood cells (RBC) per microliter blood, RBCs are the most abundant circulating cell type in humans (Eggold and Rankin, 2018). Normal erythropoiesis yields 200 billion RBCs every day, an equivalent of 40 mL of newly formed whole blood (Muckenthaler et al., 2017). Regulation of erythropoiesis in the bone marrow (BM) microenvironment depends on systemic and local factors controlling differentiation, proliferation and survival of the erythroid progenitor cells (EPC). Inherited RBC abnormalities might result in chronic hemolysis with an increased erythropoietic drive, or ineffective erythropoiesis, thereby challenging the erythropoietic system. Systemic erythropoietin (EPO) production plays a critical role in maintaining erythropoietic homeostasis under physiologic and pathologic conditions (Eggold and Rankin, 2018). Increasing evidence links EPO and erythropoiesis to skeletal homeostasis (Eggold and Rankin, 2018). First, there is a longstanding observation that patients with hemolysis have increased risk of skeletal pathology such as osteoporosis and osteonecrosis (Taher et al., 2010; Haidar et al., 2012; Eggold and Rankin, 2018; van Straaten et al., 2018). Second, removal of osteoblasts in mice resulted in increased loss of erythroid progenitors in the BM, followed by decreased amounts of hematopoietic stem cells with recovery after reappearance of osteoblasts, pointing to a critical role of osteoblasts in hemato- and erythropoiesis (Visnjic et al., 2004).

Erythropoietin, the core regulator of erythropoiesis, is an important regulator of fibroblast growth factor 23 (FGF23) production and cleavage (Clinkenbeard et al., 2017; Flamme et al., 2017; Daryadel et al., 2018; Hanudel et al., 2018; Rabadi et al., 2018; Toro et al., 2018). FGF23 is originally known as a bone-derived hormone and key player in phosphate and vitamin D metabolism. FGF23 seems to provide a link between bone mineralization and erythropoiesis (Clinkenbeard et al., 2017; Eggold and Rankin, 2018). FGF23 was first discovered as a regulator of phosphate metabolism, due to the association between hereditary phosphate wasting syndromes and *FGF23* mutations (ADHR Consortium, 2000). FGF23 induces phosphaturia, directly suppresses parathyroid hormone and the amount of 1,25(OH)<sub>2</sub>D<sub>3</sub> (active vitamin D) (Shimada et al., 2004; Quarles, 2012). FGF23 is secreted by osteocytes in response to vitamin D, parathyroid hormone and elevated levels of serum phosphate. Due to important alterations in phosphate balance in chronic kidney disease (CKD), most research on FGF23 up until now was focused on CKD (see section “EPO, Iron, CKD, and Inflammation Are Important Regulators of iFGF23

Cleavage”) (Kanbay et al., 2017). However, a new, important role for FGF23 seems to exist as regulator of erythropoiesis.

Here, we review the interplay of EPO and FGF23 in the erythroid cells of the BM. We discuss that the action of FGF23 not only depends on the amount of intact FGF23 available, but also on the amount of FGF23 cleavage which is an important factor determining its efficacy. Elucidation of the role of the EPO-FGF23 signaling pathway in hereditary anemia and chronic hemolytic diseases will add to the understanding of the pathophysiology of the diseases, of bone mineralization disorders complicating chronic hemolytic diseases, and might provide new targets for treatment downstream of EPO. An overview of FGF23 production, cleavage and signaling is provided in **Figure 1**.

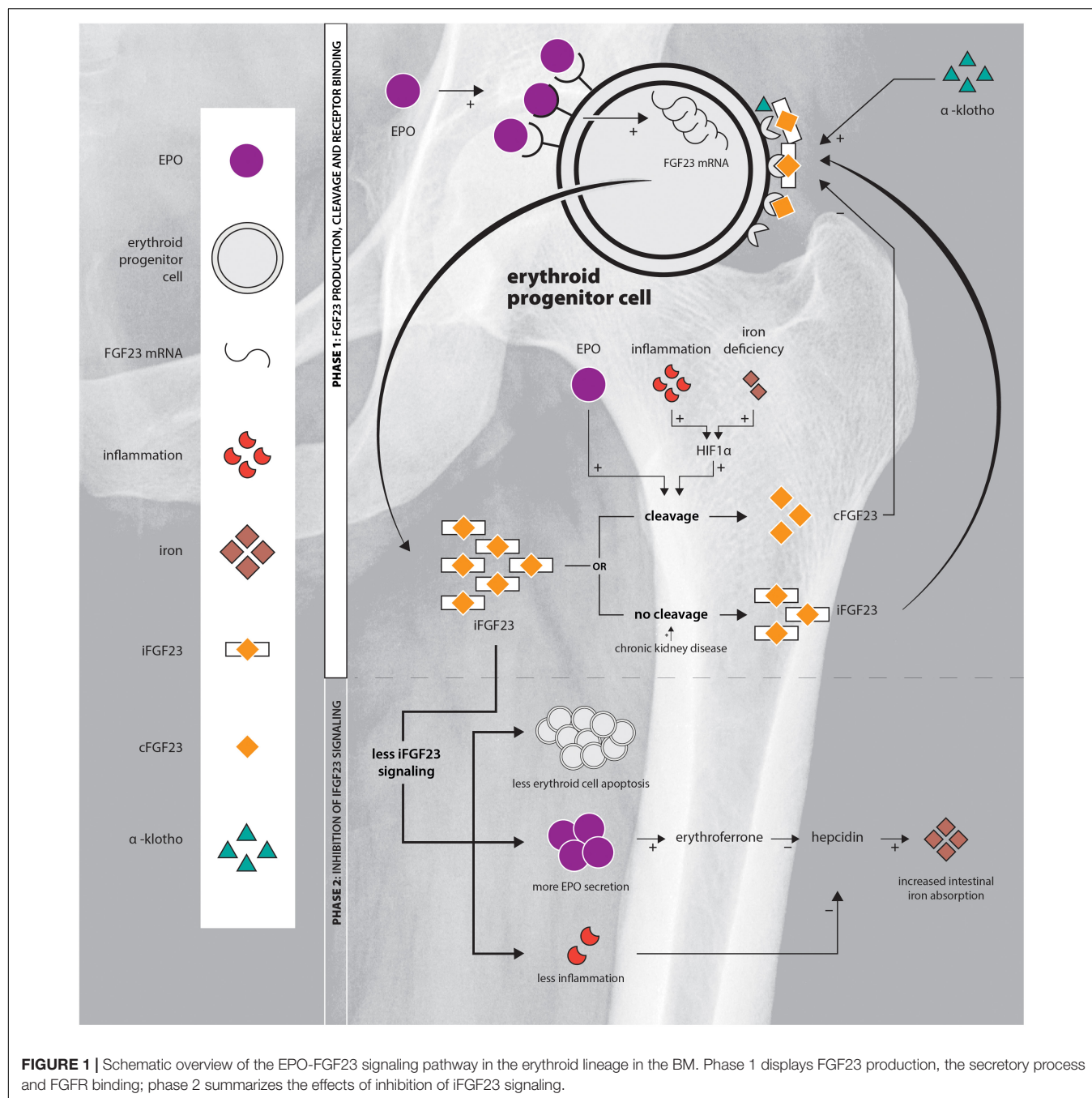
## ANEMIA AND THE EPO SIGNALING CASCADE

Erythropoietin production by renal interstitial cells, and in a smaller amount by hepatocytes, plays a critical role in maintaining erythropoietic homeostasis. The primary physiological stimulus of increased *EPO* gene transcription is tissue hypoxia, which can augment circulating EPO up to a 1000-fold in states of severe hypoxia (Jelkmann, 1992; Ebert and Bunn, 1999). Under hypoxic conditions, *EPO* transcription is augmented by binding of hypoxia inducible factor (HIF)-2 to the *EPO* gene promoter. Under normoxic conditions prolyl hydroxylases (PHD) hydroxylate HIF1 $\alpha$  and HIF2 $\alpha$ , which associate with the von Hippel-Lindau tumor suppressor protein, targeting this complex for proteasomal degradation. Low iron or oxygen conditions inhibit hydroxylation by PHD2 (Ebert and Bunn, 1999; Schofield and Ratcliffe, 2004). EPO exerts its effect on early erythroid progenitors via the EPO receptor (EPOR), with a peak receptor number at the CFU-E (Colony Forming Unit-Erythroid) stage and a decline until absence of the receptor in late basophilic erythroblasts. EPOR signaling results in survival, proliferation, and terminal differentiation (Krantz, 1991; Muckenthaler et al., 2017; Eggold and Rankin, 2018).

Besides kidney and liver, EPO expression has also been reported in brain, lung, heart, spleen, and reproductive organs. Besides kidney and liver, only EPO produced by the brain was capable to functionally regulate erythropoiesis (Weidemann et al., 2009; Haase, 2010). More recently, it was discovered that local production of EPO by osteoprogenitors and osteoblasts in the BM microenvironment, under conditions of constitutive HIF stabilization, results in selective expansion of the erythroid lineage (Rankin et al., 2012; Eggold and Rankin, 2018). The role of osteoblastic EPO in the BM microenvironment under physiologic conditions is still under investigation (Shiozawa et al., 2010). The amount of circulating EPO is normal or elevated in most forms of hereditary anemia, although the amount is often relatively low for the degree of anemia (Caro et al., 1979; Rocha et al., 2005; Zeidler and Welte, 2007). EPO levels were generally elevated in  $\beta$ -thalassemia patients with large interpatient differences partly related to age (Sukpanichnant et al., 1997; O'Donnell et al., 2007; Singer et al., 2011; Butthep et al., 2015; Schotten et al., 2017). Sickle cell disease (SCD) patients had elevated serum EPO

**Abbreviations:** ADHR, autosomal dominant hypophosphatemic rickets;  $\alpha$ -KL,  $\alpha$ -klotho; BM, bone marrow; CKD, chronic kidney disease; EPC, erythroid progenitor cell; EPO, erythropoietin; EPOR, erythropoietin receptor; FGF, fibroblast growth factor; FGFR, fibroblast growth factor receptor; GalNT3, N-acetylgalactosaminyltransferase 3; HIF, hypoxia inducible factor; HIF-PHI, hypoxia inducible factor proline hydroxylase inhibitor; PHD, prolyl hydroxylase; RBC, red blood cell; rhEPO, recombinant erythropoietin; SCD, sickle cell disease; SPC, subtilisin-like proprotein convertase; TNAP, tissue non-specific alkaline phosphatase; WT, wild-type.





concentrations ranging from the low end of expected for the degree of anemia to lower than expected (Pulte et al., 2014; Karafin et al., 2015). Off-label application of recombinant EPO (rhEPO) has been tried in selected patients to reduce transfusion requirements and improve quality of life. Responses varied and were unpredictable (Zachee et al., 1989; Singer et al., 2011; Fibach and Rachmilewitz, 2014; Han et al., 2017). Insight in components downstream of EPO in its signaling cascade might lead to insights in the EPO responsiveness in individual patients. FGF23 has shown to be one of those downstream components directly affecting erythropoiesis and providing feedback on EPO

production, as outlined in Section “Blockade of iFGF23 Signaling Results in More Erythropoiesis.”

## ERYTHROID PROGENITORS EXPRESS FGF23 IN RESPONSE TO EPO

Osseous tissue has been regarded as the major source of FGF23. Selective deletion of *FGF23* in early osteoblasts or osteocytes in a murine model demonstrated that both cell types significantly contribute to circulating FGF23. However, FGF23 was still

detectable in serum after deletion of the *FGF23* gene in both osteoblasts and osteocytes: other, non-osseous, tissues contribute to circulating FGF23 (Clinkenbeard et al., 2016). It was shown that BM, specifically the early erythroid lineage, does significantly contribute to total circulating FGF23. In wild-type (WT) mice treated with marrow ablative carboplatin followed by a 3-day course of rhEPO, serum FGF23 was 40% lower compared to controls (Clinkenbeard et al., 2017). In WT mice, baseline FGF23 mRNA in BM was comparable with osseous tissue, but the amount of FGF23 protein in BM tissue was significantly higher. Hematopoietic stem cells and EPCs, including BFU-E (Burst Forming Unit-Erythroid), CFU-E and proerythroblasts, showed more than fourfold higher amounts of FGF23 mRNA compared with whole BM including lineage specific cells. FGF23 mRNA was shown to be transiently expressed during early erythropoiesis (Toro et al., 2018). EPCs do express FGF23 mRNA under physiologic conditions, however significant increases are observed in response to EPO (Clinkenbeard et al., 2017; Daryadel et al., 2018; Toro et al., 2018). RhEPO induced FGF23 mRNA expression in BM cells 24 h after injection (Daryadel et al., 2018). Indirect immunofluorescence staining with anti-mouse FGF23 antibodies and lineage specific markers showed intense staining of erythroid progenitors and mature erythroblasts (CD71<sup>+</sup> cells) of EPO-treated mice compared to controls (Daryadel et al., 2018).

Thus, erythroid cells of the BM significantly contribute to FGF23 production and FGF23 production is increased in response to EPO. As will be discussed in Sections “FGF23 Signaling Is Regulated by Cleavage of Intact FGF23” and “EPO, Iron, CKD, and Inflammation Are Important Regulators of iFGF23 Cleavage,” the amount of cleavage of FGF23 is equally important and EPO has a strong effect on this as well.

## FGF23 SIGNALING IS REGULATED BY CLEAVAGE OF INTACT FGF23

FGF23 is formed as a full-length, biologically active protein (iFGF23). Intact FGF23 is cleaved into two fragments: the inactive N-terminal fragment of FGF23 fails to co-immunoprecipitate with FGFR (FGF receptor) complexes, which suggests that the C-terminal fragment (cFGF23) mediates binding to the FGFR (Goetz et al., 2007, 2010; Courbebaisse et al., 2017). Only intact FGF23 (iFGF23) suppresses phosphate levels in mice through the FGF receptor 1 (FGFR1) (Shimada et al., 2002; Wolf and White, 2014). cFGF23 competes with iFGF23 for binding to the FGFR, and thereby antagonizes iFGF23 signaling in mice and rats (Goetz et al., 2010; Agoro et al., 2018). Treatment with cFGF23 increased the number of early and terminally differentiated BM erythroid cells and the colony forming capacity of early progenitors to the same amount as rhEPO. These data suggest that the outcome of rhEPO treatment resembles the effects of more cFGF23. Recently, it was shown that the cFGF23 fragment itself was able to induce heart hypertrophy in SCD patients (Courbebaisse et al., 2017), probably via FGFR4 and independent from a costimulatory signal (see section “Presence of  $\alpha$ -Klotho Is Essential for Normal Erythropoiesis”) (Faul et al., 2011).

Currently, two assays are available to measure iFGF23 and cFGF23: one assay that detects the C-terminal of FGF23 which measures both cFGF23 and (full-length) iFGF23 (Immunotopics/Quidel) and one assay that only detects iFGF23 (Kainos Laboratories) (Hanudel et al., 2018). Serum half-life time is approximately identical for both iFGF23 and cFGF23 ranging from 45 to 60 min (Khosravi et al., 2007).

So, although still subject of debate, proteolytic cleavage of iFGF23 seems to abrogate its activity by two mechanisms: reduction of the amount of iFGF23 and generation of an endogenous inhibitor, cFGF23 (Goetz et al., 2010). Therefore, measurement of both iFGF23 and cFGF23 is important: alterations in the iFGF23 to cFGF23 ratio lead to alterations of iFGF23 signaling efficacy.

Regulation of FGF23 secretion includes intracellular processing in the Golgi apparatus in which iFGF23 is partially cleaved within a highly conserved subtilisin-like proprotein convertase (SPC)-site by furin or prohormone convertase 1/3, 2, and 5/6 (Figure 2). Cleavage of iFGF23 generates two fragments: the C- and N-terminal peptide fragments (20 and 12 kDa) (Benet-Pages et al., 2004; Tagliabracci et al., 2014; Yamamoto et al., 2016). Competition between phosphorylation and O-glycosylation of the SPC-site in the secretory pathway of FGF23 is an important regulatory mechanism of cleavage (Tagliabracci et al., 2014). Secretion of iFGF23 requires O-glycosylation: the glycosyltransferase N-acetylgalactosaminyltransferase 3 (GalNT3) selectively exerts O-glycosylation of amino acid residues within or in the proximity of the SPC-site and blocks cleavage of iFGF23 (Kato et al., 2006). In contrast, phosphorylation of the SPC-site promotes FGF23 proteolysis indirectly by blocking O-glycosylation. The kinase Fam20C phosphorylates iFGF23 within the SPC-site, consequently reduces glycosylation and subsequently facilitates iFGF23 cleavage (Yamamoto et al., 2016).

Summarizing, a proportion of synthesized iFGF23 will be cleaved intracellularly before secretion, the amount of intracellular cleavage is determined by competition between glycosylation (GalNT3) and phosphorylation (Fam20C) (Martin et al., 2012; Tagliabracci et al., 2014; Yamamoto et al., 2016). Various factors regulate post-translational modification, these are described in Section “EPO, Iron, CKD, and Inflammation Are Important Regulators of iFGF23 Cleavage.”

## EPO, IRON, CKD, AND INFLAMMATION ARE IMPORTANT REGULATORS OF iFGF23 CLEAVAGE

Erythropoietin, iron, inflammation, and CKD have been identified as modifiers of iFGF23 cleavage. Notably, all these factors might co-exist in patients with hereditary anemia. The amount of cleavage is determined by alterations in GalNT3 and furin. Furin plays an important role in regulation of FGF23 cleavage in iron deficiency and inflammation (Silvestri et al., 2008; David et al., 2016), whereas under conditions of high EPO GalNT3 inhibition might augment cleavage (Hanudel et al., 2018).

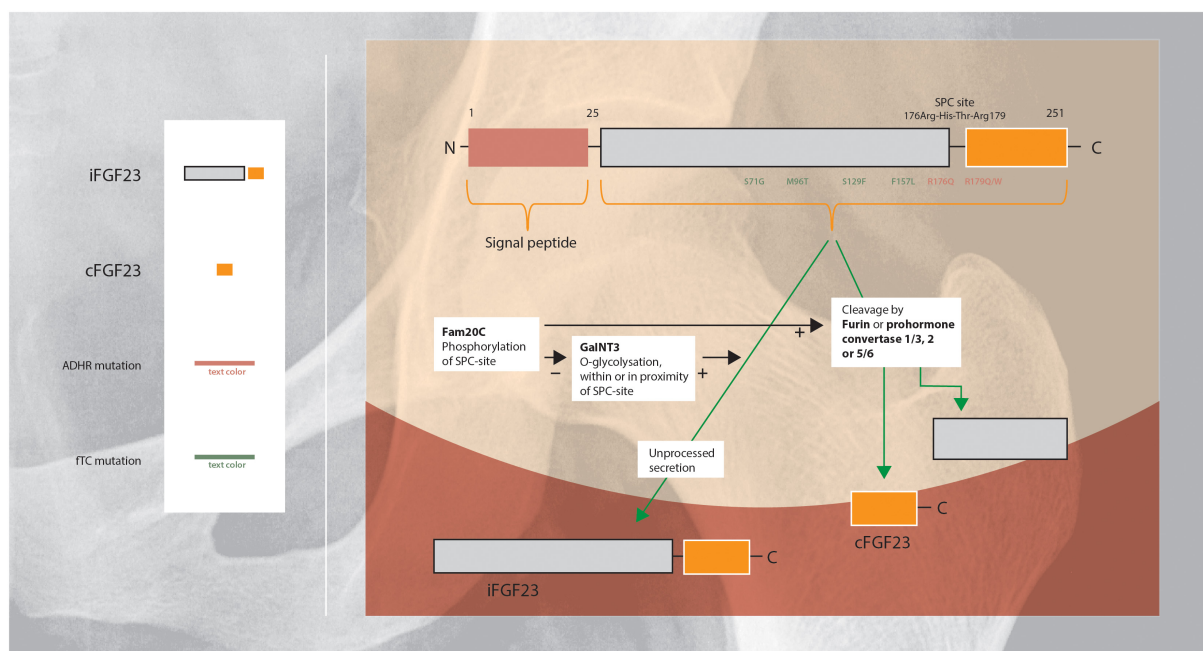


**FIGURE 2 |** Schematic overview of the regulation of FGF23 protein cleavage and secretion (Shimada et al., 2001; Saito and Fukumoto, 2009; Huang et al., 2013; Luo et al., 2019). FGF23 harbors a naturally-occurring proteolytic site at Arg176-XX-Arg179. O-Glycosylation within or in the proximity of this SPC-site of FGF23 by GalNT3 results in increased secretion of intact FGF23. Phosphorylation of the SPC-site by Fam20C indirectly promotes FGF23 cleavage by blocking O-glycosylation. ADHR is caused by mutations near the proteolytic site, that impairs proteolytic inactivation of FGF23 resulting in high levels of iFGF23 (Arg176Gln or Arg179Gln/Trp). FTC is an autosomal recessive disorder, resulting from mutations in the FGF23 gene which lead to destabilization of the tertiary structure of FGF23 and rendering it susceptible to degradation (Ser71Gly, Met96Thr, Ser129Phe, and Phe157Leu). FTC, familial tumoral calcinosis; ADHR, autosomal dominant hypophosphatemic rickets.

## Erythropoietin

Several studies report alterations of iFGF23 and cFGF23 after administration of rhEPO or under high endogenous EPO conditions, a summary is provided in the **Table 1** (Clinkenbeard et al., 2017; Flamme et al., 2017; Daryadel et al., 2018; Hanudel et al., 2018; Rabadi et al., 2018; Toro et al., 2018). Most experiments were carried out in animal models (rats and mice). Less information is available about the influence of EPO on the iFGF23/cFGF23 ratio in man.

In all animal studies one single injection or multiple-day regimen of rhEPO resulted in a significant increase in circulating cFGF23 (Clinkenbeard et al., 2017; Flamme et al., 2017; Daryadel et al., 2018; Hanudel et al., 2018; Toro et al., 2018). Increases in iFGF23 were less pronounced (Flamme et al., 2017; Hanudel et al., 2018; Toro et al., 2018), or absent (Daryadel et al., 2018), after a single injection of rhEPO. Multiple-day regimens resulted in small rises in iFGF23, less pronounced than the increase in cFGF23 (Clinkenbeard et al., 2017; Daryadel et al., 2018). EPO directly increased *FGF23* gene expression in murine hematopoietic cells (Flamme et al., 2017). Treatment of mice with an hematopoietic equipotent dose of a HIF-proline hydroxylase inhibitor (HIF-PH inhibitor) also led to a significant rise in plasma cFGF23, without an increase in circulating iFGF23. Increases in FGF23 expression after HIF-PH inhibitor treatment were mediated indirectly via EPO, as pre-administration of anti-EPO antibodies

opposed upregulation of circulating FGF23 (David et al., 2016; Flamme et al., 2017).

Effects of overexpression of endogenous EPO were investigated in a transgenic human EPO-overexpressing murine model. Results were in line with responses on rhEPO in mice: circulating cFGF23 and iFGF23 were significantly higher in EPO-overexpressing mice than in WT mice (Hanudel et al., 2018). Acute blood loss in mice, as a surrogate model for high endogenous EPO, also significantly increased circulating cFGF23, but not iFGF23 (Rabadi et al., 2018).

Only four studies (Clinkenbeard et al., 2017; Daryadel et al., 2018; Hanudel et al., 2018; Rabadi et al., 2018) explored effects of EPO on FGF23 in man. In all studies, rhEPO or a condition resulting in high endogenous EPO, increased circulating cFGF23, without (Daryadel et al., 2018; Hanudel et al., 2018) or with only minimal (Clinkenbeard et al., 2017) rise in circulating iFGF23. In a large cohort of 680 kidney transplant recipients higher EPO values were associated with increased cFGF23 values and not with iFGF23 values, independent of renal function (Hanudel et al., 2018).

Together, these data show that EPO (endogenous or exogenous) increases the total amount of circulating FGF23 (iFGF23 and cFGF23) and alters the iFGF23/cFGF23 ratio in favor of cFGF23.

It is uncertain which proteins mediate increased intracellular cleavage in the secretion pathway of iFGF23 in response to EPO.



**TABLE 1 |** Overview studies on the effects of erythropoietin (EPO) on FGF23.

| Study                                   | Model  | rhEPO   | iFGF23/cFGF23   |
|---|--|---|---|
| <b>Studies in animals</b>               |  |   |   |
| Clinkenbeard et al., 2017, pp e427–e430 | WT C57BL/6 mice  | Three-day regimen with increasing doses rhEPO                         | Max. $\pm 40\times$ increase in serum cFGF23; $\pm 2\times$ increase in serum iFGF23. Increases in cFGF23 in dose-dependent way.  |
| Rabadi et al., 2018, pp F132–F139       | C57BL/6 mice with and without 10% loss of total blood volume   | None  | 6 h: $\pm 4\times$ increase in plasma cFGF23; no increase in iFGF23.<br>cFGF23 values remained increased 48 h after blood loss.   |
| Flamme et al., 2017, p. e0186979        | Male Wistar rats   | Single injection rhEPO  | 4–6 h: $> 10\times$ increase in plasma cFGF23 (extrapolated); $\pm 2\times$ increase in plasma iFGF23 (extrapolated).   |
| Toro et al., 2018                       | WT C57BL/6 mice  | Single injection high dose HIF-PH inhibitor<br>Single injection rhEPO | 4–6 h: comparable with rhEPO. Pretreatment anti-EPO: cFGF23 response almost absent.<br>4 h: $\pm 4\times$ increase in plasma cFGF23; $\pm 2.5\times$ increase in plasma iFGF23.                           |
|   | Sprague-Dawley rats, hemorrhagic shock with 50–55% loss of total blood volume                          | None  | 24 h: $\pm 5\times$ increase in plasma cFGF23; $\pm 3.5\times$ increase in plasma iFGF23.   |
| Daryadel et al., 2018                   | WT C57BL/6 mice  | Single injection rhEPO  | 24 h: $\pm 2\times$ increase in plasma cFGF23; no increase in plasma iFGF23.  |
|   |  | 4-day regimen rhEPO   | 4 days: increase in cFGF23 and iFGF23.  |
| Hanudel et al., 2018                    | WT C57BL/6 mice with and without 0.2% adenine diet-induced CKD   | Single injection rhEPO  | 6 h: <i>non-CKD</i> cFGF23 207 $\rightarrow$ 3289 pg/mL; <i>CKD</i> cFGF23 2056 $\rightarrow$ 9376 pg/mL.<br><i>Non-CKD</i> iFGF23 187 $\rightarrow$ 385 pg/mL; <i>CKD</i> no significant rise in iFGF23. |
|   | Transgenic Tg6 mice overexpressing human EPO   | Transgenic EPO overexpression   | cFGF23 <i>WT</i> 340 pg/mL; <i>Tg6</i> 3175 pg/mL.<br>iFGF23 <i>WT</i> 317 pg/mL, <i>Tg6</i> 589 pg/mL.   |
| <b>Studies in man</b>                   |  |   |   |
| Clinkenbeard et al., 2017, pp e427–e430 | 4 patients with unexplained anemia   | Single injection rhEPO  | 6–18 h: $\pm 2\times$ increase in serum cFGF23; $\pm 1.5\times$ increase in serum cFGF23.   |
| Rabadi et al., 2018, pp F132–F139       | 131 patients admitted to ICU, categorized based on number of RBC transfusions in 48 h before admission | None  | Number of blood transfusions was associated with plasma cFGF23.   |
| Daryadel et al., 2018                   | 28 healthy volunteers  | Single injection rhEPO  | 24 h: significant increase in plasma cFGF23; plasma iFGF23 unchanged.   |
| Hanudel et al., 2018                    | 680 adult kidney transplant patients   | None  | Higher EPO values were significantly associated with increased cFGF23 and not with iFGF23; independent of renal function.   |

In mice, experiments investigating alterations in BM mRNA expression of GalNT3 after rhEPO injection were inconclusive (Daryadel et al., 2018). Meanwhile, in EPO-overexpressing mice, compared to WT mice, GalNT3 and prohormone convertase 5/6 mRNA expression were significantly decreased in bone and BM, no differences were observed in Fam20c and furin mRNA expression (Hanudel et al., 2018). Decreases in GalNT3 mRNA and absence of changes in furin and Fam20c mRNA expression were also observed in whole BM of mice after acute blood loss. However, the amount of GalNT3 mRNA expression in isolated erythroid precursors and mature erythroblasts (Ter119<sup>+</sup> cells) of these mice was unchanged (Rabadi et al., 2018). So, decreased GalNT3 expression might increase cleavage in response to high EPO, although further study is needed to elucidate the

contributory of GalNT3 and other, yet unknown, mechanisms in response to EPO.

## Iron Deficiency

Iron deficiency in WT mice resulted in a significant increase of cFGF23, with a less pronounced or even absent increase in iFGF23 (Farrow et al., 2011b; Clinkenbeard et al., 2014; David et al., 2016; Hanudel et al., 2016). Treatment of iron deficiency in CKD mice resulted in a significant decrease in whole bone FGF23 (Clinkenbeard et al., 2017). Iron deficiency induced by iron chelation stabilized pre-existing HIF1 $\alpha$  and increased FGF23 transcription (Farrow et al., 2011b; David et al., 2016). HIF1 $\alpha$  inhibition partially blocked elevations in total FGF23, and inhibited cleavage of iFGF23 (David et al.,

2016). HIF1 $\alpha$  stabilization under conditions of iron deficiency has been associated with upregulation of furin in liver cells (Silvestri et al., 2008).

Two large cohort studies support the relevance of the observations in mice in men. In a cohort of 2,000 pre-menopausal women serum iron was inversely correlated with cFGF23, but not with iFGF23 (Imel et al., 2016). And, associations between low iron parameters and high cFGF23 and iFGF23 values were found in a cohort of 3,780 elderly, with a more pronounced increase in cFGF23 (Bozentowicz-Wikarek et al., 2015).

Multiple studies examined the effects of distinct formulations of iron, oral and intravenous, in CKD patients on circulating cFGF23 and/or iFGF23 (Okada et al., 1983; Konjiki et al., 1994; Schouten et al., 2009a,b; Hryszko et al., 2012; Prats et al., 2013; Wolf et al., 2013; Block et al., 2015; Iguchi et al., 2015; Yamashita et al., 2017; Maruyama et al., 2018). Results have been inconclusive: interacting effects of rhEPO or endogenous high EPO might have influenced results. Moreover, the carbohydrate moieties of parenteral iron formulations themselves might lead to increased amounts of iFGF23 (Blazevic et al., 2014; Zoller et al., 2017).

In summary, iron deficiency leads to increased amounts of cFGF23 fragments. HIF1 $\alpha$  stabilization plays an important role in upregulation of intracellular iFGF23 cleavage. Due to co-existence of anemia, erythropoiesis-related factors might influence the iron deficiency-FGF23 pathway. Observed differences in expression of proteins directly involved in the secretory process of FGF23, furin and GalNT3, suggest that EPO is not simply an intermediary between iron deficiency and FGF23: furin plays an important role in the upregulation of iFGF23 cleavage in iron deficiency, whereas EPO might act via GalNT3 inhibition as discussed in Section “Erythropoietin” (Hanudel et al., 2018).

## Chronic Kidney Disease

Circulating total FGF23 rises progressively during early and intermediate stages of CKD and reaches levels of more than 1,000-times normal in advanced CKD. Elevated iFGF23 levels are considered as a compensatory mechanism for hyperphosphatemia, however regulation of FGF23 in CKD remains incompletely understood (Fliser et al., 2007; Gutierrez et al., 2009; Hanudel et al., 2018). Elevated total FGF23 is associated with progression of CKD (Fliser et al., 2007; Isakova et al., 2011; Portale et al., 2016), left ventricular hypertrophy (Faul et al., 2011), expression of IL-6 (Singh et al., 2016), impaired neutrophil recruitment (Rossaint et al., 2016), cardiovascular morbidity (Gutierrez et al., 2009; Faul et al., 2011; Mehta et al., 2016), and overall mortality (Isakova et al., 2011; Baia et al., 2013; Eisenga et al., 2017).

Besides the role of the kidney in clearance of iFGF23, CKD has also been identified as regulator of iFGF23 cleavage. Acute bilateral nephrectomy resulted in an immediate two- until threefold increase in iFGF23 levels with concomitant increase in iFGF23/cFGF23 ratio (Mace et al., 2015). In a murine CKD model, CKD was associated with less proteolytic cleavage of iFGF23 independent of iron status (Hanudel et al., 2016). Notably, iron deficiency, high endogenous

EPO, or administration of rhEPO still resulted in increased total FGF23 production and cleavage in CKD (Hanudel et al., 2018).

So, CKD is associated with increased total FGF23 and alteration of the iFGF23/cFGF23 ratio in favor of iFGF23. As CKD progresses toward end-stage renal disease, the iFGF23/cFGF23 ratio will approximate 1:1 (Smith et al., 2012). Co-existence of iron deficiency or rhEPO administration still influence FGF23 secretion in CKD.

## Inflammation

The association between FGF23 and inflammation has been reported in many diseases (Munoz Mendoza et al., 2012; Hanks et al., 2015; Holecki et al., 2015; Dounousi et al., 2016; Francis and David, 2016; Okan et al., 2016; Sato et al., 2016; Resende et al., 2017; Krick et al., 2018). Multiple inflammatory signaling pathways seem to interact closely to regulate FGF23 production and cleavage during acute or chronic inflammation. Additionally, other regulators of FGF23 expression and cleavage might develop under inflammatory conditions as inflammation-induced functional iron deficiency.

Regulation of FGF23 depends on chronicity of inflammation (David et al., 2016; Francis and David, 2016). In two murine models of acute inflammation, bone FGF23 mRNA expression and serum cFGF23 concentrations increased tenfold, without changes in iFGF23 (David et al., 2016). Increases in FGF23 mRNA were absent in the presence of NF $\kappa$ B (nuclear factor kappa-light-chain-enhancer of activated B cells, a canonical protein complex regulating many proinflammatory genes) inhibitor, which underlines the importance of the NF $\kappa$ B signaling pathway in regulation of FGF23 mRNA by pro-inflammatory stimuli (Ito et al., 2015). Co-treatment of bone cells with TNF or IL-1 $\beta$  and furin inhibitors resulted in increased levels of iFGF23, which suggests that increased cleavage of iFGF23 during acute inflammation is mediated by furin (McMahon et al., 2005; Ito et al., 2015; David et al., 2016). HIF1 $\alpha$  was identified as an intermediate in FGF23 mRNA upregulation: iron deficiency and hypoxia only stabilized pre-existing HIF1 $\alpha$ , where inflammation also led to increased cellular expression of HIF1 $\alpha$  in bone cell lines (David et al., 2016).

Chronic inflammation resulted in increased amounts of total FGF23 with increased amounts of iFGF23. Chronic inflammation seems to exhaust or downregulate the FGF23 cleavage system (Francis and David, 2016).

In the presence of inflammation, development of functional iron deficiency (Stefanova et al., 2017), discussed in Section “Iron Deficiency,” might contribute to increased cleavage of iFGF23 (David et al., 2016). The inflammatory cytokine IL-6 promotes hepcidin transcription in hepatocytes via the IL-6 receptor and subsequent activation of JAK tyrosine kinases and signal transducer and transcription activator 3 complexes that bind to the hepcidin promotor. Additionally, activin B stimulates formation of hepcidin transcriptional complexes via the BMP (bone morphogenetic protein)/SMAD signaling pathway (Verga Falzacappa et al., 2007; Besson-Fournier et al., 2012; Canali et al., 2016; Muckenthaler et al., 2017). Hepcidin controls the inflow of iron from enterocytes, the reticuloendothelial system and hepatocytes into the circulation via regulation of the expression



of iron exporter ferroportin (Ganz, 2011). Upregulation of hepcidin redistributes iron to the reticuloendothelial system at the expense of FGF23 producing cells including RBC precursor cells, osteocytes, and osteoblasts. Moreover, inflammation induces proteins that scavenge and relocate iron, including lactoferrin, lipocalin 2, haptoglobin, and hemopexin. These proteins contribute to inflammation-induced functional iron deficiency (Soares and Weiss, 2015).

Summarizing, inflammation does augment both FGF23 expression and its cleavage, by increased HIF1 $\alpha$  expression and stabilization and increased furin activity, but also via hepcidin-induced functional iron deficiency and subsequent non-hypoxic HIF1 $\alpha$  stabilization.

## BLOCKADE OF iFGF23 SIGNALING RESULTS IN MORE ERYTHROPOIESIS

The effects of iFGF23 signaling have been studied by direct infusion of rh-iFGF23 (Daryadel et al., 2018), and by blockage of iFGF23 signaling by knockout (Coe et al., 2014), or rh-cFGF23 injection (Agoro et al., 2018). FGF23-knockout mice displayed severe bone abnormalities, reduced lymphatic organ size, including spleen and thymus and elevated erythrocyte counts with increased RBC distribution width and reduced mean cell volume, and mean corpuscular hemoglobin (Coe et al., 2014). Knockout of the *FGF23* gene in mice resulted in a relative increase in hematopoietic stem cells, with decreased apoptosis, increased proliferative capacity of hematopoietic stem cells *in vitro* to form erythroid colonies, and an increased number of immature (pro-E, Ter119<sup>med</sup>, CD71<sup>hi</sup>) and mature erythroid cells (Ter119<sup>hi</sup>) in BM and peripheral blood. Hematopoietic changes were also observed in fetal livers, underlining the importance of FGF23 in hematopoietic stem cell generation and differentiation during embryonic development independent of the BM microenvironment. EPO, HIF1 $\alpha$ , and HIF2 $\alpha$  mRNA expression were significantly increased in BM, liver and kidney of FGF23-knockout mice, and the EPO receptor was upregulated on isolated BM mature erythroid cells. On the other hand, EPO, HIF1 $\alpha$ , and HIF2 $\alpha$  mRNA expression in osseous tissue was decreased; which might be explained by the remarkably lower osteoblast numbers in FGF23-knockout mice. Administration of rh-iFGF23 in WT mice resulted in a rapid decrease in erythropoiesis and a significant decrease in circulating EPO. *In vitro* administration of iFGF23 to FGF23-knockout BM-derived erythropoietic cells normalized erythropoiesis, normalized HIF, and EPO mRNA abundance and normalized EPOR expression (Coe et al., 2014). Alterations of EPO expression in response to iFGF23 were also observed by others: injection of rh-iFGF23 in mice reduced kidney EPO mRNA levels with 50% within 30 min, persisting over 24 h (Daryadel et al., 2018).

Inhibition of iFGF23 signaling with rh-cFGF23 in CKD mice resulted in decreased erythroid cell apoptosis, upregulation of renal and BM HIF1 $\alpha$  and subsequent EPO mRNA expression, elevated serum EPO levels and amelioration of iron deficiency. Inflammatory markers and liver hepcidin mRNA expression

declined after iFGF23 blockage (Agoro et al., 2018). Lower hepcidin expression might have followed directly from decreases in inflammation, however, might also have resulted from increased EPO expression (Wang et al., 2017).

Interestingly, the increase in erythropoiesis after iFGF23 inhibition resembles the effects of  $\alpha$ -klotho inhibition as outlined in Section “Presence of  $\alpha$ -Klotho Is Essential for Normal Erythropoiesis” (Xu et al., 2017). In summary, current studies underline the importance of FGFR signaling by FGF23 for early erythropoiesis.

## PRESENCE OF $\alpha$ -KLOTHO IS ESSENTIAL FOR NORMAL ERYTHROPOIESIS

Murine BM erythroid cells (Ter119<sup>+</sup>) express the FGF23 receptors FGFR1, 2, and 4, and a small amount of FGFR3 (Coe et al., 2014). The FGFR1, that among others regulates phosphaturia, needs three components to be activated: the FGFR itself, iFGF23, and  $\alpha$ -klotho ( $\alpha$ -KL).  $\alpha$ -KL, first described as an aging suppressor (Kuro-o et al., 1997), forms a complex with FGFR1 subgroup c, FGFR3 subgroup c or FGFR4 thereby selectively increasing the affinity of these FGFRs to FGF23 (Kurosu et al., 2006; Urakawa et al., 2006).  $\alpha$ -KL simultaneously tethers FGFR and FGF23 to create proximity and stability (Chen et al., 2018). Membrane-bound  $\alpha$ -KL is predominantly expressed in kidney, parathyroid gland and brain choroid plexus, however, shed  $\alpha$ -KL ectodomain seems to function as an on-demand cofactor (Chen et al., 2018). There is expression of  $\alpha$ -KL mRNA in BM, including BM erythroid cells (Ter119<sup>+</sup>), spleen and fetal liver cells (Coe et al., 2014; Vadakke Madathil et al., 2014). The importance of  $\alpha$ -KL for hematopoietic stem cell development and erythropoiesis was demonstrated in  $\alpha$ -KL-knockout mice. Knockout of the  $\alpha$ -KL gene resulted in a significant increase in erythropoiesis with significant increases in immature pro-erythroblasts and a relatively mature fraction of erythroblasts. *In vitro*  $\alpha$ -KL-knockout BM cells generated more erythroid colonies than BM cells of WT mice. EPO mRNA expression was significantly upregulated in  $\alpha$ -KL-knockout mice kidney, BM and liver cells, along with upregulation of HIF1 $\alpha$  and HIF2 $\alpha$  (Vadakke Madathil et al., 2014). Effects of  $\alpha$ -KL-knockout are remarkably similar to effects of iFGF23 blockade or knockout. This suggests that  $\alpha$ -KL is indeed an essential cofactor for FGF23 signaling in the regulation of erythropoiesis. However, if the link between less  $\alpha$ -KL and more EPO involves less iFGF23 signaling remains to be proven. Besides EPO, iron load seems to influence  $\alpha$ -KL. Iron overload decreased renal expression of  $\alpha$ -KL at mRNA and protein level; iron chelation suppressed the downregulation of  $\alpha$ -KL via angiotensin II (Saito et al., 2003).

Recent studies showed that FGF23 has various effects on many tissues in an  $\alpha$ -KL-dependent way, but might also act in an  $\alpha$ -KL-independent way especially under pathological conditions. The mechanism by which FGF23 activates the FGFR2 independent of  $\alpha$ -KL on leukocytes and the FGFR4 independent of  $\alpha$ -KL on cardiomyocytes is still unclear (Grabner et al., 2015; Grabner and Faul, 2016; Rossaint et al., 2016).

In conclusion,  $\alpha$ -KL seems to be essential for FGF23 signaling in erythropoiesis, as  $\alpha$ -KL-knockout resembles the effects of iFGF23 blockade or knockout on erythroid cell development.

## FGF23 EXPRESSION IN HEREDITARY ANEMIA

Currently, information about the abundance of the EPO-FGF23 pathway in hereditary anemia is limited to two studies: one study in  $\beta$ -thalassemia mice and one study in SCD patients.  $\beta$ -thalassemia intermedia mice are characterized by anemia, iron overload and high endogenous EPO. FGF23 mRNA expression in bone and BM of thalassemia intermedia mice were elevated, reaching expression levels of endogenous EPO-overexpressing, polycythemic mice. The amount of circulating iFGF23 was significantly elevated compared to WT mice (436 versus 317 pg/mL), although the increase in iFGF23 was small compared to the increase in total circulating FGF23 (3129 versus 340 pg/mL in WT mice) (Hanudel et al., 2018). Circulating FGF23 levels were measured in 77 SCD patients, no EPO measurements were available (Courbebaisse et al., 2017). Serum ferritin concentrations and estimated glomerular filtration rate were significantly higher in SCD patients than in the control group. Mean plasma cFGF23 concentrations were significantly higher in SCD patients than in healthy controls (563 versus 55 RU/mL). The magnitude of multiplication of cFGF23 in SCD patients compared to healthy controls was comparable with the multiplication of cFGF23 observed after rhEPO (Table 1). In 75% of the SCD patients cFGF23 values were above the upper limit of normal, whereas in only 10% of the SCD patients iFGF23 values were above the upper limit of normal. Unfortunately, the association between the iFGF23/cFGF23 ratio, EPO and the extent of erythropoiesis was not evaluated.

The first study underlines that the EPO-FGF23 pathway is upregulated in  $\beta$ -thalassemia intermedia and can be upregulated under iron-overloaded conditions. The second study suggests that FGF23 production and cleavage are increased in SCD, if EPO or inflammation, or another factor, is the most important driving force remains to be investigated.

The activity of the EPO-FGF23 pathway in other hereditary anemias, including BM failure syndromes, with distinct amounts of hemolysis and ineffective hematopoiesis, accompanied by distinct elevations in circulating EPO, remains to be investigated. Besides activity of the pathway, the contribution of other factors influencing FGF23 signaling in hereditary anemias, including inflammation and iron load, remains to be investigated. Moreover, the role of the individual FGFRs and  $\alpha$ -KL in FGF23 signaling in hereditary anemia is currently unknown.

## IFGF23 DIRECTLY IMPAIRS BONE MINERALIZATION

The mineral ultrastructure of bone is crucial for its mechanical and biological properties. Non-collagenous proteins, as osteocalcin and osteopontin, are secreted during osteoid

mineralization (Gericke et al., 2005). Loss of function of either or both osteocalcin and highly phosphorylated osteopontin significantly reduces crystal thickness and results in altered crystal shape (Poundarik et al., 2018). Tissue non-specific alkaline phosphatase (TNAP) is anchored to the membranes of osteoblasts and chondrocytes and to matrix vesicles released by both cells, and degrades pyrophosphate (PPi) to Pi. Pyrophosphate is an inhibitor of bone mineralization, and the regulation of pyrophosphate by TNAP controls continuous extracellular mineralization of apatite crystals. TNAP deficiency leads to accumulation of pyrophosphate, thereby decreasing mineralization (Rader, 2017).

FGF23 and EPO, are known regulators of bone mineralization, and are discussed in Section "Fibroblast Growth Factor 23." Finally, we discuss the contribution of these factors to defective bone mineralization in chronic diseases of erythropoiesis.

## Fibroblast Growth Factor 23

Both gain and loss of function mutations in the *FGF23* gene result in bone mineralization disorders (Table 2). Gain of function mutations in *FGF23* cause autosomal dominant hypophosphatemic rickets (ADHR), a disease marked by severe decreased bone mineral density (Benet-Pages et al., 2005; Farrow et al., 2011a; Goldsweig and Carpenter, 2015). The metabolic mirror of ADHR is familial tumoral calcinosis, which is associated with pathologic increase of bone mineral density and is caused by loss of function mutations in the *FGF23* or *GalNT3* gene (Farrow et al., 2011a; Goldsweig and Carpenter, 2015). So, disturbances in FGF23, either primary (congenital) or secondary (e.g., in response to high EPO), ultimately result in bone mineralization deficits.

FGF23 seems to act auto- and/or paracrine in the bone environment (Murali et al., 2016b). A model has been proposed for a local role of FGF23 signaling in bone mineralization, independent of  $\alpha$ -KL, via FGFR3. Local FGF23 signaling in osteocytes results in suppression of TNAP transcription, which leads to decreased degradation, and subsequent accumulation, of pyrophosphate and suppression of inorganic phosphate production. Both directly reduce bone mineralization. Osteopontin secretion is indirectly downregulated by FGF23 signaling: lower availability of extracellular phosphate suppresses osteopontin expression (Murali et al., 2016b). Although, acting locally, also high systemically circulating FGF23 could modulate pyrophosphate metabolism (Murali et al., 2016a,b; Andrukhova et al., 2018). Moreover, alterations in vitamin D metabolism contribute to impaired bone mineralization in response to iFGF23. 1,25(OH)<sub>2</sub>D<sub>3</sub> inhibits bone mineralization locally in osteoblasts and osteocytes via stimulation of transcription and subsequent expression of presumably inadequately phosphorylated osteopontin (Lieben et al., 2012; Murali et al., 2016b).

So, iFGF23 signaling results directly in impaired bone mineralization via TNAP suppression. Notably, current knowledge is based on FGF23-knockout models, thereby not reflecting the interplay of iFGF23 and cFGF23 (Murali et al., 2016a,b; Andrukhova et al., 2018).

TABLE 2 | FGF23-related disorders.

| Disease            | Locus   | Inheritance pattern | Genetic defect           | FGF23 function | iFGF23/cFGF23 | TmP/GFR | Serum calcium | Serum phosphate | Urinary phosphate | PTH    | 1,25(OH) <sub>2</sub> D | Bone features   | Erythropoiesis  |
|--------------------|---------|---------------------|--------------------------|----------------|---------------|---------|---------------|-----------------|-------------------|--------|-------------------------|---|---|
| ADHR (OMIM 193100) | 12p13.3 | AD                  | R176Q, R179Q/W           | GoF            | = or ↑ ↑ or = | ↓       | =             | ↓               | ↑                 | = or ↑ | = or ↓                  | Bone deformities including varus deformity lower extremities, rachitic rosary, craniostynostosis, short stature, bone pain, bone fractures. | IDA, or low serum iron, associated with elevated FGF23 in ADHR. |
| rTC (OMIM 211900)  | 12p13.3 | AR                  | S71G, M96T, S129F, F157L | LoF            | = or ↓ ↑      | ↑       | =             | ↑               | ↓                 | = or ↓ | = or ↑                  | Tumoral calcinosis, or ectopic calcifications, hyperostosis, vascular calcifications.   | Not reported.   |

Summary of laboratory parameters and clinical characteristics of disorders associated with gain of function (ADHR) (ADHR Consortium, 2000; Imel et al., 2007, 2011; Huang et al., 2013; Acar et al., 2017; Clinkenbeard and White, 2017; Michaluk and Rusinska, 2018; Luo et al., 2019) and loss of function (rTC) mutations (Ramnitz et al., 1993; Araya et al., 2005; Larsson et al., 2005a,b; Bergwitz et al., 2009; Huang et al., 2013; Clinkenbeard and White, 2017; Luo et al., 2019) in the FGF23 gene. AD, autosomal dominant; ADHRs, autosomal dominant hypophosphatemic rickets; AR, autosomal recessive; FGF23, fibroblast growth factor 23; rTC, familial tumoral calcinosis; GoF, gain of function; IDA, iron deficiency anemia; LoF, loss of function; PTH, parathyroid hormone; TmP/GFR, tubular maximum reabsorption rate of phosphate per glomerular filtration rate.

Erythropoietin

In addition to its role in erythropoiesis, EPO regulates bone homeostasis. Mice overexpressing endogenous EPO developed severe osteopenia (Hiram-Bab et al., 2015). Treatment of WT mice with rhEPO for ten days resulted in a significant reduction in trabecular bone volume and increased bone remodeling. Similar changes in bone volume were observed after increased endogenous EPO expression due to induction of acute hemolysis (Singbrant et al., 2011; Suda, 2011). Despite these observations, the action of EPO on bone homeostasis remains controversial. Effects might be dose-dependent: supraphysiologic EPO concentrations induced mineralization (Shiozawa et al., 2010; Holstein et al., 2011; Rolting et al., 2012; Sun et al., 2012; Betsch et al., 2014; Guo et al., 2014; Wan et al., 2014; Eggold and Rankin, 2018), whereas low endogenous overexpression or moderate exogenous doses of EPO impaired bone formation via EPOR signaling (Shiozawa et al., 2010; Singbrant et al., 2011; Hiram-Bab et al., 2015; Rauner et al., 2016). Whether excess cFGF23, in response to EPO, is capable to neutralize α-KL independent osseous signaling of iFGF23, is currently unknown. We hypothesize that supraphysiologic EPO concentrations suppress the iFGF23/cFGF23 ratio to a level where the amount of cFGF23 is sufficient to fully prevent signaling of iFGF23 by competitive inhibition at the FGFR3. This resembles the hypermineralization observed in patients with elevated cFGF23 in familial tumoral calcinosis based on a *GalNT3* mutation (Ramnitz et al., 2016).

Bone Mineralization in Disorders of Erythropoiesis

Impaired bone mineralization, osteoporosis, is an important complication of chronic disorders affecting erythropoiesis (Valderrabano and Wu, 2018). The etiology of low bone mass is multifactorial including marrow expansion, various endocrine causes, direct iron toxicity, side effects of iron chelation therapy, lack of physical activity and genetic factors (Tzoulis et al., 2014; De Sanctis et al., 2018). In SCD and thalassemia bone abnormalities have been attributed mainly to marrow expansion (Valderrabano and Wu, 2018), although a linear correlation between circulating EPO levels and degree of bone demineralization in patients with identical diseases lacked (Steer et al., 2017). Eighty percent of adult SCD patients had an abnormal low bone mineral density (Sarrai et al., 2007), and up to 90% of β-thalassemia patients had an elevated fracture risk (Christoforidis et al., 2007; Wong et al., 2016). More recently, among children and young adults receiving regular transfusions and adequate iron chelation therapy Z-scores were within the normal range (Christoforidis et al., 2007; Wong et al., 2016). The role of transfusions in correction of bone mineral density underlines the importance of EPO signaling in the etiology of bone disease.

Currently, it is unknown what the extent is of the contribution of high EPO and subsequent lowering the iFGF23/cFGF23 ratio, to impaired bone mineralization in patients with chronic disorders of erythropoiesis. We suggest that iFGF23 excreted by BM erythroid cells might act on the surrounding osteocytes



and osteoblasts in an auto- and/or paracrine way which will impair bone mineralization via TNAP suppression, subsequent pyrophosphate accumulation, and indirect downregulation of osteopontin (Murali et al., 2016a,b; Andrukhova et al., 2018). Hypothetically, rhEPO therapy in selected patients might increase EPO levels toward adequately elevated EPO levels, with further decline in the iFGF23/cFGF23 ratio, ultimately turning the balance toward increased bone mineralization.

## SUMMARY AND FUTURE DIRECTIONS

We have outlined the importance of the EPO-FGF23 signaling pathways in erythroid cell development and bone mineralization. Both the amount of iFGF23 and its cleavage product cFGF23 determine signaling capacity. Insight in the activity of the EPO-FGF23 signaling pathway in rare hereditary anemias with varies degrees of hemolysis and ineffective erythropoiesis and varying circulating EPO concentrations, will add to the understanding of the pathophysiology and bone complications of these diseases.

Currently, two therapeutic agents are under development, or already registered, interfering with the EPO-FGF23 axis: FGF23 antagonists (KRN23; a therapeutic antibody against the C-terminus of FGF23) and FGFR1 inhibitor (BGJ-398; a small molecule pan-FGF kinase inhibitor) (Luo et al., 2019). Both agents have been tested for disorders characterized by high iFGF23 concentrations: tumor-induced osteomalacia (iFGF23 secreting tumors), or x-linked hyperphosphatemia (*PHEX* mutation results in high iFGF23).

Administration of rhEPO decreases the iFGF23/cFGF23 ratio, inhibiting apoptosis in erythroid cells. However, both EPO and an increase in the absolute amount of iFGF23 impair bone mineralization. Hypothetically, application of selective iFGF23 antagonists, or cFGF23 agonists, might bypass non-FGF23 related side-effects of rhEPO by regulating a more downstream component of the EPO-FGF23 pathway.

Uncertainties exist regarding (long-term) application of FGF23 antagonists or FGFR1 inhibitors in human. Thereby, the influence of FGF23, and pharmacological manipulation of FGF23, on energy metabolism is unclear. FGF23 is along

with FGF21 and FGF19, both clearly associated with energy metabolism, grouped as endocrine FGFs (Luo et al., 2019).

Moreover, iFGF23 serves as a proinflammatory paracrine factor, secreted mainly by M1 proinflammatory macrophages (Hanks et al., 2015; Holecki et al., 2015; Han et al., 2016; Agoro et al., 2018; Wallquist et al., 2018). Oxygen supply in inflamed tissues is often very limited (Imtiyaz and Simon, 2010; Eltzschig and Carmeliet, 2011). This inflammation-induced hypoxia leads to increased expression of EPOR in macrophages, suppresses inflammatory macrophage signaling and promotes resolution of inflammation (Liu et al., 2015; Luo et al., 2016). In response on EPO, a substantial increase in cFGF23 compared to iFGF23 might antagonize the pro-inflammatory effects of iFGF23 or even promote development of a M2-like phenotype, characterized by immunoregulatory capacities (Rees, 2010; Liu et al., 2015; Eggold and Rankin, 2018). Several forms of hemolytic hereditary anemias present with chronic (low-grade) inflammation, which might play an important role in the vascular complications of these diseases (Frenette, 2002; Belcher et al., 2003, 2005; Aggeli et al., 2005; Rees et al., 2010; Rocha et al., 2011; Atichartakarn et al., 2014). Theoretically, cFGF23 agonists might diminish inflammation in these patients and improve clinical outcomes.

In conclusion, although first discovered as phosphate regulator, FGF23 is an important regulator of erythropoiesis being part of the EPO-FGF23 signaling pathway. A new area of research is open to extent our knowledge about FGF23 biology beyond the kidney. Experimental research is required to identify the molecular and cellular players of the EPO-FGF23 signaling pathway and the role of the various FGFRs in erythropoiesis. Thereby, to determine the clinical relevance of the pathway in patients with alterations in erythropoiesis, we propose measuring iFGF23, cFGF23, and EPO levels in patients with various forms of dyserythropoietic or hemolytic anemia, and relating these values to inflammation, bone health and vasculopathic complications.

## AUTHOR CONTRIBUTIONS

All authors listed have made a substantial, direct and intellectual contribution to the work, and approved it for publication.

## REFERENCES

- Acar, S., Demir, K., and Shi, Y. (2017). Genetic causes of rickets. *J. Clin. Res. Pediatr. Endocrinol.* 9, 88–105. doi: 10.4274/jcrpe.2017.S008
- ADHR Consortium (2000). Autosomal dominant hypophosphataemic rickets is associated with mutations in FGF23. *Nat. Genet.* 26, 345–348. doi: 10.1038/81664
- Aggeli, C., Antoniadou, C., Cosma, C., Chrysohoou, C., Tousoulis, D., Ladis, V., et al. (2005). Endothelial dysfunction and inflammatory process in transfusion-dependent patients with beta-thalassemia major. *Int. J. Cardiol.* 105, 80–84. doi: 10.1016/j.ijcard.2004.12.025
- Agoro, R., Montagna, A., Goetz, R., Aligbe, O., Singh, G., Coe, L. M., et al. (2018). Inhibition of fibroblast growth factor 23 (FGF23) signaling rescues renal anemia. *FASEB J.* 32, 3752–3764. doi: 10.1096/fj.201700667R
- Andrukhova, O., Schuler, C., Bergow, C., Petric, A., and Erben, R. G. (2018). Augmented fibroblast growth factor-23 secretion in bone locally contributes to impaired bone mineralization in chronic kidney disease in mice. *Front. Endocrinol.* 9:311. doi: 10.3389/fendo.2018.00311
- Araya, K., Fukumoto, S., Backenroth, R., Takeuchi, Y., Nakayama, K., Ito, N., et al. (2005). A novel mutation in fibroblast growth factor 23 gene as a cause of tumoral calcinosis. *J. Clin. Endocrinol. Metab.* 90, 5523–5527. doi: 10.1210/jc.2005-0301
- Atichartakarn, V., Chuncharunee, S., Archararit, N., Udomsubpayakul, U., and Aryurachai, K. (2014). Intravascular hemolysis, vascular endothelial cell activation and thrombophilia in splenectomized patients with hemoglobin E/beta-thalassemia disease. *Acta Haematol.* 132, 100–107. doi: 10.1159/000355719
- Baia, L. C., Humalda, J. K., Vervloet, M. G., Navis, G., Bakker, S. J., de Borst, M. H., et al. (2013). Fibroblast growth factor 23 and cardiovascular mortality after kidney transplantation. *Clin. J. Am. Soc. Nephrol.* 8, 1968–1978. doi: 10.2215/CJN.01880213
- Belcher, J. D., Bryant, C. J., Nguyen, J., Bowlin, P. R., Kielbik, M. C., Bischof, J. C., et al. (2003). Transgenic sickle mice have vascular



- inflammation. *Blood* 101, 3953–3959. doi: 10.1182/blood-2002-10-3313
- Belcher, J. D., Mahaseth, H., Welch, T. E., Vilback, A. E., Sonbol, K. M., Kalambur, V. S., et al. (2005). Critical role of endothelial cell activation in hypoxia-induced vasoocclusion in transgenic sickle mice. *Am. J. Physiol. Heart Circ. Physiol.* 288, H2715–H2725. doi: 10.1152/ajpheart.00986.2004
- Benet-Pages, A., Lorenz-Depiereux, B., Zischka, H., White, K. E., Econs, M. J., and Strom, T. M. (2004). FGF23 is processed by proprotein convertases but not by PHEX. *Bone* 35, 455–462. doi: 10.1016/j.bone.2004.04.002
- Benet-Pages, A., Orlik, P., Strom, T. M., and Lorenz-Depiereux, B. (2005). An FGF23 missense mutation causes familial tumoral calcinosis with hyperphosphatemia. *Hum. Mol. Genet.* 14, 385–390. doi: 10.1093/hmg/ddi034
- Bergwitz, C., Banerjee, S., Abu-Zahra, H., Kaji, H., Miyauchi, A., Sugimoto, T., et al. (2009). Defective O-glycosylation due to a novel homozygous S129P mutation is associated with lack of fibroblast growth factor 23 secretion and tumoral calcinosis. *J. Clin. Endocrinol. Metab.* 94, 4267–4274. doi: 10.1210/jc.2009-0961
- Besson-Fournier, C., Latour, C., Kautz, L., Bertrand, J., Ganz, T., Roth, M. P., et al. (2012). Induction of activin B by inflammatory stimuli up-regulates expression of the iron-regulatory peptide hepcidin through Smad1/5/8 signaling. *Blood* 120, 431–439. doi: 10.1182/blood-2012-02-411470
- Betsch, M., Thelen, S., Santak, L., Herten, M., Jungbluth, P., Miersch, D., et al. (2014). The role of erythropoietin and bone marrow concentrate in the treatment of osteochondral defects in mini-pigs. *PLoS One* 9:e92766. doi: 10.1371/journal.pone.0092766
- Blazevic, A., Hunze, J., and Boots, J. M. (2014). Severe hypophosphataemia after intravenous iron administration. *Neth. J. Med.* 72, 49–53.
- Block, G. A., Fishbane, S., Rodriguez, M., Smits, G., Shemesh, S., Pergola, P. E., et al. (2015). A 12-week, double-blind, placebo-controlled trial of ferric citrate for the treatment of iron deficiency anemia and reduction of serum phosphate in patients with CKD Stages 3–5. *Am. J. Kidney Dis.* 65, 728–736. doi: 10.1053/j.ajkd.2014.10.014
- Bozentowicz-Wikarek, M., Kocelak, P., Owczarek, A., Olszanecka-Glinianowicz, M., Mossakowska, M., Skalska, A., et al. (2015). Plasma fibroblast growth factor 23 concentration and iron status. Does the relationship exist in the elderly population? *Clin. Biochem.* 48, 431–436. doi: 10.1016/j.clinbiochem.2014.12.027
- Buttthep, P., Wisedpanichkij, R., Jindadamrongwech, S., and Fucharoen, S. (2015). Elevated erythropoietin and cytokines levels are related to impaired reticulocyte maturation in thalassemic patients. *Blood Cells Mol. Dis.* 54, 170–176. doi: 10.1016/j.bcmd.2014.11.007
- Canali, S., Core, A. B., Zumbrennen-Bullough, K. B., Merkulova, M., Wang, C. Y., Schneyer, A. L., et al. (2016). Activin B Induces Noncanonical SMAD1/5/8 Signaling via BMP Type I Receptors in Hepatocytes: evidence for a Role in Hepcidin Induction by Inflammation in Male Mice. *Endocrinology* 157, 1146–1162. doi: 10.1210/en.2015-1747
- Caro, J., Brown, S., Miller, O., Murray, T., and Erslev, A. J. (1979). Erythropoietin levels in uremic nephric and anephric patients. *J. Lab. Clin. Med.* 93, 449–458.
- Chen, G., Liu, Y., Goetz, R., Fu, L., Jayaraman, S., Hu, M. C., et al. (2018). alpha-Klotho is a non-enzymatic molecular scaffold for FGF23 hormone signalling. *Nature* 553, 461–466. doi: 10.1038/nature25451
- Christoforidis, A., Kazantzidou, E., Tsatra, I., Tsantali, H., Koliakos, G., Hatzipantelis, E., et al. (2007). Normal lumbar bone mineral density in optimally treated children and young adolescents with beta-thalassaemia major. *Hormones* 6, 334–340. doi: 10.14310/horm.2002.1111030
- Clinkenbeard, E. L., Cass, T. A., Ni, P., Hum, J. M., Bellido, T., Allen, M. R., et al. (2016). Conditional Deletion of Murine Fgf23: interruption of the normal skeletal responses to phosphate challenge and rescue of genetic hypophosphatemia. *J. Bone Miner. Res.* 31, 1247–1257. doi: 10.1002/jbmr.2792
- Clinkenbeard, E. L., Farrow, E. G., Summers, L. J., Cass, T. A., Roberts, J. L., Bayt, C. A., et al. (2014). Neonatal iron deficiency causes abnormal phosphate metabolism by elevating FGF23 in normal and ADHR mice. *J. Bone Miner. Res.* 29, 361–369. doi: 10.1002/jbmr.2049
- Clinkenbeard, E. L., Hanudel, M. R., Stayrook, K. R., Appaiah, H. N., Farrow, E. G., Cass, T. A., et al. (2017). Erythropoietin stimulates murine and human fibroblast growth factor-23, revealing novel roles for bone and bone marrow. *Haematologica* 102, e427–e430. doi: 10.3324/haematol.2017.167882
- Clinkenbeard, E. L., and White, K. E. (2017). Heritable and acquired disorders of phosphate metabolism: etiologies involving FGF23 and current therapeutics. *Bone* 102, 31–39. doi: 10.1016/j.bone.2017.01.034
- Coe, L. M., Madathil, S. V., Casu, C., Lanske, B., Rivella, S., and Sitara, D. (2014). FGF-23 is a negative regulator of prenatal and postnatal erythropoiesis. *J. Biol. Chem.* 289, 9795–9810. doi: 10.1074/jbc.M113.527150
- Courbebaisse, M., Mehel, H., Petit-Hoang, C., Ribeil, J. A., Sabbah, L., Tuloup-Minguez, V., et al. (2017). Carboxy-terminal fragment of fibroblast growth factor 23 induces heart hypertrophy in sickle cell disease. *Haematologica* 102, e33–e35. doi: 10.3324/haematol.2016.150987
- Daryadel, A., Bettoni, C., Haider, T., Imenez Silva, P. H., Schnitzbauer, U., Pastor-Arroyo, E. M., et al. (2018). Erythropoietin stimulates fibroblast growth factor 23 (FGF23) in mice and men. *Pflugers Arch.* 470, 1569–1582. doi: 10.1007/s00424-018-2171-7
- David, V., Martin, A., Isakova, T., Spaulding, C., Qi, L., Ramirez, V., et al. (2016). Inflammation and functional iron deficiency regulate fibroblast growth factor 23 production. *Kidney Int.* 89, 135–146. doi: 10.1038/ki.2015.290
- De Sanctis, V., Soliman, A. T., Elsefedy, H., Soliman, N., Bedair, E., Fiscina, B., et al. (2018). Bone disease in beta thalassemia patients: past, present and future perspectives. *Metabolism* 80, 66–79. doi: 10.1016/j.metabol.2017.09.012
- Dounousi, E., Torino, C., Pizzini, P., Cutrupi, S., Panuccio, V., D'Arrigo, G., et al. (2016). Intact FGF23 and alpha-Klotho during acute inflammation/sepsis in CKD patients. *Eur. J. Clin. Invest.* 46, 234–241. doi: 10.1111/eci.12588
- Ebert, B. L., and Bunn, H. F. (1999). Regulation of the erythropoietin gene. *Blood* 94, 1864–1877.
- Eggold, J. T., and Rankin, E. B. (2018). Erythropoiesis, EPO, macrophages, and bone. *Bone* 119, 36–41. doi: 10.1016/j.bone.2018.03.014
- Eisenga, M. F., van Londen, M., Leaf, D. E., Nolte, I. M., Navis, G., Bakker, S. J. L., et al. (2017). C-terminal fibroblast growth factor 23, iron deficiency, and mortality in renal transplant recipients. *J. Am. Soc. Nephrol.* 28, 3639–3646. doi: 10.1681/ASN.2016.12.1350
- Eltzschig, H. K., and Carmeliet, P. (2011). Hypoxia and inflammation. *N. Engl. J. Med.* 364, 656–665. doi: 10.1056/NEJMra0910283
- Farrow, E. G., Imel, E. A., and White, K. E. (2011a). Miscellaneous non-inflammatory musculoskeletal conditions. Hyperphosphatemic familial tumoral calcinosis (FGF23, GALNT3 and alphaKlotho). *Best Pract. Res. Clin. Rheumatol.* 25, 735–747. doi: 10.1016/j.berh.2011.10.020
- Farrow, E. G., Yu, X., Summers, L. J., Davis, S. I., Fleet, J. C., Allen, M. R., et al. (2011b). Iron deficiency drives an autosomal dominant hypophosphatemic rickets (ADHR) phenotype in fibroblast growth factor-23 (Fgf23) knock-in mice. *Proc. Natl. Acad. Sci. U.S.A.* 108, E1146–E1155. doi: 10.1073/pnas.1110905108
- Faul, C., Amaral, A. P., Oskouei, B., Hu, M. C., Sloan, A., Isakova, T., et al. (2011). FGF23 induces left ventricular hypertrophy. *J. Clin. Invest.* 121, 4393–4408. doi: 10.1172/JCI46122
- Fibach, E., and Rachmilewitz, E. A. (2014). Does erythropoietin have a role in the treatment of beta-hemoglobinopathies? *Hematol. Oncol. Clin. North Am.* 28, 249–263. doi: 10.1016/j.hoc.2013.11.002
- Flamme, I., Ellinghaus, P., Urrego, D., and Kruger, T. (2017). FGF23 expression in rodents is directly induced via erythropoietin after inhibition of hypoxia inducible factor proline hydroxylase. *PLoS One* 12:e0186979. doi: 10.1371/journal.pone.0186979
- Fliser, D., Kollerits, B., Neyer, U., Ankerst, D. P., Lhotta, K., Lingenhel, A., et al. (2007). Fibroblast growth factor 23 (FGF23) predicts progression of chronic kidney disease: the Mild to Moderate Kidney Disease (MMKD) Study. *J. Am. Soc. Nephrol.* 18, 2600–2608. doi: 10.1681/ASN.2006080936
- Francis, C., and David, V. (2016). Inflammation regulates fibroblast growth factor 23 production. *Curr. Opin. Nephrol. Hypertens.* 25, 325–332. doi: 10.1097/MNH.0000000000000232
- Frenette, P. S. (2002). Sickle cell vaso-occlusion: multistep and multicellular paradigm. *Curr. Opin. Hematol.* 9, 101–106. doi: 10.1097/00062752-200203000-00003
- Ganz, T. (2011). Hepcidin and iron regulation, 10 years later. *Blood* 117, 4425–4433. doi: 10.1182/blood-2011-01-258467

- Gericke, A., Qin, C., Spevak, L., Fujimoto, Y., Butler, W. T., Sorensen, E. S., et al. (2005). Importance of phosphorylation for osteopontin regulation of biomineralization. *Calcif. Tissue Int.* 77, 45–54. doi: 10.1007/s00223-004-1288-1
- Goetz, R., Beenken, A., Ibrahimi, O. A., Kalinina, J., Olsen, S. K., Eliseenkova, A. V., et al. (2007). Molecular insights into the klotho-dependent, endocrine mode of action of fibroblast growth factor 19 subfamily members. *Mol. Cell Biol.* 27, 3417–3428. doi: 10.1128/MCB.02249-06
- Goetz, R., Nakada, Y., Hu, M. C., Kurosu, H., Wang, L., Nakatani, T., et al. (2010). Isolated C-terminal tail of FGF23 alleviates hypophosphatemia by inhibiting FGF23-FGFR-Klotho complex formation. *Proc. Natl. Acad. Sci. U.S.A.* 107, 407–412. doi: 10.1073/pnas.0902006107
- Goldswieg, B. K., and Carpenter, T. O. (2015). Hypophosphatemic rickets: lessons from disrupted FGF23 control of phosphorus homeostasis. *Curr. Osteoporos. Rep.* 13, 88–97. doi: 10.1007/s11914-015-0259-y
- Grabner, A., Amaral, A. P., Schramm, K., Singh, S., Sloan, A., Yanucil, C., et al. (2015). Activation of cardiac fibroblast growth factor receptor 4 causes left ventricular hypertrophy. *Cell Metab.* 22, 1020–1032. doi: 10.1016/j.cmet.2015.09.002
- Grabner, A., and Faul, C. (2016). The role of fibroblast growth factor 23 and Klotho in uremic cardiomyopathy. *Curr. Opin. Nephrol. Hypertens.* 25, 314–324. doi: 10.1097/MNH.0000000000000231
- Guo, L., Luo, T., Fang, Y., Yang, L., Wang, L., Liu, J., et al. (2014). Effects of erythropoietin on osteoblast proliferation and function. *Clin. Exp. Med.* 14, 69–76. doi: 10.1007/s10238-012-0220-7
- Gutierrez, O. M., Januzzi, J. L., Isakova, T., Laliberte, K., Smith, K., Collerone, G., et al. (2009). Fibroblast growth factor 23 and left ventricular hypertrophy in chronic kidney disease. *Circulation* 119, 2545–2552. doi: 10.1161/CIRCULATIONAHA.108.844506
- Haase, V. H. (2010). Hypoxic regulation of erythropoiesis and iron metabolism. *Am. J. Physiol. Renal Physiol.* 299, F1–F13. doi: 10.1152/ajprenal.00174.2010
- Haidar, R., Mhaidli, H., Musallam, K. M., and Taher, A. T. (2012). The spine in beta-thalassemia syndromes. *Spine* 37, 334–339. doi: 10.1097/BRS.0b013e31821bd095
- Han, J., Zhou, J., Kondragunta, V., Zhang, X., Molokie, R. E., Gowhari, M., et al. (2017). Erythropoiesis-stimulating agents in sickle cell anaemia. *Br. J. Haematol.* 182, 602–605. doi: 10.1111/bjh.14846
- Han, X., Li, L., Yang, J., King, G., Xiao, Z., and Quarles, L. D. (2016). Counter-regulatory paracrine actions of FGF-23 and 1,25(OH)<sub>2</sub>D in macrophages. *FEBS Lett.* 590, 53–67. doi: 10.1002/1873-3468.12040
- Hanks, L. J., Casazza, K., Judd, S. E., Jenny, N. S., and Gutierrez, O. M. (2015). Associations of fibroblast growth factor-23 with markers of inflammation, insulin resistance and obesity in adults. *PLoS One* 10:e0122885. doi: 10.1371/journal.pone.0122885
- Hanudel, M. R., Chua, K., Rappaport, M., Gabayan, V., Valore, E., Goltzman, D., et al. (2016). Effects of dietary iron intake and chronic kidney disease on fibroblast growth factor 23 metabolism in wild-type and hepcidin knockout mice. *Am. J. Physiol. Renal Physiol.* 311, F1369–F1377. doi: 10.1152/ajprenal.00281.2016
- Hanudel, M. R., Eisenga, M. F., Rappaport, M., Chua, K., Qiao, B., Jung, G., et al. (2018). Effects of erythropoietin on fibroblast growth factor 23 in mice and humans. *Nephrol. Dial. Transplant.* doi: 10.1093/ndt/gfy189 [Epub ahead of print].
- Hiram-Bab, S., Liron, T., Deshet-Unger, N., Mittelman, M., Gassmann, M., Rauner, M., et al. (2015). Erythropoietin directly stimulates osteoclast precursors and induces bone loss. *FASEB J.* 29, 1890–1900. doi: 10.1096/fj.14-259085
- Holecki, M., Chudek, J., Owczarek, A., Olszanecka-Glinianowicz, M., Bozentowicz-Wikarek, M., Dulawa, J., et al. (2015). Inflammation but not obesity or insulin resistance is associated with increased plasma fibroblast growth factor 23 concentration in the elderly. *Clin. Endocrinol.* 82, 900–909. doi: 10.1111/cen.12759
- Holstein, J. H., Orth, M., Scheuer, C., Tami, A., Becker, S. C., Garcia, P., et al. (2011). Erythropoietin stimulates bone formation, cell proliferation, and angiogenesis in a femoral segmental defect model in mice. *Bone* 49, 1037–1045. doi: 10.1016/j.bone.2011.08.004
- Hryszko, T., Rydzewska-Rosolowska, A., Brzosko, S., Koc-Zorawska, E., and Mysliwiec, M. (2012). Low molecular weight iron dextran increases fibroblast growth factor-23 concentration, together with parathyroid hormone decrease in hemodialyzed patients. *Ther. Apher. Dial.* 16, 146–151. doi: 10.1111/j.1744-9987.2011.01037.x
- Huang, X., Jiang, Y., and Xia, W. (2013). FGF23 and phosphate wasting disorders. *Bone Res.* 1, 120–132. doi: 10.4248/BR201302002
- Iguchi, A., Kazama, J. J., Yamamoto, S., Yoshita, K., Watanabe, Y., Iino, N., et al. (2015). Administration of ferric citrate hydrate decreases circulating FGF23 Levels independently of serum phosphate levels in hemodialysis patients with iron deficiency. *Nephron* 131, 161–166. doi: 10.1159/000440968
- Imel, E. A., Hui, S. L., and Econs, M. J. (2007). FGF23 concentrations vary with disease status in autosomal dominant hypophosphatemic rickets. *J. Bone Miner. Res.* 22, 520–526. doi: 10.1359/jbmr.070107
- Imel, E. A., Liu, Z., McQueen, A. K., Acton, D., Acton, A., Padgett, L. R., et al. (2016). Serum fibroblast growth factor 23, serum iron and bone mineral density in premenopausal women. *Bone* 86, 98–105. doi: 10.1016/j.bone.2016.03.005
- Imel, E. A., Peacock, M., Gray, A. K., Padgett, L. R., Hui, S. L., and Econs, M. J. (2011). Iron modifies plasma FGF23 differently in autosomal dominant hypophosphatemic rickets and healthy humans. *J. Clin. Endocrinol. Metab.* 96, 3541–3549. doi: 10.1210/jc.2011-1239
- Imtiyaz, H. Z., and Simon, M. C. (2010). Hypoxia-inducible factors as essential regulators of inflammation. *Curr. Top. Microbiol. Immunol.* 345, 105–120. doi: 10.1007/82\_2010\_74
- Isakova, T., Xie, H., Yang, W., Xie, D., Anderson, A. H., Scialla, J., et al. (2011). Fibroblast growth factor 23 and risks of mortality and end-stage renal disease in patients with chronic kidney disease. *JAMA* 305, 2432–2439. doi: 10.1001/jama.2011.826
- Ito, N., Wijenayaka, A. R., Prideaux, M., Kogawa, M., Ormsby, R. T., Evdokiou, A., et al. (2015). Regulation of FGF23 expression in IDG-SW3 osteocytes and human bone by pro-inflammatory stimuli. *Mol. Cell Endocrinol.* 399, 208–218. doi: 10.1016/j.mce.2014.10.007
- Jelkmann, W. (1992). Erythropoietin: structure, control of production, and function. *Physiol. Rev.* 72, 449–489. doi: 10.1152/physrev.1992.72.2.449
- Kanbay, M., Vervloet, M., Cozzolino, M., Siropol, D., Covic, A., Goldsmith, D., et al. (2017). Novel Faces of Fibroblast Growth Factor 23 (FGF23): iron deficiency, inflammation, insulin resistance, left ventricular hypertrophy, proteinuria and acute kidney injury. *Calcif. Tissue Int.* 100, 217–228. doi: 10.1007/s00223-016-0206-7
- Karafin, M. S., Koch, K. L., Rankin, A. B., Nischik, D., Rahhal, G., Simpson, P., et al. (2015). Erythropoietic drive is the strongest predictor of hepcidin level in adults with sickle cell disease. *Blood Cells Mol. Dis.* 55, 304–307. doi: 10.1016/j.bcmd.2015.07.010
- Kato, K., Jeanneau, C., Tarp, M. A., Benet-Pages, A., Lorenz-Depiereux, B., Bennett, E. P., et al. (2006). Polypeptide GalNAc-transferase T3 and familial tumoral calcinosis. Secretion of fibroblast growth factor 23 requires O-glycosylation. *J. Biol. Chem.* 281, 18370–18377. doi: 10.1074/jbc.M602469200
- Khosravi, A., Cutler, C. M., Kelly, M. H., Chang, R., Royal, R. E., Sherry, R. M., et al. (2007). Determination of the elimination half-life of fibroblast growth factor-23. *J. Clin. Endocrinol. Metab.* 92, 2374–2377. doi: 10.1210/jc.2006-2865
- Konjiki, O., Fukaya, S., Kanou, H., Imamura, T., Iwamoto, T., and Takasaki, M. (1994). A case of hypophosphatemia induced by intravenous administration of saccharated iron oxide. *Nihon Ronen Igakkai Zasshi* 31, 805–810. doi: 10.3143/geriatrics.31.805
- Krantz, S. B. (1991). Erythropoietin. *Blood* 77, 419–434.
- Krick, S., Grabner, A., Baumlín, N., Yanucil, C., Helton, S., Grosche, A., et al. (2018). Fibroblast growth factor 23 and Klotho contribute to airway inflammation. *Eur. Respir. J.* 52:1800236. doi: 10.1183/13993003.00236-2018
- Kuro-o, M., Matsumura, Y., Aizawa, H., Kawaguchi, H., Suga, T., Utsugi, T., et al. (1997). Mutation of the mouse klotho gene leads to a syndrome resembling ageing. *Nature* 390, 45–51. doi: 10.1038/36285
- Kurosu, H., Ogawa, Y., Miyoshi, M., Yamamoto, M., Nandi, A., Rosenblatt, K. P., et al. (2006). Regulation of fibroblast growth factor-23 signaling by klotho. *J. Biol. Chem.* 281, 6120–6123. doi: 10.1074/jbc.C500457200
- Larsson, T., Davis, S. I., Garringer, H. J., Mooney, S. D., Draman, M. S., Cullen, M. J., et al. (2005a). Fibroblast growth factor-23 mutants causing familial tumoral calcinosis are differentially processed. *Endocrinology* 146, 3883–3891.
- Larsson, T., Yu, X., Davis, S. I., Draman, M. S., Mooney, S. D., Cullen, M. J., et al. (2005b). A novel recessive mutation in fibroblast growth factor-23 causes

- familial tumoral calcinosis. *J. Clin. Endocrinol. Metab.* 90, 2424–2427. doi: 10.1210/jc.2004-2238
- Lieben, L., Masuyama, R., Torrekens, S., Van Looveren, R., Schrooten, J., Baatsen, P., et al. (2012). Normocalcemia is maintained in mice under conditions of calcium malabsorption by vitamin D-induced inhibition of bone mineralization. *J. Clin. Invest.* 122, 1803–1815. doi: 10.1172/JCI45890
- Liu, Y., Luo, B., Shi, R., Wang, J., Liu, Z., Liu, W., et al. (2015). Nonerythropoietic erythropoietin-derived peptide suppresses adipogenesis, inflammation, obesity and insulin resistance. *Sci. Rep.* 5:15134. doi: 10.1038/srep15134
- Luo, B., Gan, W., Liu, Z., Shen, Z., Wang, J., Shi, R., et al. (2016). Erythropoietin signaling in macrophages promotes dying cell clearance and immune tolerance. *Immunity* 44, 287–302. doi: 10.1016/j.immuni.2016.01.002
- Luo, Y., Ye, S., Li, X., and Lu, W. (2019). Emerging structure-function paradigm of endocrine FGFs in metabolic diseases. *Trends Pharmacol. Sci.* 40, 142–153. doi: 10.1016/j.tips.2018.12.002
- Mace, M. L., Gravesen, E., Hofman-Bang, J., Olgaard, K., and Lewin, E. (2015). Key role of the kidney in the regulation of fibroblast growth factor 23. *Kidney Int.* 88, 1304–1313. doi: 10.1038/ki.2015.231
- Martin, A., David, V., and Quarles, L. D. (2012). Regulation and function of the FGF23/klotho endocrine pathways. *Physiol. Rev.* 92, 131–155. doi: 10.1152/physrev.00002.2011
- Maruyama, N., Otsuki, T., Yoshida, Y., Nagura, C., Kitai, M., Shibahara, N., et al. (2018). Ferric citrate decreases fibroblast growth factor 23 and improves erythropoietin responsiveness in hemodialysis patients. *Am. J. Nephrol.* 47, 406–414. doi: 10.1159/000489964
- McMahon, S., Grondin, F., McDonald, P. P., Richard, D. E., and Dubois, C. M. (2005). Hypoxia-enhanced expression of the proprotein convertase furin is mediated by hypoxia-inducible factor-1: impact on the bioactivation of proproteins. *J. Biol. Chem.* 280, 6561–6569. doi: 10.1074/jbc.M413248200
- Mehta, R., Cai, X., Lee, J., Scialla, J. J., Bansal, N., Sondheim, J. H., et al. (2016). Association of fibroblast growth factor 23 with atrial fibrillation in chronic kidney disease, from the chronic renal insufficiency cohort study. *JAMA Cardiol.* 1, 548–556. doi: 10.1001/jamacardio.2016.1445
- Michalus, I., and Rusinska, A. (2018). Rare, genetically conditioned forms of rickets: Differential diagnosis and advances in diagnostics and treatment. *Clin. Genet.* 94, 103–114. doi: 10.1111/cge.13229
- Muckenthaler, M. U., Rivella, S., Hentze, M. W., and Galy, B. (2017). A Red Carpet for Iron Metabolism. *Cell* 168, 344–361. doi: 10.1016/j.cell.2016.12.034
- Munoz Mendoza, J., Isakova, T., Ricardo, A. C., Xie, H., Navaneethan, S. D., Anderson, A. H., et al. (2012). Fibroblast growth factor 23 and Inflammation in CKD. *Clin. J. Am. Soc. Nephrol.* 7, 1155–1162. doi: 10.2215/CJN.13281211
- Murali, S. K., Andrukhova, O., Clinkenbeard, E. L., White, K. E., and Erben, R. G. (2016a). Excessive Osteocytic Fgf23 secretion contributes to pyrophosphate accumulation and mineralization defect in hyp mice. *PLoS Biol.* 14:e1002427. doi: 10.1371/journal.pbio.1002427
- Murali, S. K., Roschger, P., Zeitl, U., Klaushofer, K., Andrukhova, O., and Erben, R. G. (2016b). FGF23 regulates bone mineralization in a 1,25(OH)<sub>2</sub>D<sub>3</sub> and Klotho-Independent Manner. *J. Bone Miner. Res.* 31, 129–142. doi: 10.1002/jbmr.2606
- O'Donnell, A., Premawardhena, A., Arambepola, M., Allen, S. J., Peto, T. E., Fisher, C. A., et al. (2007). Age-related changes in adaptation to severe anemia in childhood in developing countries. *Proc. Natl. Acad. Sci. U.S.A.* 104, 9440–9444. doi: 10.1073/pnas.0703424104
- Okada, M., Imamura, K., Iida, M., Fuchigami, T., and Omae, T. (1983). Hypophosphatemia induced by intravenous administration of Saccharated iron oxide. *Klin. Wochenschr.* 61, 99–102. doi: 10.1007/BF01496662
- Okan, G., Baki, A. M., Yorulmaz, E., Dogru-Abbasoglu, S., and Vural, P. (2016). Fibroblast growth factor 23 and placental growth factor in patients with psoriasis and their relation to disease severity. *Ann. Clin. Lab. Sci.* 46, 174–179.
- Portale, A. A., Wolf, M. S., Messinger, S., Perwad, F., Juppner, H., Warady, B. A., et al. (2016). Fibroblast Growth Factor 23 and Risk of CKD Progression in Children. *Clin. J. Am. Soc. Nephrol.* 11, 1989–1998. doi: 10.2215/CJN.0211.0216
- Poundarik, A. A., Boskey, A., Gundberg, C., and Vashishth, D. (2018). Biomolecular regulation, composition and nanoarchitecture of bone mineral. *Sci. Rep.* 8:1191. doi: 10.1038/s41598-018-19253-w
- Prats, M., Font, R., Garcia, C., Cabre, C., Jariod, M., and Vea, A. M. (2013). Effect of ferric carboxymaltose on serum phosphate and C-terminal FGF23 levels in non-dialysis chronic kidney disease patients: post-hoc analysis of a prospective study. *BMC Nephrol.* 14:167. doi: 10.1186/1471-2369-14-167
- Pulte, E. D., McKenzie, S. E., Caro, J., and Ballas, S. K. (2014). Erythropoietin levels in patients with sickle cell disease do not correlate with known inducers of erythropoietin. *Hemoglobin* 38, 385–389. doi: 10.3109/03630269.2014.967868
- Quarles, L. D. (2012). Role of FGF23 in vitamin D and phosphate metabolism: implications in chronic kidney disease. *Exp. Cell Res.* 318, 1040–1048. doi: 10.1016/j.yexcr.2012.02.027
- Rabadi, S., Udo, I., Leaf, D. E., Waikar, S. S., and Christov, M. (2018). Acute blood loss stimulates fibroblast growth factor 23 production. *Am. J. Physiol. Renal Physiol.* 314, F132–F139. doi: 10.1152/ajprenal.00081.2017
- Rader, B. A. (2017). Alkaline phosphatase, an unconventional immune protein. *Front. Immunol.* 8:897. doi: 10.3389/fimmu.2017.00897
- Ramnitz, M. S., Gafni, R. I., and Collins, M. T. (1993). “Hyperphosphatemic Familial Tumoral Calcinosis,” in *GeneReviews(R)*, eds M. P. Adam, H. H. Ardinger, R. A. Pagon, S. E. Wallace, L. J. H. Bean, K. Stephens, et al. (Seattle, WA: University of Washington, Seattle).
- Ramnitz, M. S., Gourh, P., Goldbach-Mansky, R., Wodajo, F., Ichikawa, S., Econs, M. J., et al. (2016). Phenotypic and genotypic characterization and treatment of a cohort with familial tumoral calcinosis/hyperostosis-hyperphosphatemia syndrome. *J. Bone Miner. Res.* 31, 1845–1854. doi: 10.1002/jbmr.2870
- Rankin, E. B., Wu, C., Khatiri, R., Wilson, T. L., Andersen, R., Araldi, E., et al. (2012). The HIF signaling pathway in osteoblasts directly modulates erythropoiesis through the production of EPO. *Cell* 149, 63–74. doi: 10.1016/j.cell.2012.01.051
- Rauner, M., Franke, K., Murray, M., Singh, R. P., Hiram-Bab, S., Platzbecker, U., et al. (2016). Increased EPO levels are associated with bone loss in mice Lacking PHD2 in EPO-Producing Cells. *J. Bone Miner. Res.* 31, 1877–1887. doi: 10.1002/jbmr.2857
- Rees, A. J. (2010). Monocyte and macrophage biology: an overview. *Semin. Nephrol.* 30, 216–233. doi: 10.1016/j.semnephrol.2010.03.002
- Rees, D. C., Williams, T. N., and Gladwin, M. T. (2010). Sickle-cell disease. *Lancet* 376, 2018–2031. doi: 10.1016/S0140-6736(10)61029-X
- Resende, A. L., Elias, R. M., Wolf, M., Dos Reis, L. M., Gracioli, F. G., Santos, G. D., et al. (2017). Serum levels of fibroblast growth factor 23 are elevated in patients with active Lupus nephritis. *Cytokine* 91, 124–127. doi: 10.1016/j.cyto.2016.12.022
- Rocha, S., Costa, E., Catarino, C., Belo, L., Castro, E. M., Barbot, J., et al. (2005). Erythropoietin levels in the different clinical forms of hereditary spherocytosis. *Br. J. Haematol.* 131, 534–542. doi: 10.1111/j.1365-2141.2005.05802.x
- Rocha, S., Costa, E., Rocha-Pereira, P., Ferreira, F., Cleto, E., Barbot, J., et al. (2011). Erythropoiesis versus inflammation in Hereditary Spherocytosis clinical outcome. *Clin. Biochem.* 44, 1137–1143. doi: 10.1016/j.clinbiochem.2011.06.006
- Rolfing, J. H., Bendtsen, M., Jensen, J., Stiehler, M., Foldager, C. B., Hellfritsch, M. B., et al. (2012). Erythropoietin augments bone formation in a rabbit posterolateral spinal fusion model. *J. Orthop. Res.* 30, 1083–1088. doi: 10.1002/jor.22027
- Rossaint, J., Oehmichen, J., Van Aken, H., Reuter, S., Pavenstadt, H. J., Meersch, M., et al. (2016). FGF23 signaling impairs neutrophil recruitment and host defense during CKD. *J. Clin. Invest.* 126, 962–974. doi: 10.1172/JCI83470
- Saito, K., Ishizaka, N., Mitani, H., Ohno, M., and Nagai, R. (2003). Iron chelation and a free radical scavenger suppress angiotensin II-induced downregulation of klotho, an anti-aging gene, in rat. *FEBS Lett.* 551, 58–62. doi: 10.1016/S0014-5793(03)00894-9
- Saito, T., and Fukumoto, S. (2009). Fibroblast Growth Factor 23 (FGF23) and disorders of phosphate metabolism. *Int. J. Pediatr. Endocrinol.* 2009:496514. doi: 10.1155/2009/496514
- Sarrai, M., Duroseau, H., D'Augustine, J., Moktan, S., and Bellevue, R. (2007). Bone mass density in adults with sickle cell disease. *Br. J. Haematol.* 136, 666–672. doi: 10.1111/j.1365-2141.2006.06487.x
- Sato, H., Kazama, J. J., Murasawa, A., Otani, H., Abe, A., Ito, S., et al. (2016). Serum Fibroblast Growth Factor 23 (FGF23) in patients with rheumatoid arthritis. *Intern. Med.* 55, 121–126. doi: 10.2169/internalmedicine.55.5507
- Schofield, C. J., and Ratcliffe, P. J. (2004). Oxygen sensing by HIF hydroxylases. *Nat. Rev. Mol. Cell Biol.* 5, 343–354. doi: 10.1038/nrm1366
- Schotten, N., Laarakkers, C. M., Roelofs, R. W., Origa, R., van Kraaij, M. G., and Swinkels, D. W. (2017). EPO and hepcidin plasma concentrations in blood donors and beta-thalassemia intermedia are not related to commercially tested



- plasma ERFE concentrations. *Am. J. Hematol.* 92, E29–E31. doi: 10.1002/ajh.24636
- Schouten, B. J., Doogue, M. P., Soule, S. G., and Hunt, P. J. (2009a). Iron polymaltose-induced FGF23 elevation complicated by hypophosphataemic osteomalacia. *Ann. Clin. Biochem.* 46, 167–169. doi: 10.1258/acb.2008.008151
- Schouten, B. J., Hunt, P. J., Livesey, J. H., Frampton, C. M., and Soule, S. G. (2009b). FGF23 elevation and hypophosphatemia after intravenous iron polymaltose: a prospective study. *J. Clin. Endocrinol. Metab.* 94, 2332–2337. doi: 10.1210/jc.2008-2396
- Shimada, T., Kakitani, M., Yamazaki, Y., Hasegawa, H., Takeuchi, Y., Fujita, T., et al. (2004). Targeted ablation of Fgf23 demonstrates an essential physiological role of FGF23 in phosphate and vitamin D metabolism. *J. Clin. Invest.* 113, 561–568. doi: 10.1172/JCI19081
- Shimada, T., Mizutani, S., Muto, T., Yoneya, T., Hino, R., Takeda, S., et al. (2001). Cloning and characterization of FGF23 as a causative factor of tumor-induced osteomalacia. *Proc. Natl. Acad. Sci. U.S.A.* 98, 6500–6505. doi: 10.1073/pnas.101545198
- Shimada, T., Muto, T., Urakawa, I., Yoneya, T., Yamazaki, Y., Okawa, K., et al. (2002). Mutant FGF-23 responsible for autosomal dominant hypophosphatemic rickets is resistant to proteolytic cleavage and causes hypophosphatemia in vivo. *Endocrinology* 143, 3179–3182. doi: 10.1210/endo.143.8.8795
- Shiozawa, Y., Jung, Y., Ziegler, A. M., Pedersen, E. A., Wang, J., Wang, Z., et al. (2010). Erythropoietin couples hematopoiesis with bone formation. *PLoS One* 5:e10853. doi: 10.1371/journal.pone.0010853
- Silvestri, L., Pagani, A., and Camaschella, C. (2008). Furin-mediated release of soluble hemojuvelin: a new link between hypoxia and iron homeostasis. *Blood* 111, 924–931. doi: 10.1182/blood-2007-07-100677
- Singbrant, S., Russell, M. R., Jovic, T., Liddicoat, B., Izon, D. J., Purton, L. E., et al. (2011). Erythropoietin couples erythropoiesis, B-lymphopoiesis, and bone homeostasis within the bone marrow microenvironment. *Blood* 117, 5631–5642. doi: 10.1182/blood-2010-11-320564
- Singer, S. T., Vichinsky, E. P., Sweeters, N., and Rachmilewitz, E. (2011). Darbepoetin alfa for the treatment of anaemia in alpha- or beta- thalassaemia intermedia syndromes. *Br. J. Haematol.* 154, 281–284. doi: 10.1111/j.1365-2141.2011.08617.x
- Singh, S., Grabner, A., Yanucil, C., Schramm, K., Czaya, B., Krick, S., et al. (2016). Fibroblast growth factor 23 directly targets hepatocytes to promote inflammation in chronic kidney disease. *Kidney Int.* 90, 985–996. doi: 10.1016/j.kint.2016.05.019
- Smith, E. R., Cai, M. M., McMahon, L. P., and Holt, S. G. (2012). Biological variability of plasma intact and C-terminal FGF23 measurements. *J. Clin. Endocrinol. Metab.* 97, 3357–3365. doi: 10.1210/jc.2012-1811
- Soares, M. P., and Weiss, G. (2015). The Iron age of host-microbe interactions. *EMBO Rep.* 16, 1482–1500. doi: 10.15252/embr.201540558
- Steer, K., Stavnickuk, M., Morris, M., and Komarova, S. V. (2017). Bone health in patients with hematopoietic disorders of bone marrow origin: systematic review and meta-analysis. *J. Bone Miner. Res.* 32, 731–742. doi: 10.1002/jbmr.3026
- Stefanova, D., Raychev, A., Arezes, J., Ruchala, P., Gabayan, V., Skurnik, M., et al. (2017). Endogenous hepcidin and its agonist mediate resistance to selected infections by clearing non-transferrin-bound iron. *Blood* 130, 245–257. doi: 10.1182/blood-2017-03-772715
- Suda, T. (2011). Hematopoiesis and bone remodeling. *Blood* 117, 5556–5557. doi: 10.1182/blood-2011-03-344127
- Sukpanichnant, S., Oparitkiattikul, N., Fucharoen, S., Tanphaichitr, V. S., Hasuiki, T., and Tatsumi, N. (1997). Difference in pattern of erythropoietin response between beta-thalassemia/hemoglobin E children and adults. *Southeast Asian J. Trop. Med. Public Health* 28(Suppl. 3), 134–137.
- Sun, H., Jung, Y., Shiozawa, Y., Taichman, R. S., and Krebsbach, P. H. (2012). Erythropoietin modulates the structure of bone morphogenetic protein 2-engineered cranial bone. *Tissue Eng. Part A* 18, 2095–2105. doi: 10.1089/ten.TEA.2011.0742
- Tagliabacci, V. S., Engel, J. L., Wiley, S. E., Xiao, J., Gonzalez, D. J., Nidumanda Appaiah, H., et al. (2014). Dynamic regulation of FGF23 by Fam20C phosphorylation, GalNAc-T3 glycosylation, and furin proteolysis. *Proc Natl Acad Sci U S A* 111, 5520–5525. doi: 10.1073/pnas.1402218111
- Taher, A. T., Musallam, K. M., Karimi, M., El-Beshlawy, A., Belhoul, K., Daar, S., et al. (2010). Overview on practices in thalassemia intermedia management aiming for lowering complication rates across a region of endemicity: the OPTIMAL CARE study. *Blood* 115, 1886–1892. doi: 10.1182/blood-2009-09-243154
- Toro, L., Barrientos, V., Leon, P., Rojas, M., Gonzalez, M., Gonzalez-Ibanez, A., et al. (2018). Erythropoietin induces bone marrow and plasma fibroblast growth factor 23 during acute kidney injury. *Kidney Int.* 93, 1131–1141. doi: 10.1016/j.kint.2017.11.018
- Tzoulis, P., Ang, A. L., Shah, F. T., Berovic, M., Prescott, E., Jones, R., et al. (2014). Prevalence of low bone mass and vitamin D deficiency in beta-thalassemia major. *Hemoglobin* 38, 173–178. doi: 10.3109/03630269.2014.905792
- Urakawa, I., Yamazaki, Y., Shimada, T., Iijima, K., Hasegawa, H., Okawa, K., et al. (2006). Klotho converts canonical FGF receptor into a specific receptor for FGF23. *Nature* 444, 770–774. doi: 10.1038/nature05315
- Vadakké Madathil, S., Coe, L. M., Casu, C., and Sitara, D. (2014). Klotho deficiency disrupts hematopoietic stem cell development and erythropoiesis. *Am. J. Pathol.* 184, 827–841. doi: 10.1016/j.ajpath.2013.11.016
- Valderrabano, R. J., and Wu, J. Y. (2018). Bone and blood interactions in human health and disease. *Bone* 119, 65–70. doi: 10.1016/j.bone.2018.02.019
- van Straaten, S., Verhoeven, J., Hagens, S., Schutgens, R., van Solinge, W., van Wijk, R., et al. (2018). Organ involvement occurs in all forms of hereditary haemolytic anaemia. *Br. J. Haematol.* doi: 10.1111/bjh.15575 [Epub ahead of print].
- Verga Falzacappa, M. V., Vujic Spasic, M., Kessler, R., Stolte, J., Hentze, M. W., and Muckenthaler, M. U. (2007). STAT3 mediates hepatic hepcidin expression and its inflammatory stimulation. *Blood* 109, 353–358. doi: 10.1182/blood-2006-07-033969
- Visnjic, D., Kalajzic, Z., Rowe, D. W., Katavic, V., Lorenzo, J., and Aguila, H. L. (2004). Hematopoiesis is severely altered in mice with an induced osteoblast deficiency. *Blood* 103, 3258–3264. doi: 10.1182/blood-2003-11-4011
- Wallquist, C., Mansouri, L., Norrback, M., Hylander, B., Jacobson, S. H., Larsson, T. E., et al. (2018). Associations of fibroblast growth factor 23 with markers of inflammation and leukocyte transmigration in chronic kidney disease. *Nephron* 138, 287–295. doi: 10.1159/000485472
- Wan, L., Zhang, F., He, Q., Tsang, W. P., Lu, L., Li, Q., et al. (2014). EPO promotes bone repair through enhanced cartilaginous callus formation and angiogenesis. *PLoS One* 9:e102010. doi: 10.1371/journal.pone.0102010
- Wang, C. Y., Core, A. B., Canali, S., Zumbrennen-Bullough, K. B., Ozer, S., Umans, L., et al. (2017). Smad1/5 is required for erythropoietin-mediated suppression of hepcidin in mice. *Blood* 130, 73–83. doi: 10.1182/blood-2016-12-759423
- Weidemann, A., Kerdiles, Y. M., Knaup, K. X., Rafie, C. A., Boutin, A. T., Stockmann, C., et al. (2009). The glial cell response is an essential component of hypoxia-induced erythropoiesis in mice. *J. Clin. Invest.* 119, 3373–3383. doi: 10.1172/JCI39378
- Wolf, M., Koch, T. A., and Bregman, D. B. (2013). Effects of iron deficiency anemia and its treatment on fibroblast growth factor 23 and phosphate homeostasis in women. *J. Bone Miner. Res.* 28, 1793–1803. doi: 10.1002/jbmr.1923
- Wolf, M., and White, K. E. (2014). Coupling fibroblast growth factor 23 production and cleavage: iron deficiency, rickets, and kidney disease. *Curr. Opin. Nephrol. Hypertens.* 23, 411–419. doi: 10.1097/01.mnh.0000447020.74593.6f
- Wong, P., Fuller, P. J., Gillespie, M. T., and Milat, F. (2016). Bone disease in Thalassemia: a molecular and clinical overview. *Endocr. Rev.* 37, 320–346. doi: 10.1210/er.2015-1105
- Xu, Y., Peng, H., and Ke, B. (2017). alpha-klotho and anemia in patients with chronic kidney disease patients: a new perspective. *Exp. Ther. Med.* 14, 5691–5695. doi: 10.3892/etm.2017.5287
- Yamamoto, H., Ramos-Molina, B., Lick, A. N., Prideaux, M., Albornoz, V., Bonewald, L., et al. (2016). Posttranslational processing of FGF23 in osteocytes during the osteoblast to osteocyte transition. *Bone* 84, 120–130. doi: 10.1016/j.bone.2015.12.055
- Yamashita, K., Mizuiri, S., Nishizawa, Y., Kenichiro, S., Doi, S., and Masaki, T. (2017). Oral iron supplementation with sodium ferrous citrate reduces the serum intact and c-terminal fibroblast growth factor 23 levels of maintenance haemodialysis patients. *Nephrology* 22, 947–953. doi: 10.1111/nep.12909



- Zachee, P., Staal, G. E., Rijksen, G., De Bock, R., Couttenye, M. M., and De Broe, M. E. (1989). Pyruvate kinase deficiency and delayed clinical response to recombinant human erythropoietin treatment. *Lancet* 1, 1327–1328. doi: 10.1016/S0140-6736(89)92718-9
- Zeidler, C., and Welte, K. (2007). Hematopoietic growth factors for the treatment of inherited cytopenias. *Semin. Hematol.* 44, 133–137. doi: 10.1053/j.seminhematol.2007.04.003
- Zoller, H., Schaefer, B., and Glodny, B. (2017). Iron-induced hypophosphatemia: an emerging complication. *Curr. Opin. Nephrol. Hypertens.* 26, 266–275. doi: 10.1097/MNH.0000000000000329

**Conflict of Interest Statement:** The authors declare that the research was conducted in the absence of any commercial or financial relationships that could be construed as a potential conflict of interest.

Copyright © 2019 van Vuren, Gaillard, Eisenga, van Wijk and van Beers. This is an open-access article distributed under the terms of the Creative Commons Attribution License (CC BY). The use, distribution or reproduction in other forums is permitted, provided the original author(s) and the copyright owner(s) are credited and that the original publication in this journal is cited, in accordance with accepted academic practice. No use, distribution or reproduction is permitted which does not comply with these terms.



# Red Blood Cell Membrane Conductance in Hereditary Haemolytic Anaemias

Polina Petkova-Kirova<sup>1</sup>, Laura Hertz<sup>2,3</sup>, Jens Danielczok<sup>2</sup>, Rick Huisjes<sup>4</sup>, Asya Makhro<sup>5</sup>, Anna Bogdanova<sup>5</sup>, Maria del Mar Mañú-Pereira<sup>6</sup>, Joan-Lluis Vives Corrons<sup>7</sup>, Richard van Wijk<sup>4</sup> and Lars Kaestner<sup>2,3\*</sup>

## OPEN ACCESS

### Edited by:

Philippe Connes,  
Université Claude Bernard Lyon 1,  
France

### Reviewed by:

Stéphane Egee,  
UMR8227 Laboratoire de Biologie  
Intégrative des Modèles Marins,  
France

John Stanley Gibson,  
University of Cambridge,  
United Kingdom

### \*Correspondence:

Lars Kaestner  
lars\_kaestner@me.com

### Specialty section:

This article was submitted to  
Red Blood Cell Physiology,  
a section of the journal  
Frontiers in Physiology

**Received:** 21 January 2019

**Accepted:** 21 March 2019

**Published:** 16 April 2019

### Citation:

Petkova-Kirova P, Hertz L,  
Danielczok J, Huisjes R, Makhro A,  
Bogdanova A, Mañú-Pereira MdM,  
Vives Corrons J-L, van Wijk R and  
Kaestner L (2019) Red Blood Cell  
Membrane Conductance  
in Hereditary Haemolytic Anaemias.  
Front. Physiol. 10:386.  
doi: 10.3389/fphys.2019.00386

<sup>1</sup> Institute of Molecular Cell Biology, Saarland University, Homburg, Germany, <sup>2</sup> Theoretical Medicine and Biosciences, Saarland University, Homburg, Germany, <sup>3</sup> Experimental Physics, Saarland University, Saarbrücken, Germany, <sup>4</sup> Department of Clinical Chemistry & Haematology, University Medical Center Utrecht, Utrecht, Netherlands, <sup>5</sup> Red Blood Cell Research Group, Institute of Veterinary Physiology, Vetsuisse Faculty, Zurich Center for Integrative Human Physiology (ZIHP), University of Zürich, Zurich, Switzerland, <sup>6</sup> Vall d'Hebron Research Institute, Vall d'Hebron University Hospital, Barcelona, Spain, <sup>7</sup> Red Blood Cell Defects and Hematopoietic Disorders Unit, Josep Carreras Leukaemia Research Institute, Barcelona, Spain

Congenital haemolytic anaemias are inherited disorders caused by red blood cell membrane and cytoskeletal protein defects, deviant hemoglobin synthesis and metabolic enzyme deficiencies. In many cases, although the causing mutation might be known, the pathophysiology and the connection between the particular mutation and the symptoms of the disease are not completely understood. Thus effective treatment is lagging behind. As in many cases abnormal red blood cell cation content and cation leaks go along with the disease, by direct electrophysiological measurements of the general conductance of red blood cells, we aimed to assess if changes in the membrane conductance could be a possible cause. We recorded whole-cell currents from 29 patients with different types of congenital haemolytic anaemias: 14 with hereditary spherocytosis due to mutations in  $\alpha$ -spectrin,  $\beta$ -spectrin, ankyrin and band 3 protein; 6 patients with hereditary xerocytosis due to mutations in Piezo1; 6 patients with enzymatic disorders (3 patients with glucose-6-phosphate dehydrogenase deficiency, 1 patient with pyruvate kinase deficiency, 1 patient with glutamate-cysteine ligase deficiency and 1 patient with glutathione reductase deficiency), 1 patient with  $\beta$ -thalassemia and 2 patients, carriers of several mutations and a complex genotype. While the patients with  $\beta$ -thalassemia and metabolic enzyme deficiencies showed no changes in their membrane conductance, the patients with hereditary spherocytosis and hereditary xerocytosis showed largely variable results depending on the underlying mutation.

**Keywords:** haemolytic anemia, patch-clamp, electrophysiology, hereditary spherocytosis, hereditary xerocytosis

## INTRODUCTION

Haemolytic anaemias, characterized by the abnormal breakdown of red blood cells (RBCs), could be either acquired or inherited. The latter are a diverse group of diseases that could be classified based on the affected RBC component into membranopathies, haemoglobinopathies, and enzymopathies (Dhaliwal et al., 2004). Membranopathies are presented by hereditary spherocytosis (HS), hereditary elliptocytosis (HE) and its aggravated form pyropoikilocytosis (HPP) with defective structural membrane and cytoskeletal proteins (Iolascon et al., 2003) and by the largely heterogeneous group of stomatocytosis divided in a most general way, but not exhaustively, into overhydrated stomatocytosis (OHSt), cryohydrocytosis (CHC) and some types of familial pseudohyperkalaemia (FP) (overhydrated RBCs) and dehydrated stomatocytosis (DHSt) (hereditary xerocytosis (HX)) (dehydrated RBCs) with defective ion channels or transporters (Iolascon et al., 2003; Bruce et al., 2009). Haemoglobinopathies are presented by  $\beta$ -thalassemia (Cao and Galanello, 2010) and sickle cell disease (Ware et al., 2017) with defective hemoglobin and enzymopathies are presented most commonly by glucose-6-phosphate dehydrogenase deficiency (G6PD) (Luzzatto et al., 2016) and pyruvate kinase deficiency (PKD) (Zanella et al., 2005) but also by glutamate-cysteine ligase ( $\gamma$ -glutamylcysteine synthetase) (GCL) deficiency (Ristoff and Larsson, 1998) and glutathione reductase deficiency (van Zwieten et al., 2014). Although much is known so far, especially regarding the defective genes related to hereditary haemolytic anaemias, there are still questions, whose answers would lead to a much better understanding of the disease and possibly to a more effective treatment. A recurrent issue is if a changed membrane conductance, resulting from primary mutated channels or secondary adapted ones, does contribute to the various phenotypes. Most of the research has been done on membranopathies, understandable, primarily on the ones linked to mutations in ion channels or transporters such as band 3 protein, Rh-associated glycoprotein (RhAG), the glucose transporter GLUT1, Piezo1 and the Gardos channel (KCNN4) and accompanied by abnormal RBC cation content and disrupted volume homeostasis (Badens and Guizouarn, 2016). However, although on most occasions, the RBC cation content linked to the particular mutation has been extensively described (e.g., Stewart et al., 2011 for R730C in band 3 protein or Fermo et al., 2017 for R352H in the Gardos channel) and the defective channels, when known, expressed and studied in heterologous systems (e.g., Glogowska et al., 2017 for a number of Piezo1 mutations) with a few exceptions (Stewart et al., 2011; Andolfo et al., 2013; Shmukler et al., 2014; Fermo et al., 2017; Rotordam et al., 2018), direct electrophysiological measurements of membrane conductance in mutated RBCs have been scarce.

Thus, within the CoMMiTMenT project, by direct RBCs electrophysiological measurements in physiological solutions, we aimed to investigate whether RBC membrane conductance changes are accompanying HS due to mutations in the SPTA1 gene (coding for  $\alpha$ -spectrin), SPTB ( $\beta$ -spectrin), ANK1 (ankyrin), and SLC4A1 (band 3 protein); HX due to mutations in PIEZO1; enzymatic disorders due to glucose-6-phosphate dehydrogenase

deficiency (G6PD), pyruvate kinase deficiency (PKD), glutamate-cysteine ligase ( $\gamma$ -glutamylcysteine synthetase) (GCL) deficiency, glutathione reductase deficiency and  $\beta$ -thalassemia.

## MATERIALS AND METHODS

### Patients

Patients diagnosed with different types of haemolytic anemia were enrolled in the study after signing an informed consent. Patients' data were handled anonymously as outlined in the ethics agreements. These agreements were approved by the Medical Ethical Research Board (MERB) of the University Medical Center Utrecht, the Netherlands (UMCU) under reference code 15/426M "Disturbed ion homeostasis in hereditary hemolytic anemia" and by the Ethical Committee of Clinical Investigations of Hospital Clinic, Spain (IDIBAPS) under reference code 2013/8436. Exclusion criteria were erythrocyte transfusion in the past 90 days, age below 3 years and/or bodyweight lower than 18 kg. Blood from healthy control donors was anonymously obtained using the approved medical ethical protocol of 07/125 Mini Donor Dienst, also approved by the MERB of UMCU. The blood of the patient/patients and the healthy donor anti-coagulated in heparin was shipped overnight from the University Medical Center Utrecht (Utrecht, Netherlands) or from Institut d'Investigacions Biomèdiques August Pi i Sunyer/Hospital Clínic de Barcelona (Barcelona, Spain) to Saarland University (Homburg, Germany) without additional cooling as previously tested/simulated (Makhro et al., 2016). All patients included in the study were genetically screened for mutations by next-generation sequencing and diagnosed with the following types of anemia: 14 patients were diagnosed with HS (due to mutations in  $\alpha$ -spectrin,  $\beta$ -spectrin, ankyrin and band 3 protein), using golden standard techniques (EMA-binding, osmotic gradient ektacytometry and osmotic fragility test), 6 patients were diagnosed with hereditary xerocytosis (due to mutations in Piezo 1), 6 patients had enzymatic disorders (3 patients with glucose-6-phosphate dehydrogenase deficiency, 1 patient with pyruvate kinase deficiency, 1 patient with glutamate-cysteine ligase deficiency and 1 patient with glutathione reductase deficiency), 1 patient had  $\beta$ -thalassemia and 2 were carriers of several mutations and a complex genotype. The genotype of the patients with HS, HX and of the two patients with several mutations is given in **Table 1**. The numbering of the patients and the corresponding healthy controls is kept consistent with previous research (Hertz et al., 2017) studying the same patient group.

### Patch Clamp Analysis

Patch-clamp whole-cell measurements were performed with a NPC-16 Patchliner (Nanion Technologies, Munich, Germany) as previously described (Petkova-Kirova et al., 2018). Briefly, the resistance of the chips was between 5 and 8 M $\Omega$  with internal and external solutions as follows (in mM): KCl 70, KF 70, NaCl 10, HEPES 10, EGTA 3, CaCl<sub>2</sub> 1.2 to give free [Ca<sup>2+</sup>]<sub>i</sub> = 120 nM, pH = 7.2 adjusted with KOH (internal) and NaCl 140, KCl 4, MgCl<sub>2</sub> 5, CaCl<sub>2</sub> 2, D-glucose 5, HEPES 10, pH = 7.3 adjusted

**TABLE 1** | Patients overview.

| Patient                | Clinical presentation                    | Genotype  | Current compared to transportation control                           | Current compared to general control    |
|------------------------|--|---|--|--|
| <b>P18.1</b>           | <b>HS (<math>\alpha</math>-spectrin)</b> | <b>c.2755G &gt; T (p.Glu919); <math>\alpha^{\text{LELY}}</math></b>                   | <b>Current <math>\uparrow</math></b>                                 | <b>Current <math>\uparrow</math></b>   |
| <b>P19.1</b>           | <b>HS (<math>\alpha</math>-spectrin)</b> | <b>c.678G &gt; A (p.Glu227fs); <math>\alpha^{\text{LELY}}</math></b>                  | <b>Current <math>\uparrow</math> (not statistically significant)</b> | <b>Current <math>\uparrow</math></b>   |
| P15.1                  | HS ( $\alpha$ -spectrin)                 | c.4339-99C > T p.(?)  | No change  | No change                              |
| P20.1                  | HS ( $\alpha$ -spectrin)                 | c.[4339-99C > T; c.4347G > T] p.[(?; Lys1449Asn)]                                     | No change  | No change                              |
| P17.1 (splenectomized) | HS (ankyrin)                             | c.341C > T (p.Pro114Leu)  | Current $\downarrow$ *   | No change                              |
| P17.2                  | HS (ankyrin)                             | c.341C > T (p.Pro114Leu)  | Current $\downarrow$ *   | No change                              |
| P11.1                  | HS (ankyrin)                             | c.1943delC;c.2042delC (p.Ala648fs;p.Ala681fs)   | No change  | No change                              |
| P13.1                  | HS (ankyrin)                             | c.344T > C (p.Leu115Pro)  | No change  | No change                              |
| P13.2                  | HS (ankyrin)                             | c.344T > C (p.Leu115Pro)  | No change  | No change                              |
| P14.1                  | HS (ankyrin)                             | c.2559-2A > G (splicing)  | No change  | No change                              |
| P10.1                  | HS ( $\beta$ -spectrin)                  | c.2470C > T (p.Gln824)  | Outward current $\downarrow\downarrow$ *                             | No change                              |
| P21.1                  | HS ( $\beta$ -spectrin)                  | c.3449G > A (p.Trp1150)   | No change  | No change                              |
| P12.1                  | HS (band 3 protein)                      | c.2348T > A (p.Ile783Asn)   | Current $\downarrow$   | Inward current $\downarrow$            |
| P16.1                  | HS (band 3 protein)                      | c.2057 + 1G > A (splicing)  | No change  | No change                              |
| <b>P11.1</b>           | <b>SPTB</b>                              | <b>c.154delC; p.Arg52fs + RHAG c.808G &gt; A; p.Val270Ile</b>                         | <b>Current <math>\uparrow</math></b>                                 | <b>Current <math>\uparrow</math></b>   |
| <b>P22.1</b>           | <b>SPTA1</b>                             | <b>c.460_462dupTTG; p.Leu154dup + PKLR c.1687G &gt; A; p.Gly563Ser + del3.7Kb HBA</b> | <b>Current <math>\uparrow</math></b>                                 | <b>Current <math>\uparrow</math></b>   |
| Family 1               |  |   |  |  |
| P51.3                  | HX                                       | c. 7367G > A p.Arg2456His   | No change  | No change                              |
| P51.4                  | HX                                       | c. 7367G > A p.Arg2456His   | No change  | No change                              |
| Family 2               |  |   |  |  |
| P53.3                  | HX                                       | c. 6262C > G, p. Arg2088Gly   | No change  | No change                              |
| P53.2                  | HX                                       | c. 6262C > G, p. Arg2088Gly   | No change  | No change                              |
| Family 3               |  |   |  |  |
| P50.2                  | HX                                       | c.1276T > C p. Cys426Arg  | No change  | Outward current $\uparrow$ *           |
| Family 4               |  |   |  |  |
| <b>P52.1</b>           | <b>HX</b>                                | <b>c.7483_7488dupCTGGAG p.2495_2496dupLeuGlu</b>                                      | <b>Current <math>\downarrow</math></b>                               | <b>Current <math>\downarrow</math></b> |
| P40.1                  | G6PD                                     |   | No change  | No change                              |
| P41.1                  | G6PD                                     |   | No change  | No change                              |
| P42.1                  | G6PD                                     |   | No change  | No change                              |
| P43.1                  | GCLD                                     |   | No change  | No change                              |
| P44.1                  | GRD                                      |   | No change  | No change                              |
| P45.1                  | PKD                                      |   | No change  | No change                              |
| P60.1                  | $\beta$ -thalassemia                     |   | No change  | No change                              |

An upward arrow indicates an increase in current and a downward arrow indicates a decrease in current compared to the respective control. Two arrows label an extreme change in the designated direction. Patients that show a change in current compared to both the transportation and a general control are given in bold. Asterisks mark a deviation commented on in the main text. HS, hereditary spherocytosis; SPTB,  $\beta$ -spectrin; SPTA1,  $\alpha$ -spectrin; HX, hereditary xerocytosis; GCLD, glutamate-cysteine ligase deficiency; GRD, glutathione reductase deficiency; PKD, pyruvate kinase deficiency.

with NaOH (external). Gigaseals were considered successful if exceeding 5 G $\Omega$ . Gigaseal formation was facilitated by the use of a seal enhancing solution as recommended by the Patchliner manufacturer and containing (in mM): NaCl 80, KCl 3, MgCl<sub>2</sub> 10, CaCl<sub>2</sub> 35, HEPES 10, pH = 7.3 adjusted with NaOH. Whole-cell configuration was achieved by negative pressure suction pulses between -45 mbar and -150 mbar and its formation judged by the appearance of sharp capacitive transients. Whole-cell patch-clamp recordings were conducted at room temperature using

voltage steps from -100 to 100 mV for 500 ms in 20 mV increments at 5 s intervals, the holding potential being set at -30 mV. Data are presented as current density (current divided by capacitance, the latter estimated at the time of attaining the whole-cell configuration and by using a short test pulse of 10 mV, 5 ms) and given as means  $\pm$  SEMs ( $n$  denotes number of cells and  $N$  – number of patients). Significant differences are determined based on an unpaired  $t$ -test and Welch's correction for unequal variances, when needed, with \* denoting  $p < 0.05$ .



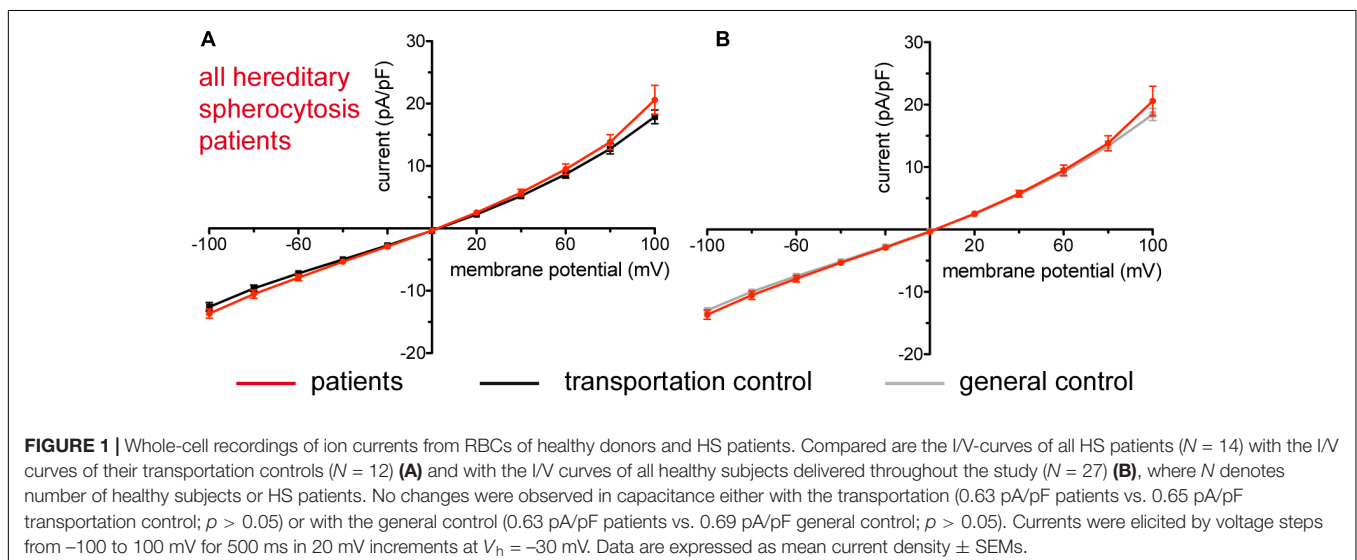
## RESULTS

Whole-cell patch clamp measurements were performed to assess possible differences in the membrane conductance of hereditary anemia patients compared to healthy controls. Regarding controls, we have compared the currents measured from the RBCs of our patients once with their transportation control, i.e., currents measured from the RBCs of a healthy subject, whose blood was delivered together with the blood of the patient, and once with a general, pooled, control, i.e., currents measured from the cells of all healthy subjects delivered throughout the study (Table 1). The rationale for this 'double comparison' is provided in the discussion. Throughout the whole study, accordingly in the manuscript, the abbreviation "P" stands for patient and "C" stands for a control, healthy subject.

### Hereditary Spherocytosis

Studied were patients with pathogenic mutations in *SPTA1* ( $\alpha$ -spectrin) (4 patients: P15.1, P18.1, P19.1, P20.1), *SPTB* ( $\beta$ -spectrin) (2 patients: P10.1 and P21.1), *ANK1* (ankyrin) (6 patients: P11.1, P13.1, P13.2, P14.1, P17.1, and P17.2), and *SLC4A1* (band 3 protein) (2 patients: P12.1 and P16.1), whose blood was delivered and, respectively, recorded from together with the blood of a healthy subject (transportation control). While no changes in the membrane conductance, nor in membrane capacitance (0.69 pA/pF general control vs. 0.63 pA/pF patients,  $p > 0.05$ ; 0.65 pA/pF transportation control vs. 0.63 pA/pF patients;  $p > 0.05$ ) were revealed with patients taken altogether (Figure 1), differences were observed in certain patients' groups as well as linked to particular mutations (Figures 3–5). Thus patients with mutations in *SPTA1* (4 patients), showed no significant differences compared to healthy controls delivered at the same days (4 healthy subjects) (Figure 2A) or compared to a control pooled over all healthy subjects included in the study (27 healthy subjects) (Figure 2B). Capacitances were not different either (0.67 pA/pF patients vs. 0.68 pA/pF transportation control,  $p > 0.05$ ; 0.67 pA/pF patients

vs. 0.69 pA/pF general control;  $p > 0.05$ ). However, the two patients, heterozygous for the *SPTA1* mutation and carrying at the same time an  $\alpha^{\text{LELY}}$  allele showed an increase in their inward current (Figure 3). Figures 3Aa,Ba consider the particular *SPTA1*  $\alpha^{\text{LELY}}$  patients [patient P18.1 (10 cells) and patient P19.1 (6 cells), respectively] vs. their transportation controls [C18 (6 cells) and C19 (7 cells), respectively]. Figures 3Ab,Bb compare the particular *SPTA1*  $\alpha^{\text{LELY}}$  patients [P18.1 (10 cells) and P19.1 (6 cells) vs. a control pooled over all the cells of all healthy subjects included in the study (175 cells)]. Figures 3Ac,Ad,Bc,Bd present raw current traces recorded from the RBCs of a healthy subject (Figures 3Ac,Bc), P18.1 (Figure 3Ad), and P19.1 (Figure 3Bd). None of the two patients showed any difference in capacitance compared with the general or with its transportation control (0.59 pA/pF P18.1 vs. 0.74 pA/pF C18,  $p > 0.05$ ; 0.59 pA/pF P18.1 vs. 0.69 pA/pF general control,  $p > 0.05$ ; 0.66 pA/pF P19.1 vs. 0.58 pA/pF C19,  $p > 0.05$ ; 0.66 pA/pF P19.1 vs. 0.69 pA/pF general control,  $p > 0.05$ ). Furthermore, while HS patients with underlying defects in *ANK1* (6 patients) showed no significant differences neither in their currents, nor in their capacitances (0.67 pA/pF patients vs. 0.63 pA/pF transportation control,  $p > 0.05$ ; 0.67 pA/pF patients vs. 0.69 pA/pF general control;  $p > 0.05$ ) compared to the control group [Figure 4Aa considered are the control healthy subjects delivered together with the patients (4 healthy subjects) and Figure 4Ab considered are all healthy subjects included in the study (27 healthy subjects)], there was a family of patients P17.1 (splenectomized) and P17.2 (with spleen) in whom an *ANK1* mutation [c.341C > T (p.Pro114Leu)] was associated with a decreased membrane conductance when compared to their own controls (Figures 4Ba,Ca, respectively) but not when compared to the pooled control of all healthy cells (Figures 4Bb,Cb, respectively). Comparison of the capacitances of P17.1 and P17.2 with their controls as well as the capacitance of C17 with the general control is as follows: 0.67 pA/pF P17.1 vs. 0.525 pA/pF C17,  $p > 0.05$ ; 0.67 pA/pF P17.1 vs. 0.69 pA/pF general control,  $p > 0.05$ ; 0.62 pA/pF P17.2 vs. 0.525 pA/pF C17,  $p > 0.05$ ; 0.62 pA/pF P17.2 vs. 0.69 pA/pF general control,



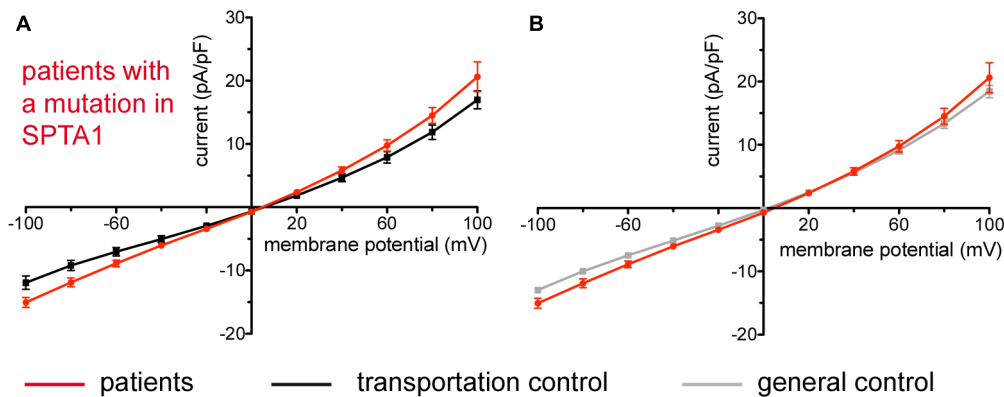


**FIGURE 2 |** Whole-cell recordings of ion currents from RBCs of healthy donors and HS patients with  $\alpha$ -spectrin mutations. Compared are the I/V-curves of all HS patients with  $\alpha$ -spectrin mutations ( $N = 4$ ) with the I/V curves of their own transportation controls ( $N = 4$ ) (A) and with the I/V curves of all healthy subjects delivered throughout the study ( $N = 27$ ) (B), where  $N$  denotes the number of healthy subjects or HS patients. No changes were observed in capacitance either with the transportation (0.67 pA/pF patients vs. 0.68 pA/pF control;  $p > 0.05$ ) or with the general control (0.67 pA/pF patients vs. 0.69 pA/pF control;  $p > 0.05$ ). Currents were elicited by voltage steps from  $-100$  to  $100$  mV for  $500$  ms in  $20$  mV increments at  $V_h = -30$  mV. Data are expressed as mean current density  $\pm$  SEMs.

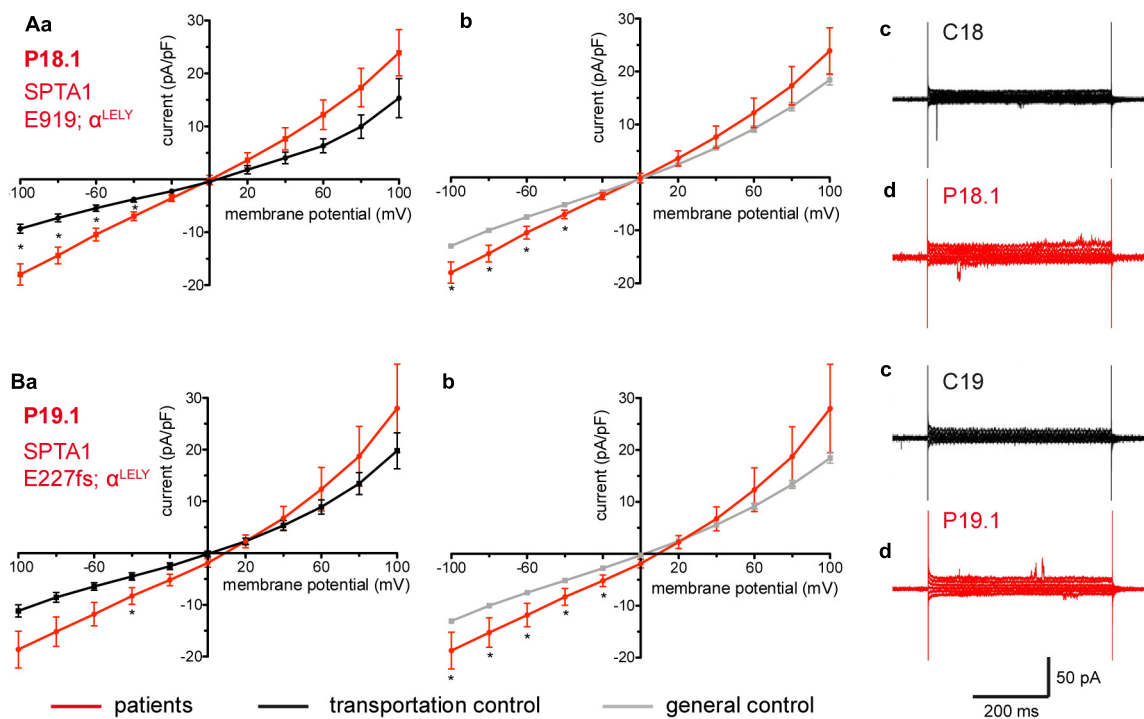


**FIGURE 3 |** Whole-cell recordings of ion currents from RBCs of healthy donors and HS patients with  $\alpha$ -spectrin mutations and carrying at the same time an  $\alpha^{\text{LELY}}$  allele. Compared are the I/V curves of P18.1 ( $n = 10$ ) with its own transportation control C18 ( $n = 6$ ) (Aa) as well as with a general control ( $n = 175$ ) (Ab), where  $n$  denotes the number of cells from the patient or the controls. As examples raw current traces recorded from the RBCs of a healthy donor (C18), whose blood was delivered together with the blood of P18.1 (Ac) and of patient P18.1 (Ad) are presented. Capacitances were not any different either with the transportation control (0.59 pA/pF P18.1 vs. 0.74 pA/pF C18;  $p > 0.05$ ) or with the general control (0.59 pA/pF patient vs. 0.69 pA/pF control;  $p > 0.05$ ). Compared are the I/V curves of P19.1 ( $n = 6$ ) with its own transportation control C19 ( $n = 7$ ) (Ba) as well as with a general control ( $n = 175$ ) (Bb), where  $n$  denotes the number of cells from the patient or the controls. As examples raw current traces recorded from the RBCs of a healthy donor (C19), whose blood was delivered together with the blood of P19.1 (Bc) and of patient P19.1 (Bd) are presented. Capacitances were not any different either with the transportation control (0.66 pA/pF P19.1 vs. 0.58 pA/pF C19;  $p > 0.05$ ) or with the general control (0.66 pA/pF patient vs. 0.69 pA/pF general control;  $p > 0.05$ ). Significant differences are determined based on an unpaired  $t$ -test with \* representing  $p < 0.05$ . Mutations below patients numbers are designated as amino acid substitutions in the respective protein. The label  $\alpha^{\text{LELY}}$  next to the mutation stands for the presence of an  $\alpha^{\text{LELY}}$  allele in the corresponding patient.

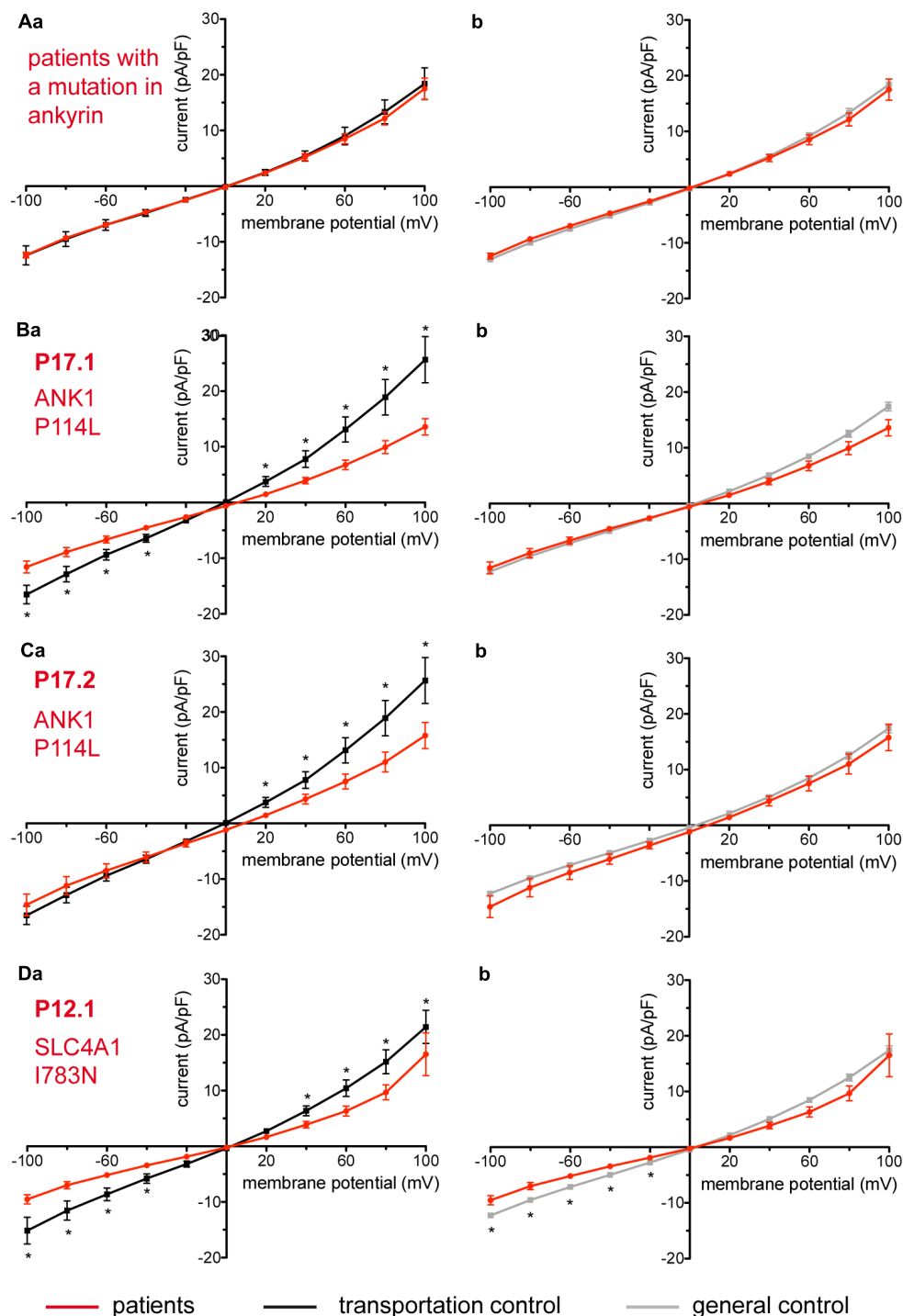


**FIGURE 4 |** Whole-cell recordings of ion currents from RBCs of healthy donors and HS patients with ankyrin mutations (A–C). Compared are the I/V-curves of all HS patients with ankyrin mutations ( $N = 6$ ) with the I/V curves of their own transportation controls ( $N = 4$ ) (Aa) and with the I/V curves of all healthy subjects delivered throughout the study ( $N = 27$ ) (Ab), where  $N$  denotes the number of healthy subjects or HS patients. No changes were observed in capacitance either with the transportation (0.67 pA/pF patients vs. 0.63 pA/pF transportation control;  $p > 0.05$ ) or with the general control (0.67 pA/pF patients vs. 0.69 pA/pF general control;  $p > 0.05$ ). Compared are the I/V curves of P17.1 ( $n = 13$ ) and its own transportation control C17 ( $n = 6$ ) (Ba) and the I/V curves of P17.2 ( $n = 11$ ) with its own transportation control C17 ( $n = 6$ ) (Ca), where  $n$  denotes the number of cells from the patient or the control. (Bb,Cb) Compare the I/V curve of a general control based on currents recorded from all cells of all healthy subjects delivered throughout the study ( $n = 175$ ) with the I/V curve of P17.1 ( $n = 13$ ) (Bb) and P17.2 ( $n = 11$ ) (Cb) ( $n$  denotes number of cells).

(Continued)

**FIGURE 4 | Continued**

Both patients 17.1 and 17.2 showed no differences in capacitance either with their transportation or with the general control (0.67 pA/pF P17.1 vs. 0.525 pA/pF C17,  $p > 0.05$ ; 0.67 pA/pF P17.1 vs. 0.69 pA/pF general control,  $p > 0.05$ ; 0.62 pA/pF P17.2 vs. 0.525 pA/pF C17,  $p > 0.05$ ; 0.62 pA/pF P17.2 vs. 0.69 pA/pF general control,  $p > 0.05$ ). However, a difference was uncovered between C17 and the general control (0.525 pA/pF C17 vs. 0.69 pA/pF general control;  $p < 0.05$ ). Whole-cell recordings of ion currents from RBCs of a healthy donor and a HS patient with band 3 protein mutation (**D**). Compared are the I/V curves of P12.1 ( $n = 17$ ) with its own transportation control C12 ( $n = 7$ ) (**Da**) as well as with a general control ( $n = 175$ ) (**Db**), where  $n$  is the number of cells of the patient or the controls. No changes were observed in capacitance either with the transportation (0.65 pA/pF P12.1 vs. 0.59 pA/pF C12;  $p > 0.05$ ) or with the general control (0.65 pA/pF P12.1 vs. 0.69 pA/pF general control;  $p > 0.05$ ). Currents were elicited by voltage steps from  $-100$  to  $100$  mV for 500 ms in 20 mV increments at  $V_h = -30$  mV. Data are expressed as mean current density  $\pm$  SEMs. Significant differences are determined based on an unpaired  $t$ -test with \* representing  $p < 0.05$ . Mutations below patients numbers are designated as amino acid substitutions in the respective protein.

$p > 0.05$ ; 0.525 pA/pF C17 vs. 0.69 pA/pF general control;  $p < 0.05$ . Moreover a patient with a band 3 protein mutation [SLC4A1 (2348T > A, Ile783Asn), P12.1 showed a decreased current compared to its own, transportation, control (C12) and to a pooled general control (**Figures 4Da,b**, respectively)]. No difference was found when the capacitance of the patient was compared with that of the general or the transportation control (0.65 pA/pF P12.1 vs. 0.59 pA/pF C12,  $p > 0.05$ ; 0.65 pA/pF P12.1 vs. 0.69 pA/pF general control,  $p > 0.05$ ). Out of the two patients with SPTB mutations (P10.1 and P21.1) (**Figures 5A,Ba,b**) one patient, P10.1, showed a significantly different conductance compared to its transportation control C10 (**Figure 5Ba**). However, based on the fact that P10.1 showed no difference with the general control (**Figure 5Bb**) and that P21.1 showed no difference either with its transportation control (**Figure 5Aa**) or with the general control (**Figure 5Ab**) as well as on the fact that C10 is very different from the general, pooled control (an outlier according to the Grubbs' test) (**Figure 5Bc**), we conclude that patients with  $\beta$ -spectrin mutations show no changes in their current. Comparison of capacitances of P21.1 and P10.1 with their controls as well as the capacitance of C10 with the general control is as follows: 0.63 pA/pF P21.1 vs. 0.69 pA/pF C21,  $p > 0.05$ ; 0.63 pA/pF P21.1 vs. 0.69 pA/pF general control,  $p > 0.05$ ; 0.68 pA/pF P10.1 vs. 0.82 pA/pF C10,  $p < 0.05$ ; 0.68 pA/pF P10.1 vs. 0.69 pA/pF general control,  $p > 0.05$ ; 0.82 pA/pF C10 vs. 0.69 pA/pF general control;  $p < 0.05$ . C10 shows a significantly increased capacitance compared to P10.1 as well as to the general control.

Two additional patients P11.1 and P22.1, carriers of several mutations and a complex genotype (*SPTB* c.154delC; p.Arg52fs + *RHAG* c.808G > A; p.Val270Ile and *SPTA1* c.460\_462dupTTG; p.Leu154dup + *PKLR* c.1687G > A; p.Gly563Ser + del3.7Kb *HBA*, respectively) show an increase in their currents (**Figures 6A,B**, respectively). The capacitances of none of the patients show any difference with their controls (0.59 pA/pF P11.1 vs. 0.66 pA/pF C11,  $p > 0.05$ ; 0.59 pA/pF P11.1 vs. 0.69 pA/pF general control,  $p > 0.05$ ; 0.61 pA/pF P22.1 vs. 0.64 pA/pF C22,  $p > 0.05$ ; 0.61 pA/pF P22.1 vs. 0.69 pA/pF general control,  $p > 0.05$ ).

## Hereditary Xerocytosis

Considered were 4 families with mutations in the *PIEZO1* gene (Family 1 with patients P51.3 and P51.4; Family 2 with P53.2 and P53.3; Family 3 with P50.2 and Family 4 with P52.1), whose blood was delivered and recorded from, together with the blood of a healthy subject (transportation control) (C51,

C53, C50, and C52, respectively). No changes in the membrane conductance or in the membrane capacitance were revealed with patients taken altogether (**Figure 7A**) as well as in two families (Family1 (P51.3 and P51.4) and Family 2 (P53.2 and P53.3) compared both to their transportation controls and to a general control (**Figures 7Ba,b,Ca,b**, respectively). However, P50.2 (Family 3), although showing no difference with its transportation control (**Figure 8Aa**), demonstrated increased conductance compared to the general, pooled, control (**Figure 8Ab**). There was also a family (Family 4 with P52.1) in which the *Piezo1* mutation (c.7483\_7488dupCTGGAG p.2495\_2496dupLeuGlu) was associated with a decreased conductance compared both to the transportation and to the general, pooled, control (**Figures 8Ba,b**, respectively). Both Family 3 and Family 4 did not show a change in their capacitance compared to their transportation or to the general control.

## Enzymopathies

Considered were 6 patients with enzymatic disorders as follows: 3 patients with glucose-6-phosphate dehydrogenase deficiency (P40.1, P41.1, and P42.1), 1 patient with pyruvate kinase deficiency (P45.1), 1 patient with glutamate-cysteine ligase deficiency (P43.1) and 1 patient with glutathione reductase deficiency (P44.1). None of the patients showed a difference in their membrane conductance or capacitance compared to a general or their own transportation control (**Figures 9, 10**).

## Beta-Thalassemia

The patient (P60.1) with  $\beta$ -thalassemia showed no difference in its membrane conductance or membrane capacitance either compared to a general or to its own, transportation, control (**Figure 11**).

## DISCUSSION

### Hereditary Spherocytosis

Electrophysiological measurements revealed additional new characteristics for HS and confirmed the heterogeneity of the disease showing that changes in membrane conductance are not an overall feature of the disease but depend on the particular, specific mutation (Huisjes et al., unpublished).

Interesting is that out of the many patients with *SPTA1* mutations it is the two patients carrying a *SPTA1*  $\alpha^{\text{LELY}}$



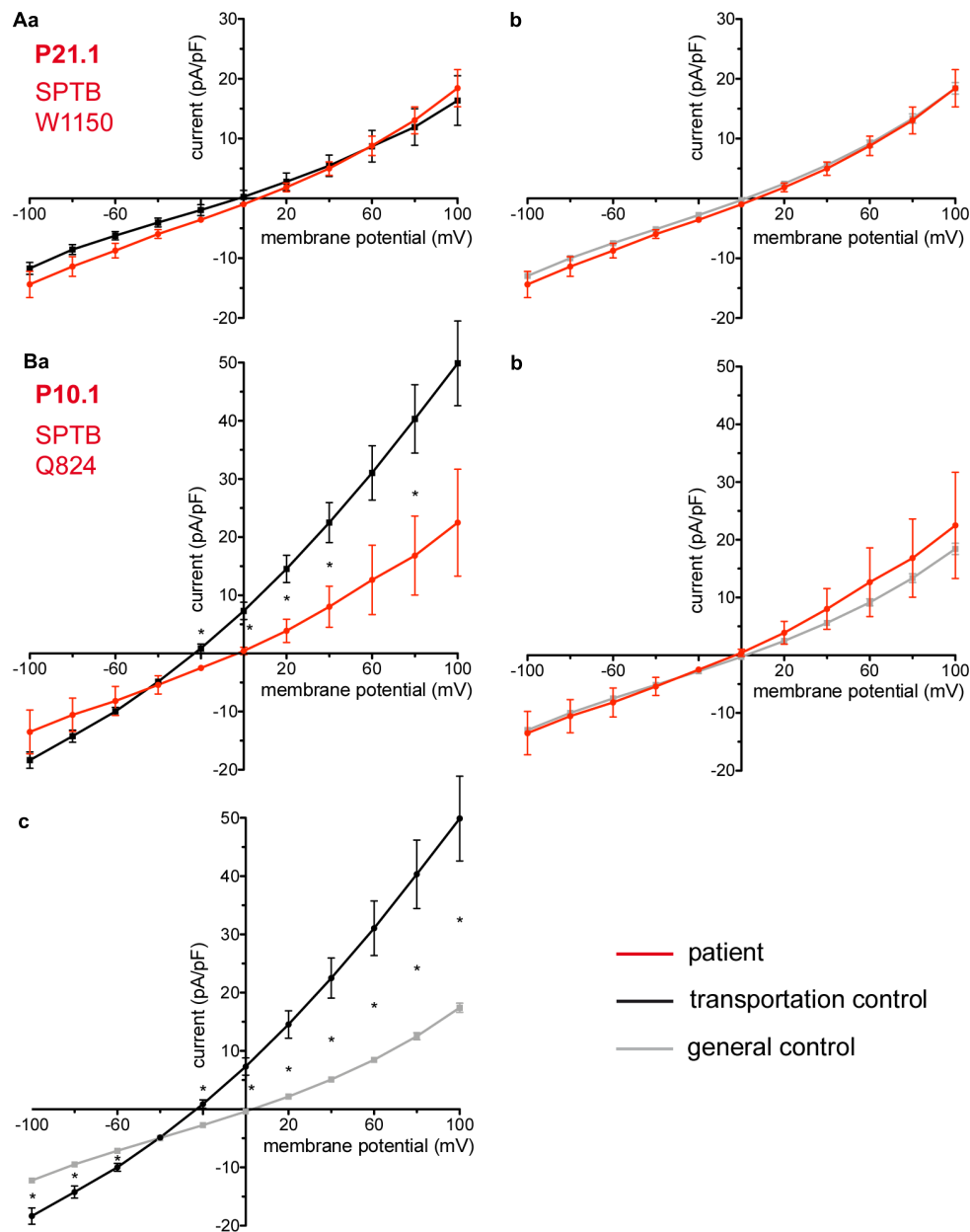
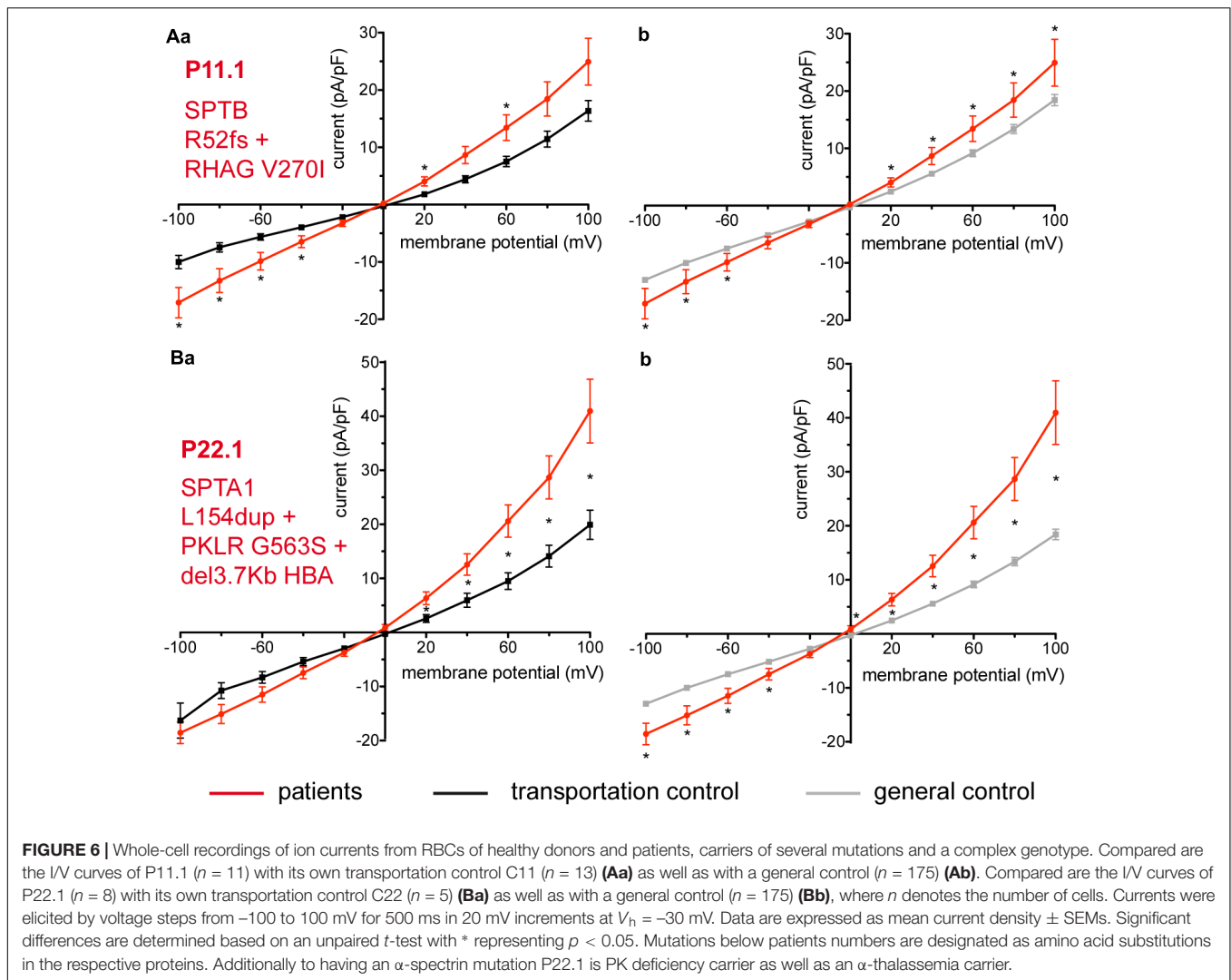


**FIGURE 5 |** Whole-cell recordings of ion currents from RBCs of healthy donors and HS patients. Whole-cell recordings of ion currents from RBCs of healthy donors and HS patients with  $\beta$ -spectrin mutations (**Aa,Ba,b**). Compared are the I/V curves of P21.1 ( $n = 8$ ) with its own transportation control C21 ( $n = 5$ ) (**Aa**) as well as with a general control ( $n = 175$ ) (**Ab**). Compared are the I/V curves of P10.1 ( $n = 3$ ) with its own transportation control C10 ( $n = 6$ ) (**Ba**) as well as with a general control ( $n = 175$ ) (**Bb**). (**Bc**) Compares the I/V curve of the transportation control of P10.1, C10 ( $n = 6$ ) with a general control ( $n = 175$ ), where  $n$  denotes the number of cells. Currents were elicited by voltage steps from  $-100$  to  $100$  mV for  $500$  ms in  $20$  mV increments at  $V_h = -30$  mV. Data are expressed as mean current density  $\pm$  SEMs. Significant differences are determined based on an unpaired  $t$ -test with \* representing  $p < 0.05$ . Mutations below patients numbers are designated as amino acid substitutions in the respective protein.

allele that show a change in their membrane conductance: an increase in their inward current. This holds true for P18.1 vs. its own transportation control and vs. the general control of 175 cells and also for patient P19.1 vs. the pooled control. Although not reaching statistical significance the inward current of P19.1 compared to its

own transportation control is also increased. Evident are the large variations within the cells of the patients for both patient P18.1 and P19.1 but especially for P19.1. This might explain why the difference in the inward current between P19.1 and its transportation control does not reach a statistical significance.



Allele  $\alpha^{\text{LELY}}$  is a common polymorphic allele and its presence in humans is by itself asymptomatic. The  $\alpha^{\text{LELY}}$  allele, however, plays the role of an exacerbating factor when it occurs in trans to an  $\alpha$ -spectrin mutation resulting in a disastrously weak spectrin network (Viel and Branton, 1996; Iolascon et al., 2003). This is because, due to their reduced ability to form dimers,  $\alpha$  chains from  $\alpha^{\text{LELY}}$  alleles are underrepresented in the mature RBC cytoskeleton. Accordingly underrepresented are any spectrin mutations found on the same allele and in turn overrepresented if found on the opposite allele (Wilmutte et al., 1997). How a destabilized cytoskeleton might have an effect on membrane conductance is a subject of speculations but as the RBC membrane has little structural integrity without the support of an intact and steady protein scaffold below, it might be that conformational changes influence the proper functioning of channels and lead to increased membrane conductance.

Noteworthy, in many cases, aggravating conditions such as an  $\alpha^{\text{LELY}}$  allele or a superimposed erythrocytic defect lead to an enhanced membrane conductance and a leaky cell. Thus P11.1 with a mutation in  $\beta$ -spectrin as well as a mutation in RHAG and

P22.1 with a mutation in  $\alpha$ -spectrin as well as being a pyruvate kinase deficiency and a thalassemia carrier show an increase both in their inward and outward current. While in the case of P22.1 such an increase cannot be straightforwardly explained as neither thalassemia nor pyruvate kinase deficiency alone give any change in conductance, P11.1 is particularly interesting. The Rh-associated glycoprotein (RhAG) coded by the RHAG gene, together with the RhD and RhCcEe proteins, is a major component of the Rh blood group system. It is essential for assembly of the Rh protein complex in the RBC membrane and for expression of the Rh antigens (Avent and Reid, 2000). The exact function of RhAG is not completely understood but it is suggested to be involved in RBC gas exchange as it promotes transmembrane  $\text{NH}_3$  transport (additionally  $\text{NH}_4^+$ ) (Bakouh et al., 2006) as well as facilitates  $\text{CO}_2$  membrane permeation (Endeward et al., 2008). More interesting is, however, that RhAG can act as a pore for monovalent cations ( $\text{Na}^+$ ,  $\text{K}^+$ , and  $\text{Li}^+$ ) and RHAG point mutations leading to Ile61Arg and Phe65Ser substitutions result in massively increased permeabilities for  $\text{K}^+$  and  $\text{Na}^+$  and to overhydrated stomatocytosis (Bruce et al., 2009).

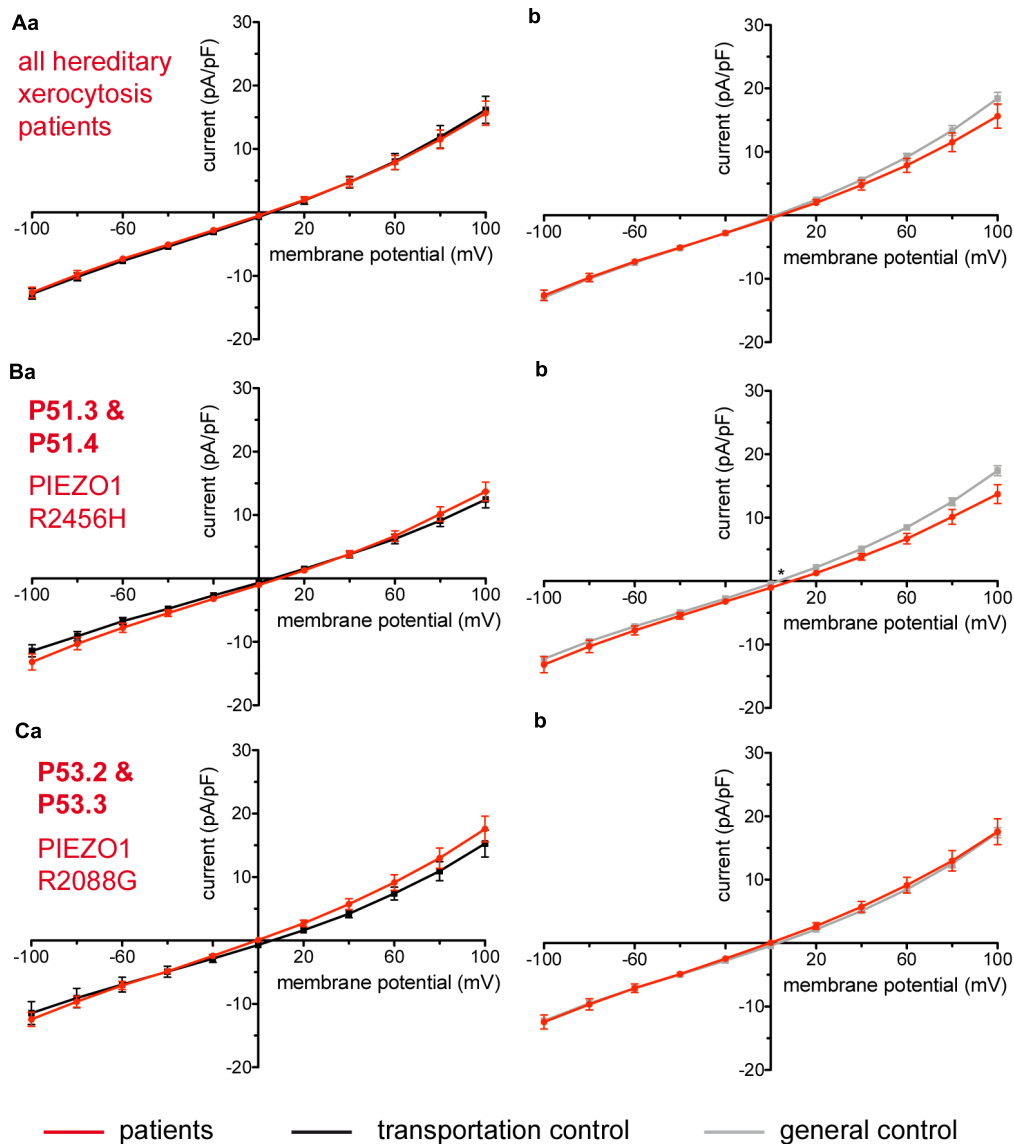
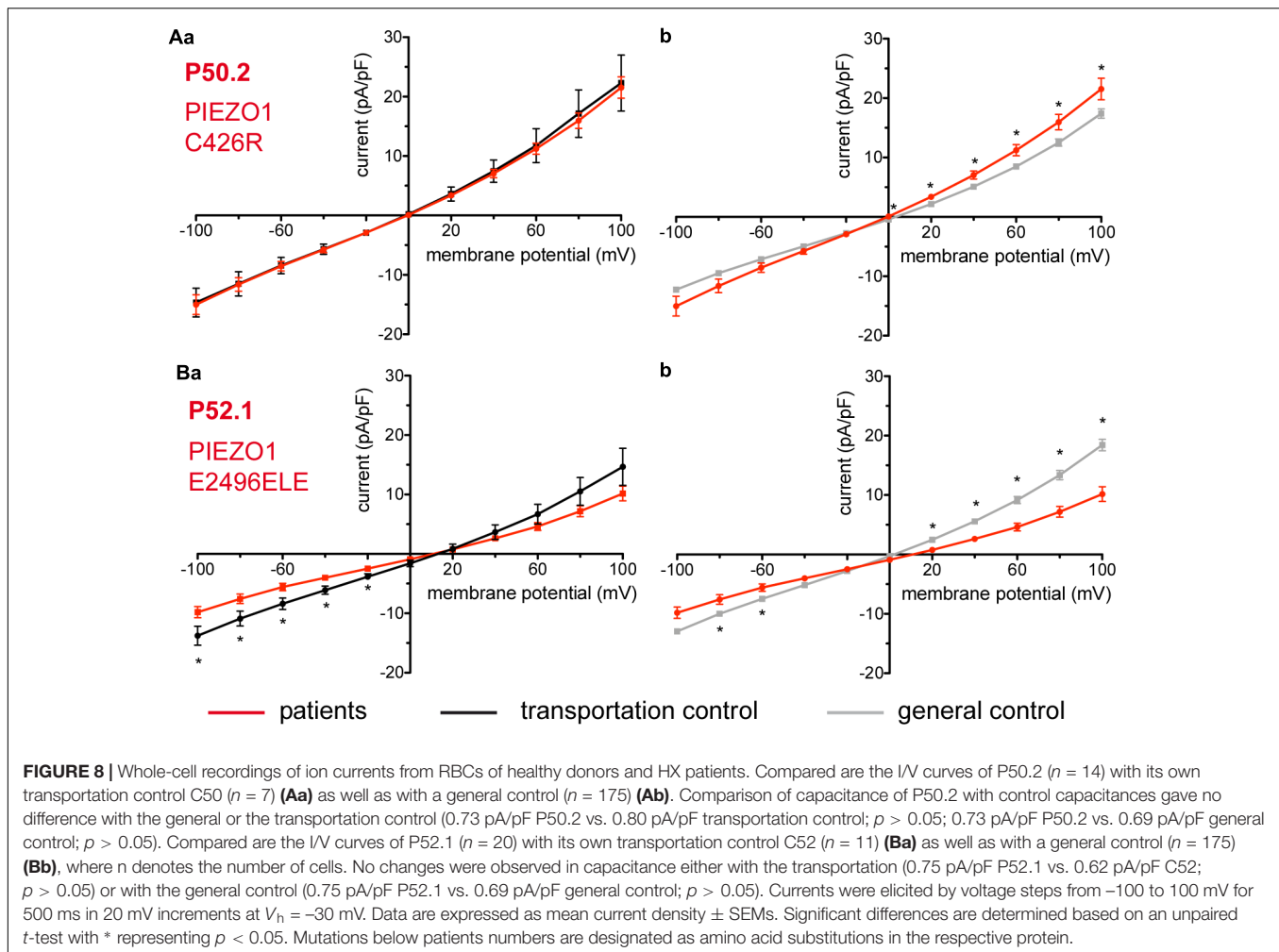


**FIGURE 7 |** Whole-cell recordings of ion currents from RBCs of healthy donors and HX patients. Compared are the I/V-curves of all HX patients ( $N = 6$ ) with the I/V curves of their own transportation controls ( $N = 4$ ) (**Aa**) and with the I/V curves of all healthy subjects delivered throughout the study ( $N = 27$ ) (**Ab**), where  $N$  denotes the number of healthy subjects or HX patients. No changes were observed in capacitance either with the transportation (0.725 pA/pF patients vs. 0.71 pA/pF transportation control;  $p > 0.05$ ) or with the general control (0.725 pA/pF patients vs. 0.69 pA/pF general control;  $p > 0.05$ ). Compared are the I/V curves of P51.3 and P51.4 pooled together (Family 1) ( $n = 22$ ) with their own transportation control C51 ( $n = 7$ ) (**Ba**) and the I/V curves of P53.2 and P53.3 pooled together (Family 2) ( $n = 27$ ) with their own transportation control C53 ( $n = 9$ ) (**Ca**), where  $n$  denotes the number of cells from the patients or the controls. (**Bb,Cb**) Compare the I/V curve of a general control based on currents recorded from all cells of all healthy subjects delivered throughout the study ( $n = 175$ ) with the I/V curve of P51.3 and P51.4 pooled together ( $n = 22$ ) (**Bb**) and P53.2 and P53.3 pooled together ( $n = 27$ ) (**Cb**) ( $n$  denotes number of cells). P51.3 and P51.4 pooled together (Family 1) and P53.2 and P53.3 pooled together (Family 2) did not show a difference in their capacitance compared to the general or transportation control (0.69 pA/pF P51.3 and P51.4 vs. 0.72 pA/pF C51,  $p > 0.05$ ; 0.69 pA/pF P51.3 and P51.4 vs. 0.69 pA/pF general control,  $p > 0.05$ ; 0.75 pA/pF P53.2 and P53.3 vs. 0.71 pA/pF P53,  $p > 0.05$ ; 0.75 pA/pF P53.2 and P53.3 vs. 0.69 pA/pF general control,  $p > 0.05$ ). Currents were elicited by voltage steps from  $-100$  to  $100$  mV for 500 ms in 20 mV increments at  $V_h = -30$  mV. Data are expressed as mean current density  $\pm$  SEMs. Significant differences are determined based on an unpaired  $t$ -test with \* representing  $p < 0.05$ . Mutations below patients numbers are designated as amino acid substitutions in the respective protein.

Expression of the mutated RhAGs in xenopus oocytes confirms the large monovalent leaks imposed by the mutations and modeling studies correlate those leaks with possibly widening the pore structures permitting passive diffusion of  $\text{Na}^+$  and  $\text{K}^+$  (Bruce et al., 2009). Mutation c.808G > A in P11.1 with a

substitution Val270Ile residing in the 5th endoloop of RhAG (Huang et al., 1999) although not linked to overhydrated stomatocytosis relates to the  $\text{Rh}^{\text{null}}$  syndrome accordingly characterized by varying degrees of chronic haemolytic anemia and spherostomatocytosis (Nash and Shojania, 1987). Without



knowing the mechanism that might relate mutation RHAG c.808G > A (or the complex defect c.808G > A+SPTB c.154delC) to changes in the RBC membrane conductance, P11.1 has been described with having less  $K^+$  in the plasma than its transportation control yet more than a non-transported normal control and a much increased activity of its  $Na^+/K^+$  pump (Huisjes et al., unpublished). Thus, it could well be that a possibly increased  $K^+$  leak underlined by the detected increased membrane conductance triggers compensatory changes, namely enhanced ion pumping that might explain the partially compensated  $K^+$  leak (i.e., that  $K^+$  in the plasma of the patient is less than  $K^+$  in the plasma of its transportation control). This is in line with observations that haemolytic diseases showing increased non- $Na^+/K^+$  pump and non- $NaK2Cl$  cotransport,  $K^+$  fluxes [ouabain- (an inhibitor of the  $Na^+/K^+$  pump) and bumetanide- (an inhibitor of the  $NaK2Cl$  cotransport) resistant  $K^+$  fluxes] are accompanied by increased  $Na^+/K^+$  pump fluxes (ouabain- sensitive fluxes) (Stewart, 2004).

Not always, however, a resulting changed membrane conductance is manifested as an increase in current. A patient (P12.1) with a mutation in band 3 protein shows a decrease in

current and, although counterintuitive, also accompanied by a significant loss of  $K^+$  from the RBC.

The major function of band 3 protein is of an anion transporter exchanging a bicarbonate for a chloride ion across the RBC plasma membrane thus ensuring efficient removal of  $CO_2$  from tissues (Guyton and Hall, 2006). However, data in the literature show that point mutations resulting in single amino acid substitutions cause  $Na^+$  and  $K^+$  leaks with anion transport activity either maintained or abolished depending on the mutation (Bruce et al., 1993, 2005; Salhany et al., 1995; Stewart et al., 2010, 2011). Those mutations causing predominantly stomatocytosis but also spherocytosis (Arakawa et al., 2015) have been suggested to induce monovalent cation leaks in one of 3 possible ways: (i) converting the anion exchanger in a non-selective cation conductor, (ii) inducing cation conductance in a still functioning exchanger and (iii) causing the anion exchanger to stimulate endogenous cation transporters (Badens and Guizouarn, 2016). The latter has been shown in heterologous expression systems (Stewart et al., 2010) as well as in RBCs (H734R) (Bogdanova et al., 2009). It could indeed be that band 3 protein is engaged in complex interactions modulating cation permeability pathways (both



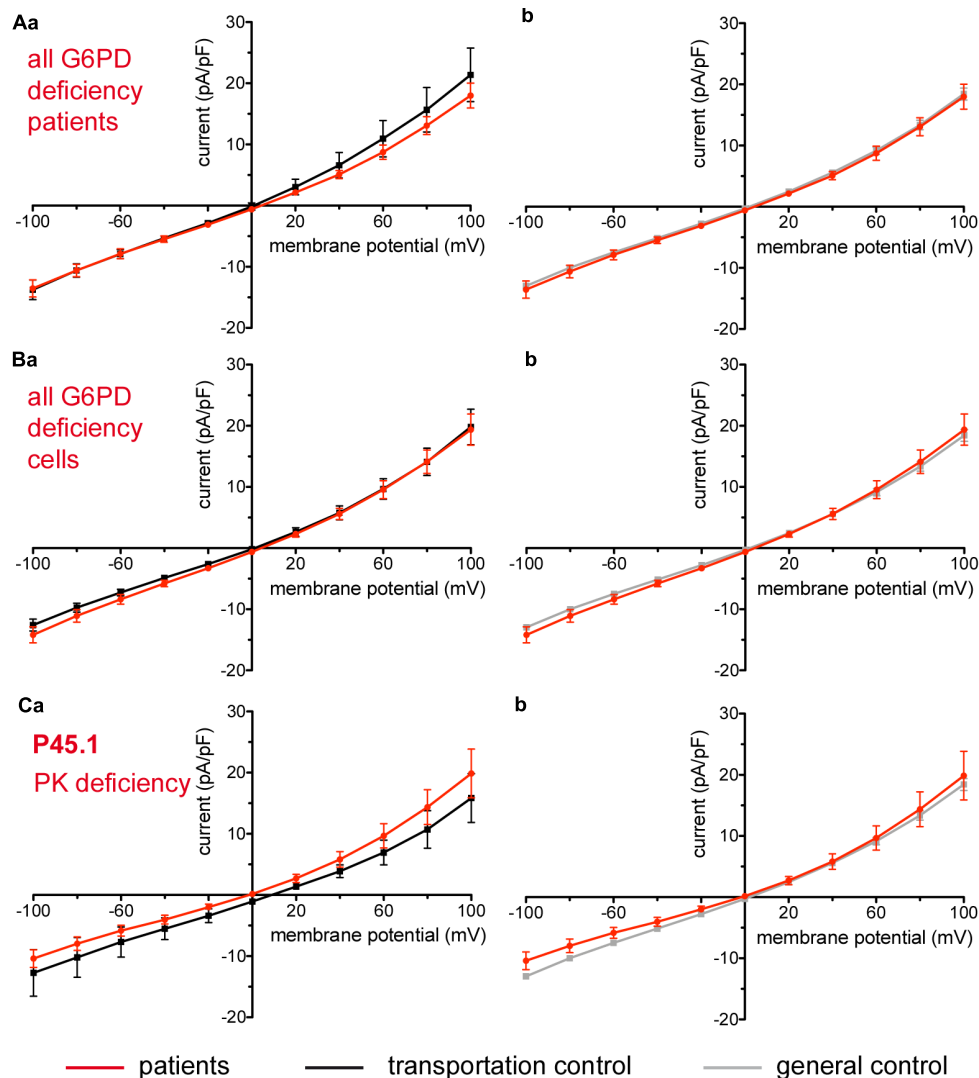


**FIGURE 9 |** Whole-cell recordings of ion currents from RBCs of healthy donors and patients with enzymopathies (glucose-6-phosphate dehydrogenase deficiency and pyruvate kinase deficiency). Compared are the I/V-curve of all glucose-6-phosphate dehydrogenase deficiency patients ( $N = 3$ ) (Aa) with the I/V curve of their own transportation controls ( $N = 3$ ) (Aa) and with the I/V curve of all healthy subjects delivered throughout the study ( $N = 27$ ) (Ab), where  $N$  denotes the number of healthy subjects or patients. Capacitance of the three patients P40.1, P41.1, P42.1 was not any different from that of the controls (0.62 pA/pF P40.1 + P41.1 + P42.1 vs. 0.68 pA/pF C40 + C41 + C42,  $p > 0.05$ ; 0.62 pA/pF P40.1 + P41.1 + P42.1 vs. 0.69 pA/pF general control,  $p > 0.05$ ). Compared are the I/V-curve of all glucose-6-phosphate dehydrogenase deficiency patients cells ( $n = 27$ ) with the I/V curve of all transportation control cells ( $n = 22$ ) (Ba) as well as with a general control ( $n = 175$ ) (Bb), where  $n$  denotes the number of cells. Compared are the I/V curves of P45.1 ("PK" below the patient number stands for pyruvate kinase deficiency) ( $n = 15$ ) with its own transportation control C45 ( $n = 5$ ) (Ca) as well as with a general control ( $n = 175$ ) (Cb). No changes were observed in capacitance either with the transportation (0.72 pA/pF P45.1 vs. 0.68 pA/pF C45;  $p > 0.05$ ) or with the general control (0.72 pA/pF P45.1 vs. 0.69 pA/pF general control;  $p > 0.05$ ). Currents were elicited by voltage steps from  $-100$  to  $100$  mV for 500 ms in 20 mV increments at  $V_h = -30$  mV. Data are expressed as mean current density  $\pm$  SEMs.

channels and transporters) and that mutations changing its conformation or its availability in the membrane might lead to multifaceted effects either increasing or decreasing membrane conductance (both of which with the detrimental result of disturbing RBC ion homeostasis). In line is a study showing kidney band 3 protein interaction with nephrin (Wu et al., 2010). The intracellular domain of nephrin interacts with TRPC6, believed to be present in erythrocytes (Foller et al., 2008; Danielczok J. et al., 2017) suggesting a possible functional link

between band 3 protein and TRPC6 in erythrocytes as well. While no changes in cation channel activity (not an increase either, regardless of the reported substantially elevated cation leak) have been detected in band 3 protein R730C RBCs [as measured by on-cell patch-clamp, (Stewart et al., 2011)] as well as in band 3 protein H734R RBCs [as judged by membrane potential changes, (Bogdanova et al., 2009)], it could be that each mutation alters in a different way endogenous permeability pathways.

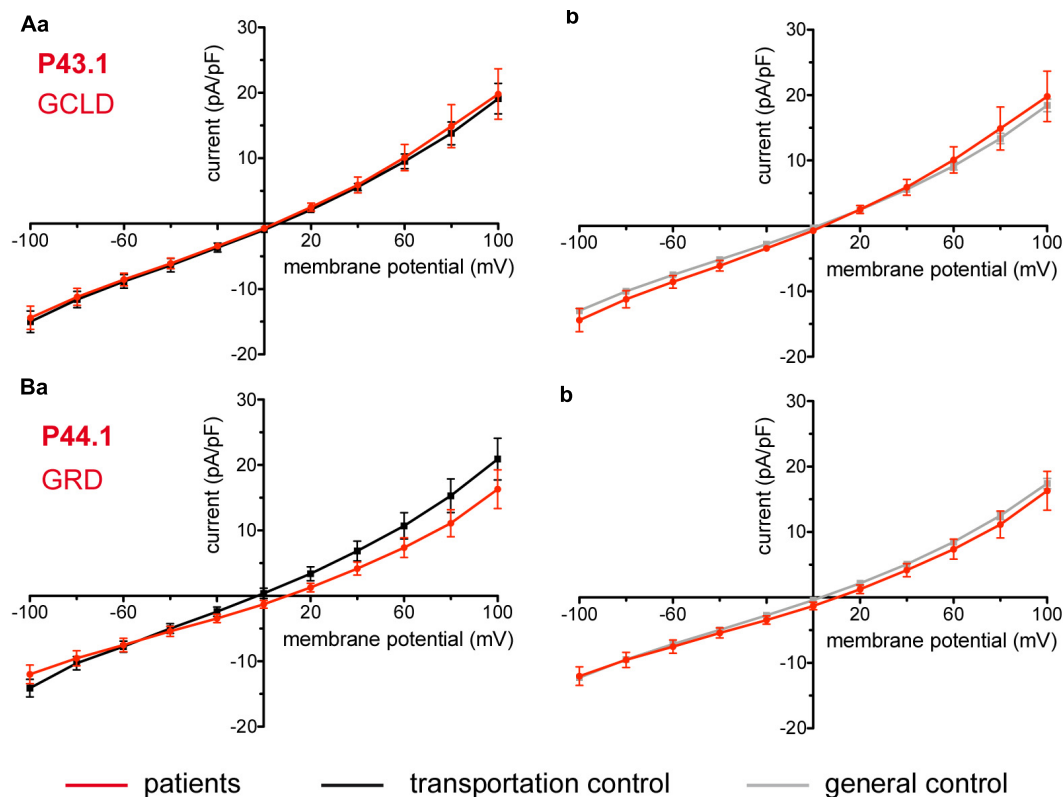


**FIGURE 10 |** Whole-cell recordings of ion currents from RBCs of healthy donors and patients with enzymopathies. Compared are the I/V curves of P43.1 (GCLD below the patient number stands for glutamate-cysteine ligase deficiency) ( $n = 6$ ) with its own transportation control C43 ( $n = 5$ ) (**Aa**) as well as with a general control ( $n = 175$ ) (**Ab**). No changes were observed in capacitance either with the transportation (0.64 pA/pF P43.1 vs. 0.65 pA/pF C43;  $p > 0.05$ ) or with the general control (0.64 pA/pF P43.1 vs. 0.69 pA/pF general control;  $p > 0.05$ ). Compared are the I/V curves of P44.1 (GRD below the patient number stands for glutathione reductase deficiency) ( $n = 9$ ) with its own transportation control C44 ( $n = 5$ ) (**Ba**) as well as with a general control ( $n = 175$ ) (**Bb**), where  $n$  denotes the number of cells. No changes were observed in capacitance either with the transportation (0.76 pA/pF P44.1 vs. 0.65 pA/pF C44;  $p > 0.05$ ) or with the general control (0.76 pA/pF P44.1 vs. 0.69 pA/pF general control;  $p > 0.05$ ). Currents were elicited by voltage steps from  $-100$  to  $100$  mV for  $500$  ms in  $20$  mV increments at  $V_h = -30$  mV. Data are expressed as mean current density  $\pm$  SEMs.

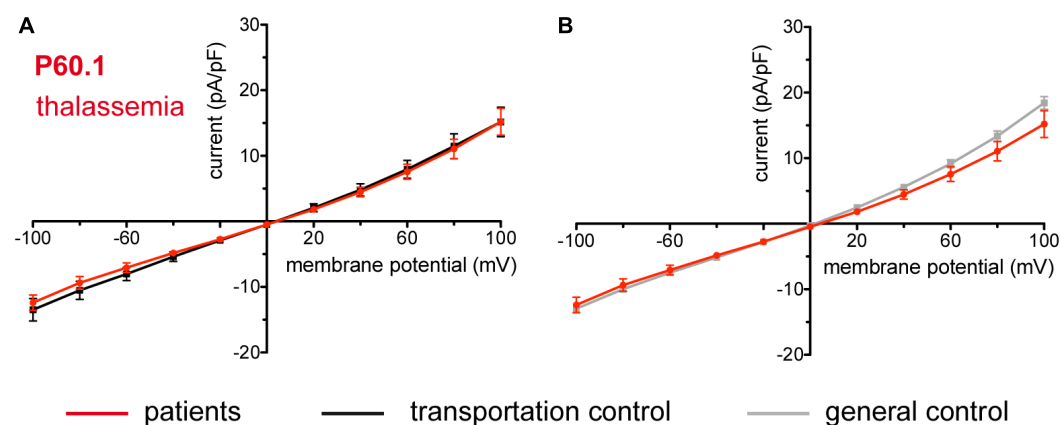


**FIGURE 11 |** Whole-cell recordings of ion currents from RBCs of healthy donors and a patient with  $\beta$ -thalassemia. Compared are the I/V curves of P60.1 ( $n = 12$ ) with its own transportation control C60 ( $n = 5$ ) (**A**) as well as with a general control ( $n = 175$ ) (**B**). No changes were observed in capacitance either with the transportation (0.72 pA/pF P60.1 vs. 0.64 pA/pF C60;  $p > 0.05$ ) or with the general control (0.72 pA/pF P60.1 vs. 0.69 pA/pF general control;  $p > 0.05$ ). Currents were elicited by voltage steps from  $-100$  to  $100$  mV for  $500$  ms in  $20$  mV increments at  $V_h = -30$  mV. Data are expressed as mean current density  $\pm$  SEMs.

Regarding mutation Ile783Asn of patient P12.1, it is not in the cytoplasmic half of the core domain of band 3 protein, where most of the mutations causing stomatocytosis are (Arakawa et al., 2015), yet it is very close to and in the same transmembrane domain (TM 12) as another mutation, namely Gly796Arg, also triggering stomatocytosis (Arakawa et al., 2015). According to (Huisjes et al., unpublished) mutation Ile783Asn is accompanied by increased  $\text{Na}^+\text{-K}^+\text{-ATPase}$  activity, a referral to stomatocytosis, yet by an osmoscan curve with a typical HS pattern and extremely low eosin-5-maleimide (EMA) staining (61%), likely reflecting strongly reduced copy numbers of band 3 protein, a referral to spherocytosis. (EMA-binding on RBCs involves the  $\epsilon\text{-NH}$  group of lysine at position 430 from band 3 protein (Nicolas et al., 2003) and is experimentally found to correlate with band 3 protein expression on RBCs (Huisjes et al., 2018). Thus the question whether it is the unavailability of band 3 protein or a possible structural and conformational change that causes the decreased outward current, remains open.

In our study, as outlined in the Results section, we have compared the currents measured from the RBCs of our patients once with their transportation control, i.e., currents measured from the RBCs of a healthy subject, whose blood was delivered together with the blood of the patient, and once with a general control, i.e., currents measured from the cells of all healthy subjects delivered throughout the study. Inevitably a question comes up, especially when there are differences in the comparisons with the two controls, which is the more appropriate one. Whereas, undoubtedly, considering the transportation control, allows us to take into account the particular transportation conditions such as temperature, vibration intensity and shipment duration, it has limitations. Such limitations are the low number of measured cells but mostly the fact that the control subject, although judged healthy, might not be a representative control. Thus in the case with C17, the control for patients P17.1 and P17.2, the averaged capacitance of C17 RBCs (0.53 pA/pF) is statistically significantly smaller than the averaged capacitance of the RBCs of the general control (0.69 pA/pF). This in turn results in an increased current density (current divided by capacitance) for the transportation control which might explain the observed difference of P17.1 and P17.2 compared to C17 but not to the general control (Figures 4B,C).

With C10, the control of P10.1, the situation is even more extreme, as, even though the averaged capacitance of the RBCs of the transportation control is higher compared to the averaged capacitance of the general control, which results in a lower current density, the current density still remains much higher than the one of the general control. The appearance of the I/V curve is also very different with the reversal potential being much shifted to the more negative values compared to the general control (Figure 5Bc). The above mentioned limitations could be avoided by considering the general control which, due to the high number of cells, is balancing (smoothing out) the effect of a healthy but unrepresentative subject and is close to an 'ideal' control. At the same time what is an advantage of the general control is simultaneously a disadvantage as it 'balances' also the specific transportation effects on the samples. A way out of accidentally coming across a non-representative

healthy subject is using the blood of several healthy subjects as a transportation control or, even better, the blood of several healthy relatives. A further problem, however, is that transportation could have different effects on the patient and on the control. This problem could be avoided by avoiding transportation itself, whenever possible.

## Hereditary Xerocytosis

Piezo 1 is a mechanically activated cation channel (Coste et al., 2010, 2012), which is permeable to monovalent cations ( $P_{\text{K}} > P_{\text{Cs}} \cong P_{\text{Na}} > P_{\text{Li}}$ ) and to most divalent cations like  $\text{Ba}^{2+}$ ,  $\text{Ca}^{2+}$ , and  $\text{Mg}^{2+}$ , but not  $\text{Mn}^{2+}$  (Gnanasambandam et al., 2015). Expressed in many tissues like kidney, lung and urinary bladder (Coste et al., 2010; Miyamoto et al., 2014), Piezo 1 has been detected in the plasma membrane of RBCs, e.g., by mass spectroscopy and immunologically (Zarychanski et al., 2012; Andolfo et al., 2013; Kaestner and Egée, 2018). A major role of Piezo1 channels in RBCs is in volume regulation and mutations in the channel have been linked to HX, a dominantly inherited haemolytic anemia, characterized by decreased  $\text{K}^+$  and increased  $\text{Na}^+$  RBCs content, as well as dehydration resulting in increased mean corpuscular hemoglobin concentrations (MCHC), a leftward shift of the osmotic gradient ektacytometry curve and increased osmotic resistance of the RBCs (Gallagher, 2013; Shmukler et al., 2014; Glogowska and Gallagher, 2015; Andolfo et al., 2016). Disease clinical manifestations are variable and may include mild to moderate haemolysis, perinatal edema and non-immune hydrops fetalis that spontaneously resolve, thrombosis, pseudohyperkalemia and sometimes severe iron overload in the course of the disease (Gallagher, 2013; Glogowska and Gallagher, 2015; Andolfo et al., 2016). Out of the four mutations in our study [R2456H (P51.3 and P51.4), R2088G (P53.3 and P53.2), C426R (P50.2), and E2496ELE (P52.1)], three (R2456H, R2088G, and E2496ELE) are known and have been extensively characterized including expression of the mutant Piezo1 channel in heterologous systems and characterization of the channel activity (Zarychanski et al., 2012; Albuisson et al., 2013; Andolfo et al., 2013; Bae et al., 2013; Sandberg et al., 2014; Shmukler et al., 2014; Glogowska et al., 2017). Two of the mutations, R2456H and E2496ELE, among the most common ones found in typical HX patients (Zarychanski et al., 2012; Albuisson et al., 2013; Andolfo et al., 2013; Shmukler et al., 2014), are in the C-terminal region, part of the pore module of Piezo1 (Coste et al., 2015; Ge et al., 2015). Those mutations do not alter the sensitivity of the channel to mechanical stimulation but cause considerable increase in the inactivation time constant thus giving rise to an increased channel activity in response to a given mechanical stimulus (Albuisson et al., 2013; Glogowska et al., 2017). Could an increased channel activity lasting only for the duration of a short mechanical stimulus explain the ion disbalance observed in HX? A possible answer is that during their circulation in the vascular system RBCs are under constant mechanical stress squeezing in capillaries and in the tiny slits of the spleen undergoing numerous rounds of mechanical stimulation with Piezo1 activation (Danielczok J.G. et al., 2017) and, in the case of Piezo1 prolonged inactivation, not being

capable of replenishing their ions. However, it is also likely that slowing of inactivation could potentially cause a slight increase in a basal Piezo1 activity (independent of mechanical stimulation) (Albuisson et al., 2013). This is supported by the study of (Andolfo et al., 2013), which demonstrates spontaneous ion channel activity in R2456H patient RBCs, blocked by GsMTx-4 and not observed in healthy cells. In addition are the on-cell patch recordings from the RBCs of another R2456H patient revealing once again an increased cation channel activity (independent of mechanical stimulation) without information on the identity of the channel (Shmukler et al., 2014). Consistent with Piezo 1 increased activity having direct or secondary effects on membrane conductance is the observed decrease in conductance in P52.1 (E2496ELE) RBCs. Also in P51.3 and P51.4 (R2456H) and P52.1 (E2496ELE) a rightward shift of the I/V curve is observed (**Figures 7Bb, 8Bb**) indicative of an upregulation/downregulation of a channel/channels. Whether the shift is pertinent to the mutations though is not explicitly clear as such a shift is not detected when patients' currents are compared with their transportation controls (**Figures 7Ba, 8Ba**). Concerning mutation C426R (P50.2) which shows an increase in current only with the general control but not with its transportation control we tend to disregard the difference shown with the general control as the transportation control was taken from a genetically related healthy subject and it indeed shows a remarkable similarity with the I/V curve of the patient (**Figure 8Aa**).

## Enzymopathies and Beta-Thalassemia

Metabolic enzyme deficiencies (glucose-6-phosphate dehydrogenase deficiency, pyruvate kinase deficiency, glutamate-cysteine ligase deficiency and glutathione reductase deficiency) as well as  $\beta$ -thalassemia are not accompanied by changes in membrane conductance. The former is consistent with the lack of changes also in the  $K^+$  and  $Na^+$  content of 11 patients with congenital non-spherocytic haemolytic anemia including pyruvate kinase deficiency (Vives Corrons and Besson, 2001).

## CONCLUSION

Trying to summarize and come up with a common channel increased activity/dysfunction or just an effect (decrease or increase in conductance) accompanying RBCs ion disbalance

disorders, we stumble upon a great variability in results. Such a variability is of course reflecting the many triggers of the disbalance and for sure not lessened by the fact that not only between different mutations but also among members of a family with the same mutation there are distinct differences starting from the severity of the disease and extending down to the cellular level. Such a summary is even harder and certainly not helped by the great variability in healthy subjects reflected in control membrane conductance measurements as seen in our study. And last but not least answers are yet heavier without so far clearly knowing how an increased  $Na^+$  and a decreased  $K^+$  can lead to overhydration as in OHSt or to dehydration as in HX. Nevertheless based on our study we conclude that changes in conductance are incurred by certain  $\alpha$ -spectrin [c.2755G > T (p.Glu919) and c.678G > A p.(Glu227fs) whenever an  $\alpha^{LELY}$  allele is present], band 3 protein [c.2348T > A p.(Ile783Asn)] and Piezo1 (c.7483\_7488dupCTGGAG p.2495\_2496dupLeuGlu) mutations as a difference is observed with both the general and the transportation control. Identification of the channel/channels that underlie the changed conductances demands future studies.

## ETHICS STATEMENT

Patients' data were handled anonymously as outlined in the ethics agreements. These agreements were approved by the Medical Ethical Research Board (MERB) of the University Medical Center Utrecht, Netherlands (UMCU) under reference code 15/426M "Disturbed ion homeostasis in hereditary hemolytic anemia" and by the Ethical Committee of Clinical Investigations of Hospital Clinic, Spain (IDIBAPS) under reference code 2013/8436.

## AUTHOR CONTRIBUTIONS

All authors listed have made a substantial, direct and intellectual contribution to the work, and approved it for publication.

## FUNDING

The research leading to these results has received funding from the European Seventh Framework Program under grant agreement number 602121 (CoMMiTMeNT).

## REFERENCES

- Albuisson, J., Murthy, S. E., Bandell, M., Coste, B., Louis-Dit-Picard, H., Mathur, J., et al. (2013). Dehydrated hereditary stomatocytosis linked to gain-of-function mutations in mechanically activated PIEZO1 ion channels. *Nat. Commun.* 4:1884. doi: 10.1038/ncomms2899
- Andolfo, I., Alper, S. L., De Franceschi, L., Auriemma, C., Russo, R., De Falco, L., et al. (2013). Multiple clinical forms of dehydrated hereditary stomatocytosis arise from mutations in PIEZO1. *Blood* 121, 3925–3935. doi: 10.1182/blood-2013-02-482489
- Andolfo, I., Russo, R., Gambale, A., and Iolascon, A. (2016). New insights on hereditary erythrocyte membrane defects. *Haematologica* 101, 1284–1294. doi: 10.3324/haematol.2016.142463
- Arakawa, T., Kobayashi-Yurugi, T., Alguel, Y., Iwanari, H., Hatae, H., Iwata, M., et al. (2015). Crystal structure of the anion exchanger domain of human erythrocyte band 3. *Science* 350, 680–684. doi: 10.1126/science.aaa4335
- Avent, N. D., and Reid, M. E. (2000). The Rh blood group system: a review. *Blood* 95, 375–387.
- Badens, C., and Guizouarn, H. (2016). Advances in understanding the pathogenesis of the red cell volume disorders. *Br. J. Haematol.* 174, 674–685. doi: 10.1111/bjh.14197



- Bae, C., Gnanasambandam, R., Nicolai, C., Sachs, F., and Gottlieb, P. A. (2013). Xerocytosis is caused by mutations that alter the kinetics of the mechanosensitive channel PIEZO1. *Proc. Natl. Acad. Sci. U.S.A.* 110, E1162–E1168. doi: 10.1073/pnas.1219777110
- Bakouh, N., Benjelloun, F., Cherif-Zahar, B., and Planelles, G. (2006). The challenge of understanding ammonium homeostasis and the role of the Rh glycoproteins. *Transfus. Clin. Biol.* 13, 139–146. doi: 10.1016/j.tracbi.2006.02.008
- Bogdanova, A. Y., Goede, J. S., Weiss, E., Bogdanov, N., Bennekou, P., Bernhardt, I., et al. (2009). Cryohydrocytosis: increased activity of cation carriers in red cells from a patient with a band 3 mutation. *Haematologica* 95, 189–198. doi: 10.3324/haematol.2009.010215
- Bruce, L. J., Guizouarn, H., Burton, N. M., Gabillat, N., Poole, J., Flatt, J. F., et al. (2009). The monovalent cation leak in overhydrated stomatocytic red blood cells results from amino acid substitutions in the Rh-associated glycoprotein. *Blood* 113, 1350–1357. doi: 10.1182/blood-2008-07-171140
- Bruce, L. J., Kay, M. M., Lawrence, C., and Tanner, M. J. (1993). Band 3 HT, a human red-cell variant associated with acanthocytosis and increased anion transport, carries the mutation Pro-868→Leu in the membrane domain of band 3. *Biochem. J.* 293, 317–320. doi: 10.1042/bj2930317
- Bruce, L. J. L., Robinson, H. C. H., Guizouarn, H. H., Borgese, F. F., Harrison, P. P., King, M.-J. M., et al. (2005). Monovalent cation leaks in human red cells caused by single amino-acid substitutions in the transport domain of the band 3 chloride-bicarbonate exchanger, AE1. *Nat. Genet.* 37, 1258–1263. doi: 10.1038/ng1656
- Cao, A., and Galanello, R. (2010). Beta-thalassemia. *Genet. Med.* 12, 61–76. doi: 10.1097/GIM.0b013e3181cd68ed
- Coste, B., Mathur, J., Schmidt, M., Earley, T. J., Ranade, S., Petrus, M. J., et al. (2010). Piezo1 and Piezo2 are essential components of distinct mechanically activated cation channels. *Science* 330, 55–60. doi: 10.1126/science.1193270
- Coste, B., Murthy, S. E., Mathur, J., Schmidt, M., Mechoulam, Y., Delmas, P., et al. (2015). Piezo1 ion channel pore properties are dictated by C-terminal region. *Nat. Commun.* 6:7223. doi: 10.1038/ncomms8223
- Coste, B., Xiao, B., Santos, J. S., Syeda, R., Grandl, J., Spencer, K. S., et al. (2012). Piezo proteins are pore-forming subunits of mechanically activated channels. *Nature* 483, 176–181. doi: 10.1038/nature10812
- Danielczok, J. G., Terriac, E., Hertz, L., Petkova-Kirova, P., Lautenschläger, F., Laschke, M. W., et al. (2017). Red blood cell passage of small capillaries is associated with transient Ca<sup>2+</sup>-mediated adaptations. *Front. Physiol.* 8:979. doi: 10.3389/fphys.2017.00979
- Danielczok, J., Hertz, L., Ruppenthal, S., Kaiser, E., Petkova-Kirova, P., Bogdanova, A., et al. (2017). Does erythropoietin regulate TRPC channels in red blood cells? *Cell. Physiol. Biochem.* 41, 1219–1228. doi: 10.1159/000464384
- Dhaliwal, G., Cornett, P. A., and Tierney, L. M. (2004). Hemolytic anemia. *Am. Fam. Physician* 69, 2599–2606.
- Endeward, V., Cartron, J.-P., Ripoché, P., and Gros, G. (2008). RhAG protein of the Rhesus complex is a CO<sub>2</sub> channel in the human red cell membrane. *FASEB J.* 22, 64–73. doi: 10.1096/fj.07-9097com
- Fermo, E., Bogdanova, A., Petkova-Kirova, P., Zaninoni, A., Marcello, A. P., Makhro, A., et al. (2017). “Gardos Channelopathy”: a variant of hereditary stomatocytosis with complex molecular regulation. *Sci. Rep.* 7:1744. doi: 10.1038/s41598-017-01591-w
- Foller, M., Kasinathan, R. S., Koka, S., Lang, C., Shumilina, E. V., Birnbaumer, L., et al. (2008). TRPC6 contributes to the Ca(2+) leak of human erythrocytes. *Cell. Physiol. Biochem.* 21, 183–192. doi: 10.1159/000113760
- Gallagher, P. G. (2013). Disorders of red cell volume regulation. *Curr. Opin. Hematol.* 20, 201–207. doi: 10.1097/MOH.0b013e32835f6870
- Ge, J., Li, W., Zhao, Q., Li, N., Chen, M., Zhi, P., et al. (2015). Architecture of the mammalian mechanosensitive Piezo1 channel. *Nature* 527, 64–69. doi: 10.1038/nature15247
- Glogowska, E., and Gallagher, P. G. (2015). Disorders of erythrocyte volume homeostasis. *Int. J. Lab. Hematol.* 37(Suppl. 1), 85–91. doi: 10.1111/ijlh.12357
- Glogowska, E., Schneider, E. R., Maksimova, Y., Schulz, V. P., Lezon-Geyda, K., Wu, J., et al. (2017). Novel mechanisms of PIEZO1 dysfunction in hereditary xerocytosis. *Blood* 130, 1845–1856. doi: 10.1182/blood-2017-05-786004
- Gnanasambandam, R., Bae, C., Gottlieb, P. A., and Sachs, F. (2015). Ionic selectivity and permeation properties of human PIEZO1 channels. *PLoS One* 10:e0125503. doi: 10.1371/journal.pone.0125503
- Guyton, A. C., and Hall, J. E. (2006). *Medical Physiology*. Amsterdam: Elsevier Saunders.
- Hertz, L., Huisjes, R., Llaudet-Planas, E., Petkova-Kirova, P., Makhro, A., Danielczok, J. G., et al. (2017). Is increased intracellular calcium in red blood cells a common component in the molecular mechanism causing anemia? *Front. Physiol.* 8:673. doi: 10.3389/fphys.2017.00673
- Huang, C. H., Cheng, G., Liu, Z., Chen, Y., Reid, M. E., Halverson, G., et al. (1999). Molecular basis for Rh(null) syndrome: identification of three new missense mutations in the Rh50 glycoprotein gene. *Am. J. Hematol.* 62, 25–32. doi: 10.1002/(SICI)1096-8652(199909)62:1<25::AID-AJH5>3.0.CO;2-K
- Huisjes, R., Satchwell, T. J., Verhagen, L. P., Schiffelers, R. M., van Solinge, W. W., Toye, A. M., et al. (2018). Quantitative measurement of red cell surface protein expression reveals new biomarkers for hereditary spherocytosis. *Int. J. Lab. Hematol.* 40, e74–e77. doi: 10.1111/ijlh.12841
- Iolascon, A., Perrotta, C., and Stewart, G. W. (2003). Red blood cell membrane defects. *Rev. Clin. Exp. Hematol.* 7, 22–56.
- Kaestner, L., and Egée, S. (2018). Commentary: voltage gating of mechanosensitive PIEZO channels. *Front. Physiol.* 9:1565. doi: 10.3389/fphys.2018.01565
- Luzzatto, L., Nannelli, C., and Notaro, R. (2016). Glucose-6-phosphate dehydrogenase deficiency. *Hematol. Oncol. Clin. North Am.* 30, 373–393. doi: 10.1016/j.hoc.2015.11.006
- Makhro, A., Huisjes, R., Verhagen, L. P., Mañú Pereira, M. D. M., Llaudet-Planas, E., Petkova-Kirova, P., et al. (2016). Red cell properties after different modes of blood transportation. *Front. Physiol.* 7:288. doi: 10.3389/fphys.2016.00288
- Miyamoto, T., Mochizuki, T., Nakagomi, H., Kira, S., Watanabe, M., Takayama, Y., et al. (2014). Functional role for Piezo1 in stretch-evoked Ca<sup>2+</sup> influx and ATP release in urothelial cell cultures. *J. Biol. Chem.* 289, 16565–16575. doi: 10.1074/jbc.M113.528638
- Nash, R., and Shojania, A. M. (1987). Hematological aspect of Rh deficiency syndrome: a case report and a review of the literature. *Am. J. Hematol.* 24, 267–275. doi: 10.1002/ajh.2830240306
- Nicolas, V., Le Van Kim, C., Gane, P., Birkenmeier, C., Cartron, J.-P., Colin, Y., et al. (2003). Rh-RhAG/ankyrin-R, a new interaction site between the membrane bilayer and the red cell skeleton, is impaired by Rh(null)-associated mutation. *J. Biol. Chem.* 278, 25526–25533. doi: 10.1074/jbc.M302816200
- Petkova-Kirova, P., Hertz, L., Makhro, A., Danielczok, J., Huisjes, R., Llaudet-Planas, E., et al. (2018). A previously unrecognized Ca<sup>2+</sup>-inhibited nonselective cation channel in red blood cells. *Hemasphere* 2:e146. doi: 10.1097/HS9.0000000000000146
- Ristoff, E., and Larsson, A. (1998). Patients with genetic defects in the gamma-glutamyl cycle. *Chem. Biol. Interact.* 11, 113–121. doi: 10.1016/S0009-2797(97)00155-5
- Rotterdam, G. M., Fermo, E., Becker, N., Barcellini, W., Brüggemann, A., Fertig, N., et al. (2018). A novel gain-of-function mutation of Piezo1 is functionally affirmed in red blood cells by high-throughput patch clamp. *Haematologica* doi: 10.3324/haematol.2018.201160 [Epub ahead of print].
- Salhany, J. M., Schopfer, L. M., Kay, M. M., Gamble, D. N., and Lawrence, C. (1995). Differential sensitivity of stilbenedisulfonates in their reaction with band 3 HT (Pro-868→Leu). *Proc. Natl. Acad. Sci. U.S.A.* 92, 11844–11848. doi: 10.1073/pnas.92.25.11844
- Sandberg, M. B., Nybo, M., Birgens, H., and Frederiksen, H. (2014). Hereditary xerocytosis and familial haemolysis due to mutation in the PIEZO1 gene: a simple diagnostic approach. *Int. J. Lab. Hematol.* 36, e62–e65. doi: 10.1111/ijlh.12172
- Shmukler, B. E., Vidorpe, D. H., Rivera, A., Auerbach, M., Brugnara, C., and Alper, S. L. (2014). Dehydrated stomatocytic anemia due to the heterozygous mutation R2456H in the mechanosensitive cation channel PIEZO1: a case report. *Blood Cells Mol. Dis.* 52, 53–54. doi: 10.1016/j.bcmd.2013.07.015
- Stewart, A. K., Kedar, P. S., Shmukler, B. E., Vidorpe, D. H., Hsu, A., Glader, B., et al. (2011). Functional characterization and modified rescue of novel AE1 mutation R730C associated with overhydrated cation leak stomatocytosis. *Am. J. Physiol. Cell Physiol.* 300, C1034–C1046. doi: 10.1152/ajpcell.00447.2010
- Stewart, A. K., Vidorpe, D. H., Heneghan, J. F., Chebib, F., Stolpe, K., Akhavein, A., et al. (2010). The GPA-dependent, spherostomatocytosis mutant AE1 E758K induces GPA-independent, endogenous cation transport in amphibian oocytes. *Am. J. Physiol. Cell Physiol.* 298, C283–C297. doi: 10.1152/ajpcell.00444.2009

- Stewart, G. W. (2004). Hemolytic disease due to membrane ion channel disorders. *Curr. Opin. Hematol.* 11, 244–250. doi: 10.1097/01.moh.0000132240.20671.33
- van Zwieten, R., Verhoeven, A. J., and Roos, D. (2014). Inborn defects in the antioxidant systems of human red blood cells. *Free Radic. Biol. Med.* 67, 377–386. doi: 10.1016/j.freeradbiomed.2013.11.022
- Viel, A., and Branton, D. (1996). Spectrin: on the path from structure to function. *Curr. Opin. Cell Biol.* 8, 49–55. doi: 10.1016/S0955-0674(96)80048-2
- Vives Corrons, L., and Besson, I. (2001). Red cell membrane Na<sup>+</sup> transport systems in hereditary spherocytosis: relevance to understanding the increased Na<sup>+</sup> permeability. *Ann. Haematol.* 80, 535–539. doi: 10.1007/s002770100342
- Ware, R. E., de Montalembert, M., Tshilolo, L., and Abboud, M. R. (2017). Sick cell disease. *Lancet* 390, 311–323. doi: 10.1016/S0140-6736(17)30193-9
- Wilmotte, R., Harper, S. L., Ursitti, J. A., Maréchal, J., Delaunay, J., and Speicher, D. W. (1997). The exon 46-encoded sequence is essential for stability of human erythroid alpha-spectrin and heterodimer formation. *Blood* 90, 4188–4196.
- Wu, F., Saleem, M. A., Kampik, N. B., Satchwell, T. J., Williamson, R. C., Blattner, S. M., et al. (2010). Anion exchanger 1 interacts with nephrin in podocytes. *J. Am. Soc. Nephrol.* 21, 1456–1467. doi: 10.1681/ASN.2009090921
- Zanella, A., Fermo, E., Bianchi, P., and Valentini, G. (2005). Red cell pyruvate kinase deficiency: molecular and clinical aspects. *Br. J. Haematol.* 130, 11–25. doi: 10.1111/j.1365-2141.2005.05527.x
- Zarychanski, R., Schulz, V. P., Houston, B. L., Maksimova, Y., Houston, D. S., Smith, B., et al. (2012). Mutations in the mechanotransduction protein PIEZO1 are associated with hereditary xerocytosis. *Blood* 120, 1908–1915. doi: 10.1182/blood-2012-04-422253

**Conflict of Interest Statement:** The authors declare that the research was conducted in the absence of any commercial or financial relationships that could be construed as a potential conflict of interest.

Copyright © 2019 Petkova-Kirova, Hertz, Danielczok, Huisjes, Makhro, Bogdanova, Mañú-Pereira, Vives Corrons, van Wijk and Kaestner. This is an open-access article distributed under the terms of the Creative Commons Attribution License (CC BY). The use, distribution or reproduction in other forums is permitted, provided the original author(s) and the copyright owner(s) are credited and that the original publication in this journal is cited, in accordance with accepted academic practice. No use, distribution or reproduction is permitted which does not comply with these terms.



# Clinical and Molecular Spectrum of Glucose-6-Phosphate Isomerase Deficiency. Report of 12 New Cases

**Elisa Fermo<sup>1\*</sup>, Cristina Vercellati<sup>1</sup>, Anna Paola Marcello<sup>1</sup>, Anna Zaninoni<sup>1</sup>, Selin Aytac<sup>2</sup>, Mualla Cetin<sup>2</sup>, Ilaria Capolsini<sup>3</sup>, Maddalena Casale<sup>4</sup>, Sabrina Paci<sup>5</sup>, Alberto Zanella<sup>1</sup>, Wilma Barcellini<sup>1</sup> and Paola Bianchi<sup>1</sup>**

<sup>1</sup> UOC Ematologia, UOS Fisiopatologia delle Anemie, Fondazione IRCCS Ca' Granda Ospedale Maggiore Policlinico di Milano, Milan, Italy, <sup>2</sup> Department of Pediatric Hematology, Faculty of Medicine, Hacettepe University, Ankara, Turkey, <sup>3</sup> Pediatric Oncohematology Section with BMT, Santa Maria della Misericordia Hospital, Perugia, Italy, <sup>4</sup> Department of Woman, Child and General and Special Surgery, University of Campania "Luigi Vanvitelli", Naples, Italy, <sup>5</sup> Dipartimento di Pediatria, ASST Santi Paolo e Carlo, Presidio Ospedale San Paolo Università di Milano, Milan, Italy

## OPEN ACCESS

### Edited by:

Lesley Jean Bruce,  
NHS Blood and Transplant,  
United Kingdom

### Reviewed by:

Prabhakar S. Kedar,  
National Institute  
of Immunohaematology (ICMR), India  
James Palis,  
University of Rochester, United States

### \*Correspondence:

Elisa Fermo  
elisa.fermo@policlinico.mi.it

### Specialty section:

This article was submitted to  
Red Blood Cell Physiology,  
a section of the journal  
Frontiers in Physiology

**Received:** 14 January 2019

**Accepted:** 04 April 2019

**Published:** 07 May 2019

### Citation:

Fermo E, Vercellati C, Marcello AP, Zaninoni A, Aytac S, Cetin M, Capolsini I, Casale M, Paci S, Zanella A, Barcellini W and Bianchi P (2019) Clinical and Molecular Spectrum of Glucose-6-Phosphate Isomerase Deficiency. Report of 12 New Cases. *Front. Physiol.* 10:467. doi: 10.3389/fphys.2019.00467

Glucose-6-phosphate isomerase (GPI, EC 5.3.1.9) is a dimeric enzyme that catalyzes the reversible isomerization of glucose-6-phosphate to fructose-6-phosphate, the second reaction step of glycolysis. GPI deficiency, transmitted as an autosomal recessive trait, is considered the second most common erythro-enzymopathy of anaerobic glycolysis, after pyruvate kinase deficiency. Despite this, this defect may sometimes be misdiagnosed and only about 60 cases of GPI deficiency have been reported. GPI deficient patients are affected by chronic non-spherocytic hemolytic anemia of variable severity; in rare cases, intellectual disability or neuromuscular symptoms have also been reported. The gene locus encoding GPI is located on chromosome 19q13.1 and contains 18 exons. So far, about 40 causative mutations have been identified. We report the clinical, hematological and molecular characteristics of 12 GPI deficient cases (eight males, four females) from 11 families, with a median age at admission of 13 years (ranging from 1 to 51); eight of them were of Italian origin. Patients displayed moderate to severe anemia, that improves with aging. Splenectomy does not always result in the amelioration of anemia but may be considered in transfusion-dependent patients to reduce transfusion intervals. None of the patients described here displayed neurological impairment attributable to the enzyme defect. We identified 13 different mutations in the *GPI* gene, six of them have never been described before; the new mutations affect highly conserved residues and were not detected in 1000 Genomes and HGMD databases and were considered pathogenic by several mutation algorithms. This is the largest series of GPI deficient patients so far reported in a single study. The study confirms the great heterogeneity of the molecular defect and provides new insights on clinical and molecular aspects of this disease.

**Keywords:** red cell disorders, chronic hemolytic anemias, red cell metabolism, glucose-6-phosphate isomerase deficiency, glycolysis

## INTRODUCTION

Glucose-6-phosphate isomerase (GPI, EC 5.3.1.9) is a dimeric enzyme that catalyzes the reversible isomerization of glucose-6-phosphate (G6P) to fructose-6-phosphate (F6P), the second reaction step of glycolysis (Kugler and Lakomek, 2000). In addition to the catalytic function of the dimeric enzyme, the monomeric form of GPI has been shown to act as a cytokine, its activities including neuroleukin (Gurney et al., 1986), myofibril-bound serine-protease inhibitor (Cao et al., 2000), autocrine motility factor (Watanabe et al., 1996), and the maturation and differentiation factor (Xu et al., 1996). More recently an unexpected relationship between GPI and phosphatidate phosphatase 1 (PAP1) activity involved in glycerolipid biosynthesis has also been reported (Haller et al., 2010).

Glucose-6-phosphate isomerase deficiency (OMIM 172400), transmitted as an autosomal recessive trait, is considered the second most common erythro-enzymopathy of anaerobic glycolysis, after pyruvate kinase deficiency. GPI deficient patients are affected by mild to severe chronic non-spherocytic hemolytic anemia (CNSHA); in rare cases intellectual disability or neuromuscular symptoms have also been reported (Van Biervliet et al., 1975; Kahn et al., 1978; Zanella et al., 1980; Schröter et al., 1985; Shalev et al., 1993; Jamwal et al., 2017).

The gene locus encoding GPI is located on chromosome 19q13.1 and contains 18 exons (Walker et al., 1995). So far, about 60 cases of GPI deficiency have been described, and more than 40 mutations have been reported at the nucleotide level (Kugler and Lakomek, 2000; Clarke et al., 2003; Repiso et al., 2006; Zhu et al., 2015; Manco et al., 2016; Jamwal et al., 2017; Zaidi et al., 2017; Kedar et al., 2018; Mojzikova et al., 2018). Missense mutations are the most common, but non-sense and splicing mutations have also been observed.

In this paper we report the clinical and molecular characterization of 12 patients affected by GPI deficiency: six new mutations of the *GPI* gene have been found and related to the clinical pattern. Long term follow-up allowed us to describe the clinical spectrum of the GPI deficiency from infancy to adulthood.

## PATIENTS AND METHODS

### Patients

Twelve patients (eight males and four females) from 11 families, with a median age at admission of 13 years (ranging from 1 to 51) were studied; eight were of Italian origin, two were Turkish, one from Pakistan and one from Romania.

### Hematological and Enzyme Assays

Blood samples were collected after obtaining written informed consent from the patients and approval from the Institutional Ethical Committee. For patients under the age of 18, written informed consent was obtained from the parents. All the diagnostic procedures and investigations were performed in accordance with the Helsinki Declaration of 1975. Routine hematological investigations were carried out according to Dacie

and Lewis (2001): complete blood count, reticulocyte count, bilirubin, serum ferritin levels, screening for abnormal/unstable hemoglobins, direct antiglobulin test. To exclude red cell membrane disorders, RBC morphology and red cell osmotic fragility tests were evaluated in all cases. When possible EMA binding tests (Bianchi et al., 2012), red cell protein content by SDS-PAGE analyses (Mariani et al., 2008), and RBC deformability analyses by LoRRca MaxSis (Laser-Assisted Optical Rotational Cell Analyzer, Mechatronics, NL) (Zaninoni et al., 2018) were performed. RBC enzymes activities were determined according to Beutler et al. (1977). The diagnosis of GPI deficiency was made through the exclusion of the most common causes of hemolytic anemia, by the demonstration of a reduced GPI activity in the probands or in the parents, and by the identification of homozygous or compound heterozygous mutations in the *GPI* gene.

### Molecular Analysis

Genomic DNA was extracted from leukocytes collected from peripheral blood, using standard manual methods (Sambrook et al., 1989). The entire coding region and intronic flanking regions of the *GPI* gene were analyzed by direct sequencing (ABI PRISM 310 Genetic Analyzer, Applied Biosystems, Warrington, United Kingdom) using the Big Dye Terminator Cycle Sequencing Kit (Applied Biosystems, Warrington, United Kingdom).

When available, total RNA was isolated from leukocytes using TRIzol (Life Technologies, Paisley, United Kingdom) and reverse transcribed to cDNA using random hexamer primers and AMV reverse transcriptase. The entire GPI cDNA was amplified by PCR and automatically sequenced. (RefSeq: ENST00000356487, UniProt P06744). **Table 1** reports the primers used for molecular analysis.

To clarify the pathogenetic effect of the genotype identified in patient seven and to exclude other concomitant causes of hemolysis, the DNA sample of the patient was

**TABLE 1** | Primers used for DNA analysis of GPI gene.

|     |                      |     |                       |
|-----|----------------------|-----|-----------------------|
| 1F  | CGCCCACGCGCCTCGCT    | 1R  | GCCCCGCGCTCCAGACC     |
| 2F  | TCTTCTGGGAACAGCTCCTG | 2R  | GAGGAGGTGACTGAGGTCTA  |
| 3F  | CGTCTGTCTGTCTCATTGGG | 3R  | GGTGAAGACACAGGGTGATG  |
| 4F  | TGTCTAGTGGATAGAGGGCC | 4R  | CCCTCCCTTAAGCTGCA     |
| 5F  | CCAGGACACGGCAGTAATGA | 5R  | ACAGCCAGGTCCCATCCCTG  |
| 6F  | GTCTGGGCACTGTTGGTCC  | 6R  | CCAAAAGGGACCAATGGCCA  |
| 7F  | GTCAGTGTCACTGACCTGCA | 7R  | CCGCCTTCACTTCCAACCTC  |
| 8F  | CTCAGAACCAAGGACTGGGA | 8R  | ATCCACCAGACCTACGAACC  |
| 9F  | TCACGGAGCACAGCTCCCT  | 9R  | GCTAGGTATGCAGCAGGTAC  |
| 10F | GTGCAAGACCAGGGACAGG  | 10R | GCATGATGTTCAAGGACACAA |
| 11F | GCCTTCCTTCGTTGCAGAAG | 11R | GCAGGATGAGTGGGAGCTG   |
| 12F | CTCTGCCAAGTCTGGCCA   | 12R | AATGGGGCAAAGAGCTCCTG  |
| 13F | TTACAGGCTTGAGCCACTGC | 13R | ACTGTGTTCAACCCACATGAC |
| 14F | GGAGGGAAGGATCTTCCAG  | 14R | GCCAACCAATGCACCAGGTT  |
| 15F | GAAGTACCAGGCGGTCTTGT | 15R | CCCATCTGTAGGACAAGCC   |
| 16F | ACCTGCACGTCTCAGCCTC  | 17R | GTGGTATGAGGAAGGCTCTAA |
| 18F | TAGGGGAGGGCCGGGAATA  | 18R | CCACAACCAGAGGGTGCTC   |



further analyzed on an NGS-targeted panel designed by SureDesign software (Agilent Technologies, Santa Clara, CA, United States), containing 40 genes associated with congenital hemolytic anemias. Libraries were obtained by the HaloPlexHS Target Enrichment System Kit and sequenced on a MiSeq platform (Illumina, San Diego, CA, United States).

## RESULTS

**Table 2** reports the main clinical and hematological data in the 12 GPI deficient patients at the time of diagnosis. In 10/12 patients, extensive clinical data, family history, and laboratory data were available, with a median follow-up of 18 years (ranging from 2 to 40 years).

Consanguinity was confirmed in one Turkish patient and suspected in another two families originating from small Italian villages. Despite the onset of anemia reported at birth or early infancy, the median age of diagnosis varied greatly, half of the cases in fact were diagnosed in adulthood (18 to 51 years) (**Figure 1**). Six patients were misdiagnosed before receiving the correct diagnosis of GPI in this study: the most common diagnostic errors were hereditary spherocytosis (four cases), thalassemia (one case), or G6PD deficiency (one case). None of the patients showed neurological symptoms attributable to GPI deficiency. Growth and intellectual disability were reported only in case 5, affected by phenylketonuria<sup>†</sup> (PKU), untreated during infancy. Case 12 had a concomitant G6PD deficiency (0.6 IU/gHb; ref. ranges: 7.2–9.6).

All the patients displayed chronic macrocytic anemia before splenectomy, with median Hb levels during follow-up of 9.4 g/dL (range 8–11.3); median VGM 119 fL (84.8–127.8), MCHC 32.1 g/dL (28.6–33), increased absolute reticulocyte number ( $210 \times 10^9/L$ , range 113–660) and increased unconjugated bilirubin. Recurrent drastic drops down of Hb levels (median 5.4 g/dL, 2.7–6.2) were reported during infection/aplastic crisis in five patients.

In 8/12 cases, information on iron status was available, serum ferritin levels were increased in most patients (median 353 ng/mL, 90–2356), two of them requiring chelation therapy due to iron overload.

All the patients displayed a normal osmotic fragility and EMA-binding test. RBC morphology, available in 9/12 patients, was unremarkable although not comparable to normal subjects; a few spherocytes, stomatocytes (ranging from 3 to 10%), echinocytes (3 to 4%), rare ovalocytes or target cells were reported. A more compromised RBC morphology was observed in the splenectomized patients (**Figure 2**). In six patients, RBC deformability was investigated by LoRRca Osmoscan analysis. Interestingly, all the them showed an altered enlarged Osmoscan curve associated with significantly increased Omin (median 156, range 126–176,  $p < 0.001$ ) and, even more, Ohyper (median 527, range 439–579,  $p < 0.001$ ). Elmax and AUC values were decreased compared to the controls (**Figure 3**).

All the patients but one displayed a reduced GPI activity (from 10 to 40% of low normal reference range). In case 8, who showed

**TABLE 2 |** Clinical and hematological data in the 12 GPI deficient patients at the time of the diagnosis.

| Pt          | Age | Sex | Neon. Jaun. | Extx    | Tx            | Tot. n. | Splenect. (age) | Colecyst. (age) | Hb g/dL                | Retics $10^9/L$ | Hb g/dL          | Retics $10^9/L$ | MCV (fL) | Unc. Bil (mg/dL) | SF (ng/mL) |
|-------------|-----|-----|-------------|---------|---------------|---------|-----------------|-----------------|------------------------|-----------------|------------------|-----------------|----------|------------------|------------|
|             |     |     |             |         |               |         |                 |                 | Pre-splenectomy        |                 | Post-splenectomy |                 |          |                  |            |
| 1           | 2   | M   | Yes         | No      | Occasional    | 4       | No              | No              | 6.1 <sup>*</sup> –10.2 | 231             | –                | –               | 103      | 1.1              | n.a.       |
| 2           | 6   | F   | No          | No      | Occasional    | 2       | No              | No              | 6.2 <sup>*</sup> –11.6 | 166             | –                | –               | 94.9     | n.a.             | n.a.       |
| 3           | 40  | M   | Yes         | Yes     | Occasional    | n.a.    | Yes (9)         | No              | n.a.                   | n.a.            | 11.5             | 445             | 126.5    | 3.56             | 2356       |
| 4           | 8   | F   | No          | No      | Occasional    | n.a.    | Yes (7)         | Yes (7)         | 9.4                    | 113             | 10               | 364             | 105.1    | 3–11.9           | 488        |
| 5           | 1   | M   | Yes         | Yes     | Occasional    | 10      | No              | No              | 10                     | n.a.            | –                | –               | 102      | 5                | 202        |
| 6           | 51  | F   | No          | no      | Occasional    | 9       | Yes (17)        | Yes (18)        | n.a.                   | n.a.            | 10.5             | 170             | 119      | 3.18             | 353        |
| 7           | 3   | M   | No          | No      | Occasional    | n.a.    | No              | No              | 11.7                   | 347             | –                | –               | 127.8    | 0.93             | 210        |
| 8           | 1   | M   | Yes         | Yes (2) | Regular (4w)  | n.a.    | No              | No              | 8.5                    | 410             | –                | –               | 84.8     | 2                | n.a.       |
| 9           | 18  | F   | No          | No      | Regular* (4w) | >50     | Yes (6)         | Yes             | 5.4 <sup>*</sup> –8.9  | 210             | 9.4              | 1420            | 127      | 13.4 (post)      | 1123       |
| 10          | 23  | M   | No          | No      | Regular* (4w) | >30     | Yes (3)         | Yes             | 2.7 <sup>*</sup> –8.4  | 660             | 9.2              | 1740            | 123      | 8.2 (post)       | 185        |
| 11          | 18  | M   | No          | No      | No            | 0       | No              | No              | 10.8                   | 200             | –                | –               | 103.3    | 4.3              | n.a.       |
| 12          | 46  | M   | Yes         | No      | No            | 0       | Yes (45)        | No              | 8.0                    | 126             | 13.9             | 342             | 101.6    | 2.7              | n.a.       |
| Ref. values |     |     |             |         |               |         |                 |                 | 12–16                  | 16–84           | 12–16            | 16–84           | 78–99    | <0.75            | 30–400     |

Tx, transfusions; SF, serum ferritin; n.a., not available; \*, case 9: every 4 weeks until splenectomy then occasional; case 10 every 4 week until splenectomy; †: during hemolytic crises.

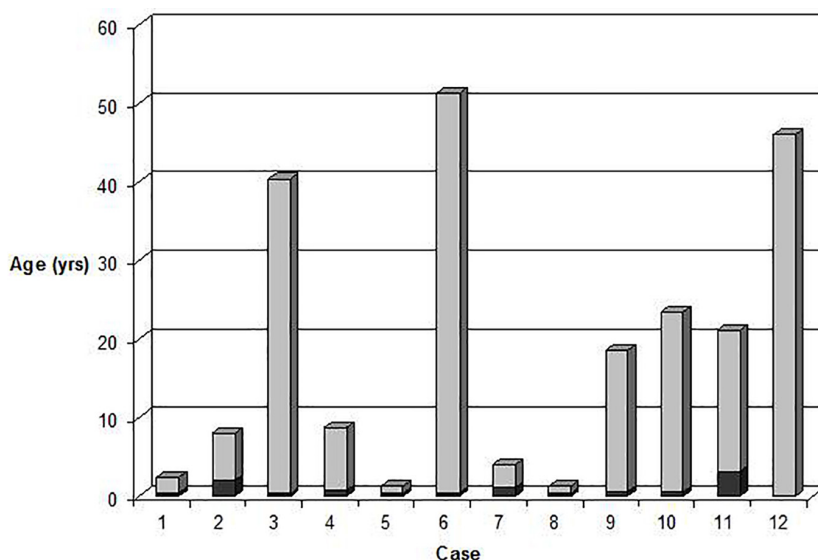


**FIGURE 1** | Age at onset of anemia (dark gray) compared with age at diagnosis (light gray) in the 12 GPI deficient patients.

normal GPI activity, the diagnosis was reached by studying the GPI activity in the parents.

### Glucose-6-Phosphate Isomerase Deficiency in Infancy

No intrauterine growth retardation and/or fetal distress were observed in this series of patients prior to birth. Information on the neonatal period was available in 11 patients. Five of them displayed anemia at birth, the remaining six in early infancy (all before 3 years of age). Neonatal jaundice was present in five patients, three of whom required exchange transfusion. During childhood all patients but two needed blood transfusions: three of them regularly with a transfusion interval of 4 to 8 weeks. The other patients were occasionally transfused in concomitance of hemolytic crises due to infections.

### Glucose-6-Phosphate Isomerase Deficiency and Splenectomy

Six patients were splenectomized, all of them before the diagnosis of GPI deficiency. Only one patient recovered from anemia; in the remaining cases, although resulting only in a slight increase of Hb levels (0.5–1 g/dL), splenectomy greatly reduced or even eliminated transfusion requirement.

Interestingly, in some patients a considerable increase of the reticulocyte counts and unconjugated bilirubin was observed after splenectomy. No thrombotic events have been reported in the six splenectomized patients, since their surgeries.

### Molecular Heterogeneity of Glucose-6-Phosphate Isomerase Deficiency

**Table 3** reports the biochemical and molecular data of the GPI deficient patients.

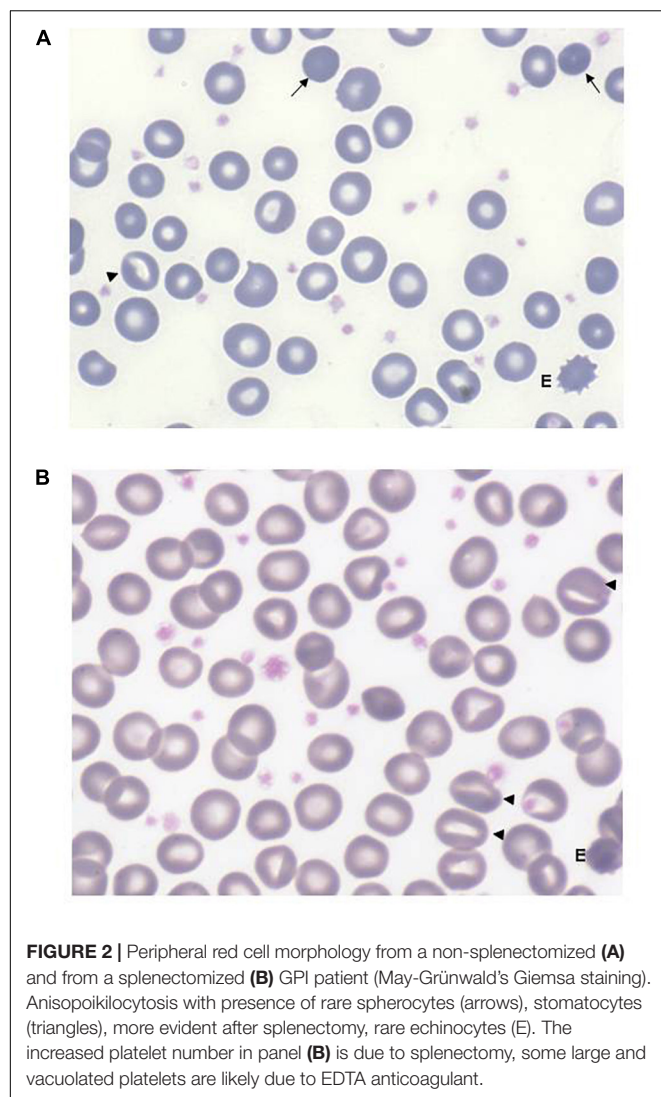
Thirteen different missense mutations were found in the GPI gene, six of them never described before (c.145G>C, p.Gly49Arg; c.269T>C, p.Ile90Thr; c.307C>G, p.Leu103Val; c.311 G>A, p.Arg104Gln; c.839T>G, p.Ile280Ser; c.921C>A, p.Phe307Leu) (**Figure 4**).

All the new mutations affect highly conserved residues, and were predicted to have pathogenic effects by Polyphen-2, Mutation Taster, and M-CAP (**Table 4**).

Seven patients were homozygote and four compounds heterozygotes for two different mutations. In patient 7, despite the sequencing of the entire GPI coding region, intronic flanking regions and promoter, we were able to find only one mutation at the heterozygous level (p.Arg472His), transmitted by the mother. In addition, we detected the polymorphism c.489A>G [synonymous variant p.Gly163=, rs1801015, GMAF 0.20070 (G), ExAC 0.11116], transmitted by the father. No other pathogenic mutations were detected by the NGS targeted sequencing of 40 genes associated with congenital hemolytic anemias, confirming that GPI deficiency was the only cause of anemia in this patient. cDNA analysis in the proband and his parents revealed a loss of heterozygosity, with only the maternal allele present at the cDNA level, suggesting that the paternal allele was not expressed or rapidly degraded. Despite this, we did not find a difference in clinical severity in these patients with respect to the other GPI patients carrying two missense mutations.

## DISCUSSION

The present cohort of GPI deficient patients represents the largest series so far described in a single study, collecting retrospective information and follow-up data over a median period of 18 years. All the cases were never reported before, consistently increasing the number of GPI patients reported



in literature (Kugler and Lakomek, 2000; Clarke et al., 2003; Repiso et al., 2006; Warang et al., 2012; Adama van Scheltema et al., 2015; Zhu et al., 2015; Manco et al., 2016; Jamwal et al., 2017; Zaidi et al., 2017; Burger et al., 2018; Kedar et al., 2018; Mojzíkova et al., 2018).

Despite the fact that GPI deficiency is considered the second most frequent RBC enzymopathy of anaerobic glycolysis after pyruvate kinase, the exact frequency of this disorder is not known and a diagnosis is often difficult to reach; this may be due to the lack of availability of the enzymatic assay, performed only in a few specialized centers, or because of the lack of knowledge about some rare disorders for which specific tests are not considered during laboratory investigations (Bianchi et al., 2018; Kedar et al., 2018; Sonaye et al., 2018). Moreover, due to the similarity in clinical presentation with other congenital hemolytic anemias, an exact diagnosis is often delayed.

An increasing number of new diagnoses might be expected in the coming years due to the advent of new NGS technologies that allow the simultaneous analysis of multiple genes associated to

rare/very rare hemolytic anemias. At least three additional GPI-deficient patients have been reported in the literature in the last 2 years using these technologies (Jamwal et al., 2017; Kedar et al., 2018; Russo et al., 2018).

The possibility to evaluate a consistent group of patients from infancy to adulthood allowed us to describe the clinical picture of GPI deficiency, which is characterized by the onset of chronic macrocytic anemia at birth or early infancy, reticulocytosis, jaundice and splenomegaly associated with mild hepatomegaly; in all the patients in which the information was available, pregnancy was uneventful with normal growth development.

This clinical pattern is in line with cases previously described by our group (Baronciani et al., 1996); however, in some patients a more severe clinical presentation, i.e., hydrops fetalis, has been reported (Ravindranath et al., 1987; Adama van Scheltema et al., 2015).

Neuromuscular impairment or mental retardation are rare complication sometimes reported in GPI deficiency (Van Biervliet et al., 1975; Kahn et al., 1978; Zanella et al., 1980; Shalev et al., 1993; Kugler et al., 1998; Jamwal et al., 2017), as well as in other glycolytic enzyme defects caused by ubiquitously expressed genes (i.e., phosphoglycerate kinase deficiency, phosphofructokinase deficiency or triosephosphate isomerase deficiency). The link between GPI deficiency and neuromuscular dysfunction has not been fully established, and has been attributed to the fact that the monomeric form of GPI is identical to neuroleukin (NLK), a neurotrophic factor that supports the survival of embryonic spinal neurons, skeletal neurons and sensory neurons; however, the proposed hypothesis on the molecular mechanism leading to a neuromuscular dysfunction are in some cases contradictory (Kugler et al., 1998; Repiso et al., 2005). Actually, only three GPI deficient cases with neurological impairment were characterized at molecular level: two of them were homozygous for mutations p.Arg347Cys and p.Arg347His, respectively, and one was compound heterozygous for mutations p.His20Pro and p.Leu339Pro (Beutler et al., 1997; Kugler et al., 1998; Jamwal et al., 2017). A large number of cases with mutations affecting amino acid Arg347 (including two in our series) have been reported with only hematological involvement, suggesting that other possible confounding factors, independent from enzyme deficiency itself, such as kernicterus (Jamwal et al., 2017) or other genetic defects in consanguineous families, may contribute to the clinical phenotype.

A long follow-up time allowed us to shine light on other possible features of GPI deficiency not yet clearly reported in literature: (a) increased sensitivity to infections that result in a dramatic drop-down of hemoglobin levels persisting also in adults, (b) a low response to splenectomy resulting only in a slight increase of Hb levels, however eliminating or reducing the transfusion requirement in all patients, (c) a tendency to increase the reticulocyte number after splenectomy, probably due to selective sequestration of younger GPI defective erythrocytes by the spleen as previously hypothesized in PK deficiency (Mentzer et al., 1971; Matsumoto et al., 1972).

Increased sensitivity to infections was reported in other GPI cases (Helleman and Van Biervliet, 1976; Repiso et al., 2006; Manco et al., 2016; Kedar et al., 2018), making this aspect relevant

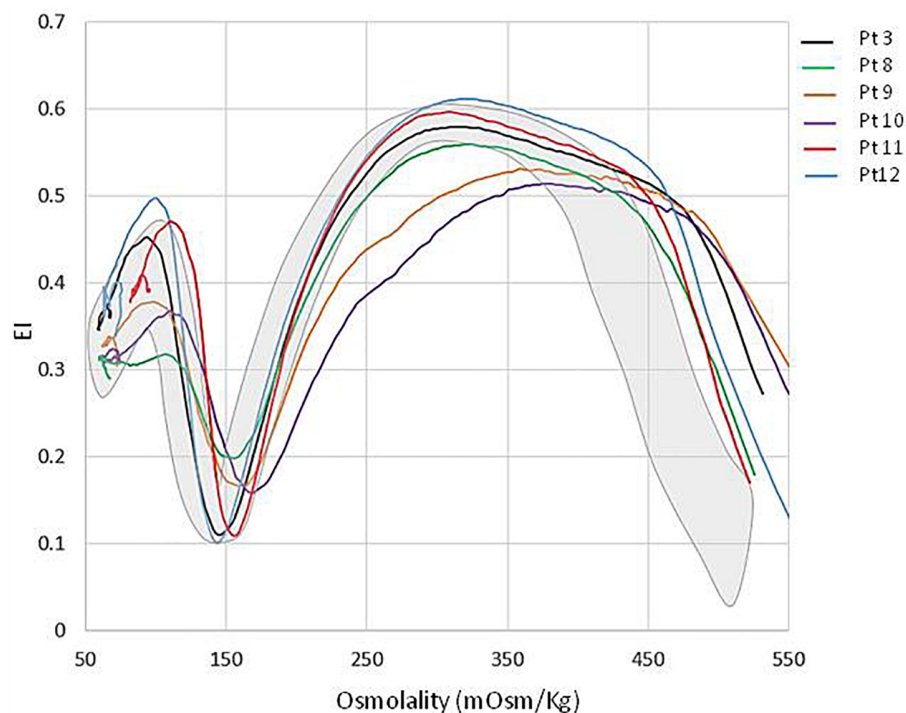


**FIGURE 3 |** LoRRca Osmoscan curve of 6 GPI deficient patients compared with normal controls (gray area).

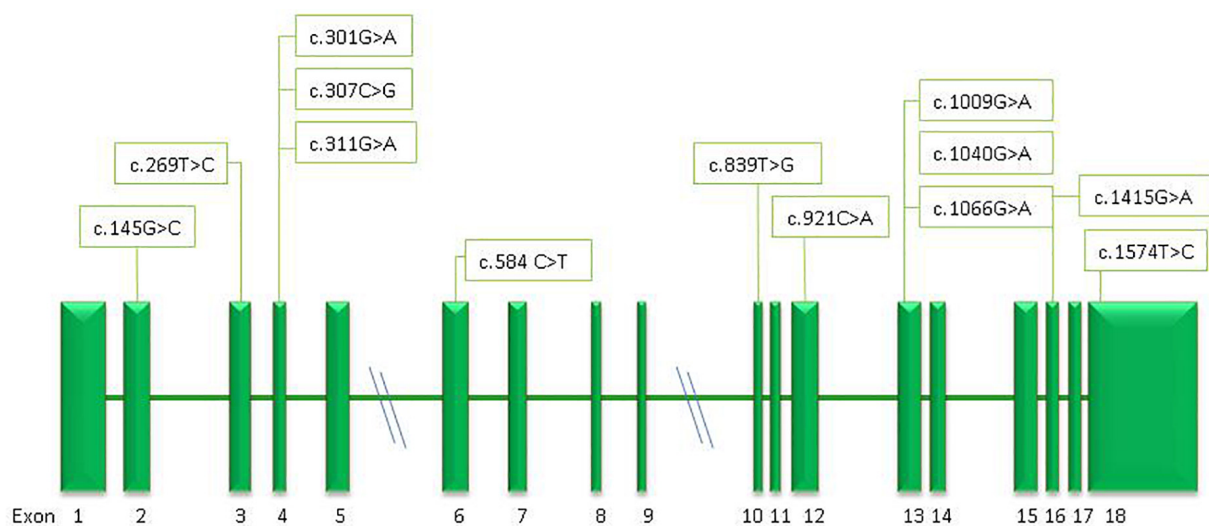


**FIGURE 4 |** Schematic representation of the *GPI* gene and position of the mutations identified in this study.

in the follow-up, suggesting that adequate vaccination coverage should be considered.

As previously reported, GPI-deficient red cells produce an altered Osmoscan profile (LoRRca analyzer), characterized by a right enlarged opened curve (Zaninoni et al., 2018). These findings, which result in a statistically significant increase of Ohyper values, offer an initial laboratory screen for patients with this rare enzyme defect. A possible explanation may reside in

an increased red cell volume, or a cellular overhydrated state resulting in cell swelling of an origin not yet investigated.

Increased thrombotic risk after splenectomy, clearly demonstrated in hereditary xerocytosis, and in overhydrated stomatocytosis (Fermo et al., 2017; Iolascon et al., 2017) has recently been reported in some enzyme defects i.e., pyruvate kinase deficiency (Grace et al., 2018). No thrombotic events have been reported in the analyzed series, or in the GPI deficient



**TABLE 3 |** Biochemical and molecular data of the GPI deficient patients.

| Pt         | GPI activity (IU/gHb) | Residual activity % | Mutation                        | Effect                         |
|------------|-----------------------|---------------------|---------------------------------|--------------------------------|
| 1          | 6                     | 10%                 | <b>c.145G&gt;C/c.921C&gt;A</b>  | <b>p.Gly49Arg/p.Phe307Leu</b>  |
| 2          | 10.5                  | 19%                 | <b>c.311 G&gt;A/c.584C&gt;T</b> | <b>p.Arg104Gln/p.Thr195Ile</b> |
| 3          | 18                    | 32%                 | <b>c.307C&gt;G/c.307C&gt;G</b>  | <b>p.Leu103Val/p.Leu103Val</b> |
| 4          | 15.7                  | 28%                 | c.301G>A/c.1009G>A              | p.Val101Met/p.Ala337Thr        |
| 5          | 13.3                  | 24%                 | c.1009G>A/c.1009G>A             | p.Ala337Thr/p.Ala337Thr        |
| 6          | 14.3                  | 26%                 | c.584C>T/c.584C>T               | p.Thr195Ile/p.Thr195Ile        |
| 7          | 16                    | 29%                 | c.489A>G (rs1801015)/c.1415G>A  | LOH/p.Arg472His                |
| 8          | 54.6                  | 98%                 | <b>c.269T&gt;C/c.1066G&gt;A</b> | <b>p.Ile90Thr/p.Asp356Asn</b>  |
| 9          | 22                    | 40%                 | c.1040G>A/c.1040G>A             | p.Arg347His/p.Arg347His        |
| 10         | 17                    | 30%                 | c.1040G>A/c.1040G>A             | p.Arg347His/p.Arg347His        |
| 11         | 20.2                  | 36.5%               | <b>c.839T&gt;G/c.839T&gt;G</b>  | <b>p.Ile280Ser/p.Ile280Ser</b> |
| 12         | 4.8                   | 9%                  | c.1574 T>C/c.1574 T>C           | p.Ile525Thr/p.Ile525Thr        |
| Ref. range | 55,3–72,3             |                     |                                 |                                |

Percentage of residual GPI activity was calculated on the lower reference value. New mutations are reported in bold.

**TABLE 4 |** List of new variants identified.

| HGVS coding | HGVS protein | GPI structure | Exon | Status | Polyphen-2            | M-CAP   | MAF1000G | MAF ExAC     | RefSeqID    |
|-------------|--------------|---------------|------|--------|-----------------------|---------|----------|--------------|-------------|
| c.145G>C    | Gly49Arg     | Lβ1-β2        | 2    | Het    | 1.000 (0.00; 1.00) D  | 0.358 P | –        | –            | –           |
| c.269T>C    | p.Ile90Thr   | Lα6-Turn      | 3    | Het    | 1.000 (0.00; 1.00) D  | 0.343 P | –        | –            | –           |
| c.307C>G    | p.Leu103Val  | α8            | 4    | Hom    | 0.649 (0.87; 0.91) PD | 0.479 P | –        | –            | –           |
| c.311 G>A   | p.Arg104Gln  | Lα8-b4        | 4    | Het    | 0.544 (0.88; 0.91) PD | 0.577 P | –        | –            | –           |
| c.839T>G    | p.Ile280Ser  | α21           | 10   | Hom    | 1.000 (0.00; 1.00) D  | 0.611 P | –        | –            | –           |
| c.921C>A    | p.Phe307Leu  | α23           | 12   | Het    | 1.000 (0.00; 1.00) D  | 0.383 P | –        | A = 0.000008 | rs754782152 |

Polyphen-2 analysis (HumDiv) PD, possibly damaging; D, probably damaging; in bracket sensitivity, specificity; M-CAP P, possibly pathogenetic (ref. Jagadeesh et al., 2016). Recommended pathogenicity threshold: Polyphen-2 > 0.8 (with misclassified pathogenetic variants 31%); M-CAP > 0.025 (with misclassified pathogenetic variants 5%).

cases reported in literature; however, we cannot exclude that this information might be lost at follow up.

Information on iron status and erythropoietic activity in GPI deficiency is scant, although it is known that iron overload may frequently occur in other more common glycolytic enzymopathies as a consequence of various factors, including hyperhaemolysis or ineffective erythropoiesis. Only iron stores (ferritin levels) were available in the present series and found to be elevated in four of seven patients, underlying the need of monitoring iron status in this disease.

Glucose-6-phosphate isomerase deficiency shows a wide molecular heterogeneity with more than 40 mutations in the GPI gene currently listed in the Human Gene Mutation Database<sup>1</sup>. Most of them are missense, covering about 93% of the total mutations identified, with only a few splicing, nonsense or frameshift mutations (Kugler and Lakomek, 2000; Manco et al., 2016). This is in line with the findings in our series, where all the different mutations identified were missense. Despite this, loss of heterozygosity at the cDNA level in patient 7, who did not show the second causative mutation, neither by Sanger sequencing nor by NGS targeted sequencing, may suggest that in GPI deficiency some drastic molecular abnormalities escape the conventional screening techniques. Interestingly, patient 7 carried the paternal allele on the silent polymorphic variant c.489A>G (p.Gly163=),

that is located in the third nucleotide of exon 6. Although we did not perform functional *in vitro* analysis of this silent mutation, we cannot exclude that the variant, although polymorphic, may interfere with the normal splicing, resulting in an unstable mRNA, rapidly degraded.

Despite the molecular heterogeneity, some recurrent mutations have been identified in GPI deficiency. This is the case of missense mutations affecting the amino acid Arg347, here detected in two brothers of Turkish origin (c.1040G>A, p.Arg347His) and already reported in literature in other unrelated patients of different ethnical origins (Walker et al., 1993; Repiso et al., 2006; Lin et al., 2009); another mutation at the same codon (c.1039 C>T, p. Arg347Cys) has also been described (Xu and Beutler, 1994; Lin et al., 2009), suggesting the presence of a mutational hotspot (Repiso et al., 2005). Arg347 is a highly conserved residue (GERP 5.65), falling in the region responsible for GPI dimerization. It has been hypothesized that a mutation in these residues causes a loss of GPI capability to dimerize, making the enzyme more susceptible to thermolability; actually, kinetic studies performed in a mutant enzyme from an homozygous p.Arg347His patient, showed that the Km for G6P and for F6P were not altered, but the thermostability was drastically reduced (Repiso et al., 2005).

Different than expected and previously reported in literature (Walker et al., 1993; Repiso et al., 2005) the cases in this series carrying mutation p.Arg347His did not show a drastic reduction

<sup>1</sup> www.hgmd.cf.ac.uk

of GPI activity (30–40% of residual activity vs. 18% reported by others); this could be explained by technical variability in the enzymatic assay, or by the very high number of reticulocytes found in our patients at the time of the assay, which may display an higher enzyme activity than mature red cells (Beutler et al., 1977). Other recurrent mutations found in this series were p.Thr195Ile and p.Val101Met, already reported in Italian patients by Baronciani et al. (1996).

## CONCLUSION

In conclusion, the study confirms the great heterogeneity of the molecular defect and provides new insights on clinical and molecular aspects of this disease.

## REFERENCES

- Adama van Scheltema, P. N., Zhang, A., Ball, L. M., Steggerda, S. J., van Wijk, R., Fransen van de Putte, D. E., et al. (2015). Successful treatment of fetal hemolytic disease due to glucose phosphate isomerase deficiency (GPI) using repeated intrauterine transfusions: a case report. *Clin. Case Rep.* 3, 862–865. doi: 10.1002/ccr3.358
- Baronciani, L., Zanella, A., Bianchi, P., Zappa, M., Alfinito, F., Iolascon, A., et al. (1996). Study of the molecular defects in glucose phosphate isomerase-deficient patients affected by chronic hemolytic anemia. *Blood* 88, 2306–2310.
- Beutler, E., Blume, K. G., Kaplan, J. C., Lohr, G. W., Ramot, B., and Valentine, W. N. (1977). International Committee for Standardization in Haematology: recommended methods for red-cell enzyme analysis. *Br. J. Haematol.* 35, 331–340. doi: 10.1111/j.1365-2141.1977.tb00589.x
- Beutler, E., West, C., Britton, H. A., Harris, J., and Forman, L. (1997). Glucosephosphate isomerase (GPI) deficiency mutations associated with hereditary nonspherocytic hemolytic anemia (HNSHA). *Blood Cells Mol. Dis.* 23, 402–409. doi: 10.1006/bcmd.1997.0157
- Bianchi, P., Fermo, E., Glader, B., Kanno, H., Agarwal, A., Barcellini, W., et al. (2018). Addressing the diagnostic gaps in pyruvate kinase deficiency: consensus recommendations on the diagnosis of pyruvate kinase deficiency. *Am. J. Hematol.* [Epub ahead of print].
- Bianchi, P., Fermo, E., Vercellati, C., Marcello, A. P., Porretti, L., Cortezzi, A., et al. (2012). Diagnostic power of laboratory tests for hereditary spherocytosis: a comparison study in 150 patients grouped according to molecular and clinical characteristics. *Haematologica* 97, 516–523. doi: 10.3324/haematol.2011.052845
- Burger, N. C. M., van Wijk, R., Bresters, D., and Schell, E. A. (2018). A novel mutation of glucose phosphate isomerase (GPI) causing severe neonatal anemia due to GPI deficiency. *J. Pediatr. Hematol. Oncol.* 41, e186–e189. doi: 10.1097/MPH.0000000000001393
- Cao, M. J., Osatomi, K., Matsude, R., Ohkubo, M., Hara, K., and Ishihara, K. (2000). Purification of a novel serine proteinase inhibitor from skeletal muscle of white croaker (*Argyrosomus argentatus*). *Biochem. Biophys. Res. Commun.* 272, 485–489. doi: 10.1006/bbrc.2000.2803
- Clarke, J. L., Vulliamy, T. J., Roper, D., Mesbah-Namin, S. A., Wild, B. J., Walker, J. I., et al. (2003). Combined glucose-6-phosphate dehydrogenase and glucosephosphate isomerase deficiency can alter clinical outcome. *Blood Cells Mol. Dis.* 30, 258–263. doi: 10.1016/s1079-9796(03)00027-5
- Dacie, J. V., and Lewis, S. M. (2001). *Practical Haematology*, 9th Edn. London: Churchill Livingstone.
- Fermo, E., Vercellati, C., Marcello, A. P., Zaninoni, A., van Wijk, R., and Mirra, N. (2017). Hereditary xerocytosis due to mutations in PIEZO1 gene associated with heterozygous pyruvate kinase deficiency and beta-thalassemia trait in two unrelated families. *Case Rep. Hematol.* 2017:2769570. doi: 10.1155/2017/2769570
- Grace, R. F., Bianchi, P., van Beers, E. J., Eber, S. W., Glader, B., Yaish, H. M., et al. (2018). Clinical spectrum of pyruvate kinase deficiency: data from the

## AUTHOR CONTRIBUTIONS

EF and PB performed the molecular analysis, analyzed the results, prepared and revised the manuscript. CV, AM, and AnZ performed the hematologic and biochemical investigations. SA, MuC, IC, MaC, SP, ALZ, and WB performed the patient follow-up and revision of the manuscript.

## FUNDING

The study was supported by the Fondazione IRCCS “Ca’ Granda” Ospedale Maggiore Policlinico Milano, Project number RC 175/04, 2015–2017.

- pyruvate kinase deficiency natural history study. *Blood* 131, 2183–2192. doi: 10.1182/blood-2017-10-810796
- Gurney, M. E., Heinrich, S. P., Lee, M. R., and Yin, H. S. (1986). Molecular cloning and expression of neuroleukin, a neurotrophic factor for spinal and sensory neurons. *Science* 234, 566–573.
- Haller, J. F., Smith, C., Liu, D., Zheng, H., Tornheim, K., Ham, G.-S., et al. (2010). Isolation of novel animal cell lines isomerase reveals mutations in glucose-6-phosphate defective in glycerolipid biosynthesis. *J. Biol. Chem.* 285, 866–877. doi: 10.1074/jbc.M109.068213
- Hellemans, P. W., and Van Biervliet, J. P. (1976). Haematological studies in a new variant of glucosephosphate isomerase deficiency (GPI Utrecht). *Helv. Paediatr. Acta* 30, 525–536.
- Iolascon, A., Andolfo, I., Barcellini, W., Corcione, F., Garçon, L., De Franceschi, L., et al. (2017). Recommendations regarding splenectomy in hereditary hemolytic anemias. *Haematologica* 102, 1304–1313. doi: 10.3324/haematol.2016.161166
- Jagadeesh, K. A., Wenger, A. M., Berger, M. J., Guturu, H., Stenson, P. D., Cooper, D. N., et al. (2016). M-CAP eliminates a majority of variants of uncertain significance in clinical exomes at high sensitivity. *Nat. Genet.* 48, 1581–1586. doi: 10.1038/ng.3703
- Jamwal, M., Aggarwal, A., Das, A., Maitra, A., Sharma, P., Krishnan, S., et al. (2017). Next-generation sequencing unravels homozygous mutation in glucose-6-phosphate isomerase, GPIc.1040G> A (p.Arg347His) causing hemolysis in an Indian infant. *Clin. Chim. Acta* 468, 81–84. doi: 10.1016/j.cca.2017.02.012
- Kahn, A., Buc, H. A., Giro, R., Cottreau, D., and Griscelli, C. (1978). Molecular and functional anomalies in two new mutant glucose-phosphate-isomerase variants with enzyme deficiency and chronic hemolysis. *Hum. Genet.* 40, 293–304. doi: 10.1007/bf00272190
- Kedar, P. S., Gupta, V., Dongerdiye, R., Chiddarwar, A., Warang, P., and Madkaikar, M. R. (2018). Molecular diagnosis of unexplained haemolytic anaemia using targeted next-generation sequencing panel revealed (p.Ala337Thr) novel mutation in GPI gene in two Indian patients. *J. Clin. Pathol.* 2019, 81–85. doi: 10.1136/jclinpath-2018-205420
- Kugler, W., Brems, K., Laspe, P., Muirhead, H., Davies, C., Winkler, H., et al. (1998). Molecular basis of neurological dysfunction coupled with haemolytic anaemia in human glucose-6-phosphate isomerase (GPI) deficiency. *Hum. Genet.* 103, 450–454. doi: 10.1007/s004390050849
- Kugler, W., and Lakomek, M. (2000). Glucose-6-phosphate isomerase deficiency. *Baillière's Best. Pract. Res. Clin. Haematol.* 13, 89–101. doi: 10.1053/beha.1999.0059
- Lin, H. Y., Kao, Y. H., Chen, S. T., and Meng, M. (2009). Effects of inherited mutations on catalytic activity and structural stability of human glucose-6-phosphate isomerase expressed in *Escherichia coli*. *Biochim. Biophys. Acta* 1794, 315–323. doi: 10.1016/j.bbapap.2008.11.004
- Manco, L., Bento, C., Victor, B. L., Pereira, J., Relvas, L., Brito, R. M., et al. (2016). Hereditary nonspherocytic hemolytic anemia caused by red cell glucose-6-phosphate isomerase (GPI) deficiency in two Portuguese patients: clinical features and molecular study. *Blood Cells Mol. Dis.* 60, 18–23. doi: 10.1016/j.bcmd.2016.06.002

- Mariani, M., Barcellini, W., Vercellati, C., Marcello, A. P., Fermo, E., Pedotti, P., et al. (2008). Clinical and hematologic features of 300 patients affected by hereditary spherocytosis grouped according to the type of the membrane protein defect. *Haematologica* 93, 1310–1317. doi: 10.3324/haematol.12546
- Matsumoto, N., Ishihara, T., Nakashima, K., Miwa, S., Uchino, F., and Kondo, M. (1972). Sequestration and destruction of reticulocytes in the spleen in pyruvate kinase deficiency hereditary non-spherocytic hemolytic anemia. *Nippon Ketsueki Gakkai zasshi* 35, 525–537.
- Mentzer, W. C. Jr., Baehner, R. L., Schmidt-Schonbeth, H., Robinson, S. H., and Nathan, D. G. (1971). Selective reticulocyte destruction in erythrocyte pyruvate kinase deficiency. *J. Clin. Invest.* 5, 688–699.
- Mojzikova, R., Koralkova, P., Holub, D., Saxova, Z., Pospisilova, D., Prochazkova, D., et al. (2018). Two novel mutations (p.(Ser160Pro) and p.(Arg472Cys) causing glucose-6-phosphate isomerase deficiency are associated with erythroid dysplasia and inappropriately suppressed hepcidin. *Blood Cells Mol. Dis.* 69, 23–29. doi: 10.1016/j.bcmd.2017.04.003
- Ravindranath, Y., Paglia, D. E., Warrier, I., Valentine, W., Nakatani, M., and Brockway, R. A. (1987). Glucose phosphate isomerase deficiency as a cause of hydrops fetalis. *N. Engl. J. Med.* 316, 258–261. doi: 10.1056/nejm198701293160506
- Repiso, A., Oliva, B., Vives Corrons, J. L., Carreras, J., and Climent, F. (2005). Glucose phosphate isomerase deficiency: enzymatic and familial characterization of Arg346His mutation. *Biochim. Biophys. Acta* 1740, 467–471. doi: 10.1016/j.bbdis.2004.10.008
- Repiso, A., Oliva, B., Vives-Corrons, J. L., Beutler, E., Carreras, J., and Climent, F. (2006). mRed cell glucose phosphate isomerase (GPI): a molecular study of three novel mutations associated with hereditary nonspherocytic hemolytic anemia. *Hum. Mutat.* 27:1159. doi: 10.1002/humu.9466
- Russo, R., Andolfo, I., Manna, F., Gambale, A., Marra, R., Rosato, B. E., et al. (2018). Multi-gene panel testing improves diagnosis and management of patients with hereditary anemias. *Am. J. Hematol.* 93, 672–682. doi: 10.1002/ajh.25058
- Sambrook, J., Fritsch, E. F., and Maniatis, T. (1989). *Molecular Cloning. A Laboratory Manual*. New York, NY: Cold Spring Harbor Laboratory Press.
- Schröter, W., Eber, S. W., Bardosi, A., Gahr, M., Gabriel, M., and Sitzmann, F. C. (1985). Generalised glucosylphosphate isomerase (GPI) deficiency causing haemolytic anaemia, neuromuscular symptoms and impairment of granulocytic function: a new syndrome due to a new stable GPI variant with diminished specific activity (GPI Homburg). *Eur. J. Paediatr.* 144, 301–305. doi: 10.1007/bf00441768
- Shalev, O., Shalev, R. S., Forman, L., and Beutler, E. (1993). GPI mount scopus  $\pm$  a variant of glucose-phosphate isomerase deficiency. *Ann. Hematol.* 67, 197–200. doi: 10.1007/bf01695868
- Sonaye, R., Sombans, S., and Ramphul, K. (2018). A case report of congenital non-spherocytic hemolytic anemia in a patient from India. *Cureus* 2018:e2478. doi: 10.7759/cureus.2478
- Van Biervliet, J. P., Van Milligen-Boersma, L., and Staal, G. E. (1975). A new variant of glucosylphosphate isomerase deficiency (GPI-Utrecht). *Clin. Chim. Acta* 65, 157–165. doi: 10.1016/0009-8981(75)90103-5
- Walker, J. I. H., Layton, D. M., Bellingham, A. J., Morgan, M. J., and Faik, P. (1993). DNA sequence abnormalities in human glucose 6-phosphate isomerase deficiency. *Hum. Mol. Gen.* 2, 327–329. doi: 10.1093/hmg/2.3.327
- Walker, J. I. H., Morgan, M. J., and Faik, P. (1995). Structure and organization of the human glucose phosphate isomerase gene (GPI). *Genomics* 29, 261–265. doi: 10.1006/geno.1995.1241
- Warang, P., Kedar, P., Ghosh, K., and Colah, R. B. (2012). Hereditary non-spherocytic hemolytic anemia and severe glucose phosphate isomerase deficiency in an Indian patient homozygous for the L487F mutation in the human GPI gene. *Int. J. Hematol.* 96, 263–267. doi: 10.1007/s12185-012-1122-x
- Watanabe, H., Takehana, K., Date, M., Shinozaki, T., and Raz, A. (1996). Tumor cell autocrine motility factor is the neuroleukin/phosphohexose isomerase polypeptide. *Cancer Res.* 56, 2960–2963.
- Xu, W., and Beutler, E. (1994). The characterization of gene mutations for human glucose phosphate isomerase deficiency associated with chronic haemolytic anemia. *J. Clin. Invest.* 94, 2326–2329. doi: 10.1172/jci117597
- Xu, W., Seiter, K., Feldman, E., Ahmed, T., and Chiao, J. W. (1996). The differentiation and maturation mediator for human myeloid leukemia cells shares homology with neuroleukin or phosphoglucose isomerase. *Blood* 87, 4502–4506.
- Zaidi, A. U., Kedar, P., Koduri, P. R., Goyette, G. W. Jr., Buck, S., Paglia, D. E., et al. (2017). Glucose phosphate isomerase (GPI) Tadikonda: characterization of a novel Pro340Ser mutation. *Pediatr. Hematol. Oncol.* 34, 449–454. doi: 10.1080/08880018.2017.1383541
- Zanella, A., Izzo, C., Rebulla, P., Perroni, L., Mariani, M., Canestri, G., et al. (1980). The first stable variant of erythrocyte glucose-phosphate isomerase associated with severe hemolytic anemia. *Am. J. Hematol.* 9, 1–11. doi: 10.1002/ajh.2830090102
- Zaninoni, A., Fermo, E., Vercellati, C., Consonni, D., Marcello, A. P., Zanella, A., et al. (2018). Use of laser assisted optical rotational cell analyzer (LoRRca MaxSis) in the diagnosis of RBC membrane disorders, enzyme defects, and congenital dyserythropoietic anemias: a monocentric study on 202 patients. *Front. Physiol.* 9:451. doi: 10.3389/fphys.2018.00451
- Zhu, X., Petrovski, S., Xie, P., Ruzzo, E. K., Lu, Y. F., McSweeney, K. M., et al. (2015). Whole-exome sequencing in undiagnosed genetic diseases: interpreting 119 trios. *Genet. Med.* 17, 774–781. doi: 10.1038/gim.2014.191

**Conflict of Interest Statement:** The authors declare that the research was conducted in the absence of any commercial or financial relationships that could be construed as a potential conflict of interest.

Copyright © 2019 Fermo, Vercellati, Marcello, Zaninoni, Aytac, Cetin, Capolsini, Casale, Paci, Zanella, Barcellini and Bianchi. This is an open-access article distributed under the terms of the Creative Commons Attribution License (CC BY). The use, distribution or reproduction in other forums is permitted, provided the original author(s) and the copyright owner(s) are credited and that the original publication in this journal is cited, in accordance with accepted academic practice. No use, distribution or reproduction is permitted which does not comply with these terms.



# Glutaraldehyde – A Subtle Tool in the Investigation of Healthy and Pathologic Red Blood Cells

Aseña Abay<sup>1,2†</sup>, Greta Simionato<sup>1,3†</sup>, Revaz Chachanidze<sup>1,4</sup>, Anna Bogdanova<sup>5</sup>, Laura Hertz<sup>1,3</sup>, Paola Bianchi<sup>6</sup>, Emile van den Akker<sup>2</sup>, Marieke von Lindern<sup>2</sup>, Marc Leonetti<sup>4</sup>, Giampaolo Minetti<sup>7</sup>, Christian Wagner<sup>1,8</sup> and Lars Kaestner<sup>1,3\*</sup>

<sup>1</sup> Dynamics of Fluids, Department of Experimental Physics, Saarland University, Saarbrücken, Germany, <sup>2</sup> Landsteiner Laboratory, Sanquin, Amsterdam, Netherlands, <sup>3</sup> Theoretical Medicine and Biosciences, Saarland University, Homburg, Germany, <sup>4</sup> Université Grenoble Alpes, CNRS, Grenoble INP, LRP, Grenoble, France, <sup>5</sup> Red Blood Cell Research Group, Institute of Veterinary Physiology, Vetsuisse Faculty and the Zurich Center for Integrative Human Physiology (ZIHP), University of Zurich, Zurich, Switzerland, <sup>6</sup> UOC Ematologia, UOS Fisiopatologia delle Anemie, Fondazione IRCCS Ca' Granda Ospedale Maggiore Policlinico, Milan, Italy, <sup>7</sup> Laboratory of Biochemistry, Department of Biology and Biotechnology, University of Pavia, Pavia, Italy, <sup>8</sup> Physics and Materials Science Research Unit, University of Luxembourg, Luxembourg City, Luxembourg

## OPEN ACCESS

### Edited by:

Angelo D'Alessandro,  
University of Colorado Denver,  
United States

### Reviewed by:

Yang Xia,  
The University of Texas Health  
Science Center at Houston,  
United States  
Allan Doctor,  
Washington University in St. Louis,  
United States

### \*Correspondence:

Lars Kaestner  
lars\_kaestner@me.com

<sup>†</sup>These authors have contributed  
equally to this work

### Specialty section:

This article was submitted to  
Red Blood Cell Physiology,  
a section of the journal  
Frontiers in Physiology

**Received:** 25 January 2019

**Accepted:** 11 April 2019

**Published:** 14 May 2019

### Citation:

Abay A, Simionato G,  
Chachanidze R, Bogdanova A,  
Hertz L, Bianchi P, van den Akker E,  
von Lindern M, Leonetti M, Minetti G,  
Wagner C and Kaestner L (2019)  
Glutaraldehyde – A Subtle Tool  
in the Investigation of Healthy  
and Pathologic Red Blood Cells.  
Front. Physiol. 10:514.  
doi: 10.3389/fphys.2019.00514

Glutaraldehyde is a well-known substance used in biomedical research to fix cells. Since hemolytic anemias are often associated with red blood cell shape changes deviating from the biconcave disk shape, conservation of these shapes for imaging in general and 3D-imaging in particular, like confocal microscopy, scanning electron microscopy or scanning probe microscopy is a common desire. Along with the fixation comes an increase in the stiffness of the cells. In the context of red blood cells this increased rigidity is often used to mimic malaria infected red blood cells because they are also stiffer than healthy red blood cells. However, the use of glutaraldehyde is associated with numerous pitfalls: (i) while the increase in rigidity by an application of increasing concentrations of glutaraldehyde is an analog process, the fixation is a rather digital event (all or none); (ii) addition of glutaraldehyde massively changes osmolality in a concentration dependent manner and hence cell shapes can be distorted; (iii) glutaraldehyde batches differ in their properties especially in the ratio of monomers and polymers; (iv) handling pitfalls, like inducing shear artifacts of red blood cell shapes or cell density changes that needs to be considered, e.g., when working with cells in flow; (v) staining glutaraldehyde treated red blood cells need different approaches compared to living cells, for instance, because glutaraldehyde itself induces a strong fluorescence. Within this paper we provide documentation about the subtle use of glutaraldehyde on healthy and pathologic red blood cells and how to deal with or circumvent pitfalls.

**Keywords:** glutaraldehyde, erythrocytes, hemolytic anemia, fixation, cell shapes, stiffness, osmolality, batch variation

## INTRODUCTION

Besides its application as disinfectant and medication, glutaraldehyde is used in biomedical research to fix cells. The principle behind the fixation is the binding of glutaraldehyde to nucleophiles of which the amino groups are the most abundant but binding to, e.g., sulfhydryl groups also occurs (Griffiths, 1993). The result is a crosslinking of the proteins of the cell (Kawahara et al., 1997),



**Figure 1.** Approximately 45–50 years ago, glutaraldehyde and its properties were a hot research topic (Richards and Knowles, 1968; Hardy et al., 1969; Robertson and Schultz, 1970; Morel et al., 1971; Gillett and Gull, 1972; Rasmussen and Albrechtsen, 1974; Squier et al., 1976). Such studies mention the abundance of this molecule in monomeric and polymeric form, discussing the formation of polymers at high temperatures and arguing the influence of monomers and polymers in fixation efficiency. Nowadays glutaraldehyde is “only” used as a tool to fix cells. Especially for rare red blood cell (RBC)-related diseases, cell shape is an important diagnostic parameter and fixation is an approach to circumvent the subtle sample transportation challenge (Makhro et al., 2016; Hertz et al., 2017). However, a large variety of protocols exist due to laboratory specific customs and habits. Even for the storage of the glutaraldehyde a non-representative poll among collaborators revealed storage from room temperature, refrigerated to frozen conditions.

Along with the fixation comes an increase in the stiffness of the cells. In the context of RBCs this increased rigidity is often used to mimic malaria infected RBCs because they are also stiffer than healthy RBCs (Aingaran et al., 2012). Furthermore, hydrodynamic studies on blood flow and RBC interactions use glutaraldehyde as a parameter to change cellular rigidity, supposing a gradual concentration dependent process increases the stiffness of the cells.

Here we summarize properties and provide original data of glutaraldehyde's action on RBCs and stress the parameters that are important in particular in respect to RBC related pathologies

to avoid pitfalls and to allow data reproducibility as well as interlaboratory-comparability.

## MATERIALS AND METHODS

### Blood Collection

Donors and patients were enrolled in the study after signing an informed consent. The procedure is approved by the local ethics committee (approval no. 51/18) and was performed in accordance with the Helsinki international ethical standards on human experimentation. Venous blood was collected into EDTA coated tubes (1.6 mg/ml). RBCs were isolated from the whole blood by washing (centrifugation,  $380 \times g$ , 5 min) 3 times with PBS (Sigma, Germany).

### Glutaraldehyde Supply

Partly because this paper reflects a collaborative project including partners at different locations and partly by purpose, different sources of glutaraldehyde have been used throughout this study. The source (supplier), the mode of storage and in which experiments/measurements they were used in are summarized in Table 1.

### RBC Stability Test

PBS solutions (39.4 ml) with various concentrations of glutaraldehyde (various suppliers) were prepared in 50 ml tubes. Packed RBCs (600  $\mu$ l) were pipetted slowly into the solution. The large tube and the high solution/cell volume ratio (65:1) was chosen to make sure the sample had sufficient volume to fix as individual cells and would not form aggregates. The tubes were placed on a tube roller for 1 h to allow for glutaraldehyde to fix. After the fixation procedure, glutaraldehyde was removed by washing the cells 3 times with PBS and resuspended in the same solution. To test the “stability” of the cells the supernatant was spectroscopically tested for hemoglobin to identify the portion of lysed cells. For the spectrophotometry each tube was resuspended completely until the whole sample appeared homogenous. Three milliliter from each sample were placed into a new tube and centrifuged at  $500 \times g$  for 5 min to get a clear distinction between the pellet and the supernatant. One milliliter from the supernatant was placed in a spectrometer cuvette and was diluted 1:3 with PBS to ensure the hemoglobin absorption value is within the limits of the spectrophotometer (Red Tide, Ocean Optics, Netherlands). The hemoglobin absorption peak of the Soret band at about 420 nm was observed and compared between the samples. As a 100% hemolysis reference, healthy RBCs were lysed with distilled water to measure the total hemoglobin content.

### Spectroscopy

To determine the ratio of glutaraldehyde monomers and polymers, UV-absorption spectroscopy was performed at room temperature. The extinction peaks are at 280 nm for monomers and at around 235 nm for polymers (Morel et al., 1971). To determine the monomer-polymer ratio, putative 1% glutaraldehyde samples were prepared in water. Spectra were recorded on these samples for wavelengths from 200 nm to

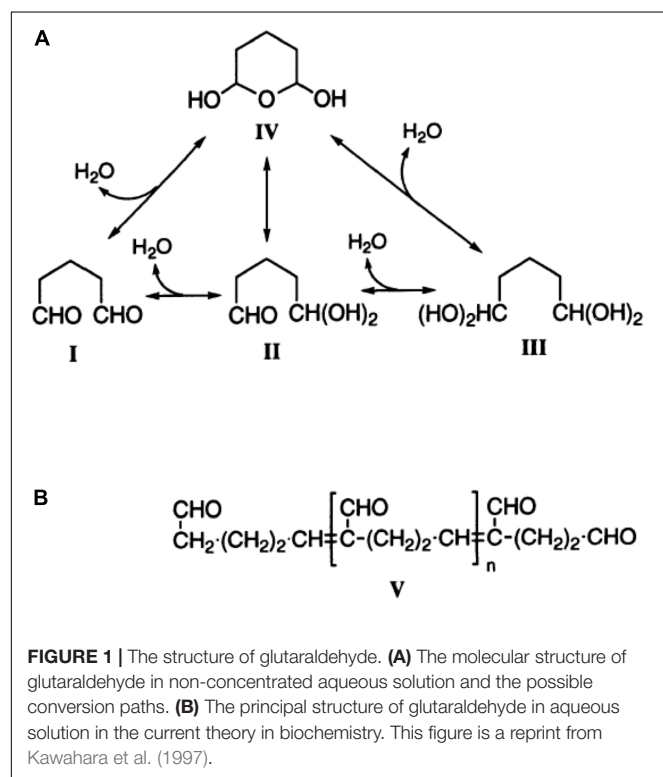


**TABLE 1** | Sources of glutaraldehyde and in which measurements they were used.

| Supplier and grade                      | Mode of storage  | Measurements used   |
|---|--|---|
| Sigma, grade I, 25% in H <sub>2</sub> O | –20°C; more than one year of storage, thawed for every use | <b>Figures 2A,C</b> ; batch 1 in <b>Figures 3B, 4B,C</b>  |
| Merck 25% in H <sub>2</sub> O           | Refrigerated   | <b>Figure 2B</b>  |
| Sigma, grade I, 25% in H <sub>2</sub> O | –20°C; fresh batch   | <b>Figures 3A,C, 5, 6B,D, 7B, 8</b> ; batch 2 in <b>Figures 3B, 4B,C</b> ; dashed line in <b>Figure 4A</b> ; bold lines in <b>Figure 6A</b> |
| Merck 25% in H <sub>2</sub> O           | room temperature for more than one year                    | batch 3 in <b>Figures 3B, 4B,C</b> ; solid line in <b>Figure 4A</b>   |
| Sigma, grade I, 50% in H <sub>2</sub> O | –20°C, aliquoted upon delivery                             | batch 4 in <b>Figures 4B,C</b> ; thin lines in <b>Figure 6A</b>   |
| Fluka 25% in H <sub>2</sub> O           | room temperature for more than one year                    | <b>Figures 7A, 9</b>  |

350 nm on Thermo Scientific Evolution 220 (Thermo Fisher, United States). To measure trypan blue's absorption spectra, 0.01% trypan blue (Sigma-Aldrich, United States) solution was prepared in PBS and recorded for wavelengths from 200 to 750 nm. The hemoglobin absorption spectrum was measured as detailed before (Kaestner et al., 2006).

The emission and excitation spectra of the glutaraldehyde induced fluorescence was measured with a Jasco FP-6500 spectrofluorometer (Jasco, Germany). RBCs were fixed with 1% glutaraldehyde from different batches for one hour, washed three times in PBS and resuspended in PBS to the concentration of 0.01125% to avoid excessive scattering. For the emission spectra measurements, excitation was set to 450 nm and the fluorescence was recorded in the range from 480 nm to 750 nm. For the excitation spectra, emission was set to 540 nm and the excitation scanned from 350 nm to 500 nm.

## Elongation Index

To compare the mechanical properties of RBCs treated with various concentrations of glutaraldehyde, their elongation index was measured by LoRRca Maxsis (Mechatronics, Netherlands). Samples were treated as outlined above (2.2 RBC stability test). For each case 25  $\mu$ l of 45% cell suspension in PBS were mixed with 5 ml of polyvinylpyrrolidone buffer (PVP, Mechatronics, Netherlands). The range of set shear was 1 to 30 Pa.

## Atomic Force Spectroscopy

In order to investigate the variation between cells at certain concentrations of glutaraldehyde, atomic force microscopy (AFM) was employed. All measurements were performed in PBS with the JPK Nanowizard 3 (Bruker, Germany) setup coupled with a microscope. Effective Young's modulus of cells was measured through force-distance curves. The variety of cantilevers of MLCT model (Bruker AFM Probes, United States) with different nominal spring constants as well as different indentation forces were tested in order to adapt measurement conditions for each glutaraldehyde concentration. Prior to the measurements cells were immobilized on the substrate with Cell-Tak (Corning, United States). Force mapping was performed for 3–5 cells of each population on a grid of 32  $\times$  32 points, corresponding to a 10  $\mu$ m  $\times$  10  $\mu$ m map. Force-distance curves were acquired at the indentation rate of 5  $\mu$ m/s. Curves were

analyzed according to the Hertz model, implemented in the JPK software. The Poisson ratio was set to 0.5.

## Measurement of Osmolality

Glutaraldehyde was added to PBS for osmolality measurements. The osmometer (Type 6, Loser Messtechnik, Germany) was checked for zero display with distilled water prior to each measurement. Glutaraldehyde solutions in PBS with various concentrations were diluted 1:10 to have a 110  $\mu$ l sample.

## Density Measurements

The densities of glutaraldehyde treated cells were determined by adjusting the density of solutions they were suspended in. In an Eppendorf tube with treated cells, the percentage of OptiPrep (Stemcell Technologies, Canada) was adjusted slowly to match the density of treated cells. To determine the cell density values, tubes with known concentration of OptiPrep were centrifuged at 500  $\times$  g. In the case where the density of the solution matched the density of the cells, no sedimentation was observed after centrifugation.

## Sample Preparation for Microscopy

Ten microliters of blood were diluted 1 to 10 in PBS and directly added to 1 ml of 1% or 0.1% glutaraldehyde in PBS. Additional samples were prepared in order to study the stability of RBCs shapes within the spherocyte-discocyte-echinocyte scale in fixative solutions. The samples were prepared by suspending 30  $\mu$ l of whole blood in 1 ml NaCl solutions with different osmolality. A hypotonic solution (131 mosmol/kg H<sub>2</sub>O) was used to form spherocytes, a hypertonic solution (800 mosmol/kg H<sub>2</sub>O) for echinocytes and an isotonic solution (290 mosmol/kg H<sub>2</sub>O) was used for discocytes. After inducing the shape transformations, 20  $\mu$ l of each cell suspension were fixed in 1 ml of the respective NaCl solutions supplemented with 1% or 0.1% glutaraldehyde. Since the addition of 1% glutaraldehyde increases the osmolality of the solutions, extra samples were fixed in respective NaCl solutions that were diluted in order to keep the same final osmolality after addition of 1% glutaraldehyde. Samples were kept in rotation (Grantbio, United Kingdom) for 1 h at room temperature. Consequently, cells were washed three times by addition of 1 ml of each respective original solution and centrifuged at 735  $\times$  g for 3 min. Finally, cells were resuspended in 1 ml of their original solution. Brightfield images of both live

and fixed cells were acquired with a 50× objective (LU Plan 50×, NA = 0.55) on an inverted microscope (Eclipse TE2000-S, Nikon, Japan).

## Staining Procedures

Eosin-5'-maleimide (EMA) membrane staining was performed on both fresh and glutaraldehyde fixed RBCs. Two microliters of blood were added to 50  $\mu$ l EMA (5 mg/ml) supplemented with 10 mM CaCl<sub>2</sub> and incubated at room temperature for 2 hours in rotation (Suemori et al., 2015). Samples were washed 3 times with 1 ml of Tyrode solution, containing in mM: 135 NaCl, 5.4 KCl, 5 glucose, 1 MgCl<sub>2</sub>, 1.5 CaCl<sub>2</sub> and 10 HEPES, pH 7.4, each time spun at 300  $\times$  g for 2 min. Cells were resuspended in 1 ml of Tyrode solution and imaged in confocal microscopy with a 100x oil objective (Plan Apo TIRE, NA = 1.49, Nikon, Japan) and an excitation wavelength of 488 nm. Glutaraldehyde induced fluorescence was examined at an excitation wavelength of 647 nm.

Some of the samples were fluorescently labeled for 3D image acquisition with confocal microscopy. Staining of the cell membrane was performed either with CellMask™ Deep Red (Life Technologies, United States) or with PKH67 (Sigma-Aldrich, United States). Living cells were stained for comparison with fixed samples. CellMask staining was performed by adding 1  $\mu$ l of CellMask stock solution (0.5  $\mu$ g/ml) into the RBCs suspension followed by incubation for 5 min and 3 washes prior to resuspension in 1 ml PBS. For PKH67, 10  $\mu$ l of packed cells were stained with 0.5  $\mu$ l PKH67 as recommended by the manufacturer and incubated at room temperature for 5 min. 3 washes followed before resuspension in 1 ml PBS. Living cells were resuspended in PBS supplemented with 0.1% bovine serum albumin.

## Flow Cytometry

Fixed cells were used for immunofluorescence tests performed by flow cytometry on cord blood to measure fetal hemoglobin (HbF) content. Ten microliters of whole cord blood were fixed for 10 min in either 0.05% or 1% glutaraldehyde in PBS. An appropriate staining buffer suggested by the company (BD Biosciences, United States) was used for next steps. After one wash, cells were permeabilized with 0.1% Triton X-100 (Sigma-Aldrich, United States) solution for 10 min. Cells were then washed and incubated with FITC mouse anti-human fetal hemoglobin antibody (BD Biosciences, United States) for 20 min at room temperature. After washes, cells were finally resuspended in 500  $\mu$ l of staining buffer and 100,000 events were recorded by flow cytometry (Gallios Flow Cytometer, Beckman Coulter, United States). Each stained sample was measured together with its respective unstained fixed sample used as a negative control. Living cells were also analyzed for comparison. Plots were obtained with the software FlowJo V10 (BD Biosciences, United States).

## 3D Imaging

Cells were placed between two glass cover slips (24 mm  $\times$  60 mm) with a suspension of beads with a 20  $\mu$ m diameter used as spacers between the cover slips. A 60× oil objective (CFI

Plan Apochromat Lambda 60× Oil, NA = 1.4) of an inverted microscope (Eclipse Ti, Nikon, Japan) was used to image. Cells were scanned using a diode laser emitting at 647 nm (LU-NV Laser Unit, Nikon, Japan) in a z-range of 20  $\mu$ m with steps of 300 nm. A spinning disk-based confocal head (CSU-W1, Yokogawa Electric Corporation, Japan) was used to generate the images. 3D reconstruction was later performed with a Matlab R2017b (MathWorks, United States) routine.

## Examination of Autofluorescence Quenching

To test the quenching of glutaraldehyde autofluorescence, fixed cells were permeabilized with 1 ml 0.1% Triton X-100 for 10 min, washed and resuspended in 1 ml PBS. Two hundred microliter of cell suspension were added to 800  $\mu$ l of 0.4% trypan blue (Sigma-Aldrich, United States) in PBS. After 15 min of incubation at room temperature, cells were washed twice and imaged as described before.

## Scanning Electron Microscopy (SEM)

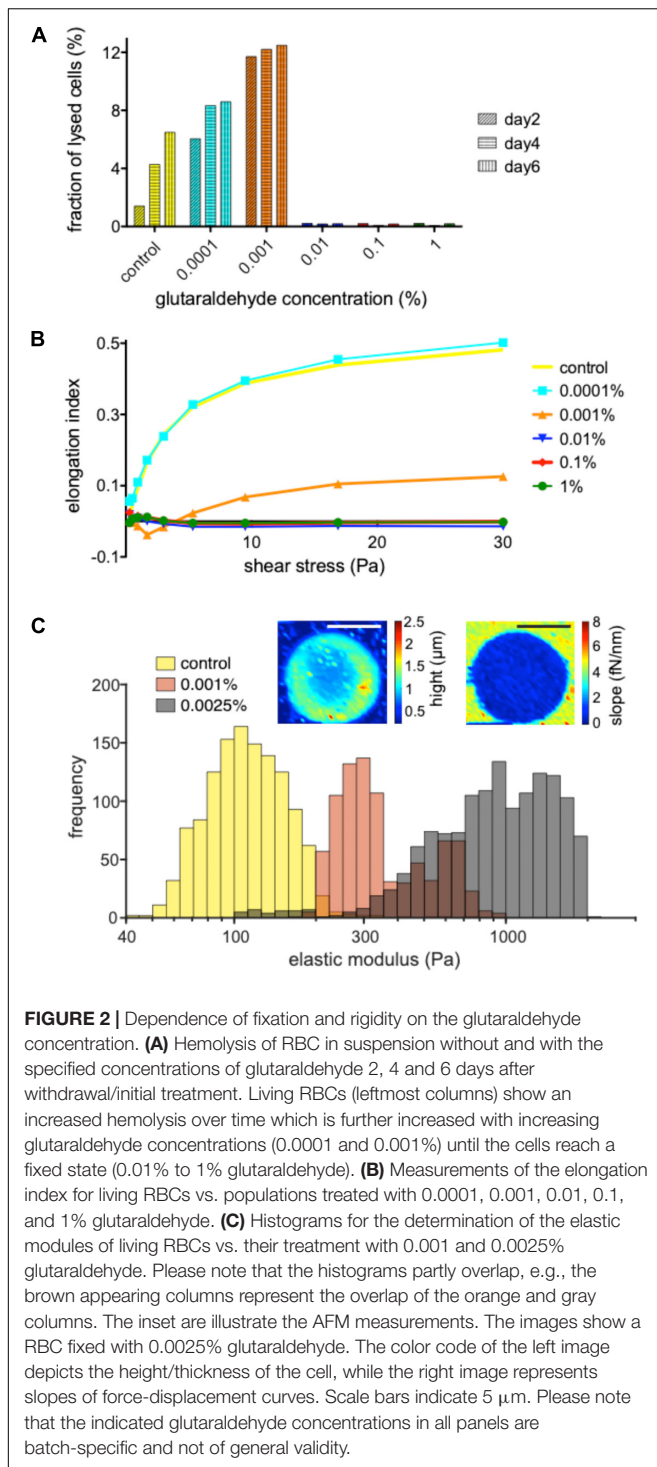
Fixed samples in 1% glutaraldehyde solution (Fluka, Germany) were centrifuged on circular glass coverslips (10 mm, Schott, Germany) for 6 min at 40  $\times$  g in a cytocentrifuge (Cytospin 2 SHANDON, United States). Sample slides were immediately resuspended in PBS to avoid sample drying and washed 3 times to remove any glutaraldehyde residues. Post fixation was done for 30 min in a solution containing 1% osmium tetroxide in PBS, followed by 3 washes in PBS, 5 min each. Samples were dehydrated in increasing ethanol concentrations: 30 min in 70% ethanol, 30 min in 80% ethanol and overnight in 100% ethanol. Cells were dried in a critical point drying (Bal-tec CPD030, United States), mounted on aluminum stubs and sputter coated with 4 nm platinum (Safematic CCU-010, Switzerland). SEM (Zeiss Supra 50 VP, Germany) imaging was performed at 10 kV with a secondary electron detector for a 5000 $\times$  magnification.

## RESULTS

### Fixation vs. Modulation of Stiffness

The protocols so far published are confusing concerning the application of the glutaraldehyde concentration because they range from 0.0005% to 8% (Morel et al., 1971; Tong and Caldwell, 1995; Guo et al., 2014) and all use the term “to fix cells” upon the application of glutaraldehyde.

Basing on the assumption that fixed cells may be conserved for a long time (ideally months or even years) with no morphological changes or lysis of the cells, we investigated the shelf life by treating samples with various glutaraldehyde concentrations kept at 4°C for 6 days. Every 2 days the supernatant sample was prepared to measure the free hemoglobin content in the suspensions. It correlates directly to the amount of lysed cells in the samples. **Figure 2A** reveals glutaraldehyde's seemingly digital (all or none) fixation property. Percentages above 0.01% showed almost no hemoglobin in the supernatant. At lower concentrations, increase in glutaraldehyde percentage increase



the hemolysis rate compared to unfixed control cells until glutaraldehyde reaches a concentration where RBCs are fixed.

To probe the stiffness of glutaraldehyde-treated RBCs we used an ektacytometer, LoRRca, a routine tool to investigate hemolytic anemias (Zaninoni et al., 2018). **Figure 2B** reveals that very low concentrations of glutaraldehyde (here: 0.0001%) resemble the mechanical behavior of living cells, while concentrations

above 0.01% glutaraldehyde are (in agreement with **Figure 2A**) indistinguishable in their elongation index plot. Interestingly, 0.001% glutaraldehyde shows indeed a curve/behavior in between the two extreme conditions. Using atomic force spectroscopy, we had a closer look in the latter range and compared living RBCs with 0.001 and 0.0025% glutaraldehyde treated RBCs (**Figure 2C**). On the one hand this plot shows that indeed the cell populations are shifted in their elastic module in dependence of the glutaraldehyde concentration. On the other hand, one can also notice a wide and overlapping spread of the elastic modulus (please note the logarithmic scale).

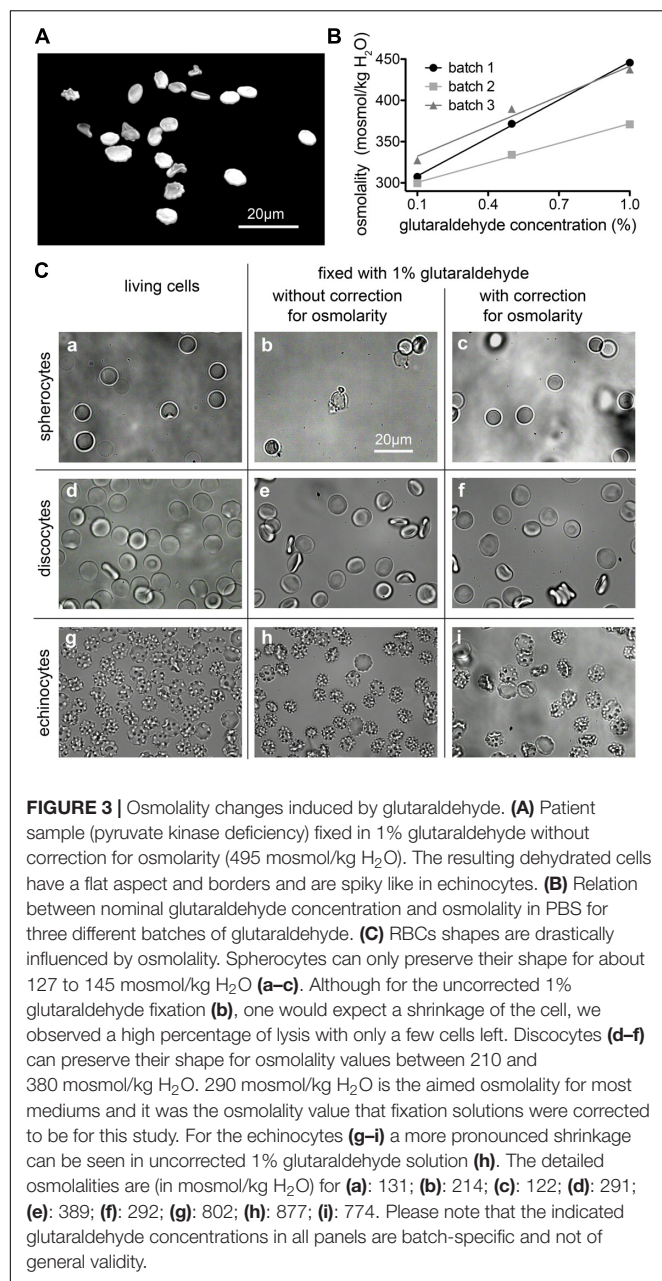
## Correction for Osmolality

Changes in the osmotic pressure result in highly deformed shapes, which lead to the formation of flattened discocytes with a clear shrunk appearance. We came across artificially deformed cells when we fixed RBCs of a patient with pyruvate kinase deficiency (**Figure 3A**). The shrinkage of the RBCs is proportional to the concentration of the glutaraldehyde (**Figures 3B,C**) and although the osmolality increase of glutaraldehyde solution scales linearly with its concentration, there are severe differences between glutaraldehyde batches as outlined in **Figure 3B**. While the change in osmolality might not be relevant in certain cell types in terms of morphology (Machado, 1967; Bone and Denton, 1971; Rasmussen, 1974), for RBCs we observed that the osmolality is essential for shape preservation (**Figure 3C**).

We are aware of the fact that glutaraldehyde may not be osmotically active. It is an uncharged, rather hydrophobic molecule that crosses the membrane, as it clearly reacts with intracellular proteins with a fast kinetics. Whether an osmotic effect could be present and relevant depends on the differential permeability of the membrane to glutaraldehyde itself and to water. Glutaraldehyde appears to act rapidly and to fix RBCs within 1 s (Sutera and Mehrjardi, 1975). Water fluxes across the RBC membrane are also fast owing to the presence of aquaporin. So the two permeabilities may be seen as to be approximately equivalent. Yet it is unknown if, and to what extent these parameters change in the time frame of glutaraldehyde reacting with the membrane, for instance affecting its own permeability coefficient and/or that of aquaporin, not to mention all the other protein-mediated transport systems of the RBC membrane. In the literature it is also argued that the buffer osmolality plays a more important role than the osmolality increase caused by glutaraldehyde addition (Barnard, 1976; González-Aguilar, 1982). Despite of all this, we have nonetheless observed that osmolality compensation by dilution of the buffer is essential for the preservation of shapes within the spherocyte-discocyte-echinocyte range, especially when glutaraldehyde is used in the high concentration range.

For discocytes, as they are the most stable shape for the cells, the range of tolerable osmolality is wide. Discocytes can preserve their shape for osmolality values between 210 and 380 mosmol/kg  $\text{H}_2\text{O}$ . Ideally 290 mosmol/kg  $\text{H}_2\text{O}$  is the aimed osmolality for most media, and it was also the osmolality value that fixation solutions were corrected for within this study. However, rare cell shapes are a lot more sensitive to





osmolality changes. For example; spherocytes can only preserve their shape for about 127 to 145 mosmol/kg H<sub>2</sub>O, which is a much narrower range.

## Monomers and Polymers

In a glutaraldehyde solution monomers and polymers coexist (compare Figure 1). Both monomers and polymers have different “fixation properties.” In particular, the higher efficiency in crosslinking due to monomers or polymers is discussed controversially (Richards and Knowles, 1968; Hardy et al., 1969; Robertson and Schultz, 1970; Gillett and Gull, 1972). While preparation/purification to yield pure monomeric and polymeric solutions requires a certain

preparation effort, the analysis of differences or variations of cell ultrastructure in electron microscopy (Bessis, 1974) goes far beyond the frame of this report. However, it is of interest to evaluate the particular composition of glutaraldehyde, which can be measured by UV-absorption spectroscopy as indicated in Figure 4A depicting the large variety of glutaraldehyde solutions used in our laboratories. The ratio of absorbance between 280 nm (monomer, Figure 4B) and 235 nm (polymer) can be taken as the monomer-polymer ratio (Figure 4C). Our results show indeed that glutaraldehyde polymerization can vary between batches. Change over time, in particular when stored at room temperature is the most likely cause for the differing ratios. In addition and independent of the polymerization, we found variations in the concentration of different glutaraldehyde batches for nominal equal concentrations as indicated by the optical density of the monomer peak depicted in Figure 4B. Therefore, it is important to document both, the monomer to polymer ratio of glutaraldehyde as well as the peak of the monomer concentration as a reference.

## Handling Pitfalls

When RBCs are pipetted into a glutaraldehyde solution they are believed to be fixed within 1 s (Sutera and Mehrjardi, 1975). This means that if the pipetting creates a considerable flow (compare also Wiegmann et al., 2017), the cellular shape adaptation to flow (Lanotte et al., 2016; Quint et al., 2017) is also conserved, which is a deviation from RBC shape in stasis (Figure 5) and must be regarded as an artifact. The cells marked by red circles in Figure 5 include knizocytes (trilobes), a clear indication for flow induced cell shape changes (Lanotte et al., 2016). Gentle pipetting is compulsory when fixing with 1% or higher glutaraldehyde concentrations. In addition a pre-dilution in saline solution of the blood sample to a hematocrit of 5% or lower proved to be helpful, due to a decrease in the viscosity of the suspension (Eckmann et al., 2000) and thus a decrease in shear stress on the cells.

In microfluidics, glutaraldehyde treated cells are often used to test deformability-based cell sorting devices, as well as to study flow of non-deformable particles (Holmes et al., 2014; Tomaiuolo et al., 2015). One common problem that often occurs while working with fixed cells is the increased sedimentation rate due to higher density of cells. This disadvantage can be improved upon by using a lower glutaraldehyde concentration for fixation. The density of cells that have been fixed with 1% was measured to be 1.21 g/ml whereas the density for 0.1% fixed cells is 1.18 g/ml, while the average cell density of living cells is 1.10 g/ml. We considered two possible reasons that could explain the increase in density of cells post-fixation: either the cross-linking caused a decrease in the cell volume (cellular dehydration), or the binding of the glutaraldehyde molecules on the cell increased the mass of the cell. Since glutaraldehyde has molar density of 0.933 g/ml (Zang et al., 2016), which is lower than both surrounding medium and the healthy cell density (1.1 g/ml), the addition of glutaraldehyde molecules to the cell membrane is unlikely to increase the density of the cell. From the density measurements

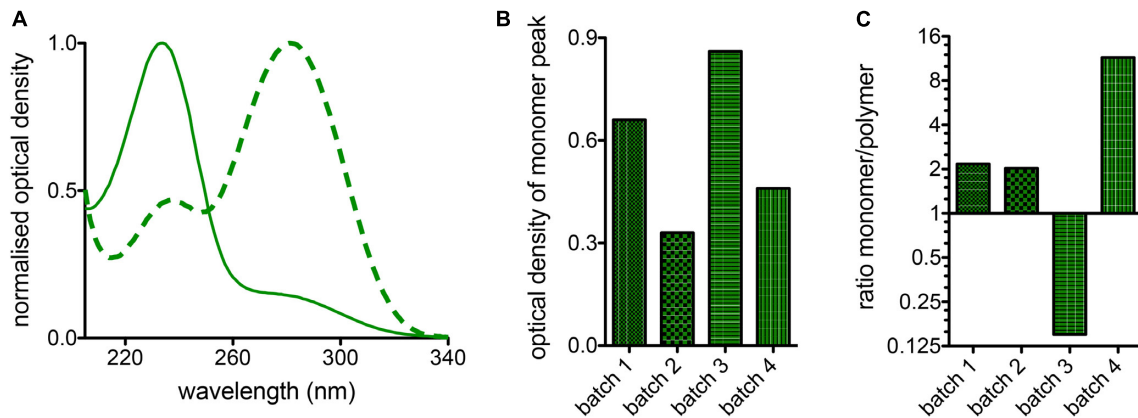


**FIGURE 4 |** Batch variations of glutaraldehyde. **(A)** Normalized absorption spectra of two different batches of glutaraldehyde in distilled water. The solid line shows predominantly the monomere peak, whereas the highest band of the dashed line represents the polymers. **(B)** Comparison of the monomer absorption peak for 4 batches of glutaraldehyde with nominally the same concentration of 1% in distilled water. **(C)** Ratio between monomers and polymers derived from 1% glutaraldehyde solutions in distilled water for 4 different batches of glutaraldehyde.

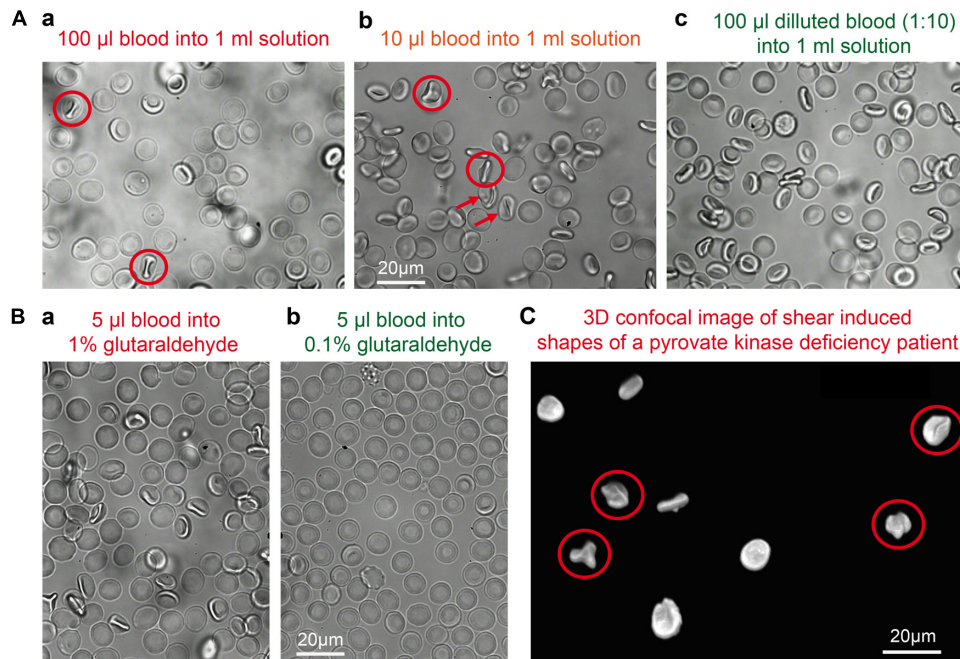
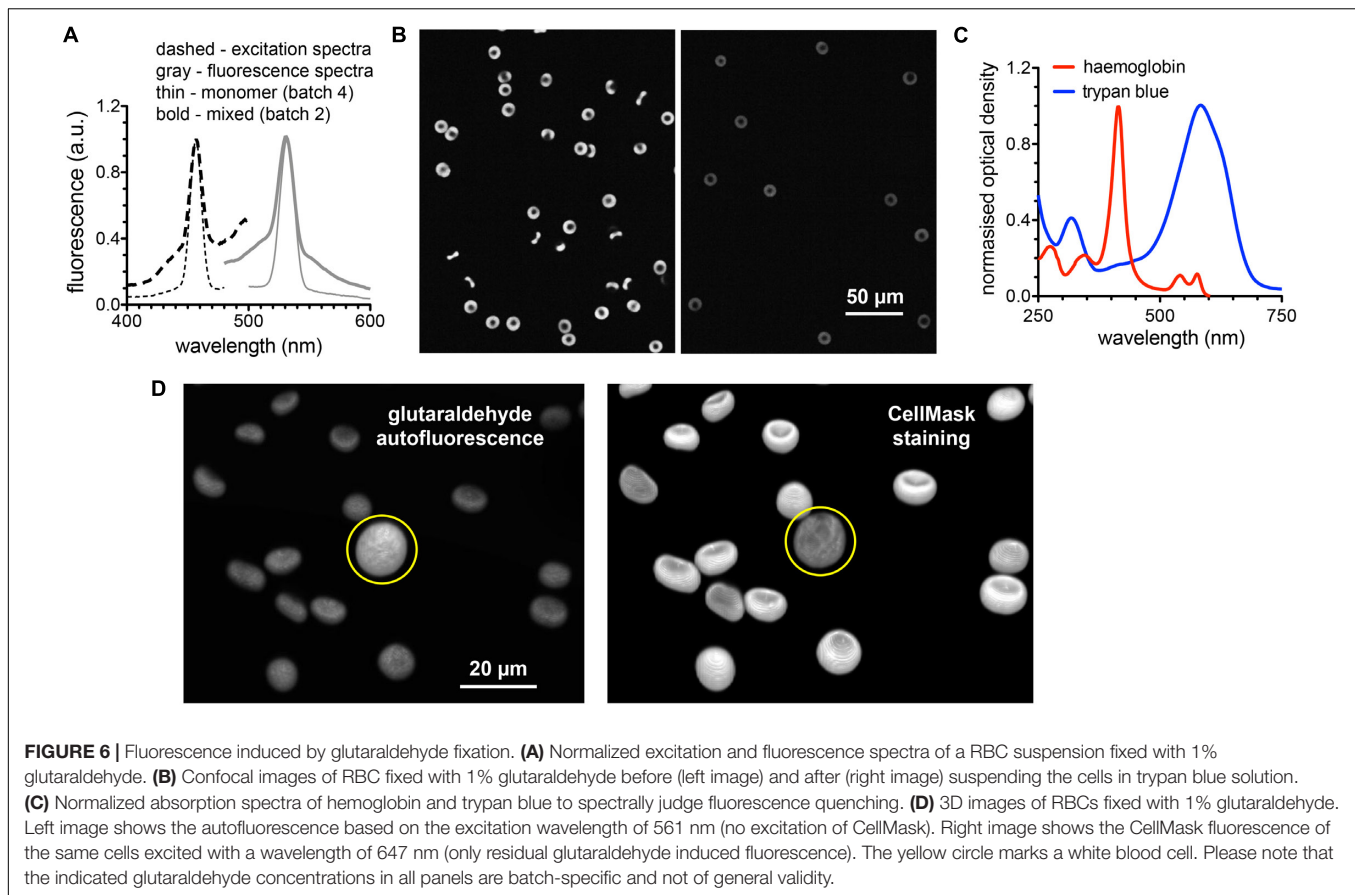


**FIGURE 5 |** Shear induced artifacts during glutaraldehyde fixation. **(A)** Representative fixation examples in 1% glutaraldehyde solution in dependence of the sample preparation. **(a)** 100 µl of whole blood pipetted into a 1% glutaraldehyde solution; **(b)** 10 µl of whole blood pipetted into a 1% glutaraldehyde solution; **(c)** 100 µl of a 1:10 diluted blood suspension pipetted into a 1% glutaraldehyde solution. Circles indicate knizocytes and arrows otherwise deformed RBCs. **(B)** Representative fixation examples of 5 µl whole blood in **(a)** 1% glutaraldehyde and **(b)** 0.1% glutaraldehyde. **(C)** Patient sample (pyruvate kinase deficiency) fixed in 1% glutaraldehyde with cells showing shear induced artifacts as the knizocytes marked with circles. Please note that the indicated glutaraldehyde concentrations in all panels are batch-specific and not of general validity.

we can calculate that 1% glutaraldehyde fixation results in approximately 9% volume decrease, whereas 0.1% fixation results in approximately 7%. A possibility to counterbalance the increase in density is the adaptation of the density of the suspension, e.g., by using OptiPrep (Stemcell Technologies, Vancouver, BC, Canada).

## Glutaraldehyde Induced Fluorescence and Staining of Fixed Cells

Staining of fixed RBCs requires to consider both the possible interference of hemoglobin with fluorescent dyes (Kaestner et al., 2006) and the fluorescence induced by glutaraldehyde. Although the autofluorescence of the glutaraldehyde itself is negligible it



forms fluorescent entities upon binding to peptides and proteins (Lee et al., 2013).

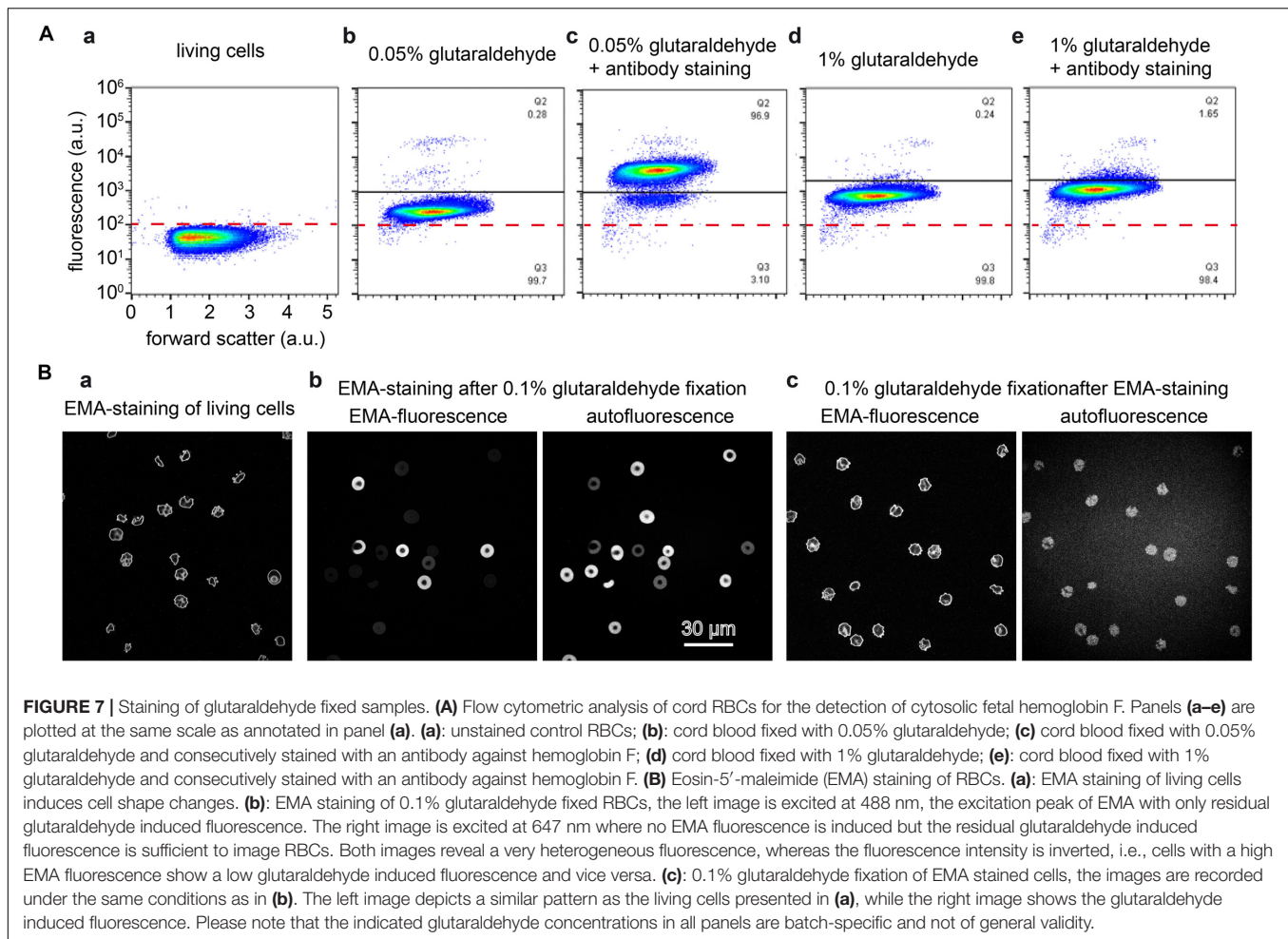
To judge the fluorescence induced by glutaraldehyde, the excitation and emission spectra of the glutaraldehyde fixed RBCs is presented in **Figure 6A**. We present spectra of cell suspensions fixed with 2 different batches of glutaraldehyde. For the almost exclusive monomeric glutaraldehyde (batch 4 in **Figure 4C**), the induced fluorescence contains distinct narrow bands (thin lines in **Figure 6A**), whereas the mixture of monomers and polymers (batch 2 in **Figure 4C**) gives in addition to the monomer band a wide band fluorescence background (bold lines in **Figure 6A**), exceeding the range of the spectra measured. This demonstrates that the induced fluorescence can be a problem in immunofluorescence staining (see also below), also considering the wide spectral range of the induced fluorescence, in particular in the presence of glutaraldehyde polymers. Especially when quantitative fluorescence intensity measurements are required, it is crucial to take the glutaraldehyde induced fluorescence into account. Therefore, we present a previously described method to quench the fluorescence by addition of trypan blue (Loike and Silverstein, 1983). Confocal sections of glutaraldehyde fixed RBCs (excitation at 488 nm) in the absence and presence of trypan blue are exemplified in **Figure 6B**. Although the fluorescence signal is reduced, it could not be completely excluded. To evaluate the putative effect of trypan blue, the absorption spectrum is depicted in **Figure 6C**.

Additionally, the absorption spectrum of hemoglobin is plotted in **Figure 6C**.

To evaluate the putative use of the glutaraldehyde induced fluorescence for RBC imaging we present in **Figure 6D** 3D-images of glutaraldehyde fixed and CellMask stained cells. While the left image in **Figure 6D** predominantly presents glutaraldehyde induced fluorescence, the right image depicts mainly CellMask fluorescence. To highlight the special properties of RBCs we choose an image that contains by chance a white blood cell (marked with a yellow circle in **Figure 6D**).

To further illustrate the scenario of interaction between glutaraldehyde and the staining of proteins of interest we present two prominent examples of (i) a cytosolic protein and (ii) a membrane protein. (i): We performed flow cytometric measurements of living RBCs and fixed cells with different concentrations of glutaraldehyde with and without additional staining of the (cytosolic) hemoglobin F (**Figure 7A**). Induced fluorescence is high at 1% glutaraldehyde but lower at decreased concentrations. Furthermore, flow cytometry data reveal higher fluorescence for samples kept in glutaraldehyde for longer time (several hours, data not shown). Moreover, cells showed different fluorescence intensities within the same sample, underlining different glutaraldehyde binding amounts between individual cells. This might reflect cell protein content, which varies between cells, e.g., in dependence of RBC age (Kaestner and Minetti, 2017). Additionally, we observe the effect that long staining with





high (1%) concentrations of glutaraldehyde prevents binding of the antibodies (**Figures 7Aa–e**). However, hemoglobin F antibodies (FITC) can distinctively be identified in 0.05% glutaraldehyde fixation. (ii): We imaged RBCs stained with EMA, which binds to the amino group of Lys-430 on RBCs membrane Band 3 protein and it is commonly used to estimate Band 3 protein abundance. **Figure 7B** compares images of living cells (**Figure 7Ba**), EMA staining after 0.1% glutaraldehyde fixation (**Figure 7Bb**) and fixation with 0.1% glutaraldehyde after EMA staining (**Figure 7Bc**).

Also the choice of the particular dye might be influenced by the glutaraldehyde. This statement goes beyond the obvious spectral selection presented above. For illustration we tested two types of cell membrane fluorescent staining dyes both on living and fixed cells: PKH dyes proved to be reliable for RBC *in vivo* staining for several weeks (Wang et al., 2013); CellMask is a popular dye to stain RBC *in vitro* (Flormann et al., 2017). While for living cells we observed a homogeneous membrane staining, the dyes did not always show to be ideal on fixed cells. PKH26 as well as PKH67 in particular resulted in the formation of visible “filaments” forming at the cell membrane (**Figure 8**). For CellMask we occasionally noticed the formation of small accumulations of dye in certain fixed samples, when staining at

low concentrations. Such an inconsistent effect could be due to the monomer/polymer ratio of the glutaraldehyde affecting the crosslinking of cells.

## Special Emphasis on Sick Cell Disease

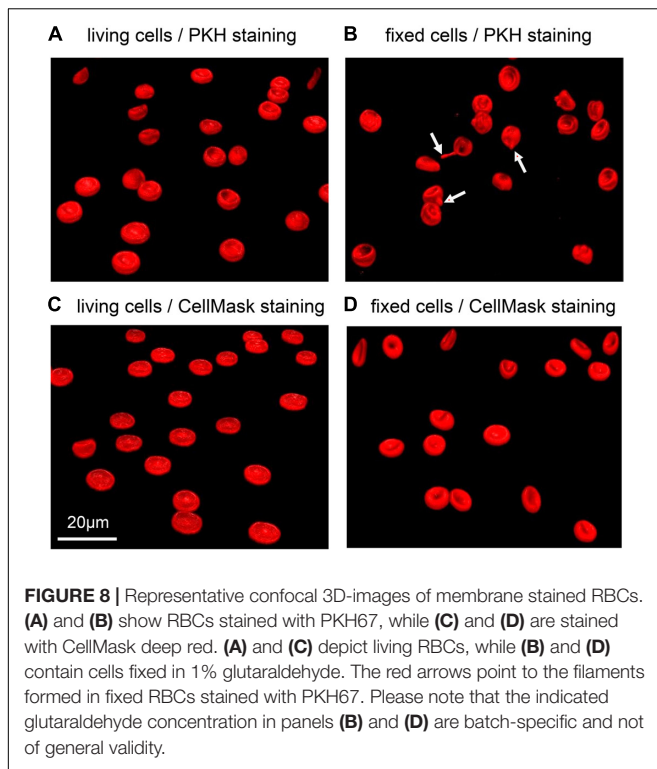
Since glutaraldehyde consumes oxygen during its reaction with compounds (Johnson, 1987), we investigated if a glutaraldehyde induced deoxygenation could cause hemoglobin crystallization in sickle cell disease patients, transforming discocytes containing oxygenated hemoglobin into sickle cells. To this end we fixed oxygenated and deoxygenated RBCs of a sickle cell disease patient with 1% of glutaraldehyde and performed scanning electron microscopy (SEM). The resulting SEM images are presented in **Figure 9**, clearly showing discocytes in oxygenated cells (**Figure 9A**) and sickled cells in deoxygenated RBCs (**Figure 9B**) of the same patient.

## DISCUSSION

### Fixation vs. Modulation of Stiffness

Previous literature gives different meanings to the concept of “fixation”: conservation of cells (Nowakowski and Luckham,

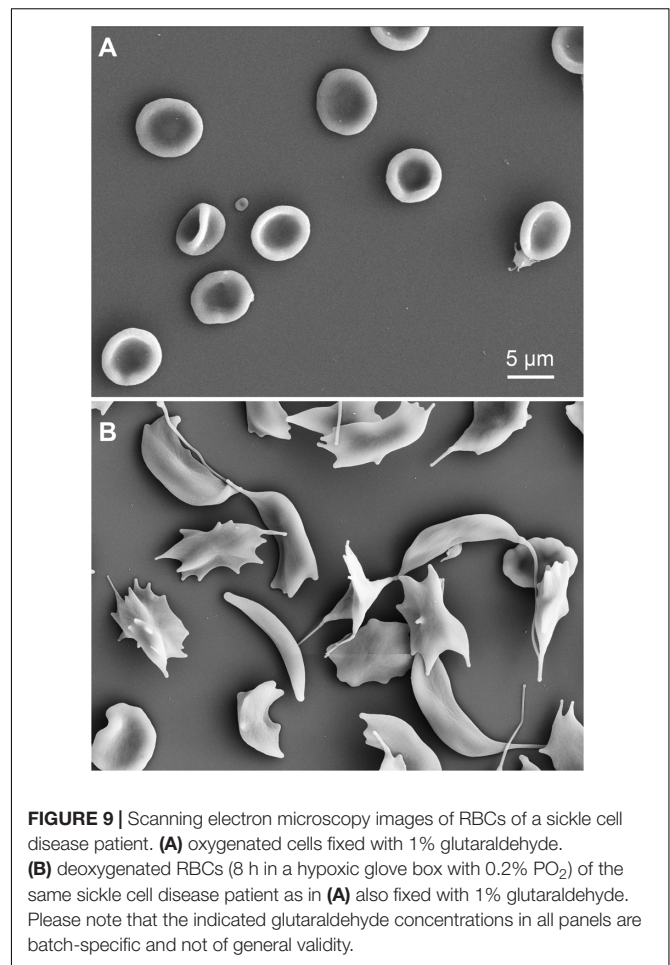




2002; Faivre et al., 2006; Karon et al., 2012) and regulation of cellular rigidity (Guo et al., 2014; Tong and Caldwell, 1995). This study emphasizes the subtle difference between the two concepts as presented in **Figures 2A,B**. Fixation of cells with glutaraldehyde and increase in cellular stiffness are two different pairs of shoes. Fixation can be thought of as a binary state (all or none), whereas rigidity can be roughly regulated at low glutaraldehyde concentrations, as shown by ektacytometry (**Figure 2B**) and atomic force spectroscopy (**Figure 2C**). However, for the latter application one should avoid the term “fixation,” because instead of being fixed, cells are rather more fragile (**Figure 2A**). Please note that the concentrations of glutaraldehyde given in **Figure 2** and in the results sections can’t be regarded as general numbers, because the batch to batch differences (**Figure 4** and discussion below), probably highly influenced by the ratio of monomers and polymers, have a tremendous influence on the fixation properties. Furthermore, glutaraldehyde appears to have a toxic effect on the cells for 0.0001 and 0.001% concentrations (**Figure 2A**), since they exhibited more lysis than the control case (living cells). The toxicity effect also can explain the increase of lysis from a 0.0001 to 0.001%.

### Correction for Osmolality

Unlike some other types of cells, RBC morphology is highly sensitive to several parameters, e.g., mechanical stress, pH changes, addition of chemical agents and osmolality differences. Because of such changes, RBC shapes are thoroughly studied in blood diseases, where genetic mutations and/or impaired cell functions affect cell shapes (Ponder, 1948; Delaunay, 2004;



Diez-Silva et al., 2010; Fermo et al., 2017). This implies that morphological analysis must be performed on reliable samples. Cell fixation is an ideal step when working with rare anemias, where patients’ samples often need to be investigated in specialized laboratories and may be stored before the analysis can be performed (**Figure 3B**). It is well known that RBC shapes are sensitive to osmolality (Reinhart et al., 2015). Adding 1% glutaraldehyde to a given solution increases the osmolality by approximately 100 mosmol/kg H<sub>2</sub>O, which results for physiological solutions in a relevant osmolality change of approximately 30%. Even if fixation occurs within seconds, the osmotic pressure difference allows water to flow in or out of the cell, affecting the shape that will be fixed. Such a water flow is also observed at higher glutaraldehyde concentrations, where the increase in osmolality is proportionally higher while fixation occurs faster (data not shown). Our results show that each shape has a different tolerance to osmolality, spherocytes being the most fragile and unstable shape (**Figure 3A**). Therefore the evaluation of spherocytes underlines the importance of osmolality correction in the fixative. If the osmolality is particularly high, discocytes appear flattened and borders slightly spiky, resembling echinocytes. Cells do not fully deform into echinocytes probably because of the simultaneous crosslinking

of glutaraldehyde while dehydration occurs. In the case of discocytes, a judgment on fixed shape quality becomes generally more difficult because the shape change is less evident and often subjective to the observer. Therefore we see a need for automated (unbiased) cell shape analysis algorithms. A visual inspection is not enough for comparison with living cells, even in 3D imaging. We can, however, mention that cells fixed in 1% corrected glutaraldehyde resemble cells fixed in 0.1% glutaraldehyde, where the osmotic imbalance after addition of glutaraldehyde to the buffer is minimal (10 mosmol/kg H<sub>2</sub>O). Therefore we suggest to verify the osmolality of the fixative solution before fixation of any samples, particularly when dealing with patients that display shape deformations, e.g., hereditary spherocytosis, sickle cell disease or pyruvate kinase deficiency. Such diseased RBCs might be more severely affected by environmental changes, like osmolality, than healthy discocytes.

## Monomers and Polymers

Glutaraldehyde solutions are mixtures of monomers and polymers as outlined in **Figure 4**. We did not investigate the advantages and disadvantages of monomers and polymers for the fixation of RBCs but this topic was previously discussed controversially (Richards and Knowles, 1968; Hardy et al., 1969; Robertson and Schultz, 1970). However, it is evident that the ratio of monomers and polymers can vary between different glutaraldehyde batches (**Figure 4C**), but the ratio can easily be determined by UV-absorption spectroscopy. Previous studies (Gillett and Gull, 1972; Rasmussen and Albrechtsen, 1974; Prentø, 1995) demonstrated that the storage temperature of glutaraldehyde is among the most important parameters for a stable preservation of the stock solution. Rasmussen (1974) has tested different storage temperatures, concluding that glutaraldehyde is most stable at  $-20^{\circ}\text{C}$ . The higher the temperature, the faster the increase in polymer formation. However, we point out that the uncontrolled formation of polymers in the stock solution will affect the impact of glutaraldehyde on osmolality, therefore making it necessary to check the osmolality increase for every prepared solution before applying osmolality correction.

## Handling Pitfalls

As stated before, RBC morphology is affected by mechanical stress, e.g., flow, to which RBCs adapt by changing their shapes into hydrodynamic ones. Pipetting results in shear of RBCs, which leads to the formation and fixation of flow shapes like knizocytes (also referred to as trilobes) (Lanotte et al., 2016), known to form at high shear rates (**Figure 5**). This highlights that the speed of fixation is extremely fast, knowing that RBCs in flow relax to the static shape in between 100 ms (Amirouche et al., 2017) and 1 s (Braunmüller et al., 2011). We observed knizocytes when fixing with 1% glutaraldehyde, but not when fixing with lower concentrations, hinting to a slower fixation for lower concentrations. Such distortions of the regular cell shape can cause confusion when diseased RBCs are under investigation (**Figure 5C**). To avoid the presence of flow induced shapes, we found it is sufficient to dilute the blood sample to hematocrits of 5% in a solution of lower viscosity, e.g., PBS.

## Staining of Fixed Cells

The fluorescence induced by glutaraldehyde is significant and covers a wide range of wavelengths (**Figures 6A, 7A**), which can be essential for the fluorescence measurement as exemplified by the measurement of hemoglobin F in cord blood RBCs using flow cytometry (**Figure 7A**) or by staining for Band 3 protein with EMA (**Figure 7B**). Although glutaraldehyde induced fluorescence can in principle be used to image RBCs (**Figures 6B,D**), the 3D-reconstruction reveals that fluorescence intensity is limited and does not reach dedicated staining such as CellMask staining (**Figure 6D**).

However, for fluorescent staining of membrane proteins that do not require permeabilization of the RBCs we recommend to first perform the membrane staining followed by the fixation. Already the staining of Band 3 protein with EMA showed severe inconsistencies that are likely to result from the fact that glutaraldehyde also binds to amino groups, i.e., EMA needs to compete with glutaraldehyde for putative binding sites (compare **Figure 7Bb**). If this is already evident for the highly abundant Band 3 protein, we expect even more severe effects for less abundant proteins and their detection using antibodies.

According to the application needed, we recommend to fix cells shortly if the autofluorescence signal is not desirable, meaning few minutes, using low concentrations to avoid higher autofluorescence than the signal coming from a specific staining. Using monomeric glutaraldehyde, the autofluorescence induced is in a narrower spectral range compared to polymeric glutaraldehyde (**Figure 6B**). This results in a several fold reduced autofluorescence at the popular laser line 488 nm, which is also advantageous in respect to the absorption properties of both hemoglobin and trypan blue (**Figure 6C**). Quenching tests revealed trypan blue to be efficient, however, not completely eliminating the signal (**Figures 6C,D**).

Membrane staining showed to be different between living and fixed cells (**Figure 8**). While CellMask is toxic at high concentrations on living cells, PKH dyes might not provide an appropriate staining on fixed cells, even at low glutaraldehyde concentrations. PKH consists of a fluorescent dye incorporated in a long aliphatic chain that inserts into membrane lipids. Due to the presence of glutaraldehyde crosslinking the membrane proteins, it might be that PKH cannot be appropriately inserted into the membrane, giving the formation of protrusions that affect the quality of the staining (**Figure 8B**). CellMask is an amphipathic molecule linked to a charged dye that can be used both for the staining of living and fixed cells and resulted in fact in a more efficient labeling of fixed cells with any tested concentration of glutaraldehyde.

## Sickle Cells

Generally, the effect of O<sub>2</sub> consumption during glutaraldehyde fixation is clearly visible in RBCs suspension, which upon fixation become darker, as a consequence of methemoglobin formation (Guillochon et al., 1986). However, up to 1% of glutaraldehyde based fixation of sickle cells we could not detect any sickling as outlined in **Figure 9A** and therefore we like to exclude hemoglobin crystallization due to deoxygenation.

## CONCLUSION

In this section we will provide general recommendations to use glutaraldehyde to fix or rigidify RBCs. Due to glutaraldehyde variations between commercial providers, batch to batch variations and conversions of glutaraldehyde during storage time, these recommendations can hardly provide particular numbers neither for the minimal glutaraldehyde concentration to fix or rigidify the cells nor for the exact osmolality compensation. Instead we recommend procedures to consider, with the aim to ease glutaraldehyde use.

- (i) We recommend to store glutaraldehyde at  $-20^{\circ}\text{C}$  in aliquots to avoid unnecessary thawing of the whole bottle for each use. Use these aliquots to prepare fresh solutions before treating the cells. This allows a maximal consistency within a series of measurements in a particular laboratory over time.
- (ii) The glutaraldehyde concentration to be used depends on the purpose and needs to be determined for the particular application and the particular glutaraldehyde batch. If fixation is required, a quick control can be done by washing the cells in distilled water prior to experiments. Fully fixed, fully non-deformable cells, will not lyse or have any morphological changes (test the supernatant for hemoglobin). In general, concentrations between 0.05 and 0.1%, fix cells but do not require osmolality compensation, limit the induced fluorescence as well as the increase in the density of cells. However, attention should be given, because fixation is not immediate but takes longer time. In contrast, concentrations of glutaraldehyde around 1% require an osmotic compensation (see below) and if induced fluorescence is not a hindering aspect, 1% glutaraldehyde provides a sound fixation and is ideal for electron microscopy applications, where often even higher percentages of glutaraldehyde are used as these methods are physically more abrasive to the cells compared to optical imaging. Additionally, we like to mention the opportunity to set a fixation at a rather low glutaraldehyde concentration, e.g., 0.05 – 0.1% and increase the concentration in a second step to 1% to avoid insufficient glutaraldehyde content.
- (iii) We suggest to measure the osmolality of the glutaraldehyde containing solution and correct it by diluting the suspension buffer when fixing with 0.5% or higher concentrations of glutaraldehyde.

## REFERENCES

- Aingaran, M., Zhang, R., Law, S. K., Peng, Z., Undisz, A., Meyer, E., et al. (2012). Host cell deformability is linked to transmission in the human malaria parasite *Plasmodium falciparum*. *Cell. Microbiol.* 14, 983–993. doi: 10.1111/j.1462-5822.2012.01786.x
- Amirouche, A., Ferrigno, R., and Faivre, M. (2017). Impact of channel geometry on the discrimination of mechanically impaired red blood cells in passive microfluidics. *Proceedings* 1:512. doi: 10.3390/proceedings1040512

- (iv) It is recommended to check the monomer/polymer ratio of the glutaraldehyde using a spectrometer and provide this ratio in the publications as a way to help interlaboratory comparability.
- (v) It is necessary to consider the appropriate staining dye and its concentration in relation to the induced autofluorescence. If cell shapes are considered, the autofluorescence is rather advantageous. Staining based on the recognition of protein structures (antibodies) or relying on the access to intracellular structures have to be handled with care and should be pre-tested on glutaraldehyde treated positive controls to show the feasibility. Trypan blue can be used to quench the autofluorescence. Staining of membrane proteins (e.g., using dyes or cluster of differentiation antibodies) should be performed prior to fixation.

## ETHICS STATEMENT

The procedure is approved by the local ethics committee (Approval No. 51/18) and was performed in accordance with the Helsinki international ethical standards on human experimentation.

## AUTHOR CONTRIBUTIONS

All authors listed have made a substantial, direct and intellectual contribution to the work, and approved it for publication.

## FUNDING

The research leading to these results has received funding from the European Framework “Horizon 2020” under grant agreement number 675115 (RELEVANCE) and from the Volkswagen Foundation (Az: 93839).

## ACKNOWLEDGMENTS

We would like to thank Dr. Rob van Zwieten and Martijn Veldhuis for assistance with the LoRRca, Matthias Jourdain and Prof. Gregor Jung for assistance with the fluorescence spectroscopy and Dr. Thomas Fischer for helpful comments and a critical discussion of the manuscript.

- Barnard, T. (1976). An empirical relationship for the formulation of glutaraldehyde-based fixatives. *J. Ultrastruct. Res.* 54, 478–786.
- Bessis, M. (1974). *Corpuscles*. Berlin: Springer-Verlag.
- Bone, Q., and Denton, E. J. (1971). The osmotic effects of electron microscope fixatives. *J. Cell Biol.* 49, 571–581. doi: 10.1083/jcb.49.3.571
- Braunmüller, S., Schmid, L., and Franke, T. (2011). Dynamics of red blood cells and vesicles in microchannels of oscillating width. *J. Phys. Condens. Matter* 23:184116. doi: 10.1088/0953-8984/23/18/184116



- Delaunay, J. (2004). The hereditary stomatocytoses: genetic disorders of the red cell membrane permeability to monovalent cations. *Semin. Hematol.* 41, 165–172. doi: 10.1053/j.seminhematol.2004.02.005
- Diez-Silva, M., Dao, M., Han, J., Lim, C. T., and Suresh, S. (2010). Shape and biomechanical characteristics of human red blood cells in health and disease. *MRS Bull.* 35, 382–388. doi: 10.1557/mrs2010.571
- Eckmann, D. M., Bowers, S., Stecker, M., and Cheung, A. T. (2000). Hematocrit, volume expander, temperature, and shear rate effects on blood viscosity. *Anesth. Analg.* 91, 539–545. doi: 10.1097/00000539-200009000-00007
- Faivre, M., Abkarian, M., Bickraj, K., and Stone, H. A. (2006). Geometrical focusing of cells in a microfluidic device: an approach to separate blood plasma. *Biorheology* 43, 147–159.
- Fermo, E., Bogdanova, A., Petkova-Kirova, P., Zaninoni, A., Marcello, A. P., Makhro, A., et al. (2017). “GardosChannelopathy”: a variant of hereditary *Stomatocytosis* with complex molecular regulation. *Sci. Rep.* 7:1744. doi: 10.1038/s41598-017-01591-w
- Flormann, D., Aouane, O., Kaestner, L., Ruloff, C., Misbah, C., Podgorski, T., et al. (2017). The buckling instability of aggregating red blood cells. *Sci. Rep.* 7:7928. doi: 10.1038/s41598-017-07634-6
- Gillett, R., and Gull, K. (1972). Glutaraldehyde-its purity and stability. *Histochemie* 30, 162–167. doi: 10.1007/bf01444063
- González-Aguilar, F. (1982). Cell volume preservation and the reflection coefficient in chemical fixation. *J. Ultrastruct. Res.* 80, 354–362. doi: 10.1016/s0022-5320(82)80048-8
- Griffiths, G. (ed.) (1993). “Fine-structure preservation,” in *Fine Structure Immunocytochemistry*, (Berlin: Springer), 9–25. doi: 10.1007/978-3-642-77095-1\_2
- Guillichon, D., Esclade, L., and Thomas, D. (1986). Effect of glutaraldehyde on haemoglobin: oxidation-reduction potentials and stability. *Biochem. Pharmacol.* 35, 317–323. doi: 10.1016/0006-2952(86)90532-0
- Guo, Q., Duffy, S. P., Matthews, K., Santoso, A. T., Scott, M. D., and Ma, H. (2014). Microfluidic analysis of red blood cell deformability. *J. Biomech.* 47, 1767–1776. doi: 10.1016/j.jbiomech.2014.03.038
- Hardy, P. M., Nicholls, A. C., and Rydon, H. N. (1969). The nature of glutaraldehyde in aqueous solution. *J. Chem. Soc. D* 1969, 565–566. doi: 10.1039/c29690000565
- Hertz, L., Huisjes, R., Llaudet-Planas, E., Petkova-Kirova, P., Makhro, A., Danielczok, J. G., et al. (2017). Is increased intracellular calcium in red blood cells a common component in the molecular mechanism causing anemia? *Front. Physiol.* 8:673. doi: 10.3389/fphys.2017.00673
- Holmes, D., Whyte, G., Bailey, J., Vergara-Irigaray, N., Ekpenyong, A., Guck, J., et al. (2014). Separation of blood cells with differing deformability using deterministic lateral displacement(†). *Interface Focus* 4:20140011. doi: 10.1098/rsfs.2014.0011
- Johnson, T. J. (1987). Glutaraldehyde fixation chemistry: oxygen-consuming reactions. *Eur. J. Cell Biol.* 45, 160–169.
- Kaestner, L., and Minetti, G. (2017). The potential of erythrocytes as cellular aging models. *Cell Death Differ.* 24, 1475–1477. doi: 10.1038/cdd.2017.100
- Kaestner, L., Tabellion, W., Weiss, E., Bernhardt, I., and Lipp, P. (2006). Calcium imaging of individual erythrocytes: problems and approaches. *Cell Calcium* 39, 13–19. doi: 10.1016/j.ceca.2005.09.004
- Karon, B. S., van Buskirk, C. M., Jaben, E. A., Hoyer, J. D., and Thomas, D. D. (2012). Temporal sequence of major biochemical events during blood bank storage of packed red blood cells. *Blood Transfus.* 10, 453–461. doi: 10.2450/2012.0099-11
- Kawahara, J.-I., Ishikawa, K., Uchimar, T., and Takaya, H. (1997). “Chemical cross-linking by glutaraldehyde between amino groups: its mechanism and effects,” in *Polymer Modification*, eds G. Swift, C. E. Carraher, and C. N. Bowman (Boston, MA: Springer), 119–131. doi: 10.1007/978-1-4899-1477-4\_11
- Lanotte, L., Mauer, J., Mendez, S., Fedosov, D. A., Fromental, J.-M., Claveria, V., et al. (2016). Red cells’ dynamic morphologies govern blood shear thinning under microcirculatory flow conditions. *Proc. Natl. Acad. Sci. U.S.A.* 113, 13289–13294. doi: 10.1073/pnas.1608074113
- Lee, K., Choi, S., Yang, C., Wu, H.-C., and Yu, J. (2013). Autofluorescence generation and elimination: a lesson from glutaraldehyde. *Chem. Commun.* 49, 3028–3030. doi: 10.1039/c3cc40799c
- Loike, J. D., and Silverstein, S. C. (1983). A fluorescence quenching technique using trypan blue to differentiate between attached and ingested glutaraldehyde-fixed red blood cells in phagocytosing murine macrophages. *J. Immunol. Methods* 57, 373–379. doi: 10.1016/0022-1759(83)90097-2
- Machado, A. B. (1967). Straight OsO<sub>4</sub> versus glutaraldehyde-OsO<sub>4</sub> in sequence as fixatives for the granular vesicles in sympathetic axons of the rat pineal body. *Stain Technol.* 42, 293–300. doi: 10.3109/10520296709115028
- Makhro, A., Huisjes, R., Verhagen, L. P., Mañú Pereira, M. D. M., Llaudet-Planas, E., Petkova-Kirova, P., et al. (2016). Red cell properties after different modes of blood transportation. *Front. Physiol.* 7:288. doi: 10.3389/fphys.2016.00288
- Morel, F. M., Baker, R. F., and Wayland, H. (1971). Quantitation of human red blood cell fixation by glutaraldehyde. *J. Cell Biol.* 48, 91–100. doi: 10.1083/jcb.48.1.91
- Nowakowski, R., and Luckham, P. (2002). Imaging the surface details of red blood cells with atomic force microscopy. *Surface Interface Anal.* 33, 118–121. doi: 10.1002/sia.1174
- Ponder, E. (1948). *Hemolysis and Related Phenomena*. New York, NY: Grune & Stratton.
- Prento, P. (1995). Glutaraldehyde for electron microscopy: a practical investigation of commercial glutaraldehydes and glutaraldehyde-storage conditions. *Histochem. J.* 27, 906–913. doi: 10.1007/bf00173845
- Quint, S., Christ, A. F., Guckenberger, A., Himbert, S., Kaestner, L., Gekle, S., et al. (2017). 3D tomography of cells in micro-channels. *Appl. Phys. Lett.* 111:103701. doi: 10.1063/1.4986392
- Rasmussen, K. E. (1974). Fixation in aldehydes. A study on the influence of the fixative, buffer, and osmolarity upon the fixation of the rat retina. *J. Ultrastruct. Res.* 46, 87–102. doi: 10.1016/s0022-5320(74)80024-9
- Rasmussen, K.-E., and Albrechtsen, J. (1974). Glutaraldehyde. The influence of pH, temperature, and buffering on the polymerization rate. *Histochemistry* 38, 19–26. doi: 10.1007/bf00490216
- Reinhart, S. A., Schulzki, T., and Reinhart, W. H. (2015). Albumin reverses the echinocytic shape transformation of stored erythrocytes. *Clin. Hemorheol. Microcirc.* 60, 437–449. doi: 10.3233/CH-141899
- Richards, F. M., and Knowles, J. R. (1968). Glutaraldehyde as a protein cross-linking reagent. *J. Mol. Biol.* 37, 231–233. doi: 10.1016/0022-2836(68)90086-7
- Robertson, E. A., and Schultz, R. L. (1970). The impurities in commercial glutaraldehyde and their effect on the fixation of brain. *J. Ultrastruct. Res.* 30, 275–287. doi: 10.1016/s0022-5320(70)80063-6
- Squier, C. A., Hart, J. S., and Churchland, A. (1976). Changes in red blood cell volume on fixation in glutaraldehyde solutions. *Histochemistry* 48, 7–16. doi: 10.1007/bf00489711
- Suemori, S., Wada, H., Nakanishi, H., Tsujioka, T., Sugihara, T., and Tohyama, K. (2015). Analysis of hereditary elliptocytosis with decreased binding of eosin-5-maleimide to red blood cells. *BioMed Res. Int.* 2015:451861. doi: 10.1155/2015/451861
- Sutera, S. P., and Mehrjardi, M. H. (1975). Deformation and fragmentation of human red blood cells in turbulent shear flow. *Biophys. J.* 15, 1–10. doi: 10.1016/S0006-3495(75)85787-0
- Tomauiolo, G., Carciati, A., Caserta, S., and Guido, S. (2015). Blood linear viscoelasticity by small amplitude oscillatory flow. *Rheol. Acta* 55, 485–495. doi: 10.1007/s00397-015-0894-3
- Tong, X., and Caldwell, K. D. (1995). Separation and characterization of red blood cells with different membrane deformability using steric field-flow fractionation. *J. Chromatogr. B Biomed. Appl.* 674, 39–47. doi: 10.1016/0378-4347(95)00297-0
- Wang, J., Wagner-Britz, L., Bogdanova, A., Ruppenthal, S., Wiesen, K., Kaiser, E., et al. (2013). Morphologically homogeneous red blood cells present a heterogeneous response to hormonal stimulation. *PLoS One* 8:e67697. doi: 10.1371/journal.pone.0067697



- Wiegmann, L., de Zélicourt, D. A., Speer, O., Muller, A., Goede, J. S., Seifert, B., et al. (2017). Influence of standard laboratory procedures on measures of erythrocyte damage. *Front. Physiol.* 8:731. doi: 10.3389/fphys.2017.00731
- Zang, Q., Mansouri, K., Williams, A. J., Judson, R. S., Allen, D. G., Casey, W. M., et al. (2016). In silico prediction of physicochemical properties of environmental chemicals using molecular fingerprints and machine learning. *J. Chem. Inf. Model.* 57, 36–49. doi: 10.1021/acs.jcim.6b00625
- Zaninoni, A., Fermo, E., Vercellati, C., Consonni, D., Marcello, A. P., Zanella, A., et al. (2018). Use of laser assisted optical rotational cell analyzer (LoRRcaMaxSis) in the diagnosis of RBC membrane disorders, enzyme defects, and congenital dyserythropoietic anemias: a monocentric study on 202 patients. *Front. Physiol.* 9:451. doi: 10.3389/fphys.2018.00451

**Conflict of Interest Statement:** The authors declare that the research was conducted in the absence of any commercial or financial relationships that could be construed as a potential conflict of interest.

Copyright © 2019 Abay, Simionato, Chachanidze, Bogdanova, Hertz, Bianchi, van den Akker, von Lindern, Leonetti, Minetti, Wagner and Kaestner. This is an open-access article distributed under the terms of the Creative Commons Attribution License (CC BY). The use, distribution or reproduction in other forums is permitted, provided the original author(s) and the copyright owner(s) are credited and that the original publication in this journal is cited, in accordance with accepted academic practice. No use, distribution or reproduction is permitted which does not comply with these terms.



# Red Blood Cell Homeostasis and Altered Vesicle Formation in Patients With Paroxysmal Nocturnal Hemoglobinuria

Joames K. Freitas Leal<sup>1</sup>, Frank Preijers<sup>2</sup>, Roland Brock<sup>1</sup>, Merel Adjobo-Hermans<sup>1</sup> and Giel Bosman<sup>1\*</sup>

<sup>1</sup>Department of Biochemistry, Radboud University Medical Center, Nijmegen, Netherlands, <sup>2</sup>Laboratory for Hematology, Department of Laboratory Medicine, Radboud University Medical Center, Nijmegen, Netherlands

## OPEN ACCESS

### Edited by:

Paola Bianchi,  
IRCCS Ca'Granda Foundation  
Maggiore Policlinico Hospital, Italy

### Reviewed by:

Mauro Magnani,  
University of Urbino Carlo Bo, Italy  
Marianna H. Antonelou,  
National and Kapodistrian  
University of Athens, Greece

### \*Correspondence:

Giel Bosman  
giel.bosman@radboudumc.nl

### Specialty section:

This article was submitted to  
Red Blood Cell Physiology,  
a section of the journal  
Frontiers in Physiology

**Received:** 20 February 2019

**Accepted:** 24 April 2019

**Published:** 15 May 2019

### Citation:

Freitas Leal JK, Preijers F, Brock R, Adjobo-Hermans M and Bosman G (2019) Red Blood Cell Homeostasis and Altered Vesicle Formation in Patients With Paroxysmal Nocturnal Hemoglobinuria. *Front. Physiol.* 10:578. doi: 10.3389/fphys.2019.00578

A subset of the red blood cells (RBCs) of patients with paroxysmal nocturnal hemoglobinuria (PNH) lacks GPI-anchored proteins. Some of these proteins, such as CD59, inhibit complement activation and protect against complement-mediated lysis. This pathology thus provides the possibility to explore the involvement of complement in red blood cell homeostasis and the role of GPI-anchored proteins in the generation of microvesicles (MVs) *in vivo*. Detailed analysis of morphology, volume, and density of red blood cells with various CD59 expression levels from patients with PNH did not provide indications for a major aberration of the red blood cell aging process in patients with PNH. However, our data indicate that the absence of GPI-anchored membrane proteins affects the composition of red blood cell-derived microvesicles, as well as the composition and concentration of platelet-derived vesicles. These data open the way toward a better understanding on the pathophysiological mechanism of PNH and thereby to the development of new treatment strategies.

**Keywords:** red blood cells, paroxysmal nocturnal hemoglobinuria, aging, thrombosis, microvesicles

## INTRODUCTION

Paroxysmal nocturnal hemoglobinuria (PNH) is a highly debilitating disease that is characterized by intravascular hemolysis, arterial, and venous thrombosis (Malato et al., 2012; Peacock-Young et al., 2018) and a variety of symptoms related to smooth muscle dystonia (DeZern and Brodsky, 2015). PNH is a rare disease with an incidence of 1–2 per 1,000,000 persons per year and is frequently associated with bone marrow failure such as aplastic anemia (Clemente et al., 2018). PNH is caused by clonal expansion of multipotent hematopoietic stem cells with somatic mutations in the *PIGA* gene. *PIGA* encodes for an enzyme that is critical in the synthesis of the first intermediate in the pathway of glycosylphosphatidylinositol (GPI) anchors. (Takeda et al., 1993; DeZern and Brodsky, 2015) As a consequence, the absence of *PIGA* activity results in hematopoietic cells that are deficient in GPI-anchored proteins. In RBCs, the absence of the GPI-anchored proteins decay-accelerating factor (DAF;

CD55) and membrane inhibitor of reactive lysis (MIRL; CD59) that protect against complement-mediated lysis renders red blood cells (RBCs) highly vulnerable to intravascular hemolysis (Risitano and Rotoli, 2008; Brodsky, 2014). This results not only in anemia but also in the release of free hemoglobin and iron, which catalyzes the generation of reactive oxygen species and subsequent NO depletion and vasoconstriction (Kahn et al., 2013; Rapido, 2017). For untreated patients, thrombosis is the most common cause of death (Hill et al., 2013; Griffin and Munir, 2017).

The monoclonal antibody eculizumab is the most effective drug used in PNH (Brodsky, 2009). Eculizumab blocks the cleavage of C5 by the C5 convertase into C5b and thereby inhibits the formation of the terminal membrane attack complex (MAC) C5b-9 and consequent hemolysis of abnormal RBCs. This reduces RBC destruction and transfusion requirements (Carroll and Sim, 2011; Risitano, 2012; Bayly-Jones et al., 2017). Nevertheless, the opsonizing effects of activated complement factors such as C3d may induce RBC phagocytosis (Risitano et al., 2009; DeZern and Brodsky, 2015).

At present, the mechanism(s) responsible for clonal expansion during hematopoiesis and the variable clinical manifestations of the disease have only partially been elucidated (Hill et al., 2017), but increased removal of RBC may contribute to the pathophysiology of PNH (Risitano and Rotoli, 2008). RBC homeostasis is dependent on the generation of young and removal of aged RBCs. The latter process is initiated by binding of senescent cell-specific IgG, the appearance of molecules that may trigger pathological reactions, such as immunoreactive epitopes on damaged membrane proteins, and exposure of phosphatidylserine (PS) in the outer leaflet of the lipid bilayer, all leading to phagocytosis (Bosman et al., 2008; Dinkla et al., 2014; Klei et al., 2017). From biophysical, immunochemical, proteomic, and metabolomic studies, a molecular picture of the pathways involved in the normal aging and removal process of RBCs has emerged: oxidative damage-induced, high-affinity binding of hemoglobin to the cytoplasmic domain of band 3, activation of  $\text{Ca}^{2+}$ -permeable channels, phosphorylation-controlled alterations in morphology and metabolism affecting ATP production and redox status, degradation of band 3 and/or aggregation of band 3 fragments, binding of IgG, and microvesicle (MV) generation (Ferru et al., 2011; Zolla and D'Alessandro, 2012; Bosman, 2016). Physiological anti-band 3 IgG has been reported to have a high affinity for dimeric C3b, thereby linking RBC phagocytosis to complement activation (Lutz and Bogdanova, 2013).

During physiological RBC aging, there is a small decrease in the content of GPI-anchored DAF and MIRL (Willekens et al., 2008), and in the content and activity of acetylcholinesterase (AChE), another GPI-anchored protein (Willekens et al., 2008; Freitas Leal et al., 2017). The latter observation suggests that the activities of DAF and/or MIRL might also decrease in healthy individuals and thereby contribute to complement-mediated opsonization and removal of old RBCs. AChE is increased in microvesicles, suggesting that changes in the distribution of GPI-anchored proteins in microdomains are associated with

microvesicle (MV) generation (Salzer and Prohaska, 2001; Freitas Leal et al., 2017). As a consequence, the absence of GPI-anchored proteins may affect the microvesiculation process. Indeed, some data indicate that microvesiculation of RBCs and platelets may be impaired in PNH patients (Whitlow et al., 1993). Also, it has been shown that activated complement induces the massive formation of vesicles with a strong pro-coagulant activity (Ninomiya et al., 1999). Thus, the absence of GPI-anchored proteins may have a pronounced effect on RBC morphology, function, and survival (Whitlow et al., 1993). In addition, exposure of the pro-coagulant and removal signal PS, which is in general associated with abnormal membrane organization and vesiculation in damaged or stressed, but not in aged RBCs (Bosman et al., 2008), has been reported to be increased in RBCs of PNH patients (Sato et al., 2010).

Here, we have selected a number of aging-associated parameters from this current knowledge of the molecular mechanisms involved in physiological RBC homeostasis (Bosman et al., 2008, 2012; Lutz and Bogdanova, 2013; Bosman, 2016; Freitas Leal et al., 2018) that might be relevant for the pathophysiology of PNH, in order to explore the effect of the absence of GPI-linked proteins on RBC structure, function, aging, and removal *in vivo*. Our data, obtained from PNH patients with various clone sizes and following various treatment regimes, indicate no significant effects of the absence of GPI-linked proteins on RBC turnover but emphasize the heuristic value of more, detailed studies on the origin, composition, and activity of RBC-derived and platelet-derived microvesicles.

## MATERIALS AND METHODS

### Red Blood Cell Sampling

Blood was collected by venipuncture from healthy volunteers and 15 patients after obtaining written informed consent, and using EDTA as anticoagulant, following the guidelines of the local medical ethical committee (CMO regio Arnhem Nijmegen) and in accordance with the Declaration of Helsinki. Leukocytes and platelets were removed as described before using Ficoll-Paque (Freitas Leal et al., 2017). The time between blood collection, fractionation, and analysis was identical for all samples.

### Red Blood Cell Fractionation and Microscopic Analysis

RBCs were fractionated according to cell density using discontinuous Percoll gradients ranging from 40% Percoll (1.060 g/ml) to 80% Percoll (1.096 g/ml) as described before (Willekens et al., 2008; Freitas Leal et al., 2017). The various RBC fractions were isolated and washed three times with Ringer's solution (Freitas Leal et al., 2017) by repeated centrifugation for 5 min at 400 g before analysis. RBC morphology was analyzed using a TCS SP5 confocal laser scanning microscope (Leica Microsystems, Mannheim, Germany) as described before (Cluitmans et al., 2015).

## Isolation and Characterization of Microvesicles From Plasma

Microvesicles (MVs) were isolated from the platelet-rich plasma (PRP) obtained after differential centrifugation as described before (Dinkla et al., 2012, 2013, 2016).

## Flow Cytometry Analysis

Classification of the RBCs according to PNH type was performed by flow cytometry using FITC-labeled CD235a (clone KC16, 1:100, Beckman Coulter, Fullerton, CA, USA) and PE-labeled CD59 (clone MEM43, 1:400, IQ products, Groningen, the Netherlands) as described before (Sutherland et al., 2015). PNH RBCs were classified based on CD59 content in type III (complete GPI-deficiency), type II (partial GPI-deficiency), and type I (normal expression) cells (Sutherland et al., 2015). APC-labeled CD71 (clone CY1G4, 1:200, Biolegend, San Diego, California, USA) was combined with PE-labeled CD59 to evaluate the percentage of reticulocytes per PNH type. FITC-labeled anti-C3c (1:200, Abcam, Cambridge, UK) and APC-labeled anti-C3d (1 µg/million cells, Assay Pro, St. Louis, Missouri, USA) were combined with PE-labeled CD59 to evaluate the degree of opsonization per PNH type. Staining of band 3 with eosin-5' maleimide (EMA, Thermo Fisher Scientific, Landsmeer, the Netherlands) was performed by incubating 1 million RBCs with 25 µl of EMA (0.5 mg/ml in Ringer's solution) in the dark at RT for 15 min. (Cobb and Beth, 1990; Crisp et al., 2011). After staining, RBCs were washed three times with Ringer's solution and analyzed by flow cytometry [FACSCalibur instrument (BD Biosciences, Franklin Lakes NJ, USA)] using CELLQuest software (BD Biosciences). Data were analyzed with FlowJo cell analysis software v.10 (FlowJo, LLC, Ashland, OR) using 200,000 events. Microvesicle analysis was performed using mixtures of PE-labeled CD59 (1:400), FITC-labeled CD235a (1:100), and PE/Cy5-labeled CD41 (1:10) by flow cytometry as previously described (Dinkla et al., 2012, 2013). Sulfate latex microspheres (0.9 µm, Invitrogen, Carlsbad CA, USA) and washed Flow-Count calibration beads (Beckman Coulter, Brea CA, USA) were used for quantification (Dinkla et al., 2012). Microvesicles were classified based on CD59 positivity in CD59-negative (complete GPI-deficiency), low CD59 (partial GPI-deficiency), and wild type (normal expression).

## Comparisons and Statistical Analyses

The exclusion criteria for the PNH patients were other hematological comorbidities besides aplastic anemia and having received a red blood cell transfusion within a period of 3 months before analysis. For most analyses, we compared PNH patients with control donors and PNH patients being treated with eculizumab with patients without eculizumab. Differences between groups were determined using a two-way ANOVA test. Non-parametric *t*-tests or one-way ANOVA tests were used to analyze differences between control and PNH samples. Wilcoxon matched pair tests were used to analyze differences between the various RBC fractions inside the groups, and the Fisher LSD test was used to compare

controls and patient samples. Two-sided *p*'s less than 0.05 were used to determine statistical significance. Relations between the various parameters were estimated using the Pearson correlation coefficient.

## RESULTS

### RBC Morphology and Phenotype

During aging *in vivo* and *in vitro*, RBCs undergo a series of morphological changes that result in the appearance of deformed, mostly spherocytic cells. Semi-quantitative analysis of these changes has been shown to be informative on RBC hemostasis and on the relationship between morphology, deformability, and survival (Cluitmans et al., 2015). Microscopic analysis of RBCs from patients with PNH showed a tendency to a decrease in the numbers of cells with the regular discocyte form and a concomitant increase in the numbers of echinocyte-like and otherwise misshapen cells, especially in the densest cell fractions (Figure 1A). The majority of the patients' RBCs were type I according to CD59 expression levels (Figure 1B), and we found no differences in the percentages of type II and type III cells between the various Percoll layers (Figure 1C). Treatment with eculizumab did not result in significant differences in CD59-deficient cells (Figure 1D).

### Membrane/Band 3 Content (Eosine 5'-Maleimide)

RBC aging is accompanied by changes in membrane organization that are associated with the appearance of removal signals and with the loss of cell membrane. Especially, changes in the integral membrane protein band 3 play a pivotal role in the generation of senescence-specific antigens, in the interaction between lipid bilayer and cytoskeleton, and in the generation of microvesicles (Willekens et al., 2008; Bosman et al., 2012; Lutz and Bogdanova, 2013; Freitas Leal et al., 2018). The amount of binding of the band 3 probe eosine 5'-maleimide (EMA) is mostly a sensitive marker of band 3 content, but also of Rh, Rh glycoprotein, and CD47, and/or of the loss of membrane (Cobb and Beth, 1990; Huisjes et al., 2018). Flow cytometric analysis of the binding of EMA showed a higher EMA signal in all RBC fractions from two different PNH patients tested, independent of cell density and treatment (Figure 2). There was no significant difference in the density-associated decrease between control donors or any of the PNH patients. Also, there was no statistically significant correlation between EMA fluorescence and the RBC size (forward scatter) in the RBC fractions of controls and PNH patients taken together ( $r = 0.31$ ,  $p = 0.18$ ,  $N = 20$ ).

### Complement Deposition (C3c and C3d)

Activation of complement may lead to deposition of complement fragments on RBC through the CR1 receptor, and the presence of C3b fragments induces phagocytosis of eculizumab-treated, CD59-negative RBCs *in vitro* (Lin et al., 2015). We therefore also probed for the presence of C3c and C3d



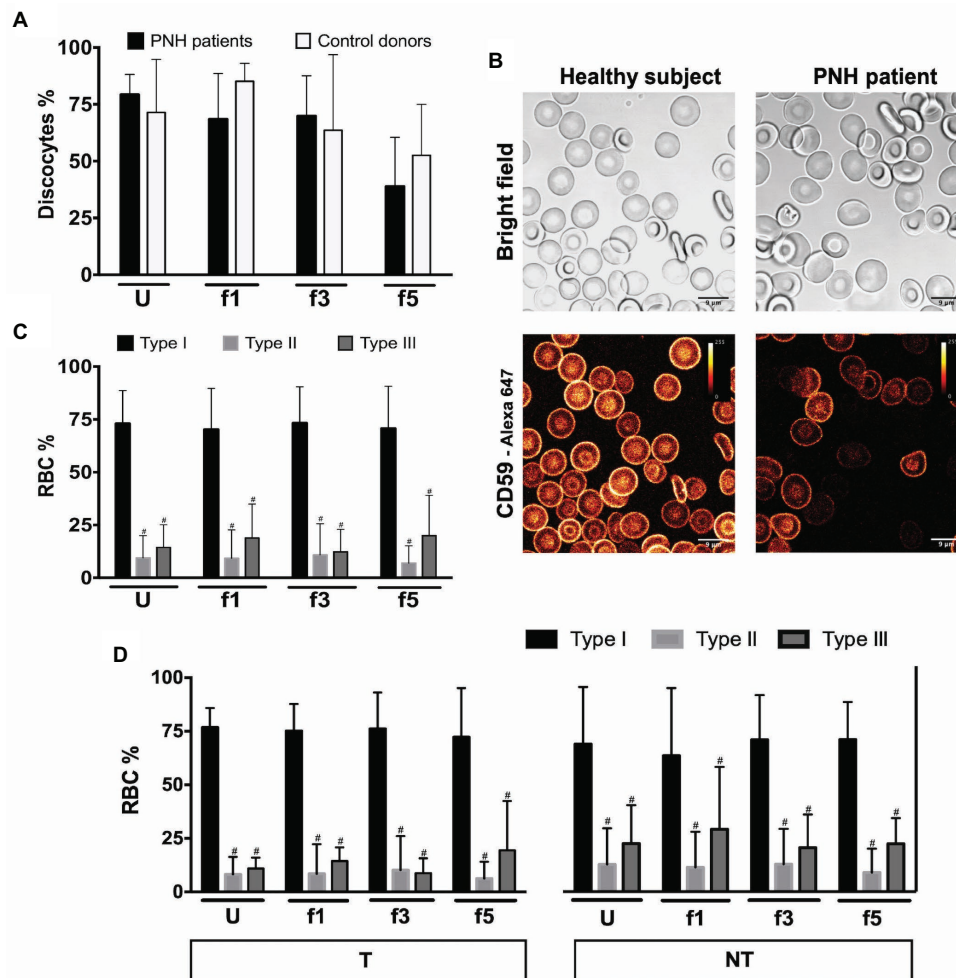


**FIGURE 1 |** RBCs morphology and phenotype of PNH patients. **(A)** Percentage of discocytes per Percoll fraction in PNH patients ( $N = 5$ ) and healthy control donors ( $N = 5$ ); **(B)** bright field and fluorescence images of anti-CD59-Alexa 647 stained RBCs from a healthy subject and a PNH patient, showing CD59 density; **(C)** RBCs of PNH patients ( $N = 9$ ) were separated according to density and analyzed by flow cytometry regarding their CD59 content (type I, II, and III); **(D)** RBCs of PNH patients being treated with eculizumab (T;  $N = 5$ ) and non-treated PNH patients (NT;  $N = 4$ ) separated according to density and analyzed by flow cytometry according to their CD59 content (type I, II, and III). \*Significantly different from type I in the same Percoll fraction ( $p < 0.05$ ). U, unseparated; f1, f3, f5, fractions of increasing density isolated by Percoll density separation (Materials and Methods).

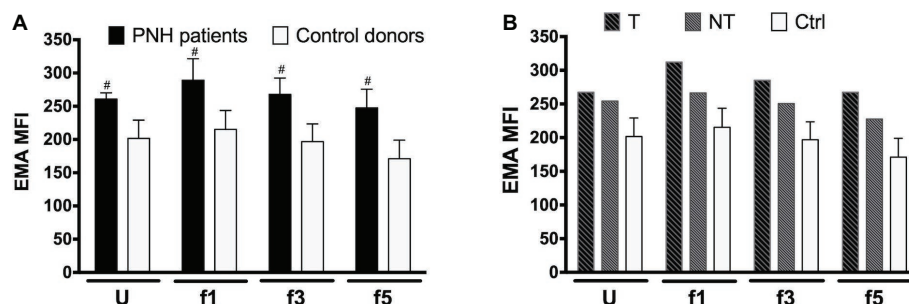


**FIGURE 2 |** Eosin 5'-maleimide Mean Fluorescence Intensity (MFI) of RBC fractions. **(A)** RBCs of PNH patients ( $N = 2$ ) and of control healthy donors ( $N = 7$ ) of various Percoll fractions were stained with eosin 5'-maleimide (EMA). The degree of staining is expressed as the mean fluorescence intensity (MFI). **(B)** EMA MFI of RBCs of a PNH patient being treated with (T) and without (NT) eculizumab, separated according to density. Ctrl, healthy donors ( $N = 7$ ). The samples were analyzed as described before (see Materials and Methods). \*Significantly different from control ( $p < 0.05$ ). U, unseparated; f1, f3, f5, fractions of increasing density isolated by Percoll density separation (Materials and Methods).

in density-separated RBCs. For both proteins, we observed a tendency to an increase in the percentage of positive cells with cell density (Figure 3). Thus, the content of RBC-bound C3c as well as C3d may increase with cell age, also on type I RBCs with a normal content of CD59 (Figure 3). These findings are in agreement with previous indications for the involvement of complement in phagocytosis *in vitro* (Lutz, 2004; Arese et al., 2005). We found no significant correlations between these parameters and treatment with eculizumab (data not shown).

## Reticulocytes

Aberrant RBC structure resulting in a decreased mean life and leading to anemia is, in many cases, compensated by increased erythropoiesis, as indicated by changes in the size of the reticulocyte fraction. The hematological data show a large variability in the size of the reticulocyte fractions of our patients, without any significant correlation with other patient variables, although most eculizumab-treated patients had higher reticulocyte numbers than the patients without eculizumab (Supplementary Table 1). Flow cytometric analysis of the RBCs of a few PNH patients showed similar data, also without significant differences between donors or RBC fractions (Figures 4A,B). In general, most reticulocytes were

found in the lightest density fractions upon Percoll separation, i.e., fraction 1 (Figure 4A), as shown before for healthy individuals (Willekens et al., 2008). The fraction of type III, CD59-lacking reticulocytes was considerably higher than the other types (Figure 4C), which may reflect a disturbed differentiation and/or maturation process in the absence of GPI-linked proteins (Sato et al., 2010).

## Microvesicles

Microvesicle generation is an integral part of the physiological RBC aging process, and changes in microvesicle concentration as well as composition occur in patients with disturbed RBC homeostasis (Freitas Leal et al., 2018). We found no significant differences in the concentrations of RBC-derived microvesicles between PNH patients and controls (Figure 5A). However, the concentration of PS-negative microvesicles in the plasma of PNH patients was higher than in the plasma of control donors (Figure 5B). The concentration of CD59-high RBC-derived microvesicles was higher than that of the other types in the plasma of control donors but not in the plasma of PNH patients (Figure 5C). Platelet-derived microvesicle concentrations were much higher in the plasma of PNH patients than in controls (Figure 5D), both the PS-positive and the PS-negative microvesicles (Figure 5E). Remarkably, almost all platelet-derived

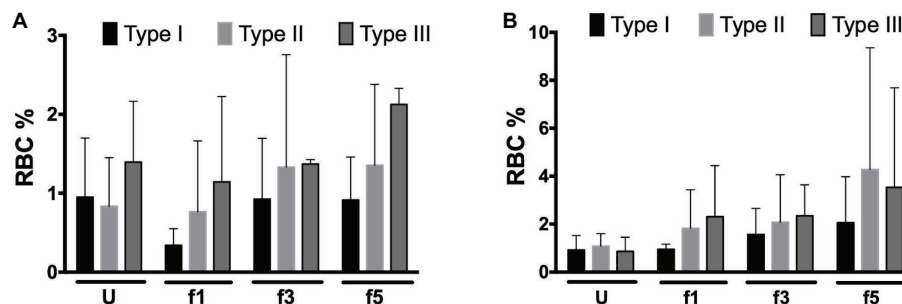


**FIGURE 3 |** Complement deposition on density-separated RBCs. **(A)** Percentage of C3c-positive RBCs in the PNH RBC population divided per CD59 content (type I, II, and III) per density (Percoll fraction;  $N = 2$ ); **(B)** percentage of C3d-positive RBCs in the PNH RBC population according to CD59 content (type I, II, and III) per Percoll fraction (type I, II, and III;  $N = 3$ ). The samples were analyzed as described before (see Materials and Methods). U, unseparated; f1, f3, f5, fractions of increasing density isolated by Percoll density separation (Materials and Methods).

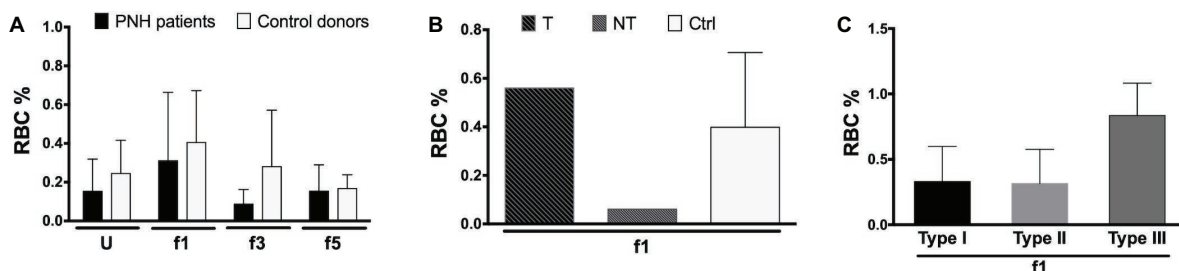


**FIGURE 4 |** Reticulocytes in patients with PNH. **(A)** Percentage of CD71-expressing RBCs from the blood of PNH patients ( $N = 2$ ) and healthy control donors RBCs ( $N = 4$ ) of various Percoll fractions after staining with APC-labeled CD71; **(B)** percentage of APC-CD71-positive RBCs of a PNH patient being treated with eculizumab (T), a non-treated PNH patient (NT), and healthy control donors in the reticulocyte-enriched Percoll fraction 1 (Ctrl;  $N = 4$ ); **(C)** percentage of APC-CD71-positive RBCs in the PNH RBC population per CD59 content (type I, II, and III) in fraction 1 ( $N = 2$ ). The samples were analyzed as described before (see Materials and Methods). U, unseparated; f1, f3, f5, fractions of increasing density isolated by Percoll density separation (Materials and Methods).

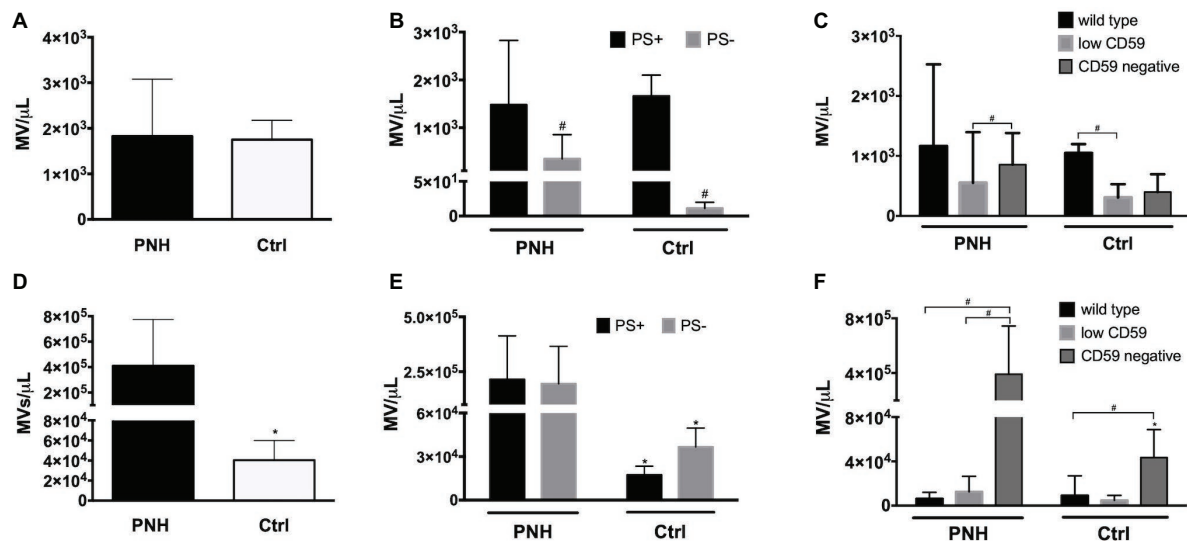


**FIGURE 5 |** Microvesicle numbers and composition in the blood of patients with PNH. **(A)** Concentration per microliter (MV/ $\mu$ L) of RBC-derived, CD235a-positive microvesicles in the blood of PNH patients ( $N = 9$ ) and control healthy donors ( $N = 6$ ); **(B)** concentration of RBC-derived microvesicles in the blood of PNH patients ( $N = 9$ ) and control healthy donors ( $N = 3$ ), distinguished according to their reactivity to Annexin V (phosphatidylserine-positive (PS+) or negative (PS-)); **(C)** RBC-derived microvesicles were categorized into wild type, CD59-low and CD59-negative PNH,  $N = 9$ ; Ctrl,  $N = 3$ ), as described for RBCs (Materials and Methods); **(D)** concentration of CD41-positive, platelet-derived microvesicles in the blood of PNH patients ( $N = 9$ ) and control healthy donors ( $N = 6$ ); **(E)** concentration of platelet-derived microvesicles according to their reactivity to Annexin V (PS+ or PS-; PNH,  $N = 9$ ; Ctrl,  $N = 3$ ); **(F)** platelet-derived microvesicles were categorized into wild type, CD59-low and CD59-negative as described for RBCs and quantified and analyzed by flow cytometry as described before (PNH,  $N = 9$ ; Ctrl,  $N = 3$ ). #Significantly different from the other parameter ( $p < 0.05$ ); \*Significantly different from the patients' samples ( $p < 0.05$ ).

microvesicles were devoid of CD59, including those from the plasma of control donors (**Figure 5F**). We observed no statistically significant correlations between the numbers of RBC-derived and platelet-derived vesicles ( $r = -0.40$ ,  $p = 0.28$ ,  $N = 9$ ).

## DISCUSSION

### RBC Aging and Generation of Microvesicles

Red blood cells of PNH patients lack the key GPI-anchored membrane proteins that protect against activated complement. We postulated that this change in membrane composition has a more wide-spread effect on membrane organization and thereby on various aspects of RBC homeostasis. The most obvious aspects derive from the role of complement in removal of senescent RBCs and the involvement of GPI-linked proteins in microdomain-associated generation of microvesicles (Lutz, 2004; Lutz and Bogdanova, 2013; de Back et al., 2014; Saha et al., 2016; Pollet et al., 2018). In this exploratory study, we did not find significant indications for a pronounced alteration of RBC homeostasis in patients with PNH, as based on cell volume, cell density, and morphology or on clinical hematology parameters, including LDH values (**Supplementary Table 1**). Thus, in most of our patients, the lack of GPI-anchored proteins does not seem to cause a major disturbance of the physiological RBC aging mechanisms.

Nevertheless, there were clear differences related to membrane composition and microvesicle formation. The EMA

measurements showed significant differences between the RBCs of PNH patients and of control donors (**Figure 2**). The tendency to a density-associated decrease in EMA staining might be due to loss of band 3 and/or membrane with aging by vesiculation, both in RBCs from control donors and from PNH patients. This has been postulated before for physiological aging *in vivo* (Willekens et al., 2008). However, the absence of a statistically significant correlation between EMA fluorescence and the RBC size, based on the cytometer parameter forward scatter, suggests that in the RBCs from PNH patients, the band 3 protein content is not a direct function of cell size. EMA staining is affected by changes in band 3 conformation and membrane organization as well (e.g., Cobb and Beth, 1990; Huisjes et al., 2018). Combined with the considerable fractions of PS-negative and CD59-lacking microvesicles in the blood of PNH patients (**Figure 5**), these data indicate that the organization of the RBC membrane, as well as the mechanism of microvesicle generation, are altered by the absence of GPI-linked proteins. This may be a direct effect, but also the consequence of the deposition of C3b. The latter not only affects lateral mobility of CD59 and band 3 molecules but also membrane viscosity and deformability (Karnchanaphanurach et al., 2009; Glodek et al., 2010). Our *in vivo* data support the involvement of GPI-linked proteins in microvesicle formation during RBC aging *in vitro* (Salzer et al., 2008; Freitas Leal et al., 2017). The differences in mechanisms leading to the generation of microvesicles with and without PS at their outside remain to be established, as well as the effect on biological activity.

Since PS exposure contributes to recognition and removal of microvesicles by macrophages (Willekens et al., 2005), its absence may not only affect their pro-coagulant activity but also their lifespan. Fusion between microvesicles and RBCs may underlie the reported transfer between CD55 and CD59 from normal RBCs to RBCs without these proteins (Sloand et al., 2004). Thus, microvesicles generated by PNH RBCs may also fuse with normal RBCs, thereby affecting their membrane organization as well. Furthermore, increased levels of RBC-derived microvesicles may affect NO bioavailability (Said et al., 2018) and induce activation of endothelial cells and tissue factor expression (Collier et al., 2013), thereby contributing to the wide-spread thrombosis in patients with PNH.

## Platelet Microvesicles and Thrombosis

Platelets without CD59 have been described to catalyze the rate of prothrombin conversion upon treatment with complement C5b-9 *in vitro*, and this was associated with an increase in microvesicle formation (Wiedmer et al., 1993). RBC-derived and platelet-derived, phosphatidylserine-positive microvesicles have been reported to be increased approximately two-fold in the blood of PNH patients (Hugel et al., 1999). We found equal concentrations of RBC-derived microvesicles in the plasma of PNH patients and healthy donors, but much larger RBC-derived, phosphatidylserine-negative microvesicle concentrations in the blood of PNH patients (Figure 5B), and larger concentrations of platelet-derived vesicles (Figure 5D). In the plasma of eculizumab-treated PNH patients, the numbers of RBC-derived vesicles were lower than in patients who had not been treated with eculizumab (Supplementary Figure S1). The absence of a statistically significant correlation between the concentrations of RBC-derived and platelet-derived microvesicles indicates that the absence of GPI-linked proteins affects microvesicle generation from RBCs and platelets through different mechanisms. Although in control donors, most platelets are CD59-positive (Jin et al., 1997), almost all platelet-derived microvesicles were CD59-negative (Figure 5). There were approximately equal concentrations of platelet-derived vesicles with and without PS at their surface (Figure 5E). These data strongly suggest that the absence of GPI-linked proteins does not only have a pronounced stimulatory effect on the generation of microvesicles but also on their composition. The latter may be related to the presence of tissue factor and is likely to affect their function (Devalet et al., 2014). Our recent finding that platelet-derived microvesicles can prevent differentiation of regulatory T-cells through P-selectin (Dinkla et al., 2016) emphasizes their pivotal role in the pathophysiology of many diseases that may include PNH (Devalet et al., 2014). Although the name suggests otherwise, most platelet-derived microvesicles originate not from platelets, but from megakaryocytes in the bone marrow (Flaumenhaft et al., 2009; Rank et al., 2010). It is not known how the absence of GPI-linked proteins affects megakaryocyte biology and/or platelet

activation. These data support the importance of an extensive characterization of origin, composition, and biological activity of CD41-positive microvesicles. Such studies may help in establishing an urgently needed, robust marker of platelet activation.

## CONCLUSION

The heterogeneity of the patient population and the concomitant small numbers available for statistical comparisons of all parameters preclude a robust answer on the question whether RBC aging is altered in patients with PNH. However, the combined results of the selected aging-associated parameters (Bosman et al., 2008, 2012; Lutz and Bogdanova, 2013) do not reveal a major aberration of the physiological RBC aging process in patients with PNH. Remarkably, formation of microvesicles by RBCs is altered in patients with PNH. This is likely due to PNH-related differences in membrane organization that is associated with the absence of GPI-linked proteins. The conspicuous lack of phosphatidylserine exposure on many RBC-derived microvesicles in PNH patients may affect their time in the circulation as well as their contribution to hemostasis and thrombosis. In platelets, PNH-related processes seem not only to induce the appearance of large numbers of phosphatidylserine-negative microvesicles but also to cause excessive formation of microvesicles. Future investigations leading to a better understanding of the mechanisms underlying vesiculation, effect of vesiculation on RBC function and survival, and effect of the various microvesicles on thrombosis in patients with PNH may be instrumental in developing new treatment strategies (Kulasekararaj et al., 2019).

## DATA AVAILABILITY

The raw data supporting the conclusions of this manuscript will be made available by the authors, without undue reservation, to any qualified researcher.

## ETHICS STATEMENT

This study was carried out in accordance with the recommendations of the medical ethical committee “CMO-Regio Arnhem Nijmegen”; with written informed consent from all subjects. All subjects gave written informed consent in accordance with the Declaration of Helsinki. The protocol was approved by the CMO-Regio Arnhem Nijmegen.

## AUTHOR CONTRIBUTIONS

JF performed all measurements, the analyses, and wrote the first version of the manuscript. FP provided the samples, some protocols, and assisted in writing the manuscript. RB, MA-H,



and GB contributed to the setup of the study, the interpretation of the data, and the writing of the manuscript.

## FUNDING

The work of JF was supported by the National Council for Scientific and Technological Development–CNPq–Brazil.

## SUPPLEMENTARY MATERIAL

The Supplementary Material for this article can be found online at: <https://www.frontiersin.org/articles/10.3389/fphys.2019.00578/full#supplementary-material>

**SUPPLEMENTARY FIGURE S1** | Microvesicle numbers and composition in the blood of patients with PNH CD59 level and treatment. **(A)** Concentration (MV/ $\mu$ l) of CD235a-positive, RBC-derived microvesicles (MVs) in the blood of PNH patients who did not receive treatment (NT;  $N = 3$ ), PNH patients who were treated with eculizumab (T;  $N = 6$ ), and control healthy donors ( $N = 6$ ); **(B)** concentration of RBC-derived microvesicles in the blood of PNH patients who did not receive treatment (NT;  $N = 3$ ), PNH patients who were being treated with eculizumab (T;  $N = 6$ ) and control donors ( $N = 6$ ) according to their reactivity to Annexin V (phosphatidylserine positive (PS+) or negative (PS−)); **(C)** RBC-derived microvesicles in the blood of PNH patients who did not receive treatment (NT;  $N = 3$ ), PNH patients who were being treated with eculizumab (T;  $N = 6$ ) categorized in wild type, CD59-low and CD59-negative as described for

RBCs (Materials and Methods); **(D)** concentration of platelet-derived microvesicles (CD41-positive) from the blood of PNH patients who did not receive treatment with eculizumab (NT;  $N = 3$ ), PNH patients who were being treated with eculizumab (T;  $N = 6$ ) and control healthy donors ( $N = 6$ ); **(E)** concentration of platelet-derived microvesicles in the blood of PNH patients who did not receive treatment with eculizumab (NT;  $N = 3$ ), PNH patients who were being treated with eculizumab (T;  $N = 6$ ) and control healthy donors ( $N = 6$ ), according to their reactivity to Annexin V (PS+ or PS−); **(F)** platelet-derived microvesicles from the blood of PNH patients who did not receive treatment with eculizumab (NT;  $N = 3$ ), PNH patients who were being treated with eculizumab (T;  $N = 6$ ) were categorized in wild type, low CD59, and CD59-negative as described for RBCs and quantified and analyzed by flow cytometry as described before (see Materials and Methods). \*Significantly different from the other parameter in the same group ( $p < 0.05$ ). \*Significantly different between groups ( $p < 0.05$ ).

**SUPPLEMENTARY TABLE 1** | Clinical data of PNH patients. AA, PNH patient with aplastic anemia; N, PNH patient without hematological comorbidities; T, in treatment; NT, not in treatment; RBC, red blood cells ( $\times 10^{12}/L$ ); RBC CS (II/III), red blood cell clone size (type II and III); Hb, hemoglobin (g/dl); Ht, hematocrit (%); MCV, mean corpuscular volume (fl); MCH, mean corpuscular hemoglobin (pg); MCHC, mean corpuscular hemoglobin concentration (g/dl); RDW, red blood cell distribution width (%); Retic, reticulocytes (promille); RBC Tr, red blood cell transfusion in the last 3 months; Leuk, Leukocytes ( $\times 10^9/L$ ); Gran CS., granulocytes clone size; Plt, platelet ( $\times 10^9/L$ ); LDH, lactate dehydrogenase (U/L); –, not available. Reference values for healthy adults: RBC: for men,  $4.7\text{--}6.1 \times 10^{12}/L$  and for women,  $4.2\text{--}5.4 \times 10^{12}/L$ ; Hb: for men,  $8.5\text{--}11$  mmol/L and for women,  $7.5\text{--}10$  mmol/dl; Ht: for men,  $0.4\text{--}0.54$  and for women,  $0.36\text{--}0.46$ ; MCV:  $80\text{--}96$  fl; MCH:  $1.7\text{--}2.1$  fmol; MCHC:  $19.3\text{--}22.5$  mmol/L; RDW:  $11.5\text{--}14.5\%$ ; Retic:  $8\text{--}26$  promille; Leuk:  $4.5\text{--}11 \times 10^9/L$ ; Plt:  $150\text{--}400 \times 10^9/L$ ; LDH:  $135\text{--}225$  U/L.

## REFERENCES

- Arese, P., Turrini, F., and Schwarzer, E. (2005). Band 3/complement-mediated recognition and removal of normally senescent and pathological human erythrocytes. *Cell. Physiol. Biochem.* 16, 133–146. doi: 10.1159/000089839
- Bayly-Jones, C., Bubeck, D., and Dunstone, M. A. (2017). The mystery behind membrane insertion: a review of the complement membrane attack complex. *Philos. Trans. R. Soc. Lond. Ser. B Biol. Sci.* 372:20160221. doi: 10.1098/rstb.2016.0221
- Bosman, G. (2016). The proteome of the red blood cell: an auspicious source of new insights into membrane-centered regulation of homeostasis. *Proteome* 4:35. doi: 10.3390/proteomes4040035
- Bosman, G. J. C. G. M., Lasonder, E., Groenen-Döpp, Y. A. M., Willekens, F. L. A., and Werre, J. M. (2012). The proteome of erythrocyte-derived microparticles from plasma: new clues for erythrocyte aging and vesiculation. *J. Proteome* 76, 203–210. doi: 10.1016/j.jprot.2012.05.031
- Bosman, G. J. C. G. M., Werre, J. M., Willekens, F. L. A., and Novotný, V. M. J. (2008). Erythrocyte ageing *in vivo* and *in vitro*: structural aspects and implications for transfusion. *Transfus. Med.* 18, 335–347. doi: 10.1111/j.1365-3148.2008.00892.x
- Brodsky, R. A. (2009). How I treat paroxysmal nocturnal hemoglobinuria. *Blood* 113, 6522–6527. doi: 10.1182/blood-2009-03-195966
- Brodsky, R. A. (2014). Paroxysmal nocturnal hemoglobinuria. *Blood* 124, 2804–2811. doi: 10.1182/blood-2014-02-522128
- Carroll, M. V., and Sim, R. B. (2011). Complement in health and disease. *Adv. Drug Deliv. Rev.* 63, 965–975. doi: 10.1016/j.addr.2011.06.005
- Clemente, M. J., Przychodzen, B., Hirsch, C. M., Nagata, Y., Bat, T., Włodarski, M. W., et al. (2018). Clonal PIGA mosaicism and dynamics in paroxysmal nocturnal hemoglobinuria. *Leukemia* 32, 2507–2511. doi: 10.1038/s41375-018-0138-5
- Cluitmans, J. C. A., Tomelleri, C., Yapici, Z., Dinkla, S., Bovee-Geurts, P., Chokkalingam, V., et al. (2015). Abnormal red cell structure and function in neuroacanthocytosis. *PLoS One* 10:e0125580. doi: 10.1371/journal.pone.0125580
- Cobb, C. E., and Beth, A. H. (1990). Identification of the Eosinyl-5-maleimide reaction site on the human erythrocyte anion-exchange protein: overlap with the reaction sites of other chemical probes. *Biochemistry* 29, 8283–8290. doi: 10.1021/bi00488a012
- Collier, M. E. W., Mah, P. M., Xiao, Y., Maraveyas, A., and Ettelaie, C. (2013). Microparticle-associated tissue factor is recycled by endothelial cells resulting in enhanced surface tissue factor activity. *Thromb. Haemost.* 110, 966–976. doi: 10.1160/TH13-01-0055
- Crisp, R. L., Solari, L., Vota, D., García, E., Míguez, G., Chamorro, M. E., et al. (2011). A prospective study to assess the predictive value for hereditary spherocytosis using five laboratory tests (cryohemolysis test, eosin-5'-maleimide flow cytometry, osmotic fragility test, autohemolysis test, and SDS-PAGE) on 50 hereditary spherocytosis fa. *Ann. Hematol.* 90, 625–634. doi: 10.1007/s00277-010-1112-0
- de Back, D. Z., Kostova, E. B., van Kraaij, M., van den Berg, T. K., and van Bruggen, R. (2014). Of macrophages and red blood cells; a complex love story. *Front. Physiol.* 5:9. doi: 10.3389/fphys.2014.00009
- Devalet, B., Mullier, F., Chatelain, B., Dogne, J.-M., and Chatelain, C. (2014). The central role of extracellular vesicles in the mechanisms of thrombosis in paroxysmal nocturnal haemoglobinuria: a review. *J. Extracell. Vesicles* 3, 1–8. doi: 10.3402/jev.v3.23304
- DeZern, A. E., and Brodsky, R. A. (2015). Paroxysmal nocturnal hemoglobinuria. A complement-mediated hemolytic anemia. *Hematol. Oncol. Clin. North Am.* 29, 479–494. doi: 10.1016/j.hoc.2015.01.005
- Dinkla, S., Brock, R., Joosten, I., and Bosman, G. J. C. G. M. (2013). Gateway to understanding microparticles: standardized isolation and identification of plasma membrane-derived vesicles. *Nanomedicine* 8, 1657–1668. doi: 10.2217/nnm.13.149
- Dinkla, S., Poppelman, M., Der Raadt, J., Atsma, F., Novotný, V. M. J., Van Kraaij, M. G. J., et al. (2014). Phosphatidylserine exposure on stored red blood cells as a parameter for donor-dependent variation in product quality. *Blood Transfus.* 12, 204–209. doi: 10.2450/2013.0106-13
- Dinkla, S., Van Cranenbroek, B., Van Der Heijden, W. A., He, X., Wallbrecher, R., Dumitriu, I. E., et al. (2016). Platelet microparticles inhibit IL-17 production

- by regulatory T cells through P-selectin. *Blood* 127, 1976–1986. doi: 10.1182/blood-2015-04-640300
- Dinkla, S., Wessels, K., Verdurmen, W. P. R., Tomelleri, C., Cluitmans, J. C. A., Fransen, J., et al. (2012). Functional consequences of sphingomyelinase-induced changes in erythrocyte membrane structure. *Cell Death Dis.* 3:e410. doi: 10.1038/cddis.2012.143
- Ferru, E., Giger, K., Pantaleo, A., Campanella, E., Grey, J., Ritchie, K., et al. (2011). Regulation of membrane-cytoskeletal interactions by tyrosine phosphorylation of erythrocyte band 3. *Blood* 117, 5998–6006. doi: 10.1182/blood-2010-11-317024
- Flaumenhaft, R., Dilks, J. R., Richardson, J., Alden, E., Patel-Hett, S. R., Battinelli, E., et al. (2009). Megakaryocyte-derived microparticles: direct visualization and distinction from platelet-derived microparticles. *Blood* 113, 1112–1121. doi: 10.1182/blood-2008-06-163832
- Freitas Leal, J. K., Adjoho-Hermans, M. J. W., and Bosman, G. J. C. G. M. (2018). Red blood cell homeostasis: mechanisms and effects of microvesicle generation in health and disease. *Front. Physiol.* 9:703. doi: 10.3389/fphys.2018.00703
- Freitas Leal, J. K., Adjoho-Hermans, M. J. W., Brock, R., and Bosman, G. J. C. G. M. (2017). Acetylcholinesterase provides new insights into red blood cell ageing *in vivo* and *in vitro*. *Blood Transfus.* 15, 232–238. doi: 10.2450/2017.0370-16
- Glodek, A. M., Mirchev, R., Golan, D. E., Khoory, J. A., Burns, J. M., Shevkopyas, S. S., et al. (2010). Ligation of complement receptor 1 increases erythrocyte membrane deformability. *Blood* 116, 6063–6071. doi: 10.1182/blood-2010-04-273904
- Griffin, M., and Munir, T. (2017). Management of thrombosis in paroxysmal nocturnal hemoglobinuria: a clinician's guide. *Ther. Adv. Hematol.* 8, 119–126. doi: 10.1177/2040620716681748
- Hill, A., DeZern, A. E., Kinoshita, T., and Brodsky, R. A. (2017). Paroxysmal nocturnal hemoglobinuria. *Nat. Rev. Dis. Primers.* 3:17028. doi: 10.1038/nrdp.2017.28
- Hill, A., Kelly, R. J., and Hillmen, P. (2013). Thrombosis in paroxysmal nocturnal hemoglobinuria. *Blood* 121, 4985–4996. doi: 10.1182/blood-2012-09-311381
- Hugel, B., Socié, G., Vu, T., Toti, F., Gluckman, E., Freyssinet, J. M., et al. (1999). Elevated levels of circulating procoagulant microparticles in patients with paroxysmal nocturnal hemoglobinuria and aplastic anemia. *Blood* 93, 3451–3456.
- Huisjes, R., Satchwell, T. J., Verhagen, L. P., Schifflers, R. M., van Solinge, W. W., Toye, A. M., et al. (2018). Quantitative measurement of red cell surface protein expression reveals new biomarkers for hereditary spherocytosis. *Int. J. Lab. Hematol.* 40, e74–e77. doi: 10.1111/ijlh.12841
- Jin, J. Y., Tooe, J. A., Marsh, J. C. W., and Gordon-Smith, E. C. (1997). Glycosylphosphatidyl-inositol (GPI)-linked protein deficiency on the platelets of patients with aplastic anaemia and paroxysmal nocturnal hemoglobinuria: two distinct patterns correlating with expression on neutrophils. *Br. J. Haematol.* 96, 493–496. doi: 10.1046/j.1365-2141.1997.d01-2047.x
- Kahn, M., Maley, J., Lasker, G., and Kadowitz, P. (2013). Updated role of nitric oxide in disorders of erythrocyte function. *Cardiovasc. Hematol. Disord. Drug Targets* 13, 83–87. doi: 10.2174/1871529X11313010009
- Karnchanaphanurach, P., Mirchev, R., Ghiran, I., Asara, J. M., Papahadjopoulos-Sternberg, B., Nicholson-Weller, A., et al. (2009). C3b deposition on human erythrocytes induces the formation of a membrane skeleton-linked protein complex. *J. Clin. Invest.* 119, 788–801. doi: 10.1172/JCI36088
- Klei, T. R. L., Meinders, S. M., van den Berg, T. K., and van Bruggen, R. (2017). From the cradle to the grave: the role of macrophages in erythropoiesis and erythrophagocytosis. *Front. Immunol.* 8. doi: 10.3389/fimmu.2017.00073
- Kulasekararaj, A. G., Hill, A., Rottinghaus, S. T., Langemeijer, S., Wells, R., Gonzalez-Fernandez, F. A., et al. (2019). Ravulizumab (ALXN1210) vs eculizumab in C5-inhibitor-experienced adult patients with PNH: the 302 study. *Blood* 133, 540–549. doi: 10.1182/blood-2018-09-876805
- Lin, Z., Schmidt, C. Q., Koutsogiannaki, S., Ricci, P., Risitano, A. M., Lambris, J. D., et al. (2015). Complement C3dg-mediated erythrophagocytosis: implications for paroxysmal nocturnal hemoglobinuria. *Blood* 126, 891–894. doi: 10.1182/blood-2015-02-625871
- Lutz, H. U. (2004). Innate immune and non-immune mediators of erythrocyte clearance. *Cell. Mol. Biol. (Noisy-le-Grand)* 50, 107–116.
- Lutz, H. U., and Bogdanova, A. (2013). Mechanisms tagging senescent red blood cells for clearance in healthy humans. *Front. Physiol.* 4:387. doi: 10.3389/fphys.2013.00387
- Malato, A., Saccullo, G., Lo Coco, L., Mancuso, S., Santoro, M., Martino, S., et al. (2012). Thrombotic complications in paroxysmal nocturnal haemoglobinuria: a literature review. *Blood Transfus.* 10, 428–435. doi: 10.2450/2012.0161-11
- Ninomiya, H., Kawashima, Y., Hasegawa, Y., and Nagasawa, T. (1999). Complement-induced procoagulant alteration of red blood cell membranes with microvesicle formation in paroxysmal nocturnal haemoglobinuria (PNH): implication for thrombogenesis in PNH. *Br. J. Haematol.* 106, 224–231. doi: 10.1046/j.1365-2141.1999.01483.x
- Peacock-Young, B., Macrae, F. L., Newton, D. J., and Ariëns, R. A. S. (2018). The prothrombotic state in paroxysmal nocturnal hemoglobinuria: a multifaceted source. *Haematologica* 103, 9–17. doi: 10.3324/haematol.2017.177618
- Pollet, H., Conrard, L., Cloos, A.-S., and Tyteca, D. (2018). Plasma membrane lipid domains as platforms for vesicle biogenesis and shedding? *Biomol. Ther.* 8:94. doi: 10.3390/biom8030094
- Rank, A., Nieuwland, R., Delker, R., Köhler, A., Toth, B., Pihusch, V., et al. (2010). Cellular origin of platelet-derived microparticles *in vivo*. *Thromb. Res.* 126, e255–e259. doi: 10.1016/j.thromres.2010.07.012
- Rapido, F. (2017). The potential adverse effects of haemolysis. *Blood Transfus.* 15, 218–221. doi: 10.2450/2017.0311-16
- Risitano, A. M. (2012). Paroxysmal nocturnal hemoglobinuria and other complement-mediated hematological disorders. *Immunobiology* 217, 1080–1087. doi: 10.1016/j.imbio.2012.07.014
- Risitano, A. M., Notaro, R., Marando, L., Serio, B., Ranaldi, D., Seneca, E., et al. (2009). Complement fraction 3 binding on erythrocytes as additional mechanism of disease in paroxysmal nocturnal hemoglobinuria patients treated by eculizumab. *Blood* 113, 4094–4100. doi: 10.1182/blood-2008-11-189944
- Risitano, A. M., and Rotoli, B. (2008). Paroxysmal nocturnal hemoglobinuria: pathophysiology, natural history and treatment options in the era of biological agents. *Biologics* 2, 205–222.
- Saha, S., Anilkumar, A. A., and Mayor, S. (2016). GPI-anchored protein organization and dynamics at the cell surface. *J. Lipid Res.* 57, 159–175. doi: 10.1194/jlr.R062885
- Said, A. S., Rogers, S. C., and Doctor, A. (2018). Physiologic impact of circulating RBC microparticles upon blood-vascular interactions. *Front. Physiol.* 8, 1–14. doi: 10.3389/fphys.2017.01120
- Salzer, U., and Prohaska, R. (2001). Stomatin, flotillin-1, and flotillin-2 are major integral proteins of erythrocyte lipid rafts. *Blood* 97, 1141–1143. doi: 10.1182/blood.V97.4.1141
- Salzer, U., Zhu, R., Luten, M., Isobe, H., Pastushenko, V., Perkmann, T., et al. (2008). Vesicles generated during storage of red cells are rich in the lipid raft marker stomatin. *Transfusion* 48, 451–462. doi: 10.1111/j.1537-2995.2007.01549.x
- Sato, S., Kozuma, Y., Hasegawa, Y., Kojima, H., Chiba, S., and Ninomiya, H. (2010). Enhanced expression of CD71, transferrin receptor, on immature reticulocytes in patients with paroxysmal nocturnal hemoglobinuria. *Int. J. Lab. Hematol.* 32, e137–e143. doi: 10.1111/j.1751-553X.2009.01148.x
- Sloand, E. M., Mainwaring, L., Keyvanfar, K., Chen, J., Maciejewski, J., Klein, H. G., et al. (2004). Transfer of glycosylphosphatidylinositol-anchored proteins to deficient cells after erythrocyte transfusion in paroxysmal nocturnal hemoglobinuria. *Blood* 104, 3782–3788. doi: 10.1182/blood-2004-02-0645
- Sutherland, D. R., Illingworth, A., Keeney, M., and Richards, S. J. (2015). “High-sensitivity detection of PNH red blood cells, red cell precursors, and white blood cells” in *Current protocols in cytometry* (Hoboken, NJ, USA: John Wiley & Sons, Inc.), 6.37.1–6.37.29.
- Takeda, J., Miyata, T., Kawagoe, K., Iida, Y., Endo, Y., Fujita, T., et al. (1993). Deficiency of the GPI anchor caused by a somatic mutation of the PIG-A gene in paroxysmal nocturnal hemoglobinuria. *Cell* 73, 703–711. doi: 10.1016/0092-8674(93)90250-T

- Whitlow, M., Iida, K., Marshall, P., Silber, R., and Nussenzweig, V. (1993). Cells lacking glycan phosphatidylinositol-linked proteins have impaired ability to vesiculate. *Blood* 81, 510–516.
- Wiedmer, T., Hall, S. E., Ortel, T. L., Kane, W. H., Rosse, W. F., and Sims, P. J. (1993). Complement-induced vesiculation and exposure of membrane prothrombinase sites in platelets of paroxysmal nocturnal hemoglobinuria. *Blood* 82, 1192–1196.
- Willekens, F. L. A., Werre, J. M., Groenen-Döpp, Y. A. M., Roerdinkholder-Stoelwinder, B., De Pauw, B., and Bosman, G. J. C. G. M. (2008). Erythrocyte vesiculation: a self-protective mechanism? *Br. J. Haematol.* 141, 549–556. doi: 10.1111/j.1365-2141.2008.07055.x
- Willekens, F. L. A., Werre, J. M., Kruijt, J. K., Roerdinkholder-Stoelwinder, B., Groenen-Döpp, Y. A. M., Van Den Bos, A. G., et al. (2005). Liver Kupffer cells rapidly remove red blood cell-derived vesicles from the circulation by scavenger receptors. *Blood* 105, 2141–2145. doi: 10.1182/blood-2004-04-1578
- Zolla, L., and D'Alessandro, A. (2012). Shaking hands with the future through omics application in transfusion medicine and clinical biochemistry. *Blood Transfus.* 10, 10–12. doi: 10.2450/2012.001S

**Conflict of Interest Statement:** The authors declare that the research was conducted in the absence of any commercial or financial relationships that could be construed as a potential conflict of interest.

Copyright © 2019 Freitas Leal, Preijers, Brock, Adjobo-Hermans and Bosman. This is an open-access article distributed under the terms of the Creative Commons Attribution License (CC BY). The use, distribution or reproduction in other forums is permitted, provided the original author(s) and the copyright owner(s) are credited and that the original publication in this journal is cited, in accordance with accepted academic practice. No use, distribution or reproduction is permitted which does not comply with these terms.



# Characterization of Two Cases of Congenital Dyserythropoietic Anemia Type I Shed Light on the Uncharacterized C15orf41 Protein

Roberta Russo<sup>1,2\*†</sup>, Roberta Marra<sup>1,2†</sup>, Immacolata Andolfo<sup>1,2</sup>, Gianluca De Rosa<sup>1,2</sup>, Barbara Eleni Rosato<sup>1,2</sup>, Francesco Manna<sup>2</sup>, Antonella Gambale<sup>1,2</sup>, Maddalena Raia<sup>2</sup>, Sule Unal<sup>3</sup>, Susanna Barella<sup>4</sup> and Achille Iolascon<sup>1,2</sup>

<sup>1</sup> Dipartimento di Medicina Molecolare e Biotecnologie Mediche, Università degli Studi di Napoli Federico II, Naples, Italy,

<sup>2</sup> CEINGE Biotecnologie Avanzate, Naples, Italy, <sup>3</sup> Division of Pediatric Hematology, Hacettepe University, Ankara, Turkey,

<sup>4</sup> SSD Talassemie, Anemie Rare e Dismetabolismi del Ferro, Ospedale Pediatrico Microcitemico Antonio Cao, Azienda Ospedaliera Brotzu, Cagliari, Italy

## OPEN ACCESS

### Edited by:

Paola Bianchi,  
IRCCS Ca' Granda Foundation  
Maggiore Policlinico Hospital, Italy

### Reviewed by:

Noemi Roy,  
University of Oxford, United Kingdom  
Theodosia A. Kalfa,  
Cincinnati Children's Hospital Medical  
Center, United States

### \*Correspondence:

Roberta Russo  
roberta.russo@unina.it

<sup>†</sup>These authors have contributed  
equally to this work

### Specialty section:

This article was submitted to  
Red Blood Cell Physiology,  
a section of the journal  
Frontiers in Physiology

Received: 23 November 2018

Accepted: 02 May 2019

Published: 22 May 2019

### Citation:

Russo R, Marra R, Andolfo I,  
De Rosa G, Rosato BE, Manna F,  
Gambale A, Raia M, Unal S, Barella S  
and Iolascon A (2019)  
Characterization of Two Cases  
of Congenital Dyserythropoietic  
Anemia Type I Shed Light on  
the Uncharacterized C15orf41  
Protein. *Front. Physiol.* 10:621.  
doi: 10.3389/fphys.2019.00621

CDA type I is a rare hereditary anemia, characterized by relative reticulocytopenia, and congenital anomalies. It is caused by biallelic mutations in one of the two genes: (i) *CDAN1*, encoding Codanin-1, which is implicated in nucleosome assembly and disassembly; (ii) *C15orf41*, which is predicted to encode a divalent metal ion-dependent restriction endonuclease with a yet unknown function. We described two cases of CDA type I, identifying the novel variant, Y94S, in the DNA binding domain of C15orf41, and the H230P mutation in the nuclease domain of the protein. We first analyzed the gene expression and the localization of C15orf41. We demonstrated that *C15orf41* and *CDAN1* gene expression is tightly correlated, suggesting a shared mechanism of regulation between the two genes. Moreover, we functionally characterized the two variants, establishing that the H230P leads to reduced gene expression and protein level, while Y94S induces a slight decrease of expression. We demonstrated that C15orf41 endogenous protein exhibits nuclear and cytosolic localization, being mostly in the nucleus. However, no altered nuclear-cytosolic compartmentalization of mutated C15orf41 was observed. Both mutants accounted for impaired erythroid differentiation in K562 cells, and H230P mutant also exhibits an increased S-phase of the cell cycle in these cells. Our functional characterization demonstrated that the two variants have different effects on the stability of the mutated mRNA, but both resulted in impaired erythroid maturation, suggesting the block of cell cycle dynamics as a putative pathogenic mechanism for C15orf41-related CDA I.

**Keywords:** CDA (I–III), *C15ORF41*, functional characterization of proteins, genetic testing, anemia

## INTRODUCTION

Congenital dyserythropoietic anemias (CDAs) are hereditary diseases, belonging to the bone marrow (BM) failure syndromes, which embrace a heterogeneous set of rare hereditary anemias that result from impaired erythropoiesis and various kinds of abnormalities during late stages of erythropoiesis (Gambale et al., 2016). Among them, CDA type I (CDA I) is characterized by anemia of variable degree, generally macrocytic, relative reticulocytopenia, and congenital anomalies, such as syndactyly,



chest deformity, and short stature. The original classification system for CDAs was based on specific erythroblasts morphological abnormalities on BM light microscopy (Roy and Babbs, 2019). The morphological pathognomonic feature of CDA I is the presence of thin chromatin bridges between the nuclei pairs of erythroblasts. On electron microscopy, heterochromatin is denser than normal, and forms demarcated clumps with small translucent vacuoles, giving rise to the metaphor of “Swiss cheese appearance” (Kellermann et al., 2010; Roy and Babbs, 2019).

CDA I is inherited as an autosomal recessive disorder caused by mutations in two different loci, *CDAN1* and *C15orf41*, which account for the 90% of CDA I cases. *CDAN1* (chr15q15.2) was the first gene in which pathogenic variants causative of CDA type I (OMIM # 224120) were identified (Dgany et al., 2002). It encodes a ubiquitously expressed and cell-cycle regulated protein, Codanin-1 (Noy-Lotan et al., 2009), which acts in nucleosome assembly and disassembly through the formation of the cytosolic Asf1-H3-H4-importin-4 complex. Codanin-1 binds directly to Asf1 via a conserved B-domain, implying a mutually exclusive interaction with the chromatin assembly factor 1 (CAF-1) and HIRA. Previous studies on osteosarcoma U-2-OS cells silenced for Codanin-1 showed accelerated DNA replication rate and increased levels of chromatin-bound Asf1, suggesting that Codanin-1 guards a limiting step in chromatin replication (Ask et al., 2012). More recently, *C15orf41* (chr15q14) was discovered as the second locus associated with CDA I (OMIM # 615631). It is an uncharacterized gene that is predicted to encode a divalent metal-ion dependent restriction endonuclease with homology to the Holliday junction resolvases (Babbs et al., 2013). It was suggested that *C15orf41*-encoded protein, similarly to Codanin-1, interacts with Asf1b (Ewing et al., 2007), supporting the hypothesis that both *C15orf41* and Codanin-1 could interplay during DNA replication and chromatin assembly (Gambale et al., 2016).

To date, only five *C15orf41* variants have been reported (Babbs et al., 2013; Palmblad et al., 2018; Russo et al., 2018). We herein described two cases of *C15orf41*-CDA I carrying the aminoacidic substitutions p.Tyr94Ser and p.His230Pro that are located in the two different domains of the *C15orf41* protein. Our functional characterization demonstrated that the two variants have different effects on the stability of the mutated mRNA. However, both mutations account for impaired erythroid maturation. This study improves the current understanding of the role of this uncharacterized protein in both the physiological conditions and the pathogenic mechanism of the disease.

## MATERIALS AND METHODS

### Patients and Genetic Testing

The diagnosis of CDA I was based on history, clinical findings, laboratory data, morphological analysis of both peripheral blood and marrow smears, and genetic testing.

Local university ethical committees approved both the DNA sampling and the collection of patients' data

from Medical Genetics Ambulatory in Naples (University Federico II, DAIMedLab).

Written informed consent was obtained from the patients for the participation in the study and the publication of the case report.

Genomic DNA preparation and mutational screening for *CDAN1*, *SEC23B*, and *C15orf41* genes by direct sequencing were performed as previously described (Russo et al., 2013). High-throughput sequencing by the custom multi-gene panel for hereditary anemias was performed as described (Russo et al., 2018).

The pathogenicity of the novel exonic variants has been evaluated by InterVar, a bioinformatics software tool for clinical interpretation of genetic variants based on the ACMG/AMP 2015 guideline<sup>1</sup>. Mainly, the pathogenicity of each variant was assessed by gathering evidence from various sources: population data, computational and predictive data, functional data, localization of the variant in a mutational hotspot and critical and well-established functional domain, and segregation data (Richards et al., 2015; Russo et al., 2018).

### Cloning and Site Direct Mutagenesis

cDNA encoding full-length wild-type (WT) *C15orf41* sequence was cloned in the pCMV-Tag1 vector for mammalian cell expression (Invitrogen) in the BglII and XhoI sites, to obtain an N-terminal tagged protein with FLAG. The point mutations c.281A > C, p.Tyr94Ser (Y94S) and c.689A > C, p.His230Pro (H230P) were introduced into the pCMV-Tag1 vector by using a QuikChange site-directed mutagenesis kit (Stratagene) (Russo et al., 2017). The coding sequence was sequenced after mutagenesis.

### Cell Cultures, Transfections, and Stable Clones Production

Hek-293, HepG2, HuH7, MG-63, HEL, and K562 cells were obtained from American Type Culture Collection (ATCC, Manassas, VA, United States). Cells were maintained in Dulbecco's modified Eagle medium (DMEM) (Invitrogen) or RPMI 1640 medium (Invitrogen) supplemented with 10% fetal bovine serum (Invitrogen), 100 U/mL penicillin (Invitrogen), and 100 mg/mL streptomycin (Invitrogen) in a humidified 5% CO<sub>2</sub> atmosphere at 37°C, according to the manufacturer's instructions. Hek-293 cells (400 × 10<sup>3</sup>) were transfected with pCMV-Tag1-*C15orf41* plasmids (2.5 µg/well) using the DNA Transfection Reagent (TransFectin Lipid Reagent, Bio-Rad) according to the manufacturer's procedures. Cells were collected 16, 24, and 48 h after the transfection to perform RNA and protein extractions. For generating K562 stably over-expressing *C15ORF41* gene, 10<sup>6</sup> cells were transfected with pCMV-Tag1-*C15orf41* plasmids using Hily Max DNA Transfection Reagent (Dojindo Laboratories). After 48 h, G418 (0.6 mg/mL) was added as a selection marker. Clones were generated according to the limiting dilution method (see **Supplementary Material** for further details).

<sup>1</sup><http://wintervar.wglab.org/>

## Erythroid Differentiation and Flow Cytometry

Erythroid differentiation of K562-*C15orf41* stable clones ( $2 \times 10^5$ /mL) was performed adding 50  $\mu$ M hemin (Sigma) to the culture medium, after 24 h of starvation (Andolfo et al., 2010). Cells were collected before hemin addition (0 days) and two days after hemin addition (2 days). For cell cycle analysis, K562 stable clones were harvested by centrifugation, resuspended in PBS containing 3.75% Nonidet P-40, 100  $\mu$ g/ml RNase A and 40  $\mu$ g/ml propidium iodide, and incubated at room temperature for 3 h in the dark. The cell antigen profile was analyzed by flow cytometry through evaluation of CD71 (proerythroblasts) and CD235a (proerythroblasts and orthochromatic erythroblasts). Samples were analyzed on a FACS flow cytometer (Becton Dickinson Immunocytometry Systems, BDIS).

## Gene Expression Analysis

Total RNA was extracted either from peripheral blood leukocytes (PBLs), reticulocytes and from cell lines using TRIzol reagent (Life Technologies). Synthesis of cDNA from total RNA (2  $\mu$ g) was performed using SensiFAST™ cDNA Synthesis Kit (Bioline). Quantitative RT-PCR (qRT-PCR) using Power SYBR Green PCR Master Mix (Applied Biosystems) was performed on Applied Biosystems 7900HT Sequence Detection System using standard cycling conditions.  $\beta$ -actin was used as internal control, while the *Neomycin* resistance gene was used as a control of transfection efficiency for K562 stable clones. Relative gene expression was calculated by using the  $2^{-\Delta C_t}$  method, as described (Russo et al., 2013).

## Subcellular Fractionation and Western Blotting

Proteins were extracted from cell lines using RIPA lysis buffer containing protease inhibitor cocktail (1 $\times$ ). Subcellular fractionation in nuclear and cytoplasmic proteins was performed using NE-PER™ Nuclear and Cytoplasmic Extraction Reagents (Thermo Fisher Scientific™). Equal amounts of protein from each lysate, as determined by a Bradford assay, were subjected to 12% sodium dodecyl sulfate-polyacrylamide gel electrophoresis (SDS-PAGE), and blotted onto polyvinylidene difluoride membranes (Biorad). Detection was performed with mouse anti-FLAG antibody (1:1000) (Sigma-Aldrich) and rabbit anti-C15orf41 (1:500) (Atlas Antibodies HPA061023). Since this antibody was recommended for immunofluorescence (IF) we tested its specificity for western blotting (WB) by using C15orf41 over-expression cells as a positive control (Bordeaux et al., 2010) (Supplementary Figure S1).

Mouse anti-TBP (TATA Binding Protein) (1:1000) (Sigma-Aldrich) and mouse anti- $\alpha$ -TUBULIN (1:5000) (Abcam) were used as a control for equal loading for cytosolic and nuclear proteins' extracts, respectively. Mouse anti- $\beta$ -actin (1:12000) (Sigma-Aldrich) was used as a loading control for total proteins' extracts. Labeled bands were visualized and densitometric analysis performed with the BioRad Chemidoc using Quantity One software (BioRad) to obtain an integrated optical density (OD) value.

## Immunofluorescence Analysis

For IF analysis  $3 \times 10^5$  cells were fixed for 10 min in 4% Paraformaldehyde (PFA, Sigma) and washed in 50 mM PBS/NH<sub>4</sub>Cl (Sigma-Aldrich, Milan, Italy). After washing in PBS 1 $\times$ , cells were allowed on 35 mm IBIDI  $\mu$ -Dishes (Ibidi GmbH, Martinsried, Germany) coated with 0.05% poly-L-lysine (Sigma-Aldrich, Milan, Italy) to adhere. Permeabilization was performed with 0.2% Triton/PBS, followed by blocking with 1% BSA/PBS. The seeded cells were immunologically stained with rabbit anti-C15orf41 antibody (1:25) (Atlas Antibodies HPA061023), mouse anti-NUCLEOPHOSMIN (1:200), and secondary antibodies (1:200) (Alexa Fluor 546 anti-rabbit, Life Technologies and Alexa Fluor 488 anti-mouse). Nuclei were stained with 1  $\mu$ g/ml DRAQ5 in PBS for 15 min at room temperature. Cells were preserved in PBS 1 $\times$  and imaged using a LEICA TCS SP8 meta confocal microscope, equipped with an oil immersion plan Apochromat 63 $\times$  objective 1.4 NA. The following settings were used: Green channel excitation of Alexa488 by the argon laser 488 nm line was detected with the 505–550 nm emission bandpass filter. Red channel excitation of Alexa546 by the Helium/Neon laser 543 nm line was detected with the 560–700 nm emission bandpass filter (using the Meta monochromator). Blue channel excitation of DRAQ5 by the blue diode laser 647 nm and emission bandpass filter.

## Statistical Analysis

Statistical significance of differences in protein and gene expression was determined using the Mann–Whitney test or Student's *t*-test. Correlation analysis of *C15orf41* with *CDAN1* gene expression was performed by Pearson correlation test. A two-sided *p*-value < 0.05 was considered statistically significant.

For the *in silico* correlation analysis between *C15orf41* and *CDAN1* gene expression in normal hematopoietic cell subpopulations we used the dataset “Normal Hematopoietic Subgroups – (GEO ID: gse19599),” stored in the R2: Genomics Analysis and Visualization Platform<sup>2</sup>, a biologist-friendly, web-based genomics analysis, and visualization application.

## RESULTS

### Clinical Cases and Genetic Testing

Clinical features and genetic data of the two probands are summarized in **Table 1**. Case 1 (A-II.2) was a 7-years-old female, second child from healthy non-consanguineous parents of Italian origin (Sardinia). At birth, cholestatic hepatopathy, dysmorphic features (bilateral syndactyly of the IV–V toes), and severe anemia (Hb 5.5 gr/dl) were observed. Family history was not indicative of anemia. At diagnosis, the proband presented transfusion-dependent normocytic anemia with a blood transfusion frequency every 15–20 days, and low reticulocyte count (**Table 1**). BM analysis showed: erythroid hyperplasia with 6% of cells showing megaloblastic features, nuclear abnormalities, and nuclear/cytoplasmic maturation

<sup>2</sup><http://r2.amc.nl>

**TABLE 1** | Clinical features of the two patients enrolled in the study.

|  | Case 1 (A-II.2)                 | Case 2 (B-II.1)*                  | Reference range <sup>‡</sup> |
|--|---------------------------------|-----------------------------------|------------------------------|
| Age at diagnosis                                     | 7 years                         | 2.4 years                         | –                            |
| Distal limb anomalies/ other features                | Toes syndactyly                 | Thoracic dysplasia; short limbs   | –                            |
| <b>Complete blood count</b>                          |                                 |                                   |                              |
| RBC ( $\times 10^6/\mu\text{L}$ )                    | 2.72                            | 3.67                              | 3.9–5.6                      |
| Hb (g/dL)  | 7.8                             | 10.6                              | 11.0–16.0                    |
| Hct (%)  | 22.2                            | 31.4                              | 33.0–45.0                    |
| MCV (fL)   | 81.6                            | 85.4                              | 70.0–91.0                    |
| MCH (pg)   | 20.2                            | 28.8                              | 23.0–33.0                    |
| MCHC (g/dL)  | 24.8                            | 33.8                              | 23.0–33.0                    |
| Retics %   | 5.8                             | 1.0                               | 0.5–2.0                      |
| Retics count ( $\times 10^3/\mu\text{L}$ )           | 158000                          | 36700                             | –                            |
| PLT ( $\times 10^3/\mu\text{L}$ )                    | –                               | 518.0                             | 150.0–450.0                  |
| <b>Biochemical, laboratory data and iron balance</b> |                                 |                                   |                              |
| Total bilirubin (mg/dL)                              | 1.90                            | 1.46                              | 0.2–1.2                      |
| LDH (U/L)  | 779                             | 511                               | 125.0–243.0                  |
| Ferritin (ng/mL)                                     | 825                             | 1512                              | 22.0–275.0                   |
| TSAT (%)   | 75                              | 89                                | 15.0–45.0                    |
| <b>C15ORF41 variants</b>                             |                                 |                                   |                              |
| HGVS (Coding) <sup>a</sup>                           | c.281A > C                      | c.689A > C                        | –                            |
| HGVS (Protein) <sup>b</sup>                          | p.Tyr94Ser                      | p.His230Pro                       | –                            |
| RefSeq ID  | rs587777101                     | –                                 | –                            |
| MAF  | C = 0.00001                     | –                                 | –                            |
| InterVar (evidence codes) <sup>§</sup>               | Pathogenic (PS1, PS3, PM2, PP4) | Likely pathogenic (PS3, PM2, PP4) | –                            |

\*Patient RP0\_39 described in Russo et al. (2018); <sup>‡</sup>Reference ranges from AOU Federico II, University of Naples, Italy; <sup>a</sup>NM\_001130010; <sup>b</sup>NP\_001123482; <sup>§</sup> InterVar evidence scores by the website <http://wintervar.wglab.org/evds.php>; PS1, same amino acid change as an established pathogenic variant; PS3, well-established functional studies show a deleterious effect; PM2, absent (or at an extremely low frequency if recessive) in population databases; PP4, patient's phenotype is highly specific for a single gene etiology; TSAT, transferrin saturation; MAF, minor allele frequency.

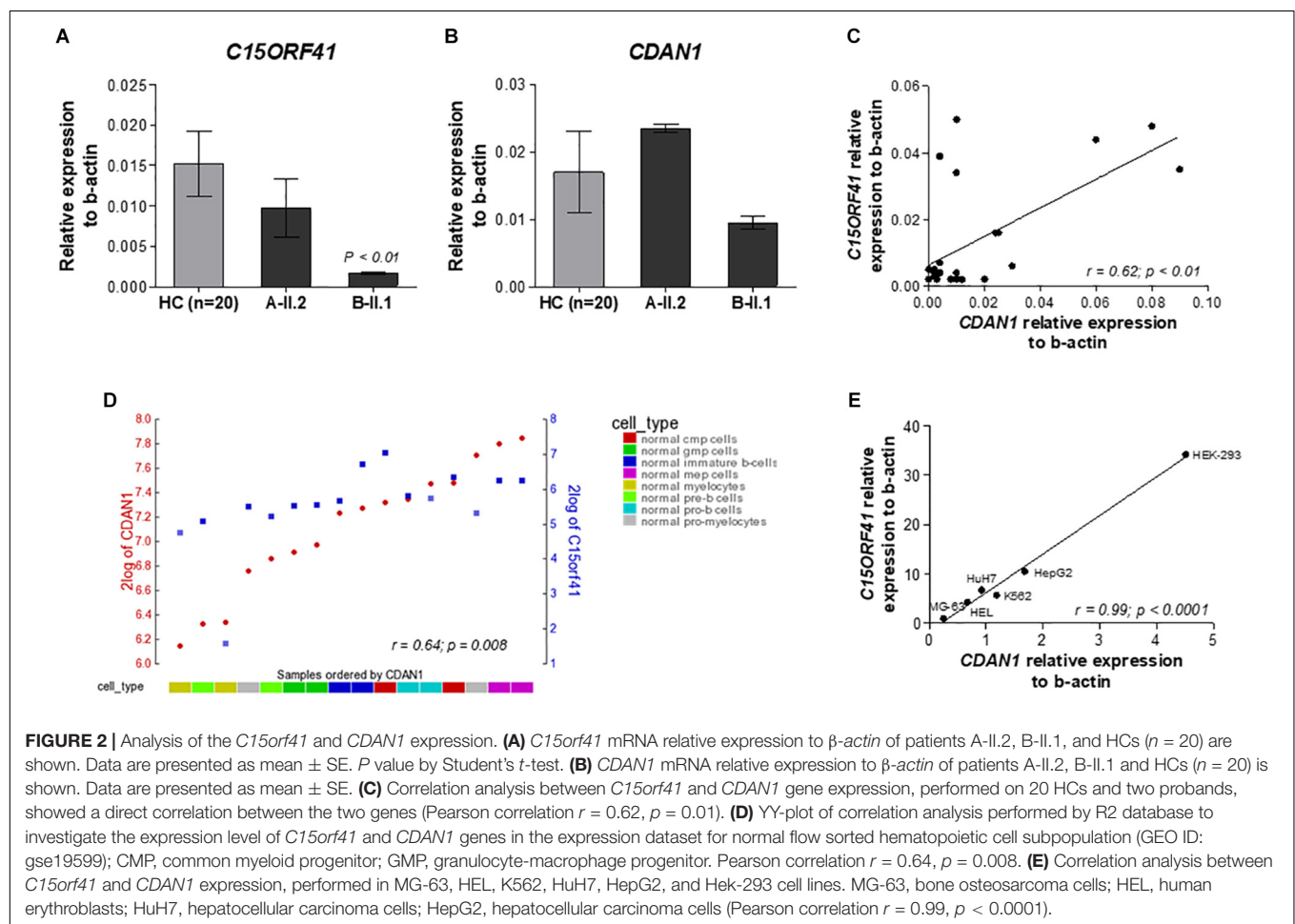
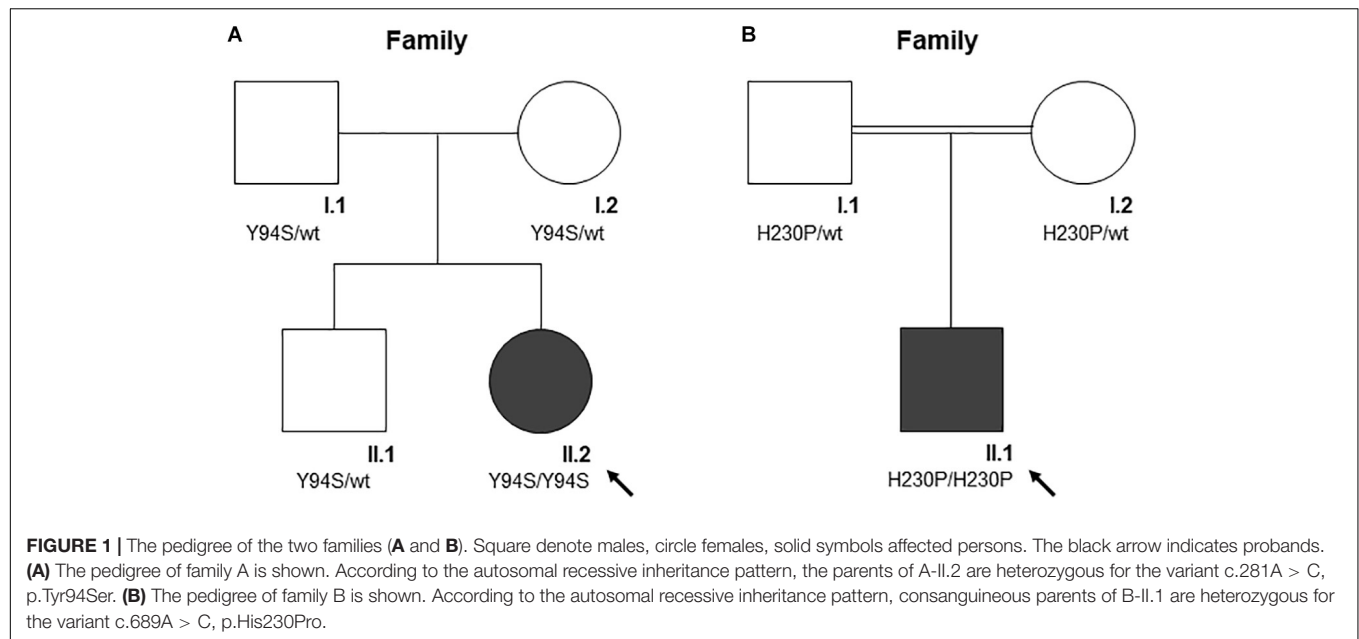
asynchrony; 4% of erythroblasts were bi- and tri-nucleated; the granulopoietic/erythropoietic ratio (G:E) = 0.53. A substantial percentage of erythroblasts showed inter-nuclear bridges (5%), a typical feature of CDA I. Accordingly, genetic testing for *CDAN1* was performed, but no causative variants were identified. Conversely, when we analyzed *C15orf41* gene, we observed the presence of the transversion c.281A > C in the homozygous state, resulting in a novel aminoacidic substitution p.Tyr94Ser (Y94S). It is an ultra-rare variant (rs587777101) with a minor allele frequency (MAF) C = 0.00001 in the ExAC database. In agreement with the recessive inheritance pattern, both parents were heterozygous (Figure 1A).

Case 2 was a 2.4-years-old male, born from 3rd degree consanguineous parents of Turkish origin. At birth, recurrent pneumonia, thoracic dysplasia, and short limbs were observed. Family history was negative for anemia or jaundice. The proband presented transfusion-dependent normocytic anemia (12 transfusions/year), low reticulocyte count, growth retardation, and increased ferritin level, suggesting an iron loading condition (Table 1). No splenomegaly was observed at physical examination and abdominal echography. BM analysis showed severe megaloblastic changes and normoblasts with double or multiple nuclei, a morphological feature suggestive of CDA II. Accordingly, we firstly performed Sanger sequencing analysis for CDA II-disease gene *SEC23B*, finding no causative variants. Then, as a second-step analysis, we enrolled the patient

in our multi-gene panel for hereditary anemias, identifying the transversion c.689A > C in *C15orf41* in the homozygous state, resulting in the amino acid substitution p.His230Pro (H230P), as reported (Russo et al., 2018). In agreement with the recessive inheritance pattern, both parents were heterozygous (Figure 1B).

### **C15orf41 and CDAN1 Gene Expression Are Directly Correlated**

To evaluate the effect of the two identified mutations on *C15orf41* gene expression, we initially analyzed *C15orf41* expression in PBLs isolated from the two probands and healthy controls (HCs). To note, *C15orf41* is a ubiquitous gene, showing a comparable level of expression in both PBLs and reticulocytes (Supplementary Figure S2). No difference in gene expression levels of the proband A-II.2 compared to those detected in HCs was observed, suggesting that Y94S variant does not affect gene expression. Conversely, we found a marked down-regulation of *C15orf41*-H230P in the second proband B-II.1 (Figure 2A). Likewise, we saw a similar trend of *CDAN1* expression in the two patients. Notably, the proband A-II.2 did not show any alterations of *CDAN1* expression compared to those seen in HCs, while the B-II.1 proband revealed a decrease of *CDAN1* expression level, although not statistically significant (Figure 2B). Of note, a direct correlation between *C15orf41* and *CDAN1* expression genes in healthy subjects was observed ( $r = 0.62$ ,  $p = 0.0006$ ) (Figure 2C). We confirmed





the *ex vivo* data on *C15orf41*-*CDAN1* correlation by *in silico* analysis of the expression dataset for normal hematopoietic cell subpopulations, obtained by R2 database (Figure 2D). Additionally, we achieved comparable results by gene expression profiling of different human cell lines (Hek-293, HepG2, HuH7, MG-63, HEL, and K562 cells), where a significant direct correlation between *C15orf41* and *CDAN1* expression was observed (Figure 2E).

## C15orf41 Localization Into Nuclear and Cytosolic Compartments

We first assessed the turnover and localization of the *C15orf41* protein in Hek293 cells transiently transfected with pCMV-tag1-*C15orf41*. Time-course analysis showed a gradual increase of *C15orf41* gene expression in cells transfected with WT clone at 16, 24, and 48 h compared to those transfected with empty vector (EV) (Figure 3A). Conversely, WB analysis on the same harvested cells revealed a marked increase of *C15orf41* protein level at 16 h after transfection, with a progressive decrease of the *C15orf41*-FLAG signal, which resulted highly down-regulated at 48 h after the transfection (Figure 3B).

To investigate *C15orf41* localization, we assessed the endogenous protein levels and localization of the protein by both WB and IF on a nuclear and a cytosolic fraction of Hek-293 cells (Figures 3C,D). Both analyses confirmed that the protein was mainly expressed in the nucleus, but also in the cytosol compartment, even if in a smaller amount, suggesting a role of the protein in these two cellular compartments (Figure 3D and Supplementary Figure S3). No co-localization of *C15orf41* with nucleoli was observed (Supplementary Figure S3).

## Characterization of C15orf41-H230P and -Y94S Mutants

To study *in vitro* the pathogenetic effect of the two variants, we evaluated gene expression and protein level of both *C15orf41*-H230P and *C15orf41*-Y94S mutants at 16 h after transfection in Hek-293. In agreement with the *ex vivo* data on both patients, we observed a sharp decrease of both gene expression and protein levels in cells over-expressing *C15orf41*-H230P mutant compared to *C15orf41*-WT ones (Figures 4A,B and Supplementary Figure S1). Conversely, only a slight reduction in gene expression and protein level in cells over-expressing *C15orf41*-Y94S was observed (Figures 4A,B and Supplementary Figure S1).

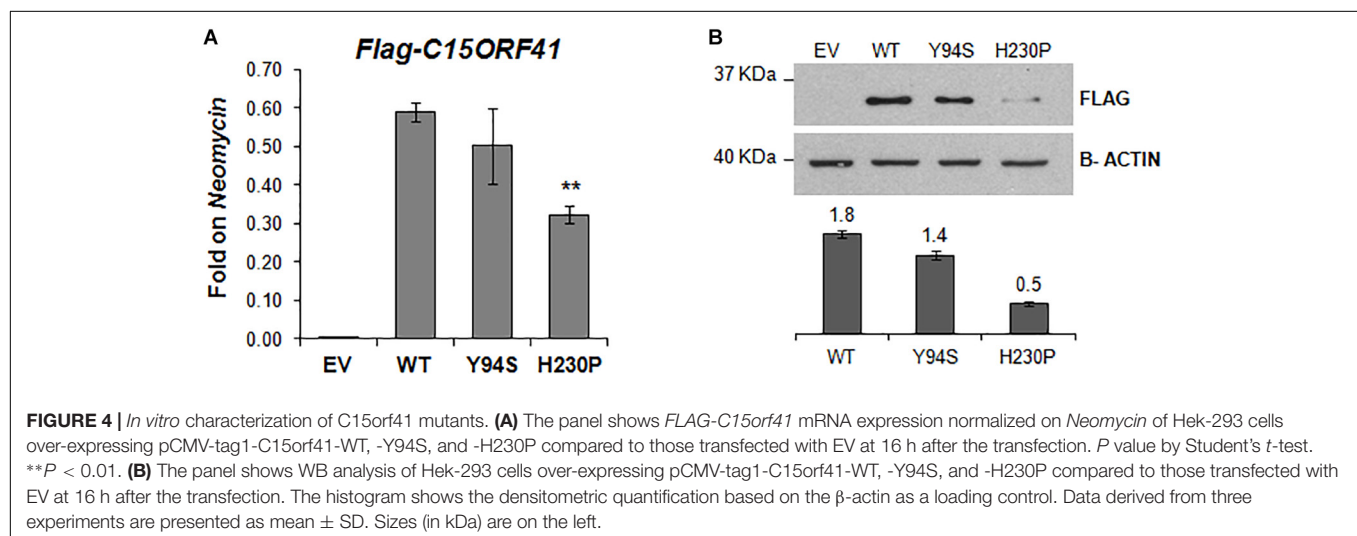
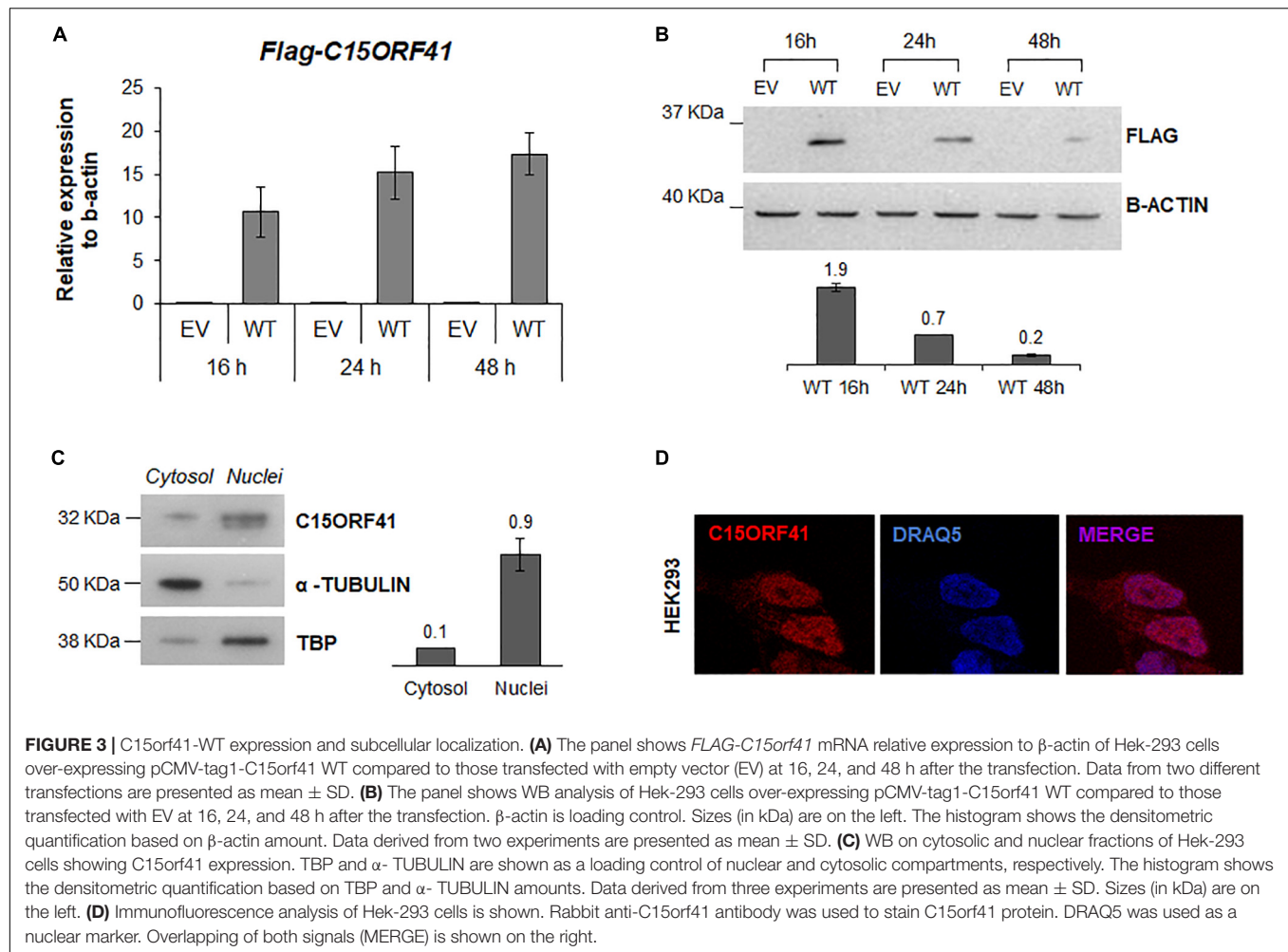
To obtain a reliable cellular model, able to be induced to erythroid differentiation, we developed K562 cells stably over-expressing *C15orf41*-WT and both mutants. Over-expressing clones were selected by measuring *Neomycin* relative gene expression in each K562 clone and comparing the digestion pattern of mutant vs. WT clones (Supplementary Figure S4). K562 selected clones WT#3 and Y94S#5 showed strong over-expression of *C15orf41* compared to those observed in K562 EV#3 clone. Instead, H230P#10 cells showed a marked gene down-regulation respect to WT#3 cells (Figure 5A). WB analysis confirmed the same trend for all the clones (Figure 5B).

To investigate if both mutants could affect erythroid differentiation, we treated K562 cells with hemin. Evaluation of CD71 and CD235 differentiation markers showed a statistically significant decreased percentage of CD71<sup>+</sup>/CD235<sup>+</sup> cells in both Y94S and H230P clones compared to the WT one (Figure 5C). Moreover, we observed a slight increase of the rate of S-phase at cell cycle analysis in K562 cells over-expressing Y94S and H230P mutants compared to WT, although not statistically significant (Figure 5D and Supplementary Figure S5). To note, immunolocalization analysis of *C15orf41* protein in K562 stable clones highlighted a preferential localization of the mutated proteins within nuclear compartment compared to WT one, similarly to those observed in Hek-293 cells transiently over-expressing *C15orf41* mutants (Figure 5E).

## DISCUSSION

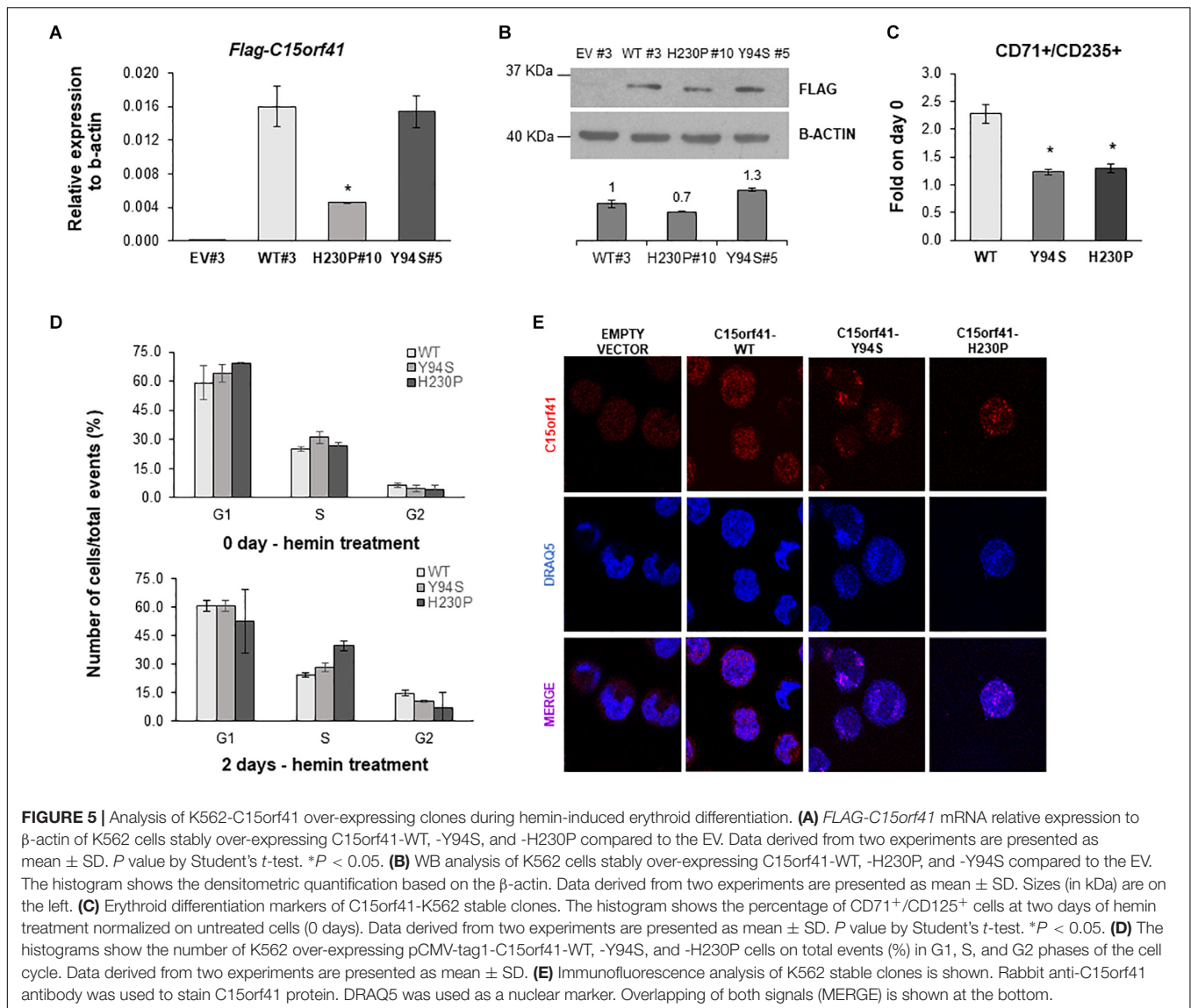
CDA type I is an autosomal recessive disorder that belongs to the heterogeneous group of inherited BM failure syndromes. To date, two causative genes have been associated to this condition: *CDAN1* that is the most frequently mutated; *C15orf41* that has been found mutated in five unrelated patients, so far (Babbs et al., 2013; Palmblad et al., 2018; Russo et al., 2018). Most of the CDA I patients exhibit lifelong macrocytic anemia with variable values of Hb. *C15orf41* patients show clinical features like *CDAN1* ones. Anyhow, a slight difference in Hb level and MCV value has been observed between the two subgroups of patients (Gambale et al., 2016).

We herein described two unrelated cases of *C15orf41*-related CDA I. Both patients presented clinical characteristics, hematological status, and morphological features of erythroblasts compatible with a suspicion of CDA I. Particularly, the presence of a substantial amount of inter-nuclear bridges between erythroblasts, a typical feature of CDA I, at the BM analysis of the case 1 (A-II.2), prompted us to perform the molecular screening of both CDA I causative genes. No causative variants in *CDAN1* were identified, while genetic testing of *C15orf41* highlighted the presence of the homozygous missense mutation Y94S. This variant resulted annotated on public databases as ultra-rare single nucleotide variant. Of note, it is a novel missense change at an amino acid residue where a different pathogenic missense change, Y94C, has been previously described (Babbs et al., 2013). Case 2 (B-II.1) was initially suspected of suffering from CDA type II, since he presented normocytic anemia and non-specific morphological erythroblast features, such as the presence of bi- and multi-nuclearity, megaloblastic changes, but no inter-nuclear bridges. Of note, among syndromes showing dyserythropoiesis, there is not a full concordance between experienced hematologists in recognition of these features (Goasguen et al., 2018). Indeed, accurate molecular screening remains the most reliable diagnosis for these patients. First genetic testing for *SEC23B* revealed no mutations in this gene. Thus, the patient was analyzed by a t-NGS panel for red blood cell disorders, that allowed us the identification of the homozygous missense variant H230P in the *C15orf41* gene (Russo et al., 2018).



To investigate the expression and subcellular localization of C15orf41, we expressed the full-length WT protein fused to a FLAG-tag. Time-course analysis evidenced an indirect correlation between gene expression and protein levels,

suggesting a rapid turnover of the protein. It was recently found that C15orf41 has at least three post-translational modification sites, such as K50 (Acetylation), T114 (Phosphorylation) and K176 (Ubiquitination) (Ahmed et al., 2018). Since



that ubiquitination is one of the most common signals for proteasome-mediated degradation (Hershko and Ciechanover, 1998), we speculated that C15orf41 is degraded via proteasome during the cell cycle. Moreover, this data is corroborated by the fact that it could be a cell cycle-regulated protein, as well as Codanin-1 (Noy-Lotan et al., 2009), and that the two proteins could interact. Our *ex vivo* and *in vitro* analyses demonstrated that *C15orf41* and *CDAN1* gene expression levels were directly correlated in patients, healthy controls, and different cell lines. Of note, Codanin-1 was proved to be part of the cytosolic Asf1-H3-H4-importin-4 complex, which is implicated in nucleosome assembly and disassembly (Ask et al., 2012).

Similarly, C15orf41 was predicted to interact with Asf1b (Ewing et al., 2007). These data suggested that both proteins are needed together to accomplish their function, thus could be regulated by the same mechanism, could control each other

in a positive feedback loop, or could interact with each other. To note, *CDAN1* and *C15orf41* are ubiquitously expressed genes, but their alterations mainly affect the erythroid lineage. One possible explanation may be that erythroid progenitors have a uniquely fast cell cycle, although CDA patients do not manifest abnormalities of other tissues containing fast-dividing cell types, such as gut epithelium or hair follicles. Other hypotheses include nuclear extrusion in erythroblasts, which requires the eviction of histones, such as H3 and H4, and C15orf41 and Codanin-1 may play a role in this process (Roy and Babbs, 2019).

The analysis of cytosolic and nuclear fractions demonstrated that C15orf41 endogenous protein exhibits mainly nuclear localization. Accordingly, nuclear localization signals and nuclear export signals were predicted in the amino acid sequence, confirming that the protein is exported from the nucleus to the cytoplasm and vice-versa. Once again, changes in C15orf41

nuclear-cytoplasmic localization could represent a mechanism, or the effect, of its regulation. According to the predicted Holliday junction resolvase function of C15ORF41 and its potential role in DNA repair machinery as guardians of genome integrity and viability, we initially hypothesized that C15orf41 could localize in the nucleoli. Indeed, it was recently demonstrated that the nucleolus, long regarded as a mere ribosome producing factory, plays a crucial role in monitoring and responding to cellular stress, as well as in DNA repair mechanisms (Mayer and Grummt, 2005; Ogawa and Baserga, 2017). However, our immunolocalization data did not support this hypothesis.

We further characterized the identified variants by both *ex vivo* and *in vitro* functional analyses. The two mutations showed different behavior. Indeed, the Y94S variation did not affect gene expression, and only slightly decreased the protein level. On the contrary, the H230P mutation induced a sharp decrease in gene expression and protein level.

Of note, Y94S variant is located in the two turn-helix-turn DNA binding domains (DBD) of the protein, together with the previously identified Y94C and P20R mutations (Babbs et al., 2013; Palmblad et al., 2018). On the contrary, H230P variant is located in the PD-(D/E) XK nuclease domain, as well as the two causative mutations L178Q and Y238C (Babbs et al., 2013; Palmblad et al., 2018). Therefore, we might assume that these variants could have a different effect on both the protein function and the pathogenetic mechanism of the disease.

Since no impaired expression of C15orf41-Y94S was observed, we speculate that this mutation could affect the three-dimensional structure of the protein and, thus, undermine the binding to the DNA.

Since CDA I mutated proteins affect mainly the erythroid lineage, we developed K562 cells stably over-expressing C15orf41 WT and mutants to induce erythroid differentiation. This cellular model allowed us to demonstrate that both mutant clones showed impaired erythroid differentiation, exhibiting a decreased percentage of CD71<sup>+</sup>/CD235<sup>+</sup> cells at two days of hemin treatment. Moreover, both Y94S and H230P clones were retained in the S phase of the cell cycle during differentiation, although with a different degree. It has been already demonstrated that there is an interdependence between S-phase progression and an essential commitment step during erythroid differentiation in which, within few hours, cells become dependent on the hormone erythropoietin, undergo activating changes in chromatin of red cell genes, and activate GATA-1, the erythroid master transcriptional regulator. Arresting S-phase progression at this time prevents the execution of this commitment step and subsequent induction of red cell genes (Pop et al., 2010). Of note, CDAN1-CDA Ia cultured erythroblasts showed an increase in S-phase cells, suggesting a cell cycle arrest (Tamary et al., 1996).

Nevertheless, based on the present data, we are not able to establish if the increased number of cells in S-phase represents faster cycling cells or a block in S-phase.

This study represents the first investigation of both the expression and the localization of C15orf41. Our *ex vivo* and *in vitro* analyses demonstrated that C15orf41 and CDAN1 are tightly correlated, suggesting a shared mechanism of regulation between the two genes and related proteins. The different behavior of both Y94S-DBD-mutation and H230P-PD-(D/E) XK-mutation could be related to the dual function of the C15orf41 protein within separate subcellular compartments. Nevertheless, both variants resulted in impaired erythroid maturation, suggesting the block of cell cycle dynamics as a putative pathogenic mechanism for C15orf41-related CDA I.

## ETHICS STATEMENT

Ethical Committee University Federico II of Naples, n. 252/18.

## AUTHOR CONTRIBUTIONS

RR, RM, and IA designed and conducted the study, and prepared the manuscript. AI critically reviewed the study. GDR and BR collaborated to the generation of cellular models. FM performed Sanger sequencing and t-NGS. MR performed flow cytometry analyses. SU, SB, and AG cared for the patients.

## FUNDING

This work was supported by grants from the Italian Ministry of University and Research (SIR to RR, RBSI144KXC); by Regione Campania CUP B63D18000350007; by Spanish foundation “Ramón Areces” (CoDysAn project to AI).

## ACKNOWLEDGMENTS

We thank Alessia Romano of the CEINGE Advanced Light Microscopy Facility for expert help in data acquisition.

## SUPPLEMENTARY MATERIAL

The Supplementary Material for this article can be found online at: <https://www.frontiersin.org/articles/10.3389/fphys.2019.00621/full#supplementary-material>

## REFERENCES

- Ahmed, M. S., Shahjaman, M., Kabir, E., and Kamruzzaman, M. (2018). Structure modeling to function prediction of uncharacterized human protein C15orf41. *Bioinformation* 14, 206–212. doi: 10.6026/97320630014206
- Andolfo, I., De Falco, L., Asci, R., Russo, R., Colucci, S., Gorrese, M., et al. (2010). Regulation of divalent metal transporter 1 (DMT1) non-IRE isoform by the microRNA Let-7d in erythroid cells. *Haematologica* 95, 1244–1252. doi: 10.3324/haematol.2009.020685
- Ask, K., Jasencakova, Z., Menard, P., Feng, Y., Almouzni, G., Groth, A., et al. (2012). Codanin-1, mutated in the anaemic disease CDAI, regulates Asf1 function in S-phase histone supply. *EMBO J.* 31, 2013–2023. doi: 10.1038/emboj.2012.55
- Babbs, C., Roberts, N. A., Sanchez-Pulido, L., McGowan, S. J., Ahmed, M. R., Brown, J. M., et al. (2013). Homozygous mutations in a predicted endonuclease



- are a novel cause of congenital dyserythropoietic anemia type I. *Haematologica* 98, 1383–1387. doi: 10.3324/haematol.2013.089490
- Bordeaux, J., Welsh, A., Agarwal, S., Killiam, E., Baquero, M., Hanna, J., et al. (2010). Antibody validation. *Biotechniques* 48, 197–209. doi: 10.2144/000113382
- Dgany, O., Avidan, N., Delaunay, J., Krasnov, T., Shalmon, L., Shalev, H., et al. (2002). Congenital dyserythropoietic anemia type I is caused by mutations in codanin-1. *Am. J. Hum. Genet.* 71, 1467–1474. doi: 10.1086/344781
- Ewing, R. M., Chu, P., Elisma, F., Li, H., Taylor, P., Climie, S., et al. (2007). Large-scale mapping of human protein-protein interactions by mass spectrometry. *Mol. Syst. Biol.* 3:89. doi: 10.1038/msb4100134
- Gambale, A., Iolascon, A., Andolfo, I., and Russo, R. (2016). Diagnosis and management of congenital dyserythropoietic anemias. *Expert Rev. Hematol.* 9, 283–296. doi: 10.1586/17474086.2016.1131608
- Goasguen, J. E., Bennett, J. M., Bain, B. J., Brunning, R., Vallespi, M. T., Tomonaga, M., et al. (2018). Dyserythropoiesis in the diagnosis of the myelodysplastic syndromes and other myeloid neoplasms: problem areas. *Br. J. Haematol.* 182, 526–533. doi: 10.1111/bjh.15435
- Hershko, A., and Ciechanover, A. (1998). The ubiquitin system. *Annu. Rev. Biochem.* 67, 425–479. doi: 10.1146/annurev.biochem.67.1.425
- Kellermann, K., Neuschwander, N., Högel, J., and Schwarz, K. (2010). The morphological diagnosis of congenital dyserythropoietic anemia: results of a quantitative analysis of peripheral blood and bone marrow cells. *Haematologica* 95, 1034–1036. doi: 10.3324/haematol.2009.014563
- Mayer, C., and Grummt, I. (2005). Cellular stress and nucleolar function. *Cell Cycle* 4, 1036–1038. doi: 10.4161/cc.4.8.1925
- Noy-Lotan, S., Dgany, O., Lahmi, R., Marcoux, N., Krasnov, T., Yissachar, N., et al. (2009). Codanin-1, the protein encoded by the gene mutated in congenital dyserythropoietic anemia type I (CDAN1), is cell cycle-regulated. *Haematologica* 94, 629–637. doi: 10.3324/haematol.2008.003327
- Ogawa, L. M., and Baserga, S. J. (2017). Crosstalk between the nucleolus and the DNA damage response. *Mol. Biosyst.* 13, 443–455. doi: 10.1039/c6mb00740f
- Palmblad, J., Sander, B., Bain, B., Klimkowska, M., and Björck, E. (2018). Congenital dyserythropoietic anemia type 1: a case with novel compound heterozygous mutations in the *C15orf41* gene. *Am. J. Hematol.* doi: 10.1002/ajh.25157 [Epub ahead of print].
- Pop, R., Shearstone, J. R., Shen, Q., Liu, Y., Hallstrom, K., Koulis, M., et al. (2010). A key commitment step in erythropoiesis is synchronized with the cell cycle clock through mutual inhibition between PU.1 and S-phase progression. *PLoS Biol.* 8:e1000484. doi: 10.1371/journal.pbio.1000484
- Richards, S., Aziz, N., Bale, S., Bick, D., Das, S., Gastier-Foster, J., et al. (2015). Standards and guidelines for the interpretation of sequence variants: a joint consensus recommendation of the american college of medical genetics and genomics and the association for molecular pathology. *Genet. Med.* 17, 405–424. doi: 10.1038/gim.2015.30
- Roy, N. B. A., and Babbs, C. (2019). The pathogenesis, diagnosis and management of CDA type I. *Br. J. Haematol.* 185, 436–449. doi: 10.1111/bjh.15817
- Russo, R., Andolfo, I., Gambale, A., De Rosa, G., Manna, F., Arillo, A., et al. (2017). GATA1 erythroid-specific regulation of SEC23B expression and its implication in the pathogenesis of congenital dyserythropoietic anemia type II. *Haematologica* 102, e371–e374. doi: 10.3324/haematol.2016.162966
- Russo, R., Andolfo, I., Manna, F., Gambale, A., Marra, R., Rosato, B. E., et al. (2018). Multi-gene panel testing improves diagnosis and management of patients with hereditary anemias. *Am. J. Hematol.* 93, 672–682. doi: 10.1002/ajh.2508
- Russo, R., Langella, C., Esposito, M. R., Gambale, A., Vitiello, F., Vallefuooco, F., et al. (2013). Hypomorphic mutations of SEC23B gene account for mild phenotypes of congenital dyserythropoietic anemia type II. *Blood Cells Mol. Dis.* 51, 17–21. doi: 10.1016/j.bcmd.2013.02.003
- Tamary, H., Shalev, H., Luria, D., Shaft, D., Zoldan, M., Shalmon, L., et al. (1996). Clinical features and studies of erythropoiesis in israeli bedouins with congenital dyserythropoietic anemia type I. *Blood* 87, 1763–1770.

**Conflict of Interest Statement:** The authors declare that the research was conducted in the absence of any commercial or financial relationships that could be construed as a potential conflict of interest.

Copyright © 2019 Russo, Marra, Andolfo, De Rosa, Rosato, Manna, Gambale, Raia, Unal, Barella and Iolascon. This is an open-access article distributed under the terms of the Creative Commons Attribution License (CC BY). The use, distribution or reproduction in other forums is permitted, provided the original author(s) and the copyright owner(s) are credited and that the original publication in this journal is cited, in accordance with accepted academic practice. No use, distribution or reproduction is permitted which does not comply with these terms.



# Corrigendum: Characterization of Two Cases of Congenital Dyserythropoietic Anemia Type I Shed Light on the Uncharacterized C15orf41 Protein

## OPEN ACCESS

### Approved by:

Frontiers Editorial Office,  
Frontiers Media SA, Switzerland

### \*Correspondence:

Roberta Russo  
roberta.russo@unina.it

†These authors have contributed  
equally to this work

### Specialty section:

This article was submitted to  
Red Blood Cell Physiology,  
a section of the journal  
Frontiers in Physiology

**Received:** 10 July 2020

**Accepted:** 13 July 2020

**Published:** 11 August 2020

### Citation:

Russo R, Marra R, Andolfo I,  
De Rosa G, Rosato BE, Manna F,  
Gambale A, Raia M, Unal S, Barella S  
and Iolascon A (2020) Corrigendum:  
Characterization of Two Cases of  
Congenital Dyserythropoietic Anemia  
Type I Shed Light on the  
Uncharacterized C15orf41 Protein.  
Front. Physiol. 11:940.  
doi: 10.3389/fphys.2020.00940

Roberta Russo<sup>1,2†</sup>, Roberta Marra<sup>1,2†</sup>, Immacolata Andolfo<sup>1,2</sup>, Gianluca De Rosa<sup>1,2</sup>,  
Barbara Eleni Rosato<sup>1,2</sup>, Francesco Manna<sup>2</sup>, Antonella Gambale<sup>1,2</sup>, Maddalena Raia<sup>2</sup>,  
Sule Unal<sup>3</sup>, Susanna Barella<sup>4</sup> and Achille Iolascon<sup>1,2</sup>

<sup>1</sup> Dipartimento di Medicina Molecolare e Biotecnologie Mediche, Università degli Studi di Napoli Federico II, Naples, Italy,

<sup>2</sup> CEINGE Biotecnologie Avanzate, Naples, Italy, <sup>3</sup> Division of Pediatric Hematology, Hacettepe University, Ankara, Turkey,

<sup>4</sup> SSD Talassemie, Anemie Rare e Dismetabolismi del Ferro, Ospedale Pediatrico Microcitemico Antonio Cao, Azienda Ospedaliera Brotzu, Cagliari, Italy

**Keywords:** CDA (I–III), C15ORF41, functional characterization of proteins, genetic testing, anemia

## A Corrigendum on

### Characterization of Two Cases of Congenital Dyserythropoietic Anemia Type I Shed Light on the Uncharacterized C15orf41 Protein

by Russo, R., Marra, R., Andolfo, I., De Rosa, G., Rosato, B. E., Manna, F., et al. (2019). *Front. Physiol.* 10:621. doi: 10.3389/fphys.2019.00621

In the published article, there was an error in affiliation 3. Instead of “SSD Talassemie, Anemie Rare e Dismetabolismi del Ferro, Ospedale Pediatrico Microcitemico Antonio Cao, Azienda Ospedaliera Brotzu, Cagliari, Italy”, it should be “Division of Pediatric Hematology, Hacettepe University, Ankara, Turkey”.

The authors apologize for this error and state that this does not change the scientific conclusions of the article in any way. The original article has been updated.

Copyright © 2020 Russo, Marra, Andolfo, De Rosa, Rosato, Manna, Gambale, Raia, Unal, Barella and Iolascon. This is an open-access article distributed under the terms of the Creative Commons Attribution License (CC BY). The use, distribution or reproduction in other forums is permitted, provided the original author(s) and the copyright owner(s) are credited and that the original publication in this journal is cited, in accordance with accepted academic practice. No use, distribution or reproduction is permitted which does not comply with these terms.



# The Spectrum of *SPTA1*-Associated Hereditary Spherocytosis

Satheesh Chonat<sup>1,2</sup>, Mary Risinger<sup>3</sup>, Haripriya Sakthivel<sup>4</sup>, Omar Niss<sup>4,5</sup>, Jennifer A. Rothman<sup>6</sup>, Loan Hsieh<sup>7</sup>, Stella T. Chou<sup>8,9</sup>, Janet L. Kwiatkowski<sup>8,9</sup>, Eugene Khandros<sup>8,9</sup>, Matthew F. Gorman<sup>10</sup>, Donald T. Wells<sup>11</sup>, Tamara Maghathe<sup>4</sup>, Neha Dagaonkar<sup>12</sup>, Katie G. Seu<sup>4</sup>, Kejian Zhang<sup>13</sup>, Wenying Zhang<sup>5,14</sup> and Theodosia A. Kalfa<sup>4,5\*</sup>

<sup>1</sup> Department of Pediatrics, Emory University School of Medicine, Atlanta, GA, United States, <sup>2</sup> Aflac Cancer and Blood Disorders Center, Children's Healthcare of Atlanta, Atlanta, GA, United States, <sup>3</sup> College of Nursing, University of Cincinnati, Cincinnati, OH, United States, <sup>4</sup> Cancer and Blood Diseases Institute, Cincinnati Children's Hospital Medical Center, Cincinnati, OH, United States, <sup>5</sup> Department of Pediatrics, University of Cincinnati College of Medicine, Cincinnati, OH, United States, <sup>6</sup> Duke University Medical Center, Durham, NC, United States, <sup>7</sup> Division of Hematology, CHOC Children's Hospital and UC Irvine Medical Center, Orange, CA, United States, <sup>8</sup> Division of Hematology, Children's Hospital of Philadelphia, Philadelphia, PA, United States, <sup>9</sup> Department of Pediatrics, Perelman School of Medicine, University of Pennsylvania, Philadelphia, PA, United States, <sup>10</sup> Kaiser Permanente Santa Clara Medical Center, Santa Clara, CA, United States, <sup>11</sup> Dell Children's Medical Center, Austin, TX, United States, <sup>12</sup> Genomics Analysis Facility, Institute for Genomic Medicine, Columbia University, New York, NY, United States, <sup>13</sup> Coyote Bioscience Co., Ltd., San Jose, CA, United States, <sup>14</sup> Laboratory of Genetics and Genomics, Division of Human Genetics, Cincinnati Children's Hospital Medical Center, Cincinnati, OH, United States

## OPEN ACCESS

### Edited by:

Paola Bianchi,  
IRCCS Ca' Granda Foundation  
Maggiore Policlinico Hospital, Italy

### Reviewed by:

Archana Mishra Agarwal,  
University of Utah Hospital,  
United States  
Hitoshi Kanno,  
Tokyo Women's Medical University,  
Japan

### \*Correspondence:

Theodosia A. Kalfa  
theodosia.kalfa@cchmc.org

### Specialty section:

This article was submitted to  
Red Blood Cell Physiology,  
a section of the journal  
Frontiers in Physiology

**Received:** 01 February 2019

**Accepted:** 11 June 2019

**Published:** 03 July 2019

### Citation:

Chonat S, Risinger M, Sakthivel H,  
Niss O, Rothman JA, Hsieh L,  
Chou ST, Kwiatkowski JL,  
Khandros E, Gorman MF, Wells DT,  
Maghathe T, Dagaonkar N, Seu KG,  
Zhang K, Zhang W and Kalfa TA  
(2019) The Spectrum  
of *SPTA1*-Associated Hereditary  
Spherocytosis.  
Front. Physiol. 10:815.  
doi: 10.3389/fphys.2019.00815

Hereditary spherocytosis (HS) is the most common red blood cell (RBC) membrane disorder causing hereditary hemolytic anemia. Patients with HS have defects in the genes coding for ankyrin (ANK1), band 3 (SLC4A1), protein 4.2 (EPB42), and  $\alpha$  (*SPTA1*) or  $\beta$ -spectrin (*SPTB*). Severe recessive HS is most commonly due to biallelic *SPTA1* mutations.  $\alpha$ -spectrin is produced in excess in normal erythroid cells, therefore *SPTA1*-associated HS ensues with mutations causing significant decrease of normal protein expression from both alleles. In this study, we systematically compared genetic, rheological, and protein expression data to the varying clinical presentation in eleven patients with *SPTA1*-associated HS. The phenotype of HS in this group of patients ranged from moderately severe to severe transfusion-dependent anemia and up to *hydrops fetalis* which is typically fatal if transfusions are not initiated before term delivery. The pathogenicity of the mutations could be corroborated by reduced *SPTA1* mRNA expression in the patients' reticulocytes. The disease severity correlated to the level of  $\alpha$ -spectrin protein in their RBC cytoskeleton but was also affected by other factors. Patients carrying the low expression  $\alpha^{\text{LEPRA}}$  allele *in trans* to a null *SPTA1* mutation were not all transfusion dependent and their anemia improved or resolved with partial or total splenectomy, respectively. In contrast, patients with near-complete or complete  $\alpha$ -spectrin deficiency have a history of having been salvaged from fatal *hydrops fetalis*, either because they were born prematurely and started transfusions early or because they had intrauterine transfusions. They have suboptimal

reticulocytosis or reticulocytopenia and remain transfusion dependent even after splenectomy; these patients require either lifetime transfusions and iron chelation or stem cell transplant. Comprehensive genetic and phenotypic evaluation is critical to provide accurate diagnosis in patients with *SPTA1*-associated HS and guide toward appropriate management.

**Keywords:** *SPTA1*,  $\alpha$ -spectrin,  $\alpha^{\text{LEPRA}}$ , hereditary spherocytosis, next generation sequencing, hemolytic anemia, *hydrops fetalis*

## INTRODUCTION

Hereditary spherocytosis (HS) is the most common red blood cell (RBC) cytoskeleton disorder causing hereditary hemolytic anemia (HHA), characterized by sphere-shaped erythrocytes (spherocytes) with increased osmotic fragility. HS can affect all ethnic groups but is more common in people of northern European ancestry where the prevalence is 1 in 1000–2500 (Gallagher, 2005). Spherocytes are formed because of loss of membrane due to quantitative defects in proteins that link the cytoskeleton to the lipid bilayer (“vertical” linkages) (Eber and Lux, 2004). The scaffolding network of the RBC cytoskeleton is assembled by  $\alpha$ - and  $\beta$ -spectrin heterodimers self-associating in a head-to-head fashion to form tetramers, bound to the lipid membrane via the anchoring complex of ankyrin, protein 4.2, and band 3 (Salomao et al., 2008). In autosomal dominant HS, which accounts for approximately 75% of cases, mutations of ankyrin (*ANK1*), band 3 (*SLC4A1*), and  $\beta$ -spectrin (*SPTB*) genes predominate. Recessive HS is most often due to compound heterozygosity for defects in the genes encoding ankyrin,  $\alpha$ -spectrin (*SPTA1*), or protein 4.2 (*EPB42*) (Eber and Lux, 2004; Gallagher, 2005; Mohandas, 2018).

Two normal *SPTA1* alleles allow for overproduction of  $\alpha$ -spectrin chains (Hanspal and Palek, 1987). Therefore, HS due to  $\alpha$ -spectrin deficiency manifests when both of the *SPTA1* alleles are affected by mutations causing significant quantitative defect. Two *SPTA1* low expression alleles were identified early-on to be associated with RBC membrane disorders and their study helped to determine the quantitative requirements of the RBC cytoskeleton for  $\alpha$ -spectrin (Wilmotte et al., 1993; Wichterle et al., 1996).  $\alpha^{\text{LELY}}$  (Low Expression LYon) has a minor allele frequency (MAF) of 25.5% (gnomad.broadinstitute.org) and consists of the mutation c.6531-12C>T in intron 45, causing partial skipping of exon 46 in half of the transcripts and consequently a 50% decrease in the amount of  $\alpha$ -spectrin (Wilmotte et al., 1993; Marechal et al., 1995).  $\alpha^{\text{LELY}}$  *in trans* to an *SPTA1* allele with a hereditary elliptocytosis (HE)-associated mutation modifies the phenotype from HE to hereditary pyropoikilocytosis (Niss et al., 2016). In contrast,  $\alpha^{\text{LELY}}$  *in trans* to a null *SPTA1* allele causes no disease, indicating that production of ~25% of normal  $\alpha$ -spectrin is enough for normal RBC cytoskeleton assembly (Delaunay et al., 2004).  $\alpha^{\text{LEPRA}}$  (Low Expression PRague) is a deep intronic *SPTA1* mutation (c.4339-99C > T). Positioned at -99 of intron 30, it activates an alternative acceptor splice site at position -70 of the same intron. The alternative splicing results in frameshift and premature termination of translation, leading to decreased  $\alpha$ -spectrin production. This allele (MAF

of 0.5% per gnomad.broadinstitute.org) produces only about 16% of full-length spectrin as compared to the normal *SPTA1* allele, based on studies with metabolic labeling of erythroblasts *in vitro* (Wichterle et al., 1996).  $\alpha^{\text{LEPRA}}$  *in trans* to a null *SPTA1* allele (leading to a total  $\alpha$ -spectrin production of about 8%) has been shown to cause severe autosomal recessive HS, with anemia and jaundice that resolve with splenectomy (Wichterle et al., 1996; Delaunay et al., 2004). Complete  $\alpha$ -spectrin deficiency has been shown to cause lethal anemia *in utero* (Whitfield et al., 1991).

We present here eleven patients with HS due to  $\alpha$ -spectrin deficiency and discuss their phenotype/genotype correlation (Table 1).

## MATERIALS AND METHODS

### Next Generation Sequencing (NGS) of Genes Associated With HHA

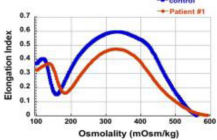
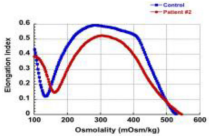
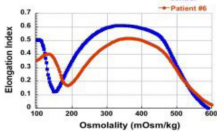
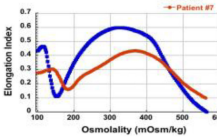
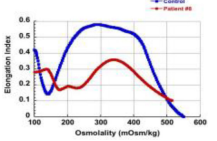
Patients with the clinical diagnosis of HHA and their parents were enrolled in an Institutional Review Board-approved research protocol based at Cincinnati Children’s Hospital Medical Center. DNA was isolated from peripheral blood (in the case of patient 9 from liver tissue preserved in paraffin after autopsy), and analyzed on an NGS HHA panel; the regions of interest for enrichment and DNA sequencing included the coding exons plus 20 bases of intronic boundaries for 32 genes known to be associated with RBC membrane and enzyme disorders and with congenital dyserythropoietic anemias: *ABCG5*, *ABCG8*, *AK1*, *ALDOA*, *ANK1*, *C15orf41*, *CDAN1*, *EPB41*, *EPB42*, *G6PD*, *GATA1*, *GCLC*, *GPI*, *GPX1*, *GSR*, *GSS*, *HK1*, *KIF23*, *KLF1*, *NT5C3A*, *PFKM*, *PGK1*, *PIEZO1*, *PKLR*, *RHAG*, *SEC23B*, *SLC2A1*(*GLUT1*), *SLC4A1*, *SPTA1*, *SPTB*, *TP11*, and *XK*. Regulatory regions and deep intronic areas of these genes with published disease-causing mutations were included in the HHA panel design. Sanger sequencing was used to confirm all mutations found in patients and in parental samples (except for parents of patients #7 and #11) to establish the phase.

### Osmotic Gradient Ektacytometry

Whole blood samples were collected in K2-EDTA-containing vials from study subjects at least 3 months after last transfusion to avoid misinterpretation from the presence of donor RBCs. Samples from healthy volunteers were collected at same time and shipped as travel controls. Specimens were stored or shipped at 4°C and were analyzed within 24 h of sample collection using



**TABLE 1** | Genetic mutations and associated phenotype in HS due to *SPTA1* mutations.

| Phenotype   | Patient | Allele 1                | Allele 2   | Age at time of report and comments   | Ektacytometry  | $\alpha$ -spectrin in RBC ghosts (% of control) |
|---|---------|-------------------------|--|--|--|---|
| GROUP I (patients 1–4)<br>Severe, recessive HS<br>(transfusion-dependent, responding to splenectomy)  | 1       | c.4339-99C > T          | c.4295del (p.L1432*)                                     | 11 year-old, chronic transfusion requirement with partial response to partial splenectomy, resolved after total splenectomy  |                   | 54%   |
|   | 2       | c.4339-99C > T          | c.5102A > T (p.L1701*)                                   | 7 year-old, chronic transfusion requirement, improved with partial splenectomy   |                   | 64%   |
|   | 3       | c.4339-99C > T          | c.3267A > T (p.Y1089*)                                   | 11 year-old, not splenectomized due to family preference, continues to require frequent transfusions   | Not evaluable in a transfused sample   |   |
|   | 4       | Mutation not identified | Gross deletion of <i>SPTA1</i>                           | 3.5 year-old, RT-PCR demonstrated significantly decreased $\alpha$ -spectrin expression; hemoglobin has normalized after recent splenectomy  | Not evaluable in a transfused sample   |   |
| GROUP II (patients 5–8)<br>Severe to moderately severe, recessive HS  | 5       | c.4339-99C > T          | c.1120C > T (p.R374*)                                    | 4 year-old, chronic transfusion requirement for first three years with improved pattern since.   | Sample not provided after age 3, when transfusion-independent  |   |
|   | 6       | c.4339-99C > T          | c.1351-1G > T  | 7 year-old, occasional transfusion requirement, resolved after splenectomy at 5 years of age   |                  | 59%   |
|   | 7       | c.4339-99C > T          | c.2671C > T (p.R891*)                                    | 4 year-old, has not been transfused so far, Hgb 7.1–8.9 g/dL, ARC 420–572 $\times 10^3/\mu\text{L}$ .  |                 | 61%   |
|   | 8       | c.4339-99C > T          | c.3257delT   | 8 year-old, transfused once as neonate, Hgb 10.6–11.8 g/dL, ARC 354–535 $\times 10^3/\mu\text{L}$ ; now Hgb 15–16 g/dL with normal ARC after splenectomy at 6 years of age (splenectomy performed because of chronic abdominal pain due to co-morbidities) |                 | Not performed.                                  |
| GROUP III (patients 9–11)<br>Life-threatening anemia in utero leading to fatal <i>hydrops fetalis</i> if untreated (transfusion-dependent, not responding to splenectomy) | 9       | c.4206delG (fs)         | c.4180delT (fs) in haplotype with c.6631C > T (p.R2211C) | Died at birth. Post-mortem diagnosis from parental studies and DNA extracted from liver tissue saved in paraffin block   | N/A  |   |
|   | 10      | c.6788+11C > T          | c.6788+11C > T   | 11 year-old, born prematurely at EGA of 33 weeks with <i>hydrops fetalis</i> , remained transfusion-dependent even after splenectomy; now doing well after matched sibling transplant  | Not evaluable in a transfused sample (required chronic transfusions up until bone marrow transplant) | 26% (performed in CD71+ cells)                  |
|   | 11      | c.6154del (p.Ala2052fs) | c.6154del (p.Ala2052fs)                                  | 2 year-old, severe in-utero anemia requiring five <i>in-utero</i> transfusions. Born with severe neonatal hyperbilirubinemia requiring exchange transfusion. Remains transfusion-dependent   | Not evaluable in a transfused sample   |   |

Of note, all the *SPTA1* variants reported here except c.4339-99C > T ( $\alpha^{\text{LEPRA}}$ ) and c.2671C > T; p.R891\* (Bogardus et al., 2014) have not been previously described.

LoRRca® MaxSis (Mechatronics, United States LLC, Warwick, RI, United States). RBC deformation was recorded while the cells were exposed to a constant shear stress of 30 Pa and an increasing osmotic gradient (0–600 mOsm/kg) in order to generate the ektacytometry curve (Da Costa et al., 2016; Zaninoni et al., 2018).

## Capillary Electrophoresis and Immunodetection

Red blood cell membrane “ghosts” were prepared from patients #1, #6, and #7, at least 3 months after last transfusion, by hypotonic lysis (Bennett, 1983) and cytoskeletal proteins were evaluated by immunodetection using the size-based capillary electrophoresis instrument Wes (ProteinSimple, San Jose, CA, United States). Capillary immuno-electrophoresis was also performed on lysates prepared from isolated CD71+ cells from patient #10 (with a similarly prepared healthy volunteer sample as control).

## Quantitative Real-Time PCR (qPCR) of Reticulocyte mRNA

Reticulocytes were magnetically isolated from whole blood collected in K2-EDTA-containing vials from patients #4 and #10, in order to validate the pathogenicity of their genotype findings, using anti-CD71 microbeads and positive selection through an AutoMACS separator (Miltenyi Biotec). A reticulocyte sample from patient 1 was prepared similarly, to be used as positive control. RNA was isolated using the QiaAmp RNA Blood Mini kit (QIAGEN) and reverse transcription was performed using the High-Capacity cDNA Reverse Transcription Kit (Applied Biosystems). *SPTA1* mRNA expression level was determined by qPCR using a StepOnePlus Real-Time PCR System (Applied Biosystems) and FAM-labeled Taqman probes (Thermo Fisher Scientific) for *SPTA1* spanning exons 48–49 (Assay ID Hs01005878\_m1) and *ACTB* (Assay ID Hs01060665\_g1) as a reference gene.

## RESULTS AND DISCUSSION

We observed three different phenotypes in patients with recessive HS due to biallelic *SPTA1* mutations, verified to be *in trans* by parental targeted sequencing (Table 1). The heterozygous parents did not have any evidence of hemolytic anemia as expected, since even  $\alpha^{\text{LELY}}$  *in trans* to a null *SPTA1* allele, producing a total of ~25% of normal  $\alpha$ -spectrin, causes no disease (Delaunay et al., 2004).

The first four patients listed in Table 1 (within Group I) had the well-known phenotype of *SPTA1*-associated HS, i.e., severe, transfusion-dependent HHA with brisk reticulocytosis (Agre et al., 1982; Wichterle et al., 1996). These patients presented with hyperbilirubinemia and non-immune hemolytic anemia soon after birth, requiring their first transfusion as neonates, before any meaningful RBC phenotypical testing could be obtained. They continued to require frequent transfusions, precluding any further erythrocyte phenotype work-up until splenectomy. Patients 1–3 had a *SPTA1* nonsense mutation (expected to lead to nonsense-mediated decay of the transcript)

*in trans* to the low expression  $\alpha^{\text{LEPRA}}$  mutation (c.4339-99C > T). Patient 1 required monthly transfusions for hemoglobin (Hgb) in the range of 6.4–7.5 g/dL with absolute reticulocyte count (ARC) of  $130\text{--}360 \times 10^9/\text{L}$  for the first four years of life, with consequent iron overload, requiring chelation treatment with deferasirox. After molecular diagnosis of *SPTA1*-associated HS utilizing NGS of the HHA panel, he underwent partial splenectomy at 4 years of age. He was able to remain transfusion-free for 18 months with Hgb 8.7–11 g/dL, but then his anemia gradually worsened with increasing transfusion requirement. He had a follow-up total splenectomy at 7 years of age; at that time the remaining splenic tissue had been impressively regrown to 435 g, based on the pathology report. The patient has had no further transfusion requirement for the past 4 years, with Hgb now in 12.7–15.8 g/dL range. Blood smear from a non-transfused blood sample after splenectomy shows many spherocytes and moderate poikilocytosis, as expected with  $\alpha$ -spectrin deficiency (Eber and Lux, 2004), and ektacytometry reveals the typical HS curve (Da Costa et al., 2016; Figure 1A). Patient 2 had a similar course for the first 2.5 years. After molecular diagnosis of *SPTA1*-associated HS, he underwent partial splenectomy and he remains transfusion-free since then with Hgb in the range of 9–10.8 g/dL and minimal regrowth of the remaining splenic tissue based on ultrasound (108–123 ml). Patient 3 has not yet had splenectomy due to parental preference and continues to require frequent transfusions.

Patient 4 had a similar clinical presentation but NGS for the HHA-panel was negative. Deletion/duplication assay by Comparative Genomic Hybridization was performed and identified a heterozygous deletion at 1q23.1 involving the *SPTA1* gene. No mutation was identified *in trans*. Since the patient remained transfusion dependent precluding phenotypical evaluation of his RBCs,  $\alpha$ -spectrin mRNA expression in his reticulocytes was evaluated by qPCR and was found decreased at levels comparable to patient 1, confirming *SPTA1*-associated recessive HS (Figure 1B). Hgb normalized at ~13 g/dL with no need for further transfusions post total splenectomy at 3 years of age.

Regrowth of the splenic remnant after partial splenectomy is a possibility, occasionally requiring a second surgery. Nevertheless, in both patients 1 and 2 who had splenectomy before 5 years of age in order to limit the transfusional iron overload, partial splenectomy was a reasonable choice with the goal to preserve splenic immune function (Englum et al., 2016). The different response of these two patients to partial splenectomy was most likely due to difference in splenic regrowth, rather than a difference in phenotypic severity.  $\alpha$ -spectrin in the erythrocyte ghosts of patient 1 was determined by immunoelectrophoresis to be 54% vs. 64% for patient 2 in comparison to normal control (Figure 1C).

Surprisingly, we identified four patients (patients 5–8 in Table 1, comprising Group II) who, despite having equivalent genotype with the first four patients of a null *SPTA1* mutation *in trans* to  $\alpha^{\text{LEPRA}}$ , appeared to have a milder phenotype, ranging from improvement in transfusion requirement after frequent transfusions in the first 2–3 years of life (patients 5 and 6)

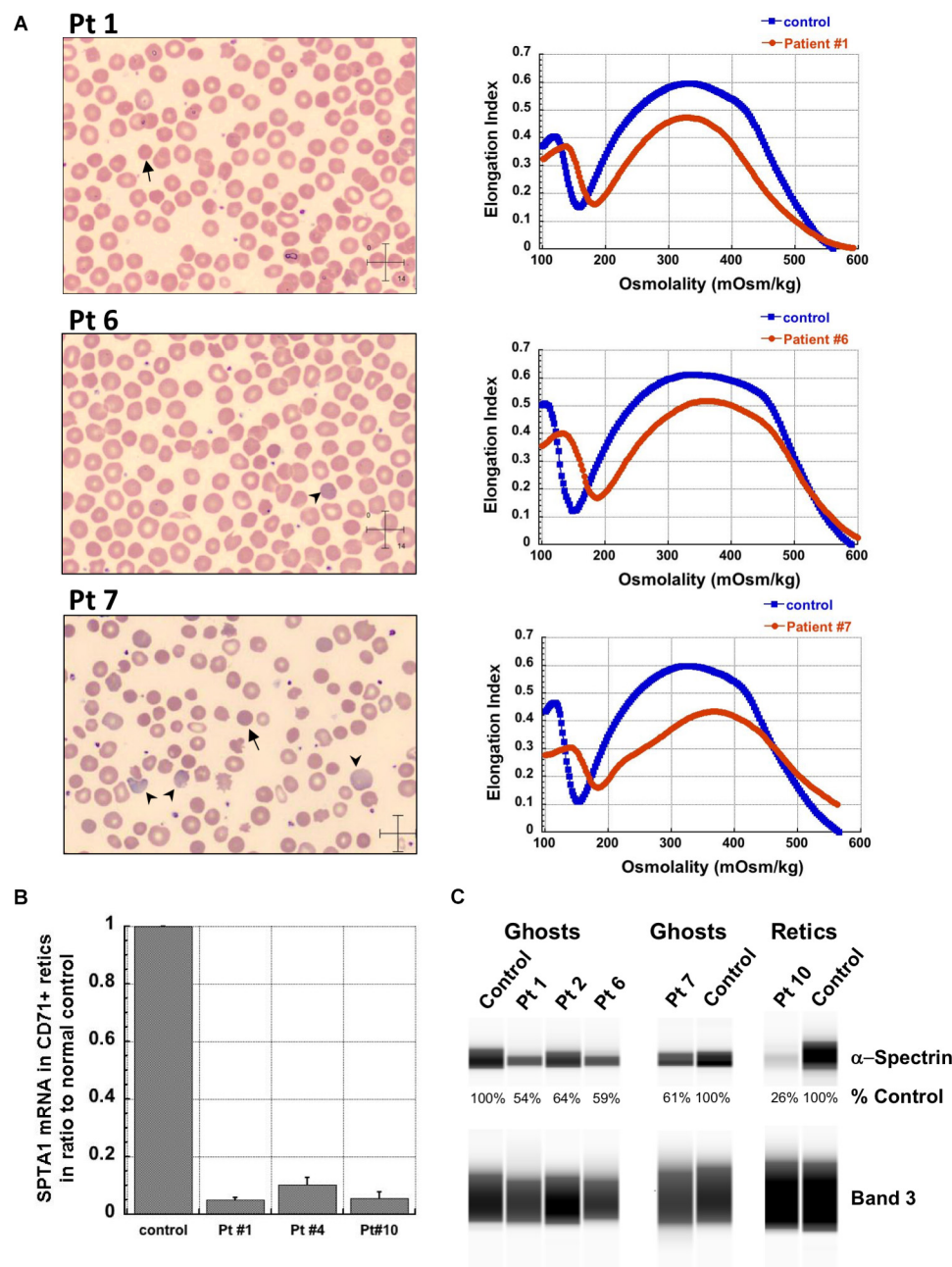


**FIGURE 1 |** Studies in peripheral blood of patients with *SPTA1*-associated HS. **(A)** Peripheral blood smears on the left from patients 1, 6 and 7 showing multiple spherocytes (arrows) lacking central pallor due to decreased surface area to volume ratio and aniso-poikilocytosis. Patient 7 also has polychromasia with increased reticulocytes (arrowheads) indicating significant hemolysis prior to splenectomy. Ektacytometry, on the right, demonstrates the typical HS curve for the patients (red) vs. control (blue). HS is characterized by increased Omin indicating decreased RBC surface to volume ratio and decreased Elmax (maximum Elongation Index) which depends mostly on the cytoskeleton mechanics. Frequently, the declining portion of the curve (represented by Ohyp, the osmolality value where the cells are at half of the maximum elongation) is also decreased (as in patient 1) indicating increased intracellular viscosity, however, it may also be normal as in patients 6 and 7 (Clark et al., 1983; Zaninoni et al., 2018). **(B)** qPCR in RNA isolated from patients' reticulocytes demonstrated severely decreased  $\alpha$ -spectrin expression. Patient 1 who has  $\alpha^{\text{LEPRA}}$  *in trans* to a null *SPTA1* mutation was found to express  $\alpha$ -spectrin at about 5% in comparison to normal control at levels similar to the original calculations for  $\alpha^{\text{LEPRA}}$  (about 16% of full-length spectrin as compared to the normal *SPTA1* allele based on studies with metabolic labeling of erythroblasts *in vitro* (Wichterle et al., 1996), and therefore a total of 8%  $\alpha$ -spectrin when  $\alpha^{\text{LEPRA}}$  is *in trans* to a null allele). qPCR appears to be a useful diagnostic assay when an unknown low-expression allele is suspected *in trans* to a null *SPTA1* mutation or deletion in a disease suspected to be severe HS, such as the case of patient 4. **(C)** Quantitation of  $\alpha$ -spectrin/band 3 ratio in RBC ghosts (Patients 1, 2, 6, and 7) and reticulocytes (Patient 10) expressed as percent of  $\alpha$ -spectrin/band 3 ratio in corresponding normal control samples by immunodetection using size-based capillary electrophoresis. Agre et al. (1985) in one of the first descriptions of HS due to  $\alpha$ -spectrin deficiency noted that the clinical severity of anemia was proportional to a degree of spectrin deficiency, ranging from 53% of normal spectrin content in severely anemic patients to 31% of normal in nearly lethal cases.

to well compensated hemolysis (patient 8). The milder severity of the disease did not seem to correlate with RBC osmotic fragility or deformability based on ektacytometry (**Figure 1A**) or the  $\alpha$ -spectrin quantitation in RBC ghosts which was only slightly lower compared to the  $\alpha$ -spectrin level in patient 2 (**Figure 1C**). Additional gene polymorphisms and mutations found in the HHA panel (**Supplementary Table S1**) did not explain the milder phenotype noted in the patients of Group II versus Group I. Heterogeneity in the level of normal  $\alpha$ -spectrin expression from the  $\alpha$ -LEPRA allele (c.4339-99C > T), variability in HIF-pathway, and erythropoietin response, and sometimes a different tolerance to anemia by patients and/or parents may be contributing to differences in the phenotype between Group I and Group II patients.

The third phenotype (Group III in **Table 1**) associated with HS due to near-complete or complete  $\alpha$ -spectrin deficiency is less well known since it has been typically embryonal lethal causing fatal *hydrops fetalis* in the third trimester of pregnancy or perinatally, such as the case of patient 9. His parents requested genetic counseling after having a fetus and a newborn child die with the clinical picture of *hydrops fetalis*. Both parents were found to carry a frameshift *SPTA1* mutation. DNA isolated from the patient's liver tissue, preserved in paraffin after autopsy, was sequenced and revealed that the patient was compound heterozygous for these *SPTA1* mutations, predicting absence of normal  $\alpha$ -spectrin production. With the progress of fetal medicine allowing prenatal diagnosis of severe anemia and *in utero* transfusions, more of these patients are now surviving to term and the disease is increasingly recognized.

Patient 10 was born prematurely at 33 weeks of gestation with severe non-immune hemolytic anemia requiring transfusion soon after birth. He remained transfusion dependent and total splenectomy did not significantly improve his hemolytic anemia. NGS for the HHA-panel revealed homozygosity for an intronic *SPTA1* variant, likely causing alternative splicing and severely decreased expression of  $\alpha$ -spectrin, as verified by qPCR (**Figure 1B**) and immunoelectrophoresis performed in lysates prepared from isolated reticulocytes. The patient is now doing well after bone marrow transplant. Patient 11, an infant of Amish-Mennonite origin required five in-utero transfusions for severe anemia and had significant neonatal hyperbilirubinemia at birth requiring exchange transfusion. HHA gene panel revealed homozygosity for a *SPTA1* frameshift mutation, explaining her severe reticulocytopenia since her reticulocytes with complete  $\alpha$ -spectrin deficiency are extremely fragile, failing to survive the shear stress in circulation.

The genetic and phenotypic information gathered from our patient cohort demonstrates that patients with recessive *SPTA1*-associated HS due to the low expression *SPTA1* variant  $\alpha^{\text{LEPRA}}$  *in trans* to a null *SPTA1* mutation respond to either partial or total splenectomy by significant improvement or resolution of anemia, respectively. In contrast, patients with near complete or complete  $\alpha$ -spectrin deficiency because of biallelic null or rare intronic *SPTA1* mutations that result in severely decreased expression of the protein, are unlikely to have a measurable response to splenectomy and require either lifetime transfusions and iron chelation or stem cell transplant. This group of patients

have typically reticulocytopenia and history of having been salvaged from fatal *hydrops fetalis*, either because they were born prematurely and started transfusions early or because they had intrauterine transfusions.

Next generation sequencing panels are robust and rapid diagnostic tools for HHA, especially when frequent transfusions preclude phenotypic evaluation of the patients' RBCs. Specialized assays such as qPCR of reticulocyte mRNA can be used for verification of the diagnosis. Comprehensive genetic and phenotypic evaluation is critical to provide insights into the variable phenotypes of patients with HHA and guide toward appropriate management.

## ETHICS STATEMENT

The manuscript is a retrospective case series, with no patient identifiable information, performed under two IRB-approved protocols in Cincinnati Children's Hospital Medical Center (CCHMC) for diagnostic, non-interventional studies of Congenital Hemolytic and Dyserythropoietic Anemias: Study #2011-1510 and Study #2015-6150. Patients and families were consented either in person in CCHMC hematology clinic or over the phone in the presence of a witness.

## AUTHOR CONTRIBUTIONS

SC, MR, KZ, WZ, and TK contributed to the conception and design of the study. SC, MR, HS, TM, ND, and KS performed the experiments. SC, ON, JR, LH, STC, JK, EK, MG, DW, and TK provided the clinical information. TK organized the database. SC and TK wrote the first draft of the manuscript. MR, HS, and KS wrote sections of the manuscript. All authors revised, read, and approved the submitted version of the manuscript.

## FUNDING

This work was supported by the National Center for Advancing Translational Sciences of the National Institutes of Health, under the award number 1UL1TR001425-01. The content is solely the responsibility of the authors and does not necessarily represent the official views of the NIH.

## ACKNOWLEDGMENTS

We are grateful to the CCHMC hematology clinical research support team, patients, and families for their enthusiastic participation in this study.

## SUPPLEMENTARY MATERIAL

The Supplementary Material for this article can be found online at: <https://www.frontiersin.org/articles/10.3389/fphys.2019.00815/full#supplementary-material>



## REFERENCES

- Agre, P., Casella, J. F., Zinkham, W. H., McMillan, C., and Bennett, V. (1985). Partial deficiency of erythrocyte spectrin in hereditary spherocytosis. *Nature* 314, 380–383. doi: 10.1038/314380a0
- Agre, P., Orringer, E. P., and Bennett, V. (1982). Deficient red-cell spectrin in severe, recessively inherited spherocytosis. *N. Engl. J. Med.* 306, 1155–1161. doi: 10.1056/NEJM198205133061906
- Bennett, V. (1983). Proteins involved in membrane-cytoskeleton association in human erythrocytes: spectrin, ankyrin, and band 3. *Meth. Enzymol.* 96, 313–324. doi: 10.1016/s0076-6879(83)96029-9
- Bogardus, H., Schulz, V. P., Maksimova, Y., Miller, B. A., Li, P., Forget, B. G., et al. (2014). Severe nondominant hereditary spherocytosis due to uniparental isodisomy at the SPTA1 locus. *Haematologica* 99, e168–e170. doi: 10.3324/haematol.2014.110312
- Clark, M. R., Mohandas, N., and Shohet, S. B. (1983). Osmotic gradient ektacytometry: comprehensive characterization of red cell volume and surface maintenance. *Blood* 61, 899–910.
- Da Costa, L., Suner, L., Galimand, J., Bonnel, A., Pascreau, T., Couque, N., et al. (2016). Diagnostic tool for red blood cell membrane disorders: assessment of a new generation ektacytometer. *Blood Cells Mol. Dis.* 56, 9–22. doi: 10.1016/j.bcmd.2015.09.001
- Delaunay, J., Nouyrigat, V., Proust, A., Schischmanoff, P. O., Cynober, T., Yvart, J., et al. (2004). Different impacts of alleles alphaLEPRA and alphaLELY as assessed versus a novel, virtually null allele of the SPTA1 gene in trans. *Br. J. Haematol.* 127, 118–122. doi: 10.1111/j.1365-2141.2004.05160.x
- Eber, S., and Lux, S. E. (2004). Hereditary spherocytosis—defects in proteins that connect the membrane skeleton to the lipid bilayer. *Semin Hematol.* 41, 118–141. doi: 10.1053/j.seminhematol.2004.01.002
- Englum, B. R., Rothman, J., Leonard, S., Reiter, A., Thornburg, C., Brindle, M., et al. (2016). Hematologic outcomes after total splenectomy and partial splenectomy for congenital hemolytic anemia. *J. Pediatr. Surg.* 51, 122–127. doi: 10.1016/j.jpedsurg.2015.10.028
- Gallagher, P. G. (2005). Red cell membrane disorders. *Hematology Am. Soc. Hematol. Educ. Program* 2005, 13–18. doi: 10.1182/asheducation-2005.1.13
- Hanspal, M., and Palek, J. (1987). Synthesis and assembly of membrane skeletal proteins in mammalian red cell precursors. *J. Cell Biol.* 105, 1417–1424. doi: 10.1083/jcb.105.3.1417
- Marechal, J., Wilmotte, R., Kanzaki, A., Dhermy, D., Garbarz, M., Galand, C., et al. (1995). Ethnic distribution of allele alpha LELY, a low-expression allele of red-cell spectrin alpha-gene. *Br. J. Haematol.* 90, 553–556. doi: 10.1111/j.1365-2141.1995.tb05583.x
- Mohandas, N. (2018). Inherited hemolytic anemia: a possessive beginner's guide. *Hematology Am. Soc. Hematol. Educ. Program* 2018, 377–381. doi: 10.1182/asheducation-2018.1.377
- Niss, O., Chonlat, S., Dagaonkar, N., Almansoori, M. O., Kerr, K., Rogers, Z. R., et al. (2016). Genotype-phenotype correlations in hereditary elliptocytosis and hereditary pyropoikilocytosis. *Blood Cells Mol. Dis.* 61, 4–9. doi: 10.1016/j.bcmd.2016.07.003
- Salomao, M., Zhang, X., Yang, Y., Lee, S., Hartwig, J. H., Chasis, J. A., et al. (2008). Protein 4.1R-dependent multiprotein complex: new insights into the structural organization of the red blood cell membrane. *Proc. Natl. Acad. Sci. U.S.A.* 105, 8026–8031. doi: 10.1073/pnas.0803225105
- Whitfield, C. F., Follweiler, J. B., Lopresti-Morrow, L., and Miller, B. A. (1991). Deficiency of alpha-spectrin synthesis in burst-forming units-erythroid in lethal hereditary spherocytosis. *Blood* 78, 3043–3051.
- Wichterle, H., Hanspal, M., Palek, J., and Jarolim, P. (1996). Combination of two mutant alpha spectrin alleles underlies a severe spherocytic hemolytic anemia. *J. Clin. Invest.* 98, 2300–2307. doi: 10.1172/JCI119041
- Wilmotte, R., Marechal, J., Morle, L., Baklouti, F., Philippe, N., Kastally, R., et al. (1993). Low expression allele alpha LELY of red cell spectrin is associated with mutations in exon 40 (alpha V/41 polymorphism) and intron 45 and with partial skipping of exon 46. *J. Clin. Invest.* 91, 2091–2096. doi: 10.1172/JCI116432
- Zaninoni, A., Fermo, E., Vercellati, C., Consonni, D., Marcello, A. P., Zanella, A., et al. (2018). Use of laser assisted optical rotational cell analyzer (lorrca maxis) in the diagnosis of rbc membrane disorders, enzyme defects, and congenital dyserythropoietic anemias: a monocentric study on 202 patients. *Front. Physiol.* 9:451. doi: 10.3389/fphys.2018.00451

**Conflict of Interest Statement:** The authors declare that the research was conducted in the absence of any commercial or financial relationships that could be construed as a potential conflict of interest.

Copyright © 2019 Chonlat, Risinger, Sakthivel, Niss, Rothman, Hsieh, Chou, Kwiatkowski, Khandros, Gorman, Wells, Maghathe, Dagaonkar, Seu, Zhang, Zhang and Kalfa. This is an open-access article distributed under the terms of the Creative Commons Attribution License (CC BY). The use, distribution or reproduction in other forums is permitted, provided the original author(s) and the copyright owner(s) are credited and that the original publication in this journal is cited, in accordance with accepted academic practice. No use, distribution or reproduction is permitted which does not comply with these terms.



# Corrigendum: The Spectrum of SPTA1-Associated Hereditary Spherocytosis

Satheesh Chonat<sup>1,2</sup>, Mary Risinger<sup>3</sup>, Haripriya Sakthivel<sup>4</sup>, Omar Niss<sup>4,5</sup>, Jennifer A. Rothman<sup>6</sup>, Loan Hsieh<sup>7</sup>, Stella T. Chou<sup>8,9</sup>, Janet L. Kwiatkowski<sup>8,9</sup>, Eugene Khandros<sup>8,9</sup>, Matthew F. Gorman<sup>10</sup>, Donald T. Wells<sup>11</sup>, Tamara Maghathe<sup>4</sup>, Neha Dagaonkar<sup>12</sup>, Katie G. Seu<sup>4</sup>, Kejian Zhang<sup>13</sup>, Wenying Zhang<sup>5,14</sup> and Theodosia A. Kalfa<sup>4,5\*</sup>

<sup>1</sup> Department of Pediatrics, Emory University School of Medicine, Atlanta, GA, United States, <sup>2</sup> Aflac Cancer and Blood Disorders Center, Children's Healthcare of Atlanta, Atlanta, GA, United States, <sup>3</sup> College of Nursing, University of Cincinnati, Cincinnati, OH, United States, <sup>4</sup> Cancer and Blood Diseases Institute, Cincinnati Children's Hospital Medical Center, Cincinnati, OH, United States, <sup>5</sup> Department of Pediatrics, University of Cincinnati College of Medicine, Cincinnati, OH, United States, <sup>6</sup> Duke University Medical Center, Durham, NC, United States, <sup>7</sup> Division of Hematology, CHOC Children's Hospital and UC Irvine Medical Center, Orange, CA, United States, <sup>8</sup> Division of Hematology, Children's Hospital of Philadelphia, Philadelphia, PA, United States, <sup>9</sup> Department of Pediatrics, Perelman School of Medicine, University of Pennsylvania, Philadelphia, PA, United States, <sup>10</sup> Kaiser Permanente Santa Clara Medical Center, Santa Clara, CA, United States, <sup>11</sup> Dell Children's Medical Center, Austin, TX, United States, <sup>12</sup> Genomics Analysis Facility, Institute for Genomic Medicine, Columbia University, New York, NY, United States, <sup>13</sup> Coyote Bioscience Co., Ltd., San Jose, CA, United States, <sup>14</sup> Laboratory of Genetics and Genomics, Division of Human Genetics, Cincinnati Children's Hospital Medical Center, Cincinnati, OH, United States

## OPEN ACCESS

### Edited by:

Paola Bianchi,  
IRCCS Ca 'Granda Foundation  
Maggiore Policlinico Hospital, Italy

### Reviewed by:

Elisa Fermo,  
IRCCS Ca 'Granda Foundation  
Maggiore Policlinico Hospital, Italy

### \*Correspondence:

Theodosia A. Kalfa  
theodosia.kalfa@cchmc.org

### Specialty section:

This article was submitted to  
Red Blood Cell Physiology,  
a section of the journal  
Frontiers in Physiology

**Received:** 03 September 2019

**Accepted:** 04 October 2019

**Published:** 18 October 2019

### Citation:

Chonat S, Risinger M, Sakthivel H,  
Niss O, Rothman JA, Hsieh L,  
Chou ST, Kwiatkowski JL,  
Khandros E, Gorman MF, Wells DT,  
Maghathe T, Dagaonkar N, Seu KG,  
Zhang K, Zhang W and Kalfa TA  
(2019) Corrigendum: The Spectrum of  
SPTA1-Associated Hereditary  
Spherocytosis.  
Front. Physiol. 10:1331.  
doi: 10.3389/fphys.2019.01331

**Keywords:** SPTA1,  $\alpha$ -spectrin,  $\alpha$ -LEPRA, hereditary spherocytosis, next generation sequencing, hemolytic anemia, hydrops fetalis

## A Corrigendum on

### The Spectrum of SPTA1-Associated Hereditary Spherocytosis

by Chonat, S., Risinger, M., Sakthivel, H., Niss, O., Rothman, J. A., Hsieh, L., et al. (2019). *Front. Physiol.* 10:815. doi: 10.3389/fphys.2019.00815

In the original article, there was a mistake in **Table 1** as published. The SPTA1 mutation of Allele 2 in Patient 1, is stated as "c.4294T>A (p.L1432\*)." The correct mutation should read "c.4295del (p.L1432\*)." The corrected **Table 1** appears below.

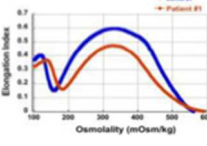
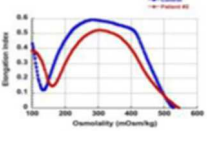
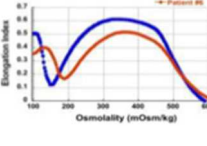
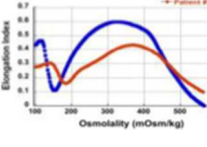
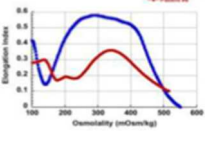
The authors apologize for this error and state that this does not change the scientific conclusions of the article in any way. The original article has been updated.

## REFERENCES

Bogardus, H., Schulz, V. P., Maksimova, Y., Miller, B. A., Li, P., Forget, B. G., et al. (2014). Severe nondominant hereditary spherocytosis due to uniparental isodisomy at the SPTA1 locus. *Haematologica* 99, e168–e170. doi: 10.3324/haematol.2014.110312

Copyright © 2019 Chonat, Risinger, Sakthivel, Niss, Rothman, Hsieh, Chou, Kwiatkowski, Khandros, Gorman, Wells, Maghathe, Dagaonkar, Seu, Zhang, Zhang and Kalfa. This is an open-access article distributed under the terms of the Creative Commons Attribution License (CC BY). The use, distribution or reproduction in other forums is permitted, provided the original author(s) and the copyright owner(s) are credited and that the original publication in this journal is cited, in accordance with accepted academic practice. No use, distribution or reproduction is permitted which does not comply with these terms.

**TABLE 1** | Genetic mutations and associated phenotype in HS due to SPTA1 mutations.

| Phenotype   | Patient | Allele 1                | Allele 2   | Age at time of report and comments   | Ektacytometry  | $\alpha$ -spectrin in RBC ghosts (% of control) |
|---|---------|-------------------------|--|--|--|---|
| GROUP I (patients 1–4)<br>Severe, recessive HS (transfusion-dependent, responding to splenectomy)   | 1       | c.4339-99C > T          | c.4295del (p.L1432*)                                     | 11 year-old, chronic transfusion requirement with partial response to partial splenectomy, resolved after total splenectomy  |                   | 54%   |
|   | 2       | c.4339-99C > T          | c.5102A > T (p.L1701*)                                   | 7 year-old, chronic transfusion requirement, improved with partial splenectomy   |                   | 64%   |
|   | 3       | c.4339-99C > T          | c.3267A > T (p.Y1089*)                                   | 11 year-old, not splenectomized due to family preference, continues to require frequent transfusions   | Not evaluable in a transfused sample   |   |
|   | 4       | Mutation not identified | Gross deletion of SPTA1                                  | 3.5 year-old, RT-PCR demonstrated significantly decreased $\alpha$ -spectrin expression; hemoglobin has normalized after recent splenectomy  | Not evaluable in a transfused sample   |   |
| GROUP II (patients 5–8)<br>Severe to moderately severe, recessive HS  | 5       | c.4339-99C > T          | c.1120C > T (p.R374*)                                    | 4 year-old, chronic transfusion requirement for first three years with improved pattern since.   | Sample not provided after age 3, when transfusion-independent  |   |
|   | 6       | c.4339-99C > T          | c.1351-1G > T  | 7 year-old, occasional transfusion requirement, resolved after splenectomy at 5 years of age   |                  | 59%   |
|   | 7       | c.4339-99C > T          | c.2671C > T (p.R891*)                                    | 4 year-old, has not been transfused so far, Hgb 7.1–8.9 g/dL, ARC 420–572 $\times 10^3/\mu\text{L}$ .  |                 | 61%   |
|   | 8       | c.4339-99C > T          | c.3257delT   | 8 year-old, transfused once as neonate, Hgb 10.6–11.8 g/dL, ARC 354–535 $\times 10^3/\mu\text{L}$ ; now Hgb 15–16 g/dL with normal ARC after splenectomy at 6 years of age (splenectomy performed because of chronic abdominal pain due to co-morbidities) |                 | Not performed.                                  |
| GROUP III (patients 9–11)<br>Life-threatening anemia in utero leading to fatal <i>hydrops fetalis</i> if untreated (transfusion-dependent, not responding to splenectomy) | 9       | c.4206delG (fs)         | c.4180delT (fs) in haplotype with c.6631C > T (p.R2211C) | Died at birth. Post-mortem diagnosis from parental studies and DNA extracted from liver tissue saved in paraffin block   | N/A  |   |
|   | 10      | c.6788+11C > T          | c.6788+11C > T   | 11 year-old, born prematurely at EGA of 33 weeks with <i>hydrops fetalis</i> , remained transfusion-dependent even after splenectomy; now doing well after matched sibling transplant  | Not evaluable in a transfused sample (required chronic transfusions up until bone marrow transplant) | 26% (performed in CD71+ cells)                  |
|   | 11      | c.6154del (p.Ala2052fs) | c.6154del (p.Ala2052fs)                                  | 2 year-old, severe in-utero anemia requiring five <i>in-utero</i> transfusions. Born with severe neonatal hyperbilirubinemia requiring exchange transfusion. Remains transfusion-dependent   | Not evaluable in a transfused sample   |   |

Of note, all the SPTA1 variants reported here except c.4339-99C > T ( $\alpha$ -LEPRA) and c.2671C > T; p.R891\* (Bogardus et al., 2014) have not been previously described.



# Receptor for Advanced Glycation End Products Antagonism Blunts Kidney Damage in Transgenic Townes Sick Mice

Emmanuelle Charrin<sup>1,2</sup>, Camille Faes<sup>1,2</sup>, Amandine Sotiaux<sup>1,2</sup>, Sarah Skinner<sup>1,2</sup>, Vincent Pialoux<sup>1,2,3</sup>, Philippe Joly<sup>1,2,4</sup>, Philippe Connes<sup>1,2,3</sup> and Cyril Martin<sup>1,2\*</sup>

<sup>1</sup>Interuniversity Laboratory of Human Movement Biology, University Claude Bernard Lyon 1, University of Lyon, Lyon, France,

<sup>2</sup>Laboratory of Excellence "GR-Ex", Paris, France, <sup>3</sup>Institut Universitaire de France, Paris, France, <sup>4</sup>Groupe Hospitalier Est, UF "Biochimie des Pathologies érythrocytaires" Centre de Biologie Est, CHU de Lyon, Lyon, France

## OPEN ACCESS

### Edited by:

Paola Bianchi,  
IRCCS Ca 'Granda Foundation  
Maggiore Policlinico Hospital, Italy

### Reviewed by:

Anna Rita Migliaccio,  
Icahn School of Medicine at Mount  
Sinai, United States  
Raffaella Colombatti,  
University Hospital of Padua, Italy

### \*Correspondence:

Cyril Martin  
cyril.martin@univ-lyon1.fr

### Specialty section:

This article was submitted to  
Red Blood Cell Physiology,  
a section of the journal  
Frontiers in Physiology

Received: 14 January 2019

Accepted: 24 June 2019

Published: 23 July 2019

### Citation:

Charrin E, Faes C, Sotiaux A,  
Skinner S, Pialoux V, Joly P,  
Connes P and Martin C (2019)  
Receptor for Advanced Glycation End  
Products Antagonism Blunts Kidney  
Damage in Transgenic Townes  
Sickle Mice.  
Front. Physiol. 10:880.  
doi: 10.3389/fphys.2019.00880

A large proportion of adult patients with sickle cell disease (SCD) develops kidney disease and is at a high risk of mortality. The contribution of advanced glycation end products and their receptor (AGE/RAGE) axis has been established in the pathogenesis of multiple kidney diseases. The aim of the present study was to determine the implication of RAGE in the development of SCD-related kidney complications in a mouse model of SCD, as this has never been investigated. 8-week-old AA (normal) and SS (homozygous SCD) Townes mice were treated with a specific RAGE antagonist (RAP) or vehicle (NaCl). After 3 weeks of treatment, red blood cell count, hematocrit, and hemoglobin levels were significantly higher in RAP-treated SS mice. Reticulocyte count and sickle cell count were reduced in RAP-SS compared to their NaCl-treated littermates. The lower NADPH oxidase activity in the kidney of RAP-treated mice compared to NaCl-treated mice suggests limited ROS production. RAP-treated SS mice had decreased NF- $\kappa$ B protein expression and activation as well as reduced TNF- $\alpha$  mRNA expression in the kidney. Glomerular area, interstitial fibrosis, tubular iron deposits, and KIM-1 protein expression were significantly reduced after RAP treatment. In conclusion, this study provides evidence supporting the pathogenic role of RAGE in kidney injuries in sickle cell mice.

**Keywords:** sickle cell disease, RAGEs, kidney, Townes mice, oxidative stress, inflammation

## INTRODUCTION

Sickle cell disease (SCD) is one of the most common severe monogenic disorders worldwide. Mutated intra-erythrocytic hemoglobin S results from the substitution of valine for glutamic acid on the sixth codon of the  $\beta$ -globin gene (HBB) and leads to the formation of sickle-shaped red blood cells (RBCs) (Ballas and Mohandas, 1996). The homozygous disease is



characterized by increased RBC fragility, decreased RBC deformability, and increased endothelial adhesion, which promote chronic hemolytic anemia and painful vaso-occlusive crises (VOC) (Rees et al., 2010; Connes et al., 2018). An imbalanced redox state and chronic inflammation also participate in the development of vasculopathy and multiple organ damage (Wood et al., 2008; Sparkenbaugh and Pawlinski, 2013; Conran and Belcher, 2018; van Beers and van Wijk, 2018). Due to its high rate of oxygen consumption and functional features, the kidney is particularly vulnerable in SCD patients. It has been estimated that 16–18% of overall mortality in patients with SCD is attributed to chronic renal failure (Platt et al., 1994). Renal manifestations of the disease include altered renal hemodynamics, renal and glomerular enlargement, and tubular deposits of iron that ultimately contribute to the development of chronic kidney disease (Nath and Hebbel, 2015).

Under oxidative conditions, advanced glycation end products (AGEs) are generated by non-enzymatic glycation and oxidation of proteins and lipids in the Maillard reaction (Singh et al., 2001). Beyond their valuable role as well-established markers of oxidative stress (Genuth et al., 2005; Koyama et al., 2007; Meerwaldt et al., 2008), it has been demonstrated that AGEs contribute to the pathophysiology of organ complications in diabetes mellitus and other chronic inflammatory diseases (Miyata et al., 1998; Huebschmann et al., 2006; Guo et al., 2012), partially through oxidative stress mechanisms/pathways (Genuth et al., 2005; Koyama et al., 2007; Meerwaldt et al., 2008). The accumulation of AGEs has been shown to participate in renal filtration alteration and glomerulopathy (Ahmed, 2005; Tan et al., 2007). The underlying molecular mechanisms involve enhanced production of pro-inflammatory cytokines, adhesion molecules, and oxidants following the activation of AGEs receptors (RAGEs) (Rojas et al., 2000; Ahmed, 2005; Goldin et al., 2006).

Although numerous SCD-related kidney complications are consistent with tissue damage induced by RAGE activation, such as albuminuria (Wendt et al., 2003), focal segmental glomerulosclerosis (Tanji et al., 2000; Wendt et al., 2003), and fibrosis (Cooper, 2004), the possible role of this receptor in the pathogenesis of SCD has been poorly investigated. To date, only two studies have reported increased plasma AGEs concentrations in children and adults with homozygous SCD at steady state with no further increase during VOC (Somjee et al., 2005; Nur et al., 2010). More recently, a third study reported increased level of AGEs in the skin of SCD patients compared to controls but the authors found no association with the clinical status of the patients (Kashyap et al., 2018). To test the hypothesis that RAGE may contribute to the development of kidney damage in SCD, we investigated the effects of RAGE inhibition on the kidney of a transgenic mouse model of SCD (Townes) expressing exclusively human sickle hemoglobin. Histological sections of the kidney, pro-inflammatory molecule expression, oxidative stress markers, and hematological parameters were analyzed in SCD mice treated with a specific antagonist peptide of RAGE.

## MATERIALS AND METHODS

### Animals

We have established a colony of Townes sickle mice in our laboratory, originally purchased from the Jackson Laboratory (Bar Harbor, ME, USA). Mouse genotypes were confirmed by PCR. Townes mice have both human  $\alpha$ - and  $\beta$ -globin genes knocked into the mouse locus, allowing the generation of littermates AA (healthy controls) and SS (homozygous SCD) mice (Wu et al., 2006). A total of 44 mice (21 females and 23 males) aged 8–9 weeks were used and maintained on a 12-h light–dark cycle with food and water *ad libitum*. The guidelines from the French Ministry of Agriculture for experimental procedures and the Institute for Laboratory Animal Research (National Academy of Sciences, USA) were followed and the protocol was approved by the regional animal care committee (#DR2013-46, Rhône-Alpes, France).

### Experimental Design

To determine the role of RAGE in SCD pathophysiology, RAGE antagonist peptide (RAP; 5 mg kg<sup>-1</sup>, #553031, Merck Millipore, Molsheim, France) was administered in 8- to 9-week-old AA and SS mice *via* intraperitoneal (IP) injection, 5 days per week for 3 weeks, as previously proposed (Arumugam et al., 2012). Saline solution (NaCl 0.9%) IP injection was used as a control.

### Tissue Sampling

The day after the last injection, mice were anesthetized with an IP injection of pentobarbital (50 mg/kg, Doletal®, Vétoquinol, Lure, France) and blood was collected by a retro-orbital venipuncture into EDTA tubes for hematological analysis. Mice were euthanatized by exsanguination with a 0.9% NaCl transcardial perfusion for 70 s. One kidney was collected and immediately frozen in liquid nitrogen for oxidative stress and qRT-PCR analyses. The second kidney was conditioned for histology (*vide infra*).

### Hematology

An ABX Micros 60 automat (Horiba, Montpellier, France) was used for the following hematological measurements: hematocrit (Hct); red blood cell (RBC) count; hemoglobin concentration; mean corpuscular volume (MCV); RBC distribution width (RDW); mean corpuscular hemoglobin concentration (MCHC); mean corpuscular hemoglobin (MCH); white blood cell (WBC) count; lymphocyte, monocyte, and granulocyte counts. The percentage of reticulocytes and sickle cells was blindly assessed on smears stained with brilliant cresyl blue (860867, Sigma-Aldrich, St-Louis, MO, USA) by two investigators under a light microscope (BX43 Microscope, Olympus, Tokyo, Japan).

### qRT-PCR for Cytokines mRNA Expression

Total mRNA from kidney was isolated using Tri Reagent LS (Euromedex, Souffelweyersheim, France) according to the manufacturer's instructions, purified with DNase I (EN0525, ThermoFisher scientific, Waltham, MA, USA), and concentrated

at 80 ng.µl<sup>-1</sup>. One thousand nanograms per sample of total mRNA were reverse transcribed to cDNA with the reverse transcriptase RNase Hminus (Promega, Madison, WI, USA) using oligo (T)15 (Eurogentec, Seraing, Belgium). RT calibration was done in the presence of 80 pg. of a synthetic external and non-homologous poly(A) Standard RNA (SmRNA) used to normalize the reverse transcription of mRNAs of biological samples (Morales and Bezin, patent WO2004.092414). Real-time qPCR analysis was performed on a Rotor-Gene Q system (Qiagen, Venlo, Netherlands) by using the Rotor-Gene SYBR® green PCR kit (Qiagen, Venlo, Netherlands). The thermal profiles consisted of 15 min at 95°C for denaturing followed by 45 cycles of amplifications (15 s at 94°C for denaturation, 30 s at 58°C for annealing and, 6 s at 72°C for extension). Results obtained for the targeted mRNAs were normalized against the SmRNA. The primer pair used was: *Tumor necrosis factor-α* (TNF-α; M13049.1) forward 5' CTG TAG CCC ACG TCG TAG C 3', reverse 5' TTG AGA TCC ATG CCG TTG 3' (97 bp), *Interleukine-1β* (IL-1β; NM 008361.3) forward 5' TTG ACG GAC CCC AAA AGA T 3', reverse 5' AGC TGG ATG CTC TCA TCA GG 3' (73 bp); *Interleukine-6* (IL-6; M24221) forward 5' GCT ACC AAA CTG GAT ATA ATC AGG A 3', reverse 5' CCA GGT AGC TAT GGT ACT CCA GAA 3' (78 bp); *Vascular cell adhesion molecule-1* (VCAM-1; NM 011693.2) forward 5' TGG TGA AAT GGA ATC TGA ACC 3', reverse 5' CCC AGA TGG TGG TTT CCT T 3' (86 bp).

## Oxidative Stress and Antioxidant Assessment

Kidney was homogenized (10%, w/v) in PBS 1X + EDTA 0.5 mM in ice. After centrifugation at 12,000 g for 10 min at 4°C, the supernatant was collected for measurement of oxidative stress markers. Homogenate aliquots were stored at -80°C. Protein concentrations were determined using the BCA protein assays Kit (Novagen, Darmstadt, Germany) in accordance with the manufacturer's instructions. All of the chemicals used for oxidative stress measurements were purchased from Sigma-Aldrich (St-Louis, MO, USA) and spectrophotometric measurements were performed on TECAN Infinite 2000 plate reader (Männedorf, Switzerland). Results were standardized per mg of total protein. Glutathione peroxidase (GPx) activity was determined by the modified method of Paglia and Valentine (Paglia and Valentine, 1967). GPx activity was determined by measuring the rate of NADPH extinction after addition of glutathione reductase, reduced glutathione and NADPH using hydrogen peroxide (H<sub>2</sub>O<sub>2</sub>) as substrate as previously described (Charrin et al., 2015). NADPH oxidase activity was quantified as the formation rate of formazan blue from nitroblue tetrazolium and the superoxide radicals produced by NADPH oxidase in the presence of NADPH.

## Histology

The kidneys were harvested and fixed in a 4% paraformaldehyde (Sigma-Aldrich, St Louis, MO, USA) in a 0.1 M phosphate

buffer solution for 2 h. They were then incubated in 25% sucrose (Sigma-Aldrich, St Louis, MO, USA) for 24 h for cryopreservation and gently frozen in -40°C isopentane (VWR, West Chester, PA, USA) before storage at -80°C. Seven-micrometer sections were cut and stained with hematoxylin-eosin, Masson's trichrome, and Perl's Blue. All observations in light microscopy were performed using a light microscope Olympus BX43 (Olympus Corporation, Tokyo, Japan), images were captured with a video camera SC30 (Olympus Corporation, Tokyo, Japan) coupled to an image analysis system (AnalySIS® getIT! 5.1; Olympus Soft Imaging Solutions GmbH, Münster, Germany). The area of 50 glomeruli per mouse was measured using Image J.

## Immunostaining

Briefly, antigen retrieval was performed by immersing frozen sections in 0.01 M citrate buffer (pH 6.0), at 95°C for 25 min. Slides were then incubated in blocking solution (TBS + 3% donkey serum) at room temperature for 1 h 30 min. Endogenous biotin and peroxidase activity were blocked before staining, by using commercial avidin/biotin and peroxidase kits, respectively (Vector Lab, Burlingame, CA, USA). Slides were incubated overnight at 4°C with the following primary antibodies: rabbit polyclonal anti-NF-κB p65 (sc-372, dilution 1:200, Santa Cruz Biotechnology, CA), mouse monoclonal anti-phosphorylated NF-κB p65 Ser536 (sc-136,548, dilution 1:200, Santa Cruz Biotechnology), or rat monoclonal anti-KIM1 (sc-53,769, dilution 1:50, Santa Cruz Biotechnology). After washing, sections were then incubated with a biotinylated donkey anti-rabbit (711-065-152, dilution 1:2,000; Jackson Immuno-Research, Suffolk, UK), donkey anti-mouse (715-065-150, dilution 1:5,000; Jackson Immuno-Research), or donkey anti-rat antibody (712-065-153, dilution 1:2,000; Jackson Immuno-Research). Exposure was performed with the avidin-biotin enzyme complex (Vectastain Elite ABC standard peroxidase Kit; Vector Lab, Burlingame, CA, USA) and the substrate 3,3'-diaminobenzidine (DAB Peroxidase Substrate Kit; Vector Lab, Burlingame, CA, USA). ImageJ® software with the "Immunoratio" plugin was used to semi-quantify NF-κB p65, phosphorylated NF-κB p65 Ser536, and KIM-1 expression in 30–50 randomly selected cortical areas. This score was measured by determining the total tissue area on the original picture while the DAB-positive area was defined using ImageJ's automatic threshold on the DAB component, obtained as previously described (Tuominen et al., 2010).

## Statistics

Statistical analyses were performed using Statistica Software (Tulsa, OK, USA). All variables were tested for normality and variance homogeneity. Data were analyzed using two-way ANOVA followed by planned comparisons or Student's *t*-test when appropriate. A "*p*-value" inferior to 0.05 was considered statistically significant. The data were expressed as means ± SD.



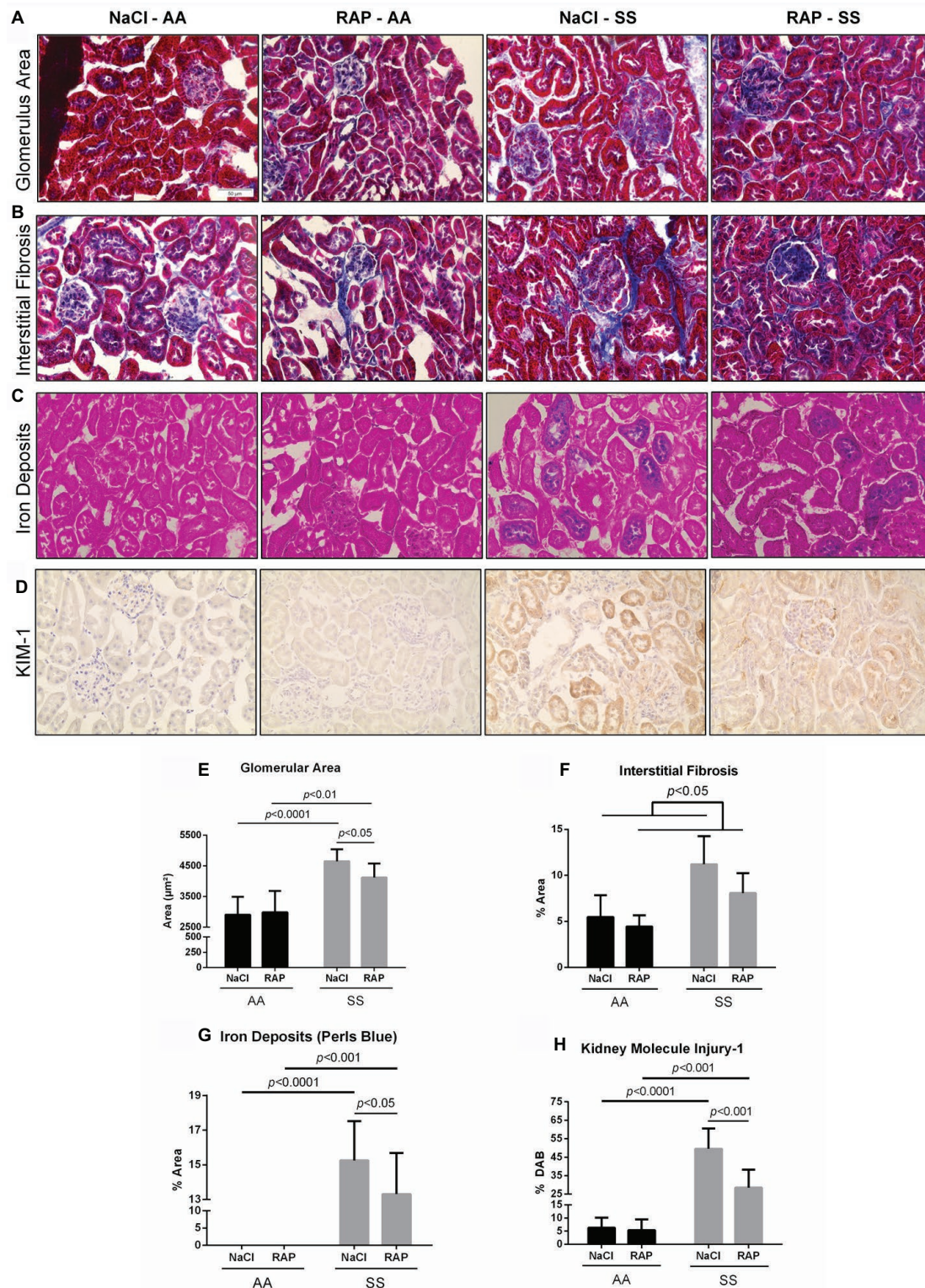


**FIGURE 1 |** Histopathological analysis of changes in morphology of 11- to 12-week-old AA and SS mice kidneys after 3 weeks of treatment with RAGE antagonist peptide. Representative images with Masson's trichrome staining (**A,B**) for determining glomerular area and interstitial fibrosis and Perl's Blue staining (**C**) for determining iron deposits (**D**) representative images of KIM-1 stained kidney sections. Magnification:  $\times 400$ . Quantification of glomerular area (**E**), interstitial fibrosis (**F**), tubular iron deposits (**G**), and KIM-1 expression (**H**). Values are means  $\pm$  SD. NaCl-AA ( $n = 6$ ; three females and three males), RAP-AA ( $n = 6$ ; four females and two males), NaCl-SS ( $n = 7$ ; three females and four males), RAP-SS ( $n = 7$ ; three females and four males). Scale bar = 50  $\mu$ m.

## RESULTS

### Receptor for Advanced Glycation End Product Blockade Blunts Kidney Damage in SS mice

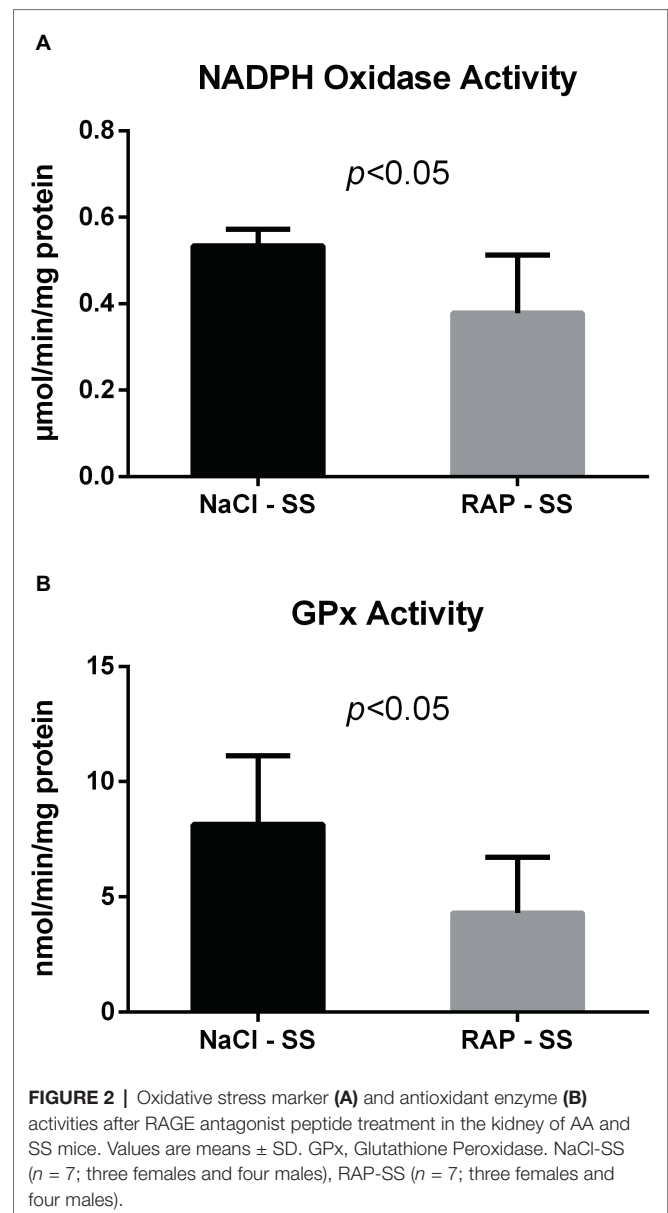
Renal histology as assessed by Masson's trichrome staining revealed glomerular hypertrophy demonstrated by higher glomerular area ( $p < 0.05$ ; **Figures 1A,E**) and higher interstitial fibrosis ( $p < 0.05$ ; **Figures 1B,F**) in SS compared to AA mice. Remarkably, RAGE inhibition lowered the glomerular area in SS mice ( $p < 0.05$ ; **Figures 1A,E**). In addition, an overall treatment effect on interstitial fibrosis was detectable in the RAP-treated group compared with the NaCl-treated group ( $p < 0.05$ ; **Figures 1B,F**). Marked accumulation of iron deposits was observed on kidney sections of SS mice stained by Perl's Blue compared to their AA littermates ( $p < 0.01$ ; **Figures 1C,G**) but the number of iron-positive tubules was significantly decreased in RAP-SS compared to NaCl-SS mice (**Figures 1C,G**). Finally, while tubular and glomerular accumulation of KIM-1 was exacerbated in SS compared to AA mice, RAGE blockade blunted KIM-1 immunostaining in SS when compared to NaCl-SS mice (**Figures 1D,H**). Results were similar between male and female mice (data not shown).

### Receptor for Advanced Glycation End Product Inhibition Modulates NADPH Oxidase and Glutathione Peroxidase Activity in SS mice

We next examined whether NADPH oxidase – which can be activated by RAGE (Wautier et al., 2001) – was modulated by RAGE antagonist peptide (RAP) treatment in the kidney of sickle cell mice. Both NADPH oxidase and GPx activities were reduced in the kidney of RAP-SS compared to NaCl-SS mice ( $p < 0.05$ ; **Figure 2**).

### Blockade With Receptor for Advanced Glycation End Product Antagonist Peptide Decreases Kidney Inflammation

To further understand the role of RAGE on kidney pathophysiology in sickle cell mice, we assessed NF- $\kappa$ B protein expression and TNF- $\alpha$  gene expression, key pro-inflammatory molecule acting downstream of the RAGE pathway. After 3 weeks of treatment, phosphorylated NF- $\kappa$ Bp65 Ser536 staining was lower ( $p < 0.05$ ) in RAP-SS compared to NaCl-SS mice (**Figures 3A,B**). RAP treatment did not significantly change ( $p = 0.06$ ) total NF- $\kappa$ Bp65 expression on SS mice kidney sections in comparison with their NaCl-treated littermates (**Figures 3C,D**). Finally, TNF- $\alpha$  mRNA expression was five times greater in the kidney of NaCl-SS (**Table 1**) than in NaCl-AA mice. In contrast, TNF- $\alpha$  mRNA was significantly reduced in RAP-SS kidney ( $p < 0.05$ ; **Table 1**) compared with that of NaCl-SS. The seemingly present increase in TNF- $\alpha$  mRNA after RAP is not significant in the AA group. No significant difference was detected for IL-1, IL-6,



and VCAM-1 mRNA expression in SS group after RAP treatment (**Table 1**).

### Receptor for Advanced Glycation End Product Inhibition Limits Anemia

Hematological changes are detailed in **Figure 4**. MCV, RDW, MCH, WBCs, and reticulocyte count were significantly higher in the SS group while MCHC, hematocrit, RBCs, and hemoglobin level were lower in SS mice than in their AA littermates (**Table 2, Figure 4**). In RAP-treated SS mice, there was no treatment effect on WBCs (**Table 2**). However, RBC count and hemoglobin level were increased ( $p < 0.05$ ; **Figures 4A–C**). Sickle cell percentage as well as reticulocyte count decreased in RAP-treated SS compared to NaCl-SS mice ( $p < 0.05$ ; **Figures 4D,E**).



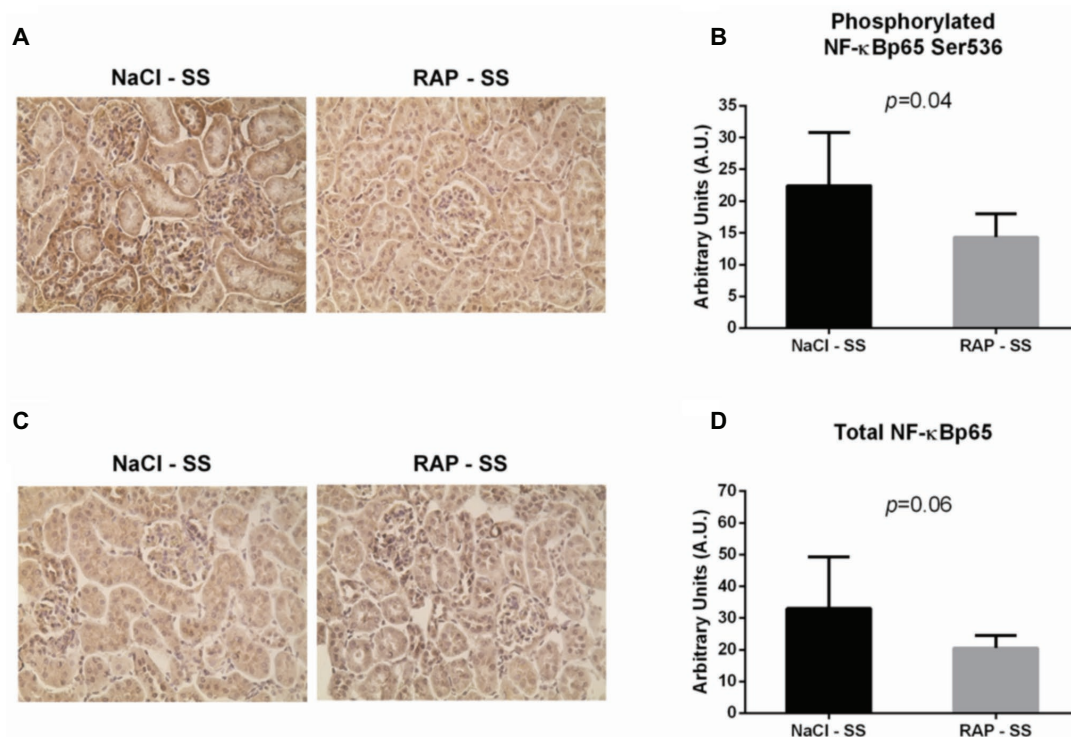


**FIGURE 3 |** Effect of RAP treatment on protein and mRNA expression of molecules acting downstream of the RAGE signaling pathway. Kidney sections from NaCl-SS and RAP-SS mice were subjected to immunohistochemistry using anti-NF-κBp65 IgG (A) and anti-phosphorylated NF-κBp65 Ser 536 IgG (B). Magnification:  $\times 400$ . Staining score (C,D) was determined using ImageJ plugin "Immunoratio". Values are means  $\pm$  SD. NaCl-SS ( $n = 7$ ; three females and four males), RAP-SS ( $n = 7$ ; three females and four males).

**TABLE 1 |** Renal mRNA expression of inflammatory and adhesion cell markers in NaCl- or RAP-treated AA and SS mice.

|                               | NaCl-AA             | RAP-AA              | NaCl-SS              | RAP-SS                             |
|-------------------------------|---------------------|---------------------|----------------------|------------------------------------|
| TNF- $\alpha$ (No. of copies) | 50.1 $\pm$ 49.5     | 110.4 $\pm$ 88.7    | 247.3 $\pm$ 187.2*   | 132.9 $\pm$ 105.4 <sup>§</sup>     |
| IL-1 $\beta$ (No. of copies)  | 261.0 $\pm$ 173.7   | 232.8 $\pm$ 89.6    | 578.9 $\pm$ 254.9    | 602.2 $\pm$ 299.9 <sup>†</sup>     |
| IL-6 (No. of copies)          | 93.3 $\pm$ 97.8     | 36.0 $\pm$ 25.6     | 113.6 $\pm$ 59.8     | 185.1 $\pm$ 191.0                  |
| VCAM-1 (No. of copies)        | 4905.5 $\pm$ 4601.6 | 7716.9 $\pm$ 2556.3 | 13790.8 $\pm$ 6839.5 | 25046.9 $\pm$ 19009.7 <sup>†</sup> |

IL-1 $\beta$ , Interleukin-1 $\beta$ ; IL-6, Interleukin-6; VCAM-1, Vascular Cell Adhesion Molecule-1.

\* $p < 0.01$  vs. NaCl-AA; <sup>†</sup> $p < 0.05$  vs. RAP-AA; <sup>§</sup> $p < 0.05$  vs. NaCl-SS.

NaCl-AA ( $n = 6$ ; three females and three males), RAP-AA ( $n = 6$ ; four females and two males), NaCl-SS ( $n = 7$ ; three females and four males), RAP-SS ( $n = 7$ ; three females and four males).

## DISCUSSION

The current study aimed to investigate the effect of RAGE inhibition on markers of kidney damage as well as on markers of oxidative stress and inflammation in the kidney of homozygous sickle mice. In support of our hypothesis, the results of the present study demonstrated for the first time that a RAGE blockade (1) dampened kidney damage, as evidenced by reduced glomerular hypertrophy, interstitial fibrosis, iron deposition, and KIM-1 protein expression in SS mice; (2) reduced the activation of both NADPH oxidase and NF-κBp65 acting downstream of the AGE/RAGE signaling pathway; (3) increased hematocrit, RBC count, and hemoglobin level, and decreased reticulocyte count and sickle cell count in SS mice.

While SS mice displayed common renal manifestations of SCD, i.e., glomerular hypertrophy (Elfenbein et al., 1974; Bhathena and Sondheimer, 1991), interstitial fibrosis (Walker et al., 1971; Alhwiesh, 2014), iron overload (Walker et al., 1971; Buckalew and Someren, 1974), and KIM-1 overexpression (Sundaram et al., 2011; Hamideh et al., 2014) – a specific marker of tubular injuries – RAP treatment minimized kidney injuries in these mice. Our findings are in agreement with those of a previous study performed in diabetic mice where administration of soluble RAGE reduced glomerular area (Wendt et al., 2003). In nephropathies, it was reported that glomerular hypertrophy results from podocyte hypertrophy and extracellular matrix (ECM) accumulation (Li et al., 2007), and RAGE activation was shown to contribute to both of these pathological

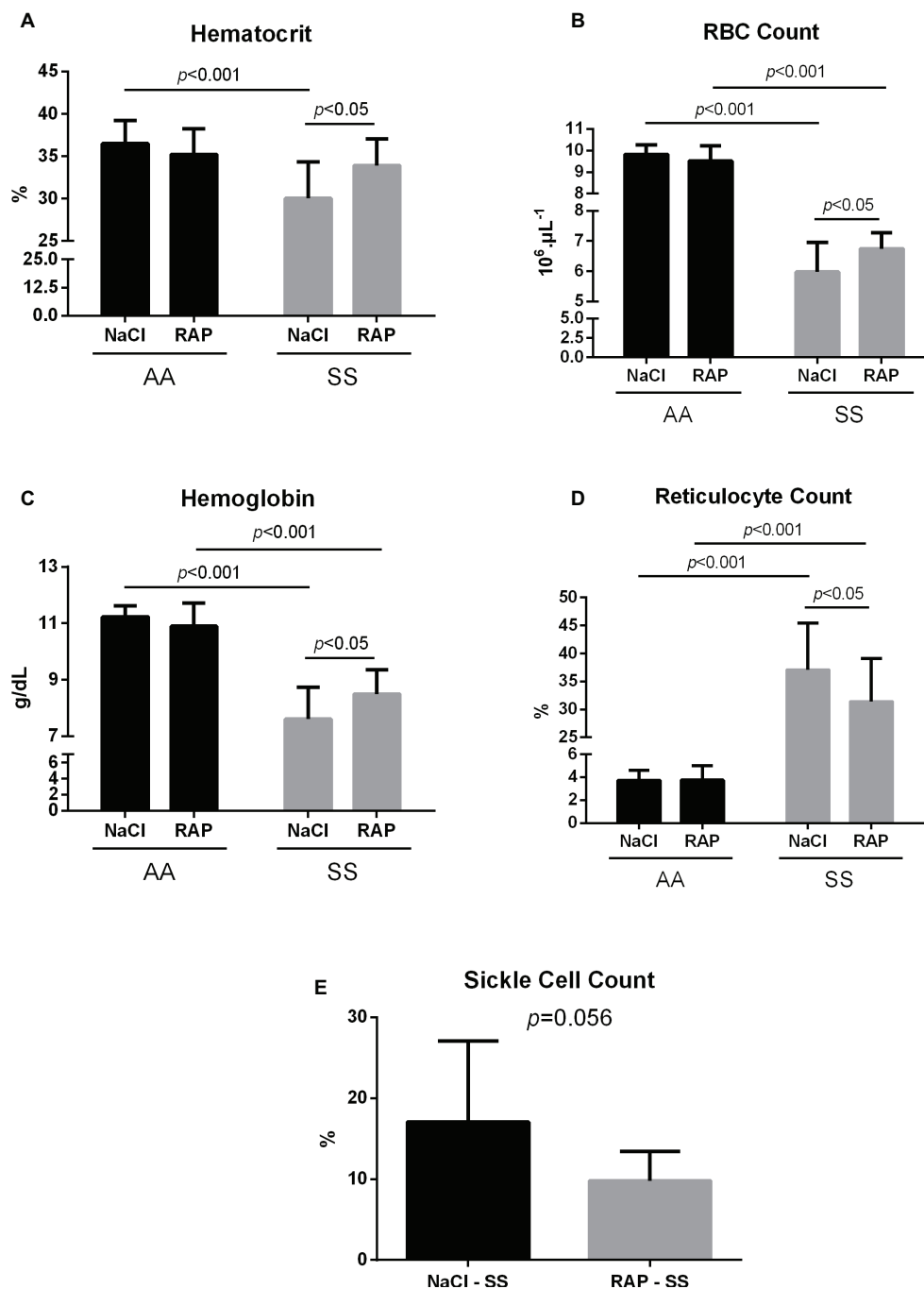


**FIGURE 4 |** Mean hematocrit (A), red blood cell count (B), hemoglobin levels (C), reticulocyte count (D), and sickle cell count (E) after treatment in AA and SS mice. Values are means  $\pm$  SD. RBC: Red Blood Cell. NaCl-AA ( $n = 13$ ; five females and eight males), RAP-AA ( $n = 12$ ; seven females and five males), NaCl-SS ( $n = 10$ ; five females and five males), RAP-SS ( $n = 9$ ; four females and five males).

changes (Liebisch et al., 2014; Zhao et al., 2014). Through the inhibition of the expression of the protein NIPPI1, AGE/RAGE interaction induced cell cycle arrest and concomitant podocyte hypertrophy. Interestingly, the activation of this pathway was NF- $\kappa$ B/TNF- $\alpha$  dependent (Liebisch et al., 2014). Similarly, ECM accumulation has been shown to be mediated

by the AGE/RAGE axis and the NF- $\kappa$ B signaling pathway, which are involved in ECM synthesis and myofibroblast differentiation (Zhao et al., 2014). Thus, both glomerular hypertrophy and interstitial fibrosis – which also results from ECM accumulation in the interstitium and myofibroblast differentiation (Farris and Colvin, 2012) – may be sustained

**TABLE 2 |** Hematological indices in NaCl- or RAP-treated AA and SS mice.

|  | NaCl-AA    | RAP-AA     | NaCl-SS     | RAP-SS       |
|--|------------|------------|-------------|--------------|
| MCV (fl)   | 37.2 ± 2.5 | 37.2 ± 2.0 | 50.6 ± 4.1* | 50.2 ± 2.2†  |
| RDW (%)  | 15.3 ± 0.6 | 15.3 ± 1.1 | 23.0 ± 2.1* | 22.4 ± 1.5†  |
| MCHC (g dl <sup>-1</sup> )                       | 31.3 ± 0.8 | 30.9 ± 1.7 | 25.3 ± 0.9* | 25.2 ± 0.8†  |
| MCH (pg)   | 12.0 ± 0.9 | 11.5 ± 0.5 | 12.8 ± 0.9* | 12.7 ± 0.7†  |
| WBC (10 <sup>3</sup> µl <sup>-1</sup> )          | 4.8 ± 1.2  | 4.2 ± 1.9  | 43.2 ± 6.7* | 47.7 ± 11.0† |
| Lymphocytes (10 <sup>3</sup> µl <sup>-1</sup> )  | 3.6 ± 0.8  | 3.3 ± 1.5  | 38.1 ± 6.1* | 42.9 ± 9.3†  |
| Monocytes (10 <sup>3</sup> µl <sup>-1</sup> )    | 0.4 ± 0.2  | 0.3 ± 0.2  | 2.2 ± 0.8*  | 1.9 ± 0.8†   |
| Granulocytes (10 <sup>3</sup> µl <sup>-1</sup> ) | 0.9 ± 0.4  | 0.6 ± 0.3  | 2.9 ± 1.4*  | 2.9 ± 1.9†   |

Values are presented as means ± SD. MCV, Mean corpuscular volume; RDW, Red blood cell distribution width; MCHC, Mean corpuscular hemoglobin concentration; MCH, Mean corpuscular hemoglobin; WBC, White blood cell.

\**p* < 0.001 vs. NaCl-AA; †*p* < 0.001 vs. RAP-AA.

NaCl-AA (*n* = 13; five females and eight males), RAP-AA (*n* = 12; seven females and five males), NaCl-SS (*n* = 10; five females and five males), RAP-SS (*n* = 9; four females and five males).

by AGE/RAGE/NF-κB signaling in sickle cell mice. Nevertheless, additional quantitative measurements on the expression of fibrosis markers (i.e., Col1α1, α-SMA, Vimentin, Fibronectin) are required to confirm this assumption. Tubular iron deposition is a common feature of SCD, as free plasma HbS pass through the glomerular filtration barrier and are incorporated into renal tubules (Nath and Hebbel, 2015). As iron deposits in the cortex of SCD patients were associated with intravascular hemolysis, one could hypothesize that the decrease in tubular iron deposits measured in our SS mice might be related to the reduced anemia we observed after RAP treatment. Interestingly, we observed an increase in hematocrit, RBC count, and hemoglobin level and a decrease in reticulocyte count in RAP-treated sickle mice that could suggest that RAGE may play a significant role in anemia. This finding could most likely be explained by decreased hemolysis rather than increased erythropoietic process, as a previous study reported a role of AGEs in the pathophysiology of chronic hemolysis-associated organ complications in SCD (Nur et al., 2010). Nevertheless, further studies are required to elucidate the role of the AGE/RAGE pathway on hemolytic processes. Finally, KIM-1 is commonly used to assess acute tubular injury as it is expressed specifically on damaged tubules but is undetectable in healthy ones (van Timmeren et al., 2007). In a recent study, urinary KIM-1 levels were reduced in diabetic RAGE-KO mice compared to diabetic wildtype mice (Thallas-Bonke et al., 2013), which is consistent with the results in the present study. Furthermore, KIM-1 has been shown to be associated with renal fibrosis and inflammation (Humphreys et al., 2013), which further supports the implication of the RAGE signaling pathway in SCD-related kidney disease.

Considerable evidence demonstrates increased oxidative stress in sickle cell disease (Chirico and Pialoux, 2012; Charrin et al., 2016). The primary mechanism by which RAGE generates oxidative stress is *via* the activation of NADPH oxidase (Gao et al., 2008). The downward RAP treatment effect on renal NADPH oxidase activity could suggest blunted basal oxidative stress in mice treated with RAGE antagonist that may explain the lower GPx activity in RAP-SS compared to vehicle-SS mice.

This hypothesis is supported by previous work showing reduced NADPH oxidase activity and nitrotyrosine levels in a glomerulosclerosis mouse model either knocked-out for RAGE or treated with soluble RAGEs (sRAGEs) (Guo et al., 2008). In these mice, RAGE blockade also improved albuminuria and limited glomerular sclerosis. Additionally, other studies reported decreased intracellular reactive oxygen species (ROS) after inhibition of RAGE with either RAGE-shRNA in renal fibroblasts (Chen et al., 2010) or RAGE antibody in renal mesangial cells (Ide et al., 2010). Collectively, our data strongly suggest that RAGE blockade is likely to ameliorate oxidative stress status in the kidney of sickle mice and may further support the hypothesis of a reduced anemia after RAP treatment.

As inflammation plays a key role in the pathophysiology of SCD (Hoppe, 2014) and is potentiated by RAGE activation (Goldin et al., 2006), we assessed protein expression of a key inflammatory molecule, i.e., NF-κBp65, and one of its target genes (i.e., TNF-α) at the mRNA level (Figure 3, Table 1). In the kidney of our vehicle-SS Townes mice, the high gene expression of pro-inflammatory cytokine TNF-α strengthens the assumption of a renal pro-inflammatory state in SCD (Akohoue et al., 2007; Hebbel et al., 2009; Krishnan et al., 2010). Interestingly, RAP treatment dampened phosphorylated NF-κBp65 expression in our SS mice. Consistent with this, it was reported that blockade of RAGE with either soluble RAGE or FPS-ZM1 suppressed NF-κB pathway in a murine model of systolic overload-induced heart failure (Liu et al., 2016). In addition, Flyvbjerg et al. reported a decrease in renal NF-κB expression along with an overall improvement of kidney function after treatment with RAGE antibody in obese Type 2 diabetic mice (Flyvbjerg et al., 2004). Thus, in the present study, inhibition of NF-κB in RAP-SS mice could explain the reduction of TNF-α mRNA levels to close to the levels observed in healthy mice. In line with this observation, recent studies showed decreased cardiac TNF-α mRNA expression in a mouse model of inflammatory heart disease knocked-out for RAGE (Bangert et al., 2016) and lower hepatic TNF-α mRNA in RAGE-/- mice after ischemia/reperfusion injury (Zeng et al., 2009). A similar drop in aortic TNF-α mRNA occurred in sinoaortic denervated rats treated with sRAGEs, acting as a decoy for RAGE (Wu et al., 2013). In this context, our data suggest that RAGE inhibition could weaken pro-inflammatory processes in the kidney of sickle cell mice.

In conclusion, our data suggest that specific inhibition of RAGE could blunt anemia-related markers. Both RAP-mediated reduced oxidative stress markers and decreased pro-inflammatory molecule expression might take part in reducing the hemolytic process as well as the glomerular hypertrophy, interstitial fibrosis, and iron deposits in the kidney of sickle cell mice. Although further studies are warranted to elucidate the role of RAGE on kidney function in sickle cell disease, our data demonstrate that this receptor seems to be an important pathogenic factor in the development of renal changes in SCD mice. Only one clinical grade antagonist of RAGE (Azelaagon: TTP488) has been tested in Alzheimer's disease patients only, in Phase I, II

(Burstein et al., 2014, BMC Neurobiol.), and III clinical trials (NCT02080364, Clinicaltrial.gov). Results of Phase III are not available at this time.

## Limitations

Our study has some limitations. The study was primarily designed to investigate acute effects of RAGE inhibition on sickle cell mice. Therefore, no functional nor mechanistic experiments were performed and thus no definitive conclusions about kidney function can be drawn.

## ETHICS STATEMENT

Comité d'Éthique en Expérimentation Animale CEEA-55 Project 2017020817227030\_v1.

## REFERENCES

- Ahmed, N. (2005). Advanced glycation endproducts—role in pathology of diabetic complications. *Diabetes Res. Clin. Pract.* 67, 3–21. doi: 10.1016/j.diabres.2004.09.004
- Akhoue, S. A., Shankar, S., Milne, G. L., Morrow, J., Chen, K. Y., Ajayi, W. U., et al. (2007). Energy expenditure, inflammation, and oxidative stress in steady-state adolescents with sickle cell anemia. *Pediatr. Res.* 61, 233–238. doi: 10.1203/pdr.0b013e31802d7754
- Alhwiesh, A. (2014). An update on sickle cell nephropathy. *Saudi J. Kidney Dis. Transpl.* 25, 249–265. doi: 10.4103/1319-2442.128495
- Arumugam, T., Ramachandran, V., Gomez, S. B., Schmidt, A. M., and Logsdon, C. D. (2012). S100P-derived RAGE antagonistic peptide reduces tumor growth and metastasis. *Clin. Cancer Res.* 18, 4356–4364. doi: 10.1158/1078-0432.CCR-12-0221
- Ballas, S. K., and Mohandas, N. (1996). Pathophysiology of vaso-occlusion. *Hematol. Oncol. Clin. North Am.* 10, 1221–1239. doi: 10.1016/S0889-8588(05)70396-8
- Bangert, A., Andrassy, M., Müller, A.-M., Bockstahler, M., Fischer, A., Volz, C. H., et al. (2016). Critical role of RAGE and HMGB1 in inflammatory heart disease. *Proc. Natl. Acad. Sci. USA* 113, E155–E164. doi: 10.1073/pnas.1522881113
- Bhathena, D. B., and Sondheimer, J. H. (1991). The glomerulopathy of homozygous sickle hemoglobin (SS) disease: morphology and pathogenesis. *J. Am. Soc. Nephrol.* 1, 1241–1252.
- Buckalew, V. M., and Someren, A. (1974). Renal manifestations of sickle cell disease. *Arch. Intern. Med.* 133, 660–669. doi: 10.1001/archinte.1974.00320160154014
- Burstein, A. H., Grimes, I., Galasko, D. R., Aisen, P. S., Sabbagh, M., and Mjalli, A. M. (2014). Effect of TTP488 in patients with mild to moderate Alzheimer's disease. *BMC Neurol.* 14:12. doi: 10.1186/1471-2377-14-12
- Charrin, E., Aufradet, E., Douillard, A., Romdhani, A., Souza, G. D., Bessaad, A., et al. (2015). Oxidative stress is decreased in physically active sickle cell SAD mice. *Br. J. Haematol.* 168, 747–756. doi: 10.1111/bjh.13207
- Charrin, E., Ofori-Acquah, S. F., Nader, E., Skinner, S., Connes, P., Pialoux, V., et al. (2016). Inflammatory and oxidative stress phenotypes in transgenic sickle cell mice. *Blood Cells Mol. Dis.* 62, 13–21. doi: 10.1016/j.bcmd.2016.10.020
- Chen, S.-C., Guh, J.-Y., Hwang, C.-C., Chiou, S.-J., Lin, T.-D., Ko, Y.-M., et al. (2010). Advanced glycation end-products activate extracellular signal-regulated kinase via the oxidative stress-EGF receptor pathway in renal fibroblasts. *J. Cell. Biochem.* 109, 38–48. doi: 10.1002/jcb.22376
- Chirico, E. N., and Pialoux, V. (2012). Role of oxidative stress in the pathogenesis of sickle cell disease. *IUBMB Life* 64, 72–80. doi: 10.1002/iub.584
- Connes, P., Renoux, C., Romana, M., Abkarian, M., Joly, P., Martin, C., et al. (2018). Blood rheological abnormalities in sickle cell anemia. *Clin. Hemorheol. Microcirc.* 68, 165–172. doi: 10.3233/CH-189005
- Conran, N., and Belcher, J. D. (2018). Inflammation in sickle cell disease. *Clin. Hemorheol. Microcirc.* 68, 263–299. doi: 10.3233/CH-189012

## AUTHOR CONTRIBUTIONS

EC and CM participated in the design of the study. EC, CF, and AS performed the experiments. EC, CF, SS, VP, PJ, PC, and CM wrote the manuscript.

## FUNDING

This study was conducted with research funding from Institut Universitaire de France (to PC and VP).

## ACKNOWLEDGMENTS

We thank Patrice Del Carmine for technical support.

- Cooper, M. E. (2004). Importance of advanced glycation end products in diabetes-associated cardiovascular and renal disease. *Am. J. Hypertens.* 17, 31S–38S. doi: 10.1016/j.amjhyper.2004.08.021
- Elfenbein, I. B., Patchefsky, A., Schwartz, W., and Weinstein, A. G. (1974). Pathology of the glomerulus in sickle cell anemia with and without nephrotic syndrome. *Am. J. Pathol.* 77, 357–374.
- Farris, A. B., and Colvin, R. B. (2012). Renal interstitial fibrosis: mechanisms and evaluation in: current opinion in nephrology and hypertension. *Curr. Opin. Nephrol. Hypertens.* 21, 289–300. doi: 10.1097/MNH.0b013e3283521cfa
- Flyvbjerg, A., Denner, L., Schrijvers, B. F., Tilton, R. G., Mogensen, T. H., Paludan, S. R., et al. (2004). Long-term renal effects of a neutralizing RAGE antibody in obese type 2 diabetic mice. *Diabetes* 53, 166–172. doi: 10.2337/diabetes.53.1.166
- Gao, X., Zhang, H., Schmidt, A. M., and Zhang, C. (2008). AGE/RAGE produces endothelial dysfunction in coronary arterioles in type 2 diabetic mice. *Am. J. Physiol. Heart Circ. Physiol.* 295, H491–H498. doi: 10.1152/ajpheart.00464.2008
- Genuth, S., Sun, W., Cleary, P., Sell, D. R., Dahms, W., Malone, J., et al. (2005). Glycation and carboxymethyllysine levels in skin collagen predict the risk of future 10-year progression of diabetic retinopathy and nephropathy in the diabetes control and complications trial and epidemiology of diabetes interventions and complications participants with type 1 diabetes. *Diabetes* 54, 3103–3111. doi: 10.2337/diabetes.54.11.3103
- Goldin, A., Beckman, J. A., Schmidt, A. M., and Creager, M. A. (2006). Advanced glycation end products sparking the development of diabetic vascular injury. *Circulation* 114, 597–605. doi: 10.1161/CIRCULATIONAHA.106.621854
- Guo, J., Ananthakrishnan, R., Qu, W., Lu, Y., Reiniger, N., Zeng, S., et al. (2008). RAGE mediates podocyte injury in adriamycin-induced glomerulosclerosis. *J. Am. Soc. Nephrol.* 19, 961–972. doi: 10.1681/ASN.2007101109
- Guo, W. A., Knight, P. R., and Raghavendran, K. (2012). The receptor for advanced glycation end products and acute lung injury/acute respiratory distress syndrome. *Intensive Care Med.* 38, 1588–1598. doi: 10.1007/s00134-012-2624-y
- Hamideh, D., Raj, V., Harrington, T., Li, H., Margolles, E., Amole, F., et al. (2014). Albuminuria correlates with hemolysis and NAG and KIM-1 in patients with sickle cell anemia. *Pediatr. Nephrol.* 29, 1997–2003. doi: 10.1007/s00467-014-2821-8
- Hebbel, R. P., Vercellotti, G. M., and Nath, K. A. (2009). A systems biology consideration of the vasculopathy of sickle cell anemia: the need for multi-modality chemo-prophylaxis. *Cardiovasc. Hematol. Disord. Drug Targets* 9, 271–292. doi: 10.2174/1871529X10909040271
- Hoppe, C. C. (2014). Inflammatory mediators of endothelial injury in sickle cell disease. *Hematol. Oncol. Clin. North Am.* 28, 265–286. doi: 10.1016/j.hoc.2013.11.006
- Huebschmann, A. G., Regensteiner, J. G., Vlassara, H., and Reusch, J. E. B. (2006). Diabetes and advanced glycoxidation end products. *Diabetes Care* 29, 1420–1432. doi: 10.2337/dc05-2096



- Humphreys, B. D., Xu, F., Sabbiseti, V., Grgic, I., Naini, S. M., Wang, N., et al. (2013). Chronic epithelial kidney injury molecule-1 expression causes murine kidney fibrosis. *J. Clin. Invest.* 123, 4023–4035. doi: 10.1172/JCI45361
- Ide, Y., Matsui, T., Ishibashi, Y., Takeuchi, M., and Yamagishi, S. (2010). Pigment epithelium-derived factor inhibits advanced glycation end product-elicited mesangial cell damage by blocking NF- $\kappa$ B activation. *Microvasc. Res.* 80, 227–232. doi: 10.1016/j.mvr.2010.03.015
- Kashyap, L., Alsaheel, A., Ranck, M., Gardner, R., Maynard, J., and Chalew, S. A. (2018). Sickle cell disease is associated with elevated levels of skin advanced glycation endproducts. *J. Pediatr. Hematol. Oncol.* 40, 285–289. doi: 10.1097/MPH.0000000000001128
- Koyama, Y., Takeishi, Y., Arimoto, T., Niizeki, T., Shishido, T., Takahashi, H., et al. (2007). High serum level of pentosidine, an advanced glycation end product (AGE), is a risk factor of patients with heart failure. *J. Card. Fail.* 13, 199–206. doi: 10.1016/j.cardfail.2006.11.009
- Krishnan, S., Setty, Y., Betal, S. G., Vijender, V., Rao, K., Dampier, C., et al. (2010). Increased levels of the inflammatory biomarker C-reactive protein at baseline are associated with childhood sickle cell vasocclusive crises. *Br. J. Haematol.* 148, 797–804. doi: 10.1111/j.1365-2141.2009.08013.x
- Li, J. J., Kwak, S. J., Jung, D. S., Kim, J.-J., Yoo, T.-H., Ryu, D.-R., et al. (2007). Podocyte biology in diabetic nephropathy. *Kidney Int. Suppl.* 106, S36–S42. doi: 10.1038/sj.ki.5002384
- Liebisch, M., Bondeva, T., Franke, S., Daniel, C., Amann, K., and Wolf, G. (2014). Activation of the receptor for advanced glycation end products induces nuclear inhibitor of protein phosphatase-1 suppression. *Kidney Int.* 86, 103–117. doi: 10.1038/ki.2014.3
- Liu, Y., Yu, M., Zhang, Z., Yu, Y., Chen, Q., Zhang, W., et al. (2016). Blockade of receptor for advanced glycation end products protects against systolic overload-induced heart failure after transverse aortic constriction in mice. *Eur. J. Pharmacol.* 791, 535–543. doi: 10.1016/j.ejphar.2016.07.008
- Meerwaldt, R., Links, T., Zeebregts, C., Tio, R., Hillebrands, J.-L., and Smit, A. (2008). The clinical relevance of assessing advanced glycation endproducts accumulation in diabetes. *Cardiovasc. Diabetol.* 7:29. doi: 10.1186/1475-2840-7-29
- Miyata, T., Ishiguro, N., Yasuda, Y., Ito, T., Nangaku, M., Iwata, H., et al. (1998). Increased pentosidine, an advanced glycation end product, in plasma and synovial fluid from patients with rheumatoid arthritis and its relation with inflammatory markers. *Biochem. Biophys. Res. Commun.* 244, 45–49. doi: 10.1006/bbrc.1998.8203
- Nath, K. A., and Heibel, R. P. (2015). Sickle cell disease: renal manifestations and mechanisms. *Nat. Rev. Nephrol.* 11, 161–171. doi: 10.1038/nrneph.2015.8
- Nur, E., Brandjes, D. P., Schnog, J.-J. B., Otten, H.-M., Fijnvandraat, K., Schalkwijk, C. G., et al. (2010). Plasma levels of advanced glycation end products are associated with haemolysis-related organ complications in sickle cell patients. *Br. J. Haematol.* 151, 62–69. doi: 10.1111/j.1365-2141.2010.08320.x
- Paglia, D. E., and Valentine, W. N. (1967). Studies on the quantitative and qualitative characterization of erythrocyte glutathione peroxidase. *J. Lab. Clin. Med.* 70, 158–169.
- Platt, O. S., Brambilla, D. J., Rosse, W. F., Milner, P. F., Castro, O., Steinberg, M. H., et al. (1994). Mortality in sickle cell disease—life expectancy and risk factors for early death. *N. Engl. J. Med.* 330, 1639–1644. doi: 10.1056/NEJM199406093302303
- Rees, D. C., Williams, T. N., and Gladwin, M. T. (2010). Sickle-cell disease. *Lancet* 376, 2018–2031. doi: 10.1016/S0140-6736(10)61029-X
- Rojas, A., Romay, S., González, D., Herrera, B., Delgado, R., and Otero, K. (2000). Regulation of endothelial nitric oxide synthase expression by albumin-derived advanced glycosylation end products. *Circ. Res.* 86, e50–e54. doi: 10.1161/01.RES.86.3.e50
- Singh, R., Barden, A., Mori, T., and Beilin, L. (2001). Advanced glycation end-products: a review. *Diabetologia* 44, 129–146. doi: 10.1007/s001250051591
- Somjee, S. S., Warrier, R. P., Thomson, J. L., Ory-Ascani, J., and Hempe, J. M. (2005). Advanced glycation end-products in sickle cell anaemia. *Br. J. Haematol.* 128, 112–118. doi: 10.1111/j.1365-2141.2004.05274.x
- Sparkenbaugh, E., and Pawlinski, R. (2013). Interplay between coagulation and vascular inflammation in sickle cell disease. *Br. J. Haematol.* 162, 3–14. doi: 10.1111/bjh.12336
- Sundaram, N., Bennett, M., Wilhelm, J., Kim, M.-O., Atweh, G., Devarajan, P., et al. (2011). Biomarkers for early detection of sickle nephropathy. *Am. J. Hematol.* 86, 559–566. doi: 10.1002/ajh.22045
- Tan, A. L. Y., Forbes, J. M., and Cooper, M. E. (2007). AGE, RAGE, and ROS in diabetic nephropathy. *Semin. Nephrol.* 27, 130–143. doi: 10.1016/j.semnephrol.2007.01.006
- Tanji, N., Markowitz, G. S., Fu, C., Kislinger, T., Taguchi, A., Pischetsrieder, M., et al. (2000). Expression of advanced glycation end products and their cellular receptor RAGE in diabetic nephropathy and nondiabetic renal disease. *J. Am. Soc. Nephrol.* 11, 1656–1666.
- Thallas-Bonke, V., Coughlan, M. T., Tan, A. L., Harcourt, B. E., Morgan, P. E., Davies, M. J., et al. (2013). Targeting the AGE-RAGE axis improves renal function in the context of a healthy diet low in advanced glycation end-product content. *Nephrology* 18, 47–56. doi: 10.1111/j.1440-1797.2012.01665.x
- Tuominen, V. J., Ruotoistenmäki, S., Viitanen, A., Jumppanen, M., and Isola, J. (2010). ImmunoRatio: a publicly available web application for quantitative image analysis of estrogen receptor (ER), progesterone receptor (PR), and Ki-67. *Breast Cancer Res.* 12:R56. doi: 10.1186/bcr2615
- van Beers, E. J., and van Wijk, R. (2018). Oxidative stress in sickle cell disease; more than a DAMP squib. *Clin. Hemorheol. Microcirc.* 68, 239–250. doi: 10.3233/CH-189010
- van Timmeren, M. M., van den Heuvel, M. C., Bailly, V., Bakker, S. J. L., van Goor, H., and Stegeman, C. A. (2007). Tubular kidney injury molecule-1 (KIM-1) in human renal disease. *J. Pathol.* 212, 209–217. doi: 10.1002/path.2175
- Walker, B. R., Alexander, F., Birdsall, T. R., and Warren, R. L. (1971). Glomerular lesions in sickle cell nephropathy. *JAMA* 215, 437–440. doi: 10.1001/jama.1971.03180160037009
- Wautier, M.-P., Chappey, O., Corda, S., Stern, D. M., Schmidt, A. M., and Wautier, J.-L. (2001). Activation of NADPH oxidase by AGE links oxidant stress to altered gene expression via RAGE. *Am. J. Physiol. Endocrinol. Metab.* 280, E685–E694. doi: 10.1152/ajpendo.2001.280.5.E685
- Wendt, T. M., Tanji, N., Guo, J., Kislinger, T. R., Qu, W., Lu, Y., et al. (2003). RAGE drives the development of glomerulosclerosis and implicates podocyte activation in the pathogenesis of diabetic nephropathy. *Am. J. Pathol.* 162, 1123–1137. doi: 10.1016/S0002-9440(10)63909-0
- Wood, K. C., Hsu, L. L., and Gladwin, M. T. (2008). Sickle cell disease vasculopathy: a state of nitric oxide resistance. *Free Radic. Biol. Med.* 44, 1506–1528. doi: 10.1016/j.freeradbiomed.2008.01.008
- Wu, F., Feng, J.-Z., Qiu, Y.-H., Yu, F.-B., Zhang, J.-Z., Zhou, W., et al. (2013). Activation of receptor for advanced glycation end products contributes to aortic remodeling and endothelial dysfunction in sinoaortic denervated rats. *Atherosclerosis* 229, 287–294. doi: 10.1016/j.atherosclerosis.2013.04.033
- Wu, L.-C., Sun, C.-W., Ryan, T. M., Pawlik, K. M., Ren, J., and Townes, T. M. (2006). Correction of sickle cell disease by homologous recombination in embryonic stem cells. *Blood* 108, 1183–1188. doi: 10.1182/blood-2006-02-004812
- Zeng, S., Dun, H., Ippagunta, N., Rosario, R., Zhang, Q. Y., Lefkowitz, J., et al. (2009). Receptor for advanced glycation end product (RAGE)-dependent modulation of early growth response-1 in hepatic ischemia/reperfusion injury. *J. Hepatol.* 50, 929–936. doi: 10.1016/j.jhep.2008.11.022
- Zhao, J., Randive, R., and Stewart, J. A. (2014). Molecular mechanisms of AGE/RAGE-mediated fibrosis in the diabetic heart. *World J. Diabetes* 5, 860–867. doi: 10.4239/wjd.v5.i6.860

**Conflict of Interest Statement:** The authors declare that the research was conducted in the absence of any commercial or financial relationships that could be construed as a potential conflict of interest.

Copyright © 2019 Charrin, Faes, Sotiaux, Skinner, Pialoux, Joly, Connes and Martin. This is an open-access article distributed under the terms of the Creative Commons Attribution License (CC BY). The use, distribution or reproduction in other forums is permitted, provided the original author(s) and the copyright owner(s) are credited and that the original publication in this journal is cited, in accordance with accepted academic practice. No use, distribution or reproduction is permitted which does not comply with these terms.



# CoDysAn: A Telemedicine Tool to Improve Awareness and Diagnosis for Patients With Congenital Dyserythropoietic Anemia

Cristian Tornador<sup>1,2</sup>, Edgar Sánchez-Prados<sup>3</sup>, Beatriz Cadenas<sup>4,5,6</sup>, Roberta Russo<sup>7,8</sup>, Veronica Venturi<sup>9</sup>, Immacolata Andolfo<sup>7,8</sup>, Ines Hernández-Rodríguez<sup>10</sup>, Achille Iolascon<sup>7,8</sup> and Mayka Sánchez<sup>1,9\*</sup>

<sup>1</sup> BloodGenetics S.L., Barcelona, Spain, <sup>2</sup> Teresa Moreto Foundation, Barcelona, Spain, <sup>3</sup> Bioinformatics for Health Sciences Master Programme, Universitat Pompeu Fabra, Barcelona, Spain, <sup>4</sup> Whole Genix SL., Barcelona, Spain, <sup>5</sup> Universitat de Vic-Universitat Central de Catalunya, Vic, Spain, <sup>6</sup> Iron Metabolism: Regulation and Diseases Group, Josep Carreras Leukaemia Research Institute, Campus Can Ruti, Barcelona, Spain, <sup>7</sup> Department of Molecular Medicine and Medical Biotechnologies, University of Naples Federico II, Naples, Italy, <sup>8</sup> CEINGE-Biotecnologie Avanzate, Naples, Italy, <sup>9</sup> Iron Metabolism: Regulation and Diseases Group, Department of Basic Sciences, Faculty of Medicine and Health Sciences, Universitat Internacional de Catalunya, Barcelona, Spain, <sup>10</sup> Haematology Service, Hospital Germans Trias i Pujol University Hospital, Oncology Catalan Institute, Barcelona, Spain

## OPEN ACCESS

### Edited by:

Richard Van Wijk,  
Utrecht University, Netherlands

### Reviewed by:

Anna Rita Migliaccio,  
Icahn School of Medicine at Mount  
Sinai, United States  
Pedro Cabrales,  
University of California, San Diego,  
United States

### \*Correspondence:

Mayka Sánchez  
msanchezfe@uic.es

### Specialty section:

This article was submitted to  
Red Blood Cell Physiology,  
a section of the journal  
Frontiers in Physiology

**Received:** 28 March 2019

**Accepted:** 02 August 2019

**Published:** 13 September 2019

### Citation:

Tornador C, Sánchez-Prados E, Cadenas B, Russo R, Venturi V, Andolfo I, Hernández-Rodríguez I, Iolascon A and Sánchez M (2019) CoDysAn: A Telemedicine Tool to Improve Awareness and Diagnosis for Patients With Congenital Dyserythropoietic Anemia. *Front. Physiol.* 10:1063. doi: 10.3389/fphys.2019.01063

Congenital Dyserythropoietic Anemia (CDA) is a heterogeneous group of hematological disorders characterized by chronic hyporegenerative anemia and distinct morphological abnormalities of erythroid precursors in the bone marrow. In many cases, a final diagnosis is not achieved due to different levels of awareness for the diagnosis of CDAs and lack of use of advanced diagnostic procedures. Researchers have identified five major types of CDA: types I, II, III, IV, and X-linked dyserythropoietic anemia and thrombocytopenia (XLDT). Proper management in CDA is still unsatisfactory, as the different subtypes of CDA have different genetic causes and different but overlapping patterns of signs and symptoms. For this reason, we developed a new telemedicine tool that will help doctors to achieve a faster diagnostic for this disease. Using open access code, we have created a responsive webpage named CoDysAn (**C**ongenital **D**yserythropoietic **A**nemia) that includes practical information for CDA awareness and a step-by-step diagnostic tool based on a CDA algorithm. The site is currently available in four languages (Catalan, Spanish, Italian, and English). This telemedicine webpage is available at <http://www.codysan.eu>.

**Keywords:** telemedicine tool, congenital dyserythropoietic anemia, diagnosis, algorithm, hematological disease

## INTRODUCTION

Congenital Dyserythropoietic Anemia (CDA) is a heterogeneous group of hematological disorders characterized by chronic hyporegenerative anemia and distinct morphological abnormalities of erythroid precursors in the bone marrow. Patients with CDA present congenital and chronic anemia of variable degree with a reticulocytosis not corresponding to the degree of anemia (ineffective erythropoiesis), jaundice and frequently splenomegaly and/or hepatomegaly (Iolascon et al., 2012, 2013).

Five classical types of CDAs (I–II–III–IV and XLDTA) have been defined based on bone marrow morphology. Among all types, CDA type II is the most common and well-known form. Genetically,

CDA type Ia (OMIM 224120) and CDA type Ib (OMIM 615631) are caused by mutations in codanin 1 (*CDAN1*) (chr 15q15.2) and *C15orf41* (chr15q14) genes, respectively (Dgany et al., 2002; Babbs et al., 2013). CDA type II (OMIM 224100) is due to pathogenic variants in Sec23 homolog B, coat complex II component (*SEC23B*) gene (chr20p11.23) (Bianchi et al., 2009; Schwarz et al., 2009). Few patients with CDA type III (OMIM 105600) have been described: they present the same mutation in the Kinesin Family Member 23 (*KIF23*) gene (chr15q23) (Liljeholm et al., 2013). CDA type IV (OMIM 613673) is due to mutations in the Kruppel Like Factor 1 (*KLF1*) gene (chr19p13.13) (Arnaud et al., 2010; Jaffray et al., 2013). Finally, X-linked dyserythropoietic anemia and thrombocytopenia (XLDAT) (OMIM 300367) is caused by mutations in transcription factor GATA Binding Protein 1 (*GATA1*) gene (chr Xp11.23) (Nichols et al., 2000; Del Vecchio et al., 2005). CDA types I and II are inherited in an autosomal recessive manner, CDA type III and IV present an autosomal dominant inheritance pattern and X-linked dyserythropoietic anemia with thrombocytopenia has an X-linked mode of inheritance.

Depending on the type of CDA, different treatments have been established. Allogenic bone marrow transplantation has been successfully employed in a few severe cases of CDAI and CDAIL. CDA III patients may require a transfusion only during times of extreme anemia e.g., pregnancy or surgery. Treatment focuses on hemoglobin normalization with the administration of interferon (IFN) alpha is used with success in CDA I patients with *CDAN1* mutations; however, patients bearing a mutation in a different gene i.e., *C15ORF41* were unresponsive to this same treatment. Severe cases of fetal anemia associated with CDAI, CDAIL, and XLTDa may require intrauterine transfusions. Blood iron levels should be closely monitored in CDA I, CDAIL, and other CDA patients undergoing regular transfusions. In these cases, morbidity may be severe due to iron overload complications that can be fatal if left untreated (Gambale et al., 2016; Palmer et al., 2018); therefore, it is imperative to monitor iron overload and induce iron depletion, when needed, by iron chelation. This working classification of CDA is still in use in clinical practice; however, the identification of the mutated genes involved in the majority of CDA subgroups will improve the diagnostic possibilities and allow a better classification of CDA patients. At present, in many cases, a final diagnosis is not achieved due to different levels of awareness for the diagnosis of CDAs and lack of use of advanced diagnostic procedures. In addition, there are families that fulfill the general definition of CDAs, but do not conform to any of the classical CDA variants. Therefore, it is very plausible that new forms of CDA may exist. These new forms will be possibly identified if a proper diagnosis is achieved in each patient suspected with CDA. Toward this goal, we have developed a new telemedicine tool named CoDysAn (Congenital Dyserythropoietic Anemia) for the management and diagnosis of patients with this disease.

The aim of CoDysAn webpage is to provide a freely accessible website where general public, patients and medical doctors can better understand and learn more about this disease. Moreover,

CoDysAn web page includes a diagnosis algorithm tool to ease the classification and diagnostic of CDA types.

## METHODS

### Patients and Validation

CoDysAn web algorithm has been developed with a set of 24 patients genetically diagnosed of different types of CDA (18 CDA type II, 1 CDA type Ib, 4 CDA type Ia, and 1 XLTDa) and with a set of 19 additional patients genetically diagnosed of non-CDA hereditary anemias including eight hereditary spherocytosis, four patients with pyruvate kinase defects, one patient with pyruvate kinase defect and a beta thalassemia trait, one patient with defects in hemolytic anemia due to adenylate kinase deficiency (AK1) gene, one patient with X-linked sideroblastic anemia, three patients with dehydrated hereditary stomatocytosis type 1 (DHS1) and one patient with dehydrated hereditary stomatocytosis type 2 (DHS2). A different set of 23 CDAIL patients was utilized to independently validate the algorithm. Patients were previously reported (Iolascon et al., 2009; Schwarz et al., 2009; Russo et al., 2010, 2011, 2013, 2014, 2016, 2018; Unal et al., 2014; Andolfo et al., 2015, 2018; Di Pierro et al., 2015) and diagnosed at the Medical Genetics Unit of A.O.U. Federico II, CEINGE-Biotecnologie Avanzate (Napoli).

### Design of Web Server

CoDysAn is implemented in PHP, HTML5, CSS, and Javascript. The web server is executed in a XAMPP. Network visualization and interactive exploration modules are based on several open-source projects: Bootstrap, jQuery and Filezilla. The source code of the diagnostic tool algorithm is implemented in php at <http://www.codysan.eu/diagnostics-tool.html>. It is integrated within this web page between lines 661 and 1,204 in four steps corresponding to the four steps of the form. The code can be checked by typing in a browser: “view-source: <http://www.codysan.eu/diagnostics-tool.html>.”

### Implementation

CoDysAn algorithm is based on the diagnostic workflow previously proposed (Iolascon et al., 2012; Gambale et al., 2016). This algorithm is based on hematological parameters depending on age and gender (Table 1). Age is split in three groups: from 0 to 6 months old; from 6 months to 12 years old; and older than 12 years. Hematological tested parameters include: hemoglobin levels, mean corpuscular volume (MCV), reticulocytes count and platelets count. Exclusion of other possible causes of anemia is also considered in the final step of the algorithm. Reference values for hematological data are adapted from general hematological reference books (Rabinovitch, 1990; Wakeman et al., 2007; Hoffman et al., 2018).

## RESULTS

### CoDysAn Scope

Following previous experience of the group in developing telemedicine tools for management and diagnosis of patients (HIGHFERRITIN Web server <http://highferritin.imppc.org/>

**TABLE 1** | Parameter thresholds used by the diagnostic CoDysAn algorithm.

| Parameter     |   | 0–6 months | 6 months to 12 years | > 12 years | Units               |
|---------------|---|------------|----------------------|------------|---------------------|
| Hemoglobin    | M | 9.5–18     | 11–15.5              | 13–17.5    | g/dL                |
|               | F | 9.5–18     | 11–15.5              | 12–16      |                     |
| MCV*          | M | 77.5–111.5 | 74–89.5              | 80–100     | fL                  |
|               | F | 77.5–111.5 | 74–89.5              | 80–100     |                     |
| Reticulocytes | M | 61–134     | 24–114               | 29–95      | ×10 <sup>9</sup> /L |
|               | F | 67–142     | 40–162               | 27–91      |                     |
| Platelets     | M | 145–450    | 145–450              | 145–450    | ×10 <sup>9</sup> /L |
|               | F | 145–450    | 145–450              | 145–450    |                     |

\*MCV stands for Mean Corpuscular Volume. M stands for male and F stands for female.

tool) (Altes et al., 2014), we have developed CoDysAn web tool. CoDysAn is a user-friendly webpage for a better awareness on the rare hereditary hematological diseases, congenital dyserythropoietic anemias (CDAs). CoDysAn webpage includes a step-by-step diagnostic algorithm based on **Figure 1**. The site is freely available at URL <http://www.codysan.eu> in four languages (Catalan, Spanish, Italian, and English).

## Webpage Structure and Design

The CoDysAn website is currently containing seven sections (see **Supplementary Figure 1** to visualize several screenshots of different sections of CoDysAn webpage): A home or main webpage section including links to other sections of the site to make information more accessible; The CoDysAn section, where one can find information about congenital dyserythropoietic anemia (CDA) disease, the CoDysAn project as a whole research project, the privacy policy, cookies policy and medical disclaimer reminding that, as any other telemedicine project, CoDysAn diagnostic tool is a preliminary diagnostic test and expert medical doctors should be contacted for a conclusive diagnosis; The diagnostic section, including the CDA algorithm flowchart (**Figure 1**) and a step-by-step diagnostic tool with specific instructions on how to use it; The collaborators section, including links to the contributors for the CoDysAn project, patient associations and links to similar web tools, such as HIGHFERRITIN web server; A resource section, including news on the CoDysAn project, bibliographical references and reference values used for the diagnostic algorithm (see also **Table 1**); An opinion section containing a Google form that allows users to express their opinion and degree of satisfaction with the website; A contact section, where users can directly contact CoDysAn developers to address any doubt regarding the webpage.

## Diagnostic Telemedicine Tool

The diagnostic algorithm used for setting up the CoDysAn diagnostic tool is depicted in **Figure 1**. A step-by-step and user-friendly form will progressively ask relevant patient information; in the first stage, age, gender and hemoglobin levels should be provided to discern if the patient has hyperhemoglobinemia (high hemoglobin values in regards to the reference value), anemia or if the values are inside the normal range, in which case the web tool will return a text indicating that there is no anemia.

Due to fluctuations in the hematological parameters, the algorithm correlates to the reference values for the hematological provided data (hemoglobin level, reticulocytes, platelets, etc.) according to age and gender, see **Table 1**. To simplify the algorithm, we have only considered three different age ranges, from 0 to 6 months, from 6 to 12 years, and older than 12 years old.

If anemia is detected, i.e., the hemoglobin levels are below the normal values for the indicated gender and age range, the algorithm will ask for three additional hematological parameters: mean corpuscular volume (MCV), reticulocytes count, and platelets count.

Users can change the input units of the provided hematological parameter. These values are converted to the international system of reference units and the value is used to check if the parameters are within range for their given thresholds (see **Table 1**).

Depending on the data provided, a new form will appear asking to exclude specific possible causes of macrocytic, normocytic or microcytic anemia. At least one alternative cause of anemia should be excluded to proceed with the diagnostic tool. In the following step, the user is asked to select additional patient's clinical or biochemical factors, such as binucleated erythroblasts, malformations or electron microscopy features.

Finally, depending on the provided information, CoDysAn tool will return a result of clinical suspicion (any of the CDA types) if it applies, or a brief explanation if there is no clinical suspicion of CDA.

If a clinical suspicion of CDA is indicated, the user has the option to search for world-wide genetic laboratories that provide clinical diagnostic tests for a particular CDA gene via the button "Search Lab." The list of world-wide genetic laboratories is taken from the NCBI's Genetic Testing Registry (GTR) webpage (Rubinstein et al., 2013). There is also the possibility to refresh the webpage and perform a new diagnostic test via the button "New diagnostic."

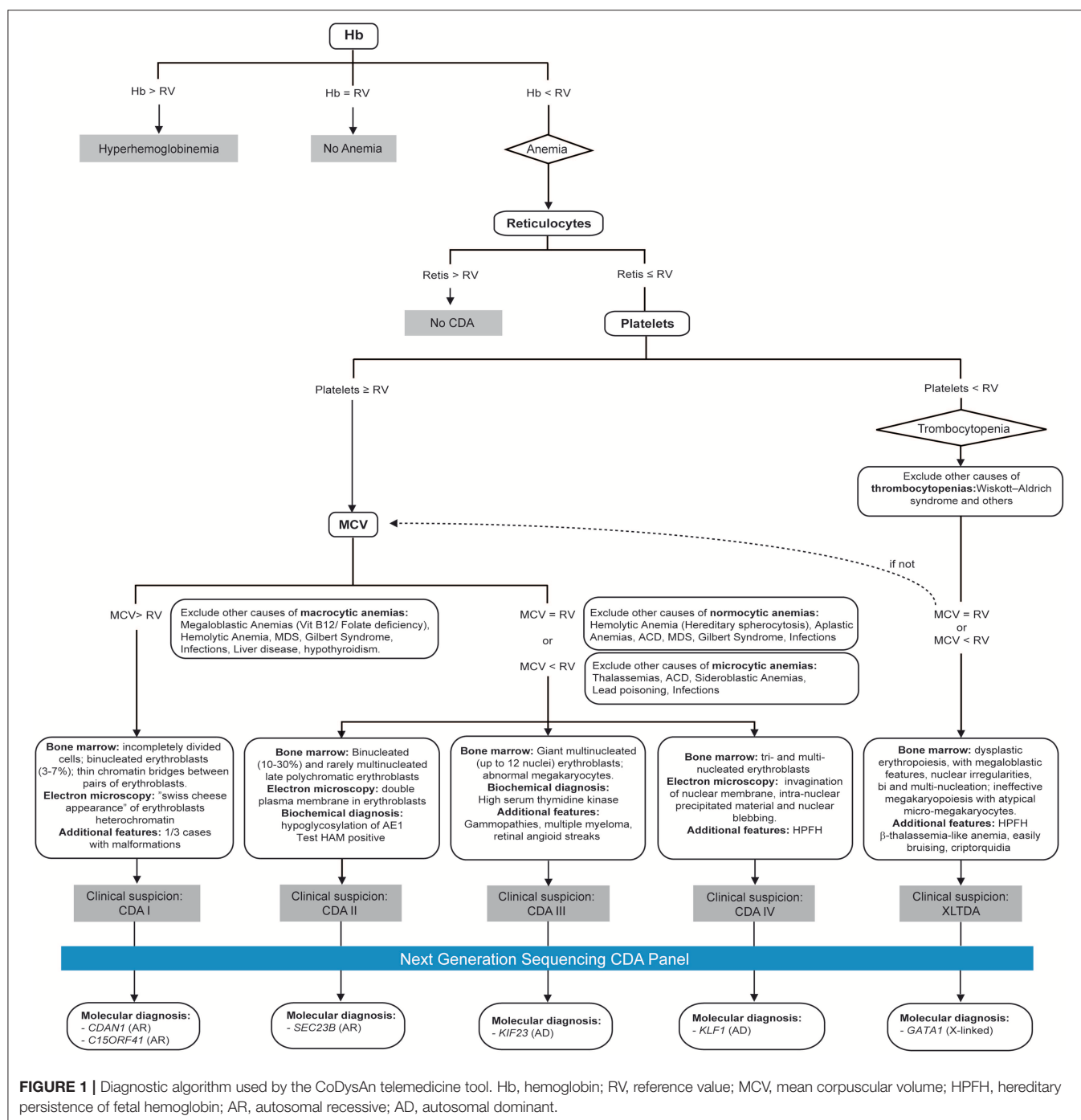
## Validation

The CodysAn algorithm has been designed with 43 patients with hereditary anemia, including 24 patients genetically diagnosed with different types of CDA (18 CDA type II, 1 CDA type Ib, 4 CDA type IIa, and 1 XLTD) and 19 additional patients genetically diagnosed with non-CDA hereditary anemias. The algorithm achieved a specificity of 89.5% and a sensibility of 87.5%. An additional set of 23 patients (all CDA II) was utilized to validate the algorithm, which returned a specificity of 87%.

## DISCUSSION

Telemedicine webpages and tools are significantly changing the way medical doctors and patients approach health care and diagnosis (Dinesen et al., 2016). CoDysAn telemedicine tool is a webpage intended to increase awareness about the rare disease CDA as, currently, patients suffering from this disease are under-diagnosed (Russo et al., 2014). The content of the webpage serves as an informative and training resource for the general public, patients and medical doctors. The use of this





tool presents limits: patients should be considered as a whole entity and multiple biochemical determinations are needed due to daily parameters' variability within the same subject. Although hematological reference ranges are useful in results interpretation and in clinical decision-making, it should be borne in mind that variations within the population may affect some outcomes. CoDysAn incorporates a diagnostic algorithm that proved to be useful for a preliminary diagnostic. It will help medical doctors to know which molecular diagnostics they should request,

reducing time and effort necessary for the diagnostic of CDA and allowing a direct implementation of a proper treatment once reached a definitive molecular diagnosis. Few reference centers are now offering genetic diagnostic panels screening the six known genes causing CDA. CoDysAn algorithm is connected to the NCBI Genetic Testing Registry (GTR) in a way to inform medical doctors about the existence of these accredited diagnostic centers to perform a complete genetic test, if required. This telemedicine tool aims to inform the general public and aid in

the diagnosis of CDA. It is not intended as an attempt to practice medicine or provide specific medical advice and it should not be used to replace or overrule a qualified health care provider's judgment. Users should not rely upon this website for self-medication. We believe that CoDysAn webpage will positively contribute to improve medical and scientific communication on the anemia field.

## DATA AVAILABILITY

All datasets generated for this study are included in the manuscript and/or the **Supplementary Files**.

## AUTHOR CONTRIBUTIONS

MS designed the webpage, designed the study, and wrote the manuscript. ES-P, CT, and BC created the webpage and wrote the diagnostic algorithm. BC designed **Figure 1**. IA and RR translated the CoDysAn webpage to Italian. AI, IA, and RR provided the patients data to test CoDysAn algorithm. VV wrote and revised the manuscript. IH-R helped with reference values and **Table 1**. All authors read and approved the final version of the manuscript.

## REFERENCES

- Altes, A., Perez-Lucena, M. J., Bruguera, M., and Grp Iberico, F. (2014). Systematic approach to the diagnosis of hyperferritinemia. *Med. Clin. (Barc)*. 142, 412–417. doi: 10.1016/j.medcli.2013.06.010
- Andolfo, I., Russo, R., Manna, F., Shmukler, B. E., Gambale, A., Vitiello, G., et al. (2015). Novel Gardos channel mutations linked to dehydrated hereditary stomatocytosis (xerocytosis). *Am. J. Hematol.* 90, 921–926. doi: 10.1002/ajh.24117
- Andolfo, I., Russo, R., Rosato, B. E., Manna, F., Gambale, A., Brugnara, C., et al. (2018). Genotype-phenotype correlation and risk stratification in a cohort of 123 hereditary stomatocytosis patients. *Am. J. Hematol.* 93, 1509–1517. doi: 10.1002/ajh.25276
- Arnaud, L., Saison, C., Helias, V., Lucien, N., Steschenko, D., Giarratana, M. C., et al. (2010). A Dominant mutation in the gene encoding the erythroid transcription factor KLF1 causes a congenital dyserythropoietic anemia. *Am. J. Hum. Genet.* 87, 721–727. doi: 10.1016/j.ajhg.2010.10.010
- Babbs, C., Roberts, N. A., Sanchez-Pulido, L., McGowan, S. J., Ahmed, M. R., Brown, J. M., et al. (2013). Homozygous mutations in a predicted endonuclease are a novel cause of congenital dyserythropoietic anemia type I. *Haematologica* 98, 1383–1387. doi: 10.3324/haematol.2013.089490
- Bianchi, P., Fermo, E., Vercellati, C., Boschetti, C., Barcellini, W., Iurlo, A., et al. (2009). Congenital dyserythropoietic anemia type II (CDAIL) is caused by mutations in the SEC23B gene. *Hum. Mutat.* 30, 1292–1298. doi: 10.1002/humu.21077
- Del Vecchio, G. C., Giordani, L., De Santis, A., and De Mattia, D. (2005). Dyserythropoietic anemia and thrombocytopenia due to a novel mutation in GATA-1. *Acta Haematol.* 114, 113–116. doi: 10.1159/000086586
- Dgany, O., Avidan, N., Delaunay, J., Krasnov, T., Shalmon, L., Shalev, H., et al. (2002). Congenital dyserythropoietic anemia type I is caused by mutations in codanin-1. *Am. J. Hum. Genet.* 71, 1467–1474. doi: 10.1086/344781
- Di Pierro, E., Russo, R., Karakas, Z., Brancaloni, V., Gambale, A., Kurt, I., et al. (2015). Congenital erythropoietic porphyria linked to GATA1-R216W mutation: challenges for diagnosis. *Eur. J. Haematol.* 94, 491–497. doi: 10.1111/ejh.12452

## FUNDING

The CoDysAn project was supported by a research grant from Ramón Areces Foundation (Reference CIVP18A1857) to MS and AI, and by a collaborative agreement between the patient associations Pablo Ugarte Association (APU) and Patient and Relative Association of Congenital Dyserythropoietic Anemia (ADISCON).

## ACKNOWLEDGMENTS

We would like to thank Nuria Centeno from UPF for Master Project advisor tasks and Francisco Fuster from Josep Carreras Leukaemia Research Institute for assistance with the opinion questionnaire. This work was performed in the context of the Experimental Sciences and Technology Ph.D. program of the University of Vic (UVic).

## SUPPLEMENTARY MATERIAL

The Supplementary Material for this article can be found online at: <https://www.frontiersin.org/articles/10.3389/fphys.2019.01063/full#supplementary-material>

- Dinesen, B., Nonnecke, B., Lindeman, D., Toft, E., Kidholm, K., Jethwani, K., et al. (2016). Personalized telehealth in the future: a global research agenda. *J. Med. Internet Res.* 18:e53. doi: 10.2196/jmir.5257
- Gambale, A., Iolascon, A., Andolfo, I., and Russo, R. (2016). Diagnosis and management of congenital dyserythropoietic anemias. *Expert Rev. Hematol.* 9, 283–296. doi: 10.1586/17474086.2016.1131608
- Hoffman, R., Benz, E. J. Jr., Silberstein, L. E., Heslop, H., Weitz, J., and Anastasi, J. (2018). *Hematology: Basic Principles and Practice, 7th Edn*. Philadelphia, PA: Elsevier Saunders.
- Iolascon, A., Esposito, M. R., and Russo, R. (2012). Clinical aspects and pathogenesis of congenital dyserythropoietic anemias: from morphology to molecular approach. *Haematologica* 97, 1786–1794. doi: 10.3324/haematol.2012.072207
- Iolascon, A., Heimpel, H., Wahlén, A., and Tamary, H. (2013). Congenital dyserythropoietic anemias: molecular insights and diagnostic approach. *Blood* 122, 2162–2166. doi: 10.1182/blood-2013-05-468223
- Iolascon, A., Russo, R., Esposito, M. R., Asci, R., Piscopo, C., Perrotta, S., et al. (2009). Molecular analysis of 42 patients with congenital dyserythropoietic anemia type II: new mutations in the SEC23B gene and a search for a genotype-phenotype relationship. *Haematologica* 95, 708–715. doi: 10.3324/haematol.2009.014985
- Jaffray, J. A., Mitchell, W. B., Gnanapragasam, M. N., Seshan, S. V., Guo, X., Westhoff, C. M., et al. (2013). Erythroid transcription factor EKLF/KLF1 mutation causing congenital dyserythropoietic anemia type IV in a patient of Taiwanese origin: review of all reported cases and development of a clinical diagnostic paradigm. *Blood Cells Mol. Dis.* 51, 71–75. doi: 10.1016/j.bcmd.2013.02.006
- Liljeholm, M., Irvine, A. F., Vikberg, A. L., Norberg, A., Month, S., Sandström, H., et al. (2013). Congenital dyserythropoietic anemia type III (CDA III) is caused by a mutation in kinesin family member, KIF23. *Blood* 121, 4791–4799. doi: 10.1182/blood-2012-10-461392
- Nichols, K. E., Crispino, J. D., Poncz, M., White, J. G., Orkin, S. H., Maris, J. M., et al. (2000). Familial dyserythropoietic anaemia and thrombocytopenia due to an inherited mutation in GATA1. *Nat. Genet.* 24, 266–270. doi: 10.1038/73480
- Palmer, W. C., Vishnu, P., Sanchez, W., Aqel, B., Riegert-Johnson, D., Seaman, L. A. K., et al. (2018). Diagnosis and management of genetic iron overload disorders. *J. Gen. Intern. Med.* 33, 2230–2236. doi: 10.1007/s11606-018-4669-2

- Rabinovitch, A. (1990). Hematology reference ranges. *Arch. Pathol. Lab. Med.* 114:1189.
- Rubinstein, W. S., Maglott, D. R., Lee, J. M., Kattman, B. L., Malheiro, A. J., Ovetsky, M., et al. (2013). The NIH genetic testing registry: a new, centralized database of genetic tests to enable access to comprehensive information and improve transparency. *Nucleic Acids Res.* 41, D925–D935. doi: 10.1093/nar/gks1173
- Russo, R., Andolfo, I., Manna, F., De Rosa, G., De Falco, L., Gambale, A., et al. (2016). Increased levels of ERFE-encoding FAM132B in patients with congenital dyserythropoietic anemia type II. *Blood* 128, 1899–1902. doi: 10.1182/blood-2016-06-724328
- Russo, R., Andolfo, I., Manna, F., Gambale, A., Marra, R., Rosato, B. E., et al. (2018). Multi-gene panel testing improves diagnosis and management of patients with hereditary anemias. *Am. J. Hematol.* 93, 672–682. doi: 10.1002/ajh.25058
- Russo, R., Esposito, M. R., Asci, R., Gambale, A., Perrotta, S., Ramenghi, U., et al. (2010). Mutational spectrum in congenital dyserythropoietic anemia type II: identification of 19 novel variants in SEC23B gene. *Am. J. Hematol.* 85, 915–920. doi: 10.1002/ajh.21866
- Russo, R., Gambale, A., Esposito, M. R., Serra, M. L., Troiano, A., De Maggio, I., et al. (2011). Two founder mutations in the SEC23B gene account for the relatively high frequency of CDA II in the Italian population. *Am. J. Hematol.* 86, 727–732. doi: 10.1002/ajh.22096
- Russo, R., Gambale, A., Langella, C., Andolfo, I., Unal, S., and Iolascon, A. (2014). Retrospective cohort study of 205 cases with congenital dyserythropoietic anemia type II: definition of clinical and molecular spectrum and identification of new diagnostic scores. *Am. J. Hematol.* 89, E169–E175. doi: 10.1002/ajh.23800
- Russo, R., Langella, C., Esposito, M. R., Gambale, A., Vitiello, F., Vallefucio, F., et al. (2013). Hypomorphic mutations of SEC23B gene account for mild phenotypes of congenital dyserythropoietic anemia type II. *Blood Cells Mol. Dis.* 51, 17–21. doi: 10.1016/j.bcmd.2013.02.003
- Schwarz, K., Iolascon, A., Verissimo, F., Trede, N. S., Horsley, W., Chen, W., et al. (2009). Mutations affecting the secretory COPII coat component SEC23B cause congenital dyserythropoietic anemia type II. *Nat. Genet.* 41, 936–940. doi: 10.1038/ng.405
- Unal, S., Russo, R., Gumruk, F., Kuskonmaz, B., Cetin, M., Sayli, T., et al. (2014). Successful hematopoietic stem cell transplantation in a patient with congenital dyserythropoietic anemia type II. *Pediatr. Transplant.* 18, E130–E133. doi: 10.1111/petr.12254
- Wakeman, L., Al-Ismail, S., Benton, A., Beddall, A., Gibbs, A., Hartnell, S., et al. (2007). Robust, routine haematology reference ranges for healthy adults. *Int. J. Lab. Hematol.* 29, 279–283. doi: 10.1111/j.1365-2257.2006.00883.x

**Conflict of Interest Statement:** CT was employed by company BloodGenetics SL. BC was employed by company Whole Genix SL.

The remaining authors declare that the research was conducted in the absence of any commercial or financial relationships that could be construed as a potential conflict of interest.

Copyright © 2019 Tornador, Sánchez-Prados, Cadenas, Russo, Venturi, Andolfo, Hernández-Rodríguez, Iolascon and Sánchez. This is an open-access article distributed under the terms of the Creative Commons Attribution License (CC BY). The use, distribution or reproduction in other forums is permitted, provided the original author(s) and the copyright owner(s) are credited and that the original publication in this journal is cited, in accordance with accepted academic practice. No use, distribution or reproduction is permitted which does not comply with these terms.



# Clinical Diagnosis of Red Cell Membrane Disorders: Comparison of Osmotic Gradient Ektacytometry and Eosin Maleimide (EMA) Fluorescence Test for Red Cell Band 3 (AE1, SLC4A1) Content for Clinical Diagnosis

Ahmar Urooj Zaidi<sup>1\*</sup>, Steven Buck<sup>1,2</sup>, Manisha Gadgeel<sup>2</sup>, Miguel Herrera-Martinez<sup>2</sup>, Araathi Mohan<sup>2</sup>, Kenya Johnson<sup>2</sup>, Shruti Bagla<sup>2</sup>, Robert M. Johnson<sup>2</sup> and Yaddanapudi Ravindranath<sup>1,2</sup>

## OPEN ACCESS

### Edited by:

Richard Van Wijk,  
Utrecht University, Netherlands

### Reviewed by:

Norbert Nemeth,  
University of Debrecen, Hungary  
Giovanna Tomaiuolo,  
University of Naples Federico II, Italy  
Archana Mishra Agarwal,  
University of Utah Hospital,  
United States

### \*Correspondence:

Ahmar Urooj Zaidi  
ahmar@wayne.edu

### Specialty section:

This article was submitted to  
Red Blood Cell Physiology,  
a section of the journal  
Frontiers in Physiology

**Received:** 06 February 2019

**Accepted:** 19 May 2020

**Published:** 19 June 2020

### Citation:

Zaidi AU, Buck S, Gadgeel M, Herrera-Martinez M, Mohan A, Johnson K, Bagla S, Johnson RM and Ravindranath Y (2020) Clinical Diagnosis of Red Cell Membrane Disorders: Comparison of Osmotic Gradient Ektacytometry and Eosin Maleimide (EMA) Fluorescence Test for Red Cell Band 3 (AE1, SLC4A1) Content for Clinical Diagnosis. *Front. Physiol.* 11:636. doi: 10.3389/fphys.2020.00636

<sup>1</sup> Children's Hospital of Michigan, Detroit, MI, United States, <sup>2</sup> Wayne State University School of Medicine, Detroit, MI, United States

The measurement of band 3 (AE1, SLC4A1, CD233) content of red cells by eosin-5-maleimide (EMA) staining is swiftly replacing conventional osmotic fragility (OF) test as a tool for laboratory confirmation of hereditary spherocytosis across the globe. Our group has systematically evaluated the EMA test as a method to screen for a variety of anemias in the last 10 years, and compared these results to those obtained with the osmotic gradient ektacytometry (osmoscans) which we have used over three decades. Our overall experience allowed us to characterize the distinctive patterns with the two tests in several congenital erythrocyte membrane disorders, such as hereditary spherocytosis (HS), hereditary elliptocytosis (HE), Southeast Asian Ovalocytosis (SAO), hereditary pyropoikilocytosis (HPP) variants, erythrocyte volume disorders, various red cell enzymopathies, and hemoglobinopathies. A crucial difference between the two methodologies is that osmoscans measure red blood cell deformability of the entire sample of RBCs, while the EMA test examines the band 3 content of individual RBCs. EMA content is influenced by cell size as smaller red cells have lower amount of total membrane than larger cells. The SAO mutation alters the EMA binding site resulting in a lower EMA MCF even as the band 3 content itself is unchanged. Thus, EMA scan results should be interpreted with caution and both the histograms and dot plots should be analyzed in the context of the clinical picture and morphology.

**Keywords:** red blood cell, anemia, membrane, Hematology, erythrocyte

## INTRODUCTION

Our ability to accurately recognize the mechanistic basis of red cell disorders is continuing to evolve, none more so than the erythrocyte membrane disorders and enzymopathies. The human erythrocyte is the most abundant cell in the human body (Bianconi et al., 2013) and perhaps the most studied cell. There are approximately 20 major proteins and over 800 minor proteins in the red



blood cell membrane. Integral membrane proteins are organized around band 3, an anion-exchange channel. The membrane skeleton, primarily composed of spectrin, actin and its associated proteins complete the composition of the phospholipid bilayer enabling it to maintain its shape (Lux, 2016). There are several other proteins that manage the regulation of volume and hydration that are implicated in rare, but important, disorders of the red blood cell membrane (Andolfo et al., 2016).

There have been many important contributions to red blood cell membrane science since the original osmotic fragility (OF) test (Hunter, 1940). One such contribution came almost four decades ago, the ektacytometer (Bessis et al., 1980). The ektacytometer is a laser diffractometer that measures the deformability potential of a population of red blood cells over an osmotic gradient, and allows the characterization of many of the common red blood cell membranopathies. Red cells undergo shape change from discoid to elliptocyte configuration as they traverse through the capillaries and the micropores in the splenic sinusoids. This *in vivo* phenomenon is mimicked in the ektacytometer. The cells are exposed to an increasing osmotic gradient, and cell deformability (shift from discoid to elliptical shape) is gauged by how light scatters as the cell responds to shear forces. The result of this test, is a characteristic graph (the Osmoscan), that shows the amount of deformability on the *y*-axis, and osmolality on the *x*-axis (**Figure 1**; Mohandas et al., 1980).

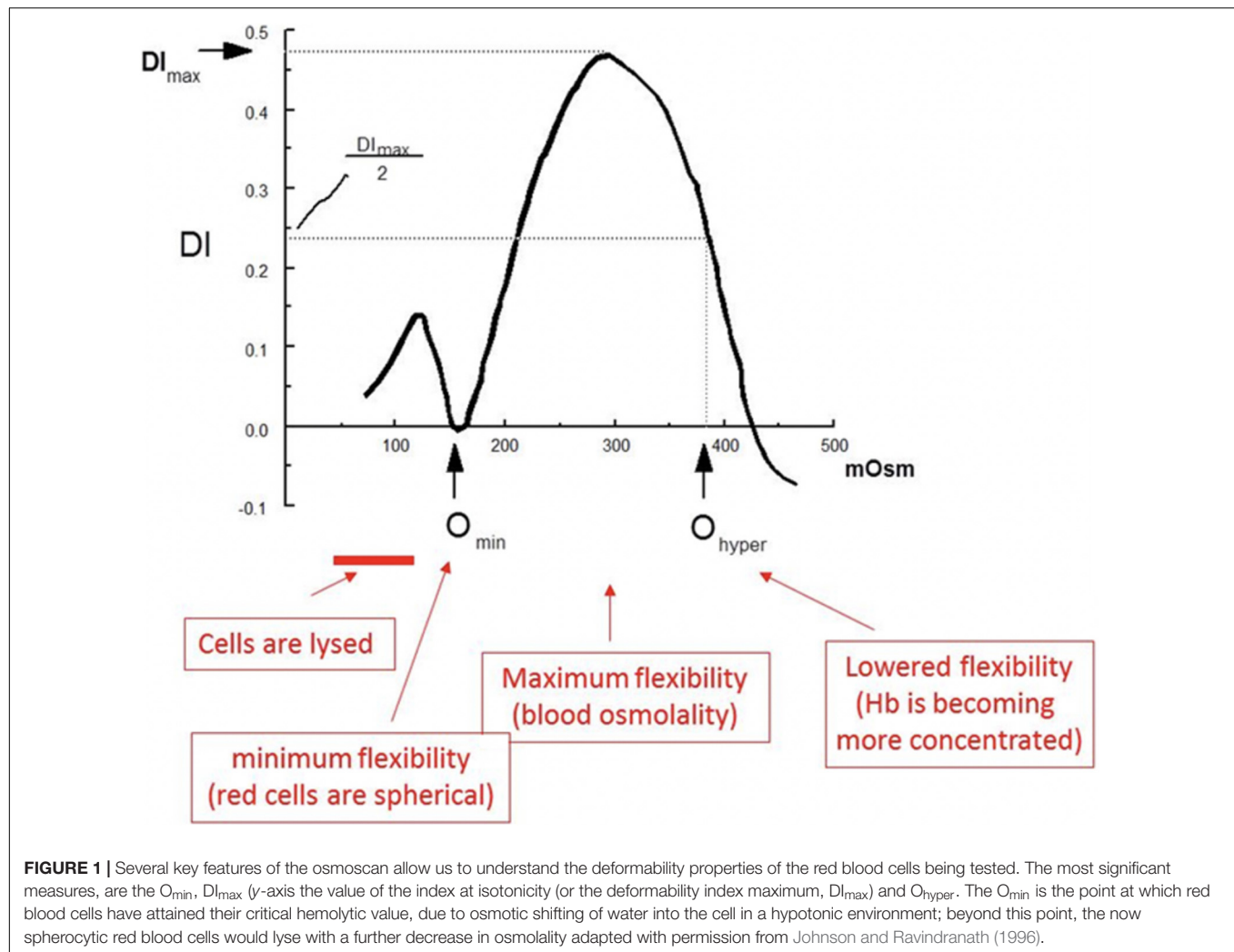
The major components of the red cells that determine deformability are the biconcave shape of the red cells, the membrane fluidity and the internal viscosity of the cell. There are several key features of the osmoscan that allow us to understand the deformability properties of the red blood cells being tested (Clark et al., 1983). The most significant measures, are the  $O_{min}$ ,  $DI_{max}$  (*y* axis the value of the index at isotonicity or the ellipticity/deformability index maximum,  $EI/DI_{max}$ ), and  $O_{hyper}$ . The  $O_{min}$  is the point at which red blood cells have attained their critical hemolytic value, due to osmotic shifting of water into the cell in a hypotonic environment; beyond this point, the now spherocytic red blood cells would lyse with a further decrease in osmolality. Thus, the EI at  $O_{min}$  measures the changes in surface to volume (S/V) ratio. The deformability index maximum is the index value at isotonicity, and the point at which red blood cells have attained the maximum ellipticity ( $DI_{max}$ ,  $EI_{max}$ ). Deformability index reflects the membrane integrity and elasticity. The  $O_{hyper}$  is the osmolality at which the index is midway between the maximal deformability and  $O_{min}$ .  $O_{hyper}$  is increased in states of cellular hydration either because of decreased mean corpuscular hemoglobin concentration or net increase of water content (such as stomatocytosis/cryohydrocytosis). These values, when compared to normal red blood cells provide unique signatures in cells with membrane pathologies. However, despite the ability of the ektacytometer to aid in the clinical diagnosis of red blood cell membrane disorders (Groner et al., 1980; Johnson and Ravindranath, 1996), its use was limited until recently because of the non-availability of the original Technicon made instruments. A newer clinical grade version with digitized osmoscans, LoRRca Maxxis®, has become available and its usage will expand. Even with the new-generation ektacytometer gaining

increasing popularity, the ability of centers to perform this test remains limited and yet approved by US FDA for clinical testing (Da Costa et al., 2016).

Almost 20 years after the introduction of ektacytometry, King et al. (2000) devised a simple alternative to standard OF test for laboratory confirmation of HS by using eosin maleimide fluorescence to measure band 3 content (AE1, SLC4A1). HS cells lose membrane through vesiculation, and along with it band-3 protein. The test uses the functional property of the fluorochrome, eosin-5-maleimide (EMA), which covalently binds to the 430th residue (lysine) on the first extracellular loop of band 3 (Cobb and Beth, 1990). This test provides investigators with insight on the amount of band 3, or functional loss of membrane, that exists in pathologic red blood cell. The results of the EMA test are reported as mean channel fluorescence (MCF) compared to a control sample- MCF ratio (patient's MCF/control MCF). However, as described below, the slope of the EMA curve on both sides indicates valuable information on the variation in cell size; trailing shoulders on the right side is prominent in patients with high reticulocyte count and the leading shoulder on the left indicates presence of fragmented red cells. Thus, EMA test should be interpreted not solely on the MCF, but also on the overall pattern of EMA intensity. The measurement of band 3 content by flow cytometry has enabled for rapid diagnosis of spherocytosis in intact red blood cells and is fast replacing the OF test.

A crucial difference between the ektacytometry and EMA test is that osmoscans measure red blood cell deformability of the entire sample of RBCs, while the EMA test examines the band 3 content of individual RBCs. One is a measure of deformability under shear stress (function) and the other an estimate of a critical membrane protein (structure). Further, the ektacytometer is a test that simulates flow of red blood cells through the vasculature, and is able to capture the spirit of the dynamic red blood cell; the test is a measure of RBC geometry, cytoplasmic viscosity, cell volume regulation and fluidity of the membrane (Mohandas et al., 1980). The testing is limited by the availability of the instrument, the need for specialized staff and the need to delay analysis after transfusion (Da Costa et al., 2016). The EMA is user-friendly, with quick turnaround time of testing, and flow cytometers are readily available in most institutions. Though the EMA only describes reduction in band 3 protein and does not interact with other integral proteins, it can serve as a reliable indirect measure of cytoskeletal health (King et al., 2004) but mild defects may result in indeterminate results (Bolton-Maggs et al., 2012).

Our group has systematically evaluated both the EMA test and osmoscans obtained as a method to screen for a variety of anemias over the past 10 years and compared these results. Our experience allowed us to characterize distinctive patterns in a variety of congenital hemolytic anemias (red cell membrane disorders, erythrocyte volume disorders, enzymopathies/hemoglobinopathies) and as well in some acquired disorders. We have not systematically evaluated the OF test by flow cytometry (Won and Suh, 2009; Crisp et al., 2012). In this review, we will describe both the ektacytometry-osmoscans and EMA tests from patients and the lessons we have learned from practical experience.



## MATERIALS AND METHODS

All individuals studied were patients at the Children's Hospital of Michigan/Wayne State University School of Medicine, and the data has been collected from routine clinical testing. This review was approved by the Wayne State University Human Investigation Committee. We reviewed records of children with suspected red blood cell membranopathies or anemias who underwent both osmotic gradient ektacytometry and flow cytometry studies using eosin-5-maleimide from 2007 to 2017. In all cases, the peripheral blood smears were reviewed by members of the division of Pediatric Hematology/Oncology. Osmotic gradient ektacytometry was performed on an ektacytometer manufactured by Technicon Instruments (Miles Diagnostics, Tarrytown, NY, United States). This instrument includes two pumps to generate buffer gradients, a microprocessor that controls the viscometer motor and gradient pumps, an image analyzer and a keyboard with a display. For standard clinical testing, the rotor speed was set at 150 RPM, operating at a shear stress of 159.3 dynes/cm<sup>3</sup> (all of the tests were done by Gerard Goyette until 2015 and following his untimely death by MG). The

analog curves were digitized (done by MHM and KJ) and  $O_{min}$  and  $O_{max}$  values were used to compare diagnostic reliability in dominant HS and general characteristics of the curves relative to normal were used to describe changes in other membrane disorders. For EMA flow cytometry, cells were stained in the dark for 30 min at room temperature with agitation, washed with 1 ml cold PBS, and re-suspended in 0.5 ml PBS plus fixative (PBS plus 0.5% formaldehyde). Acquisition was performed on a Coulter XL Flow Cytometer (Coulter Corp., Miami, FL, United States) equipped with a 488 nm Argon laser. Results were analyzed using EXPO-32 software (by SB and MG). We reviewed complete blood counts on the days of the sampling and entered them into a database without patient identifiers.

## Cases

**Table 1.** Number of patients for each disorder.

### Hereditary Spherocytosis (HS)

Hereditary spherocytosis (HS) is the most commonly inherited red blood cell membranopathy with significant clinical heterogeneity. Features like anemia, jaundice and splenomegaly

TABLE 1 | Number of cases.

|    |                               |
|----|-------------------------------|
| 43 | Hereditary Spherocytosis      |
| 8  | Hereditary Elliptocytosis     |
| 3  | Hereditary Pyropoikilocytosis |
| 3  | ABO Incompatibility           |
| 4  | AIHA                          |
| 3  | Southeast Asian Ovalocytosis  |
| 3  | Erythrocyte Volume Disorders  |

are common, and jaundice may be the only sign in neonates (Ribeiro et al., 2000; Delaunay, 2007; An and Mohandas, 2008; Nussenzveig et al., 2014; Andolfo et al., 2016; Da Costa et al., 2016). Hydrops fetalis is an exceedingly rare complication in HS (Gallagher et al., 1995; Ribeiro et al., 2000). While the molecular defects are protean, in general, it is the weakened vertical linkages between the membrane skeleton and the lipid bilayer's integral proteins that drive this disease process (Palek and Lux, 1983; Perrotta et al., 2008). This disruption of linkage between the lipid bilayer and the cytoskeleton via ankyrin (band 2.1) results in echinocyte formation. More specifically defects in ankyrin, band 3, beta spectrin, alpha spectrin or protein 4.2 cause spherocytosis through loss of membrane surface area. As erythrocytes age they begin to exhibit a variety of membrane abnormalities including the loss of potassium and water, leading to cell dehydration and increased cell density, and the loss of surface area, likely owing

to gradual release of membrane microvesicles (Lux, 2014). The spherocyte generates characteristic results on osmoscans with the entire curve being inside of the control- $O_{min}$  is increased,  $EI/DI_{Max}$  is lower and  $O_{hyper}$  is reduced. The three aspects of HS cells driving these changes are the loss of surface area, reduced S/V ratio and the high internal viscosity (Clark et al., 1983). The loss of band 3 content results in decreased EMA binding. The MCF (mean channel of fluorescence) is reduced variably with the histogram shifted to left (see Figure 2).

In 43 patients with HS, the EMA MCF was  $395.69 \pm 53.48$ , whereas in 76 normal controls the value is  $514.50 \pm 15.25$  (Zaidi et al., 2015; Table 2). Thus compared to controls HS is easily diagnosable disease by either EMA or osmoscan. The severity of spherocytic defect, can be depicted in an osmoscan based on the degree of reduction in the y-coordinate of the elongation index's maximum point (Johnson and Ravindranath, 1996). Figure 2A shows a typical osmoscan of three samples: control (black line), mild HS (blue line), and severe HS (red line). In patients with low MCF and this typical osmoscan tracing, a diagnosis of HS is certain. There is good correlation between values for  $O_{min}$ , S/V ratio and MCF in dominant HS (Zaidi et al., 2015). However, in our cohort of patients, we were unable to find any replicable association or relationship with clinical indicators of severity-hemoglobin/hematocrit, reticulocyte counts, bilirubin and other red blood cell parameters (MCHC, MCH, MCV, RDW) with either  $O_{min}$  or MCF values. This suggests that phagocytosis of damaged red cells and the extent of compensatory erythropoietic

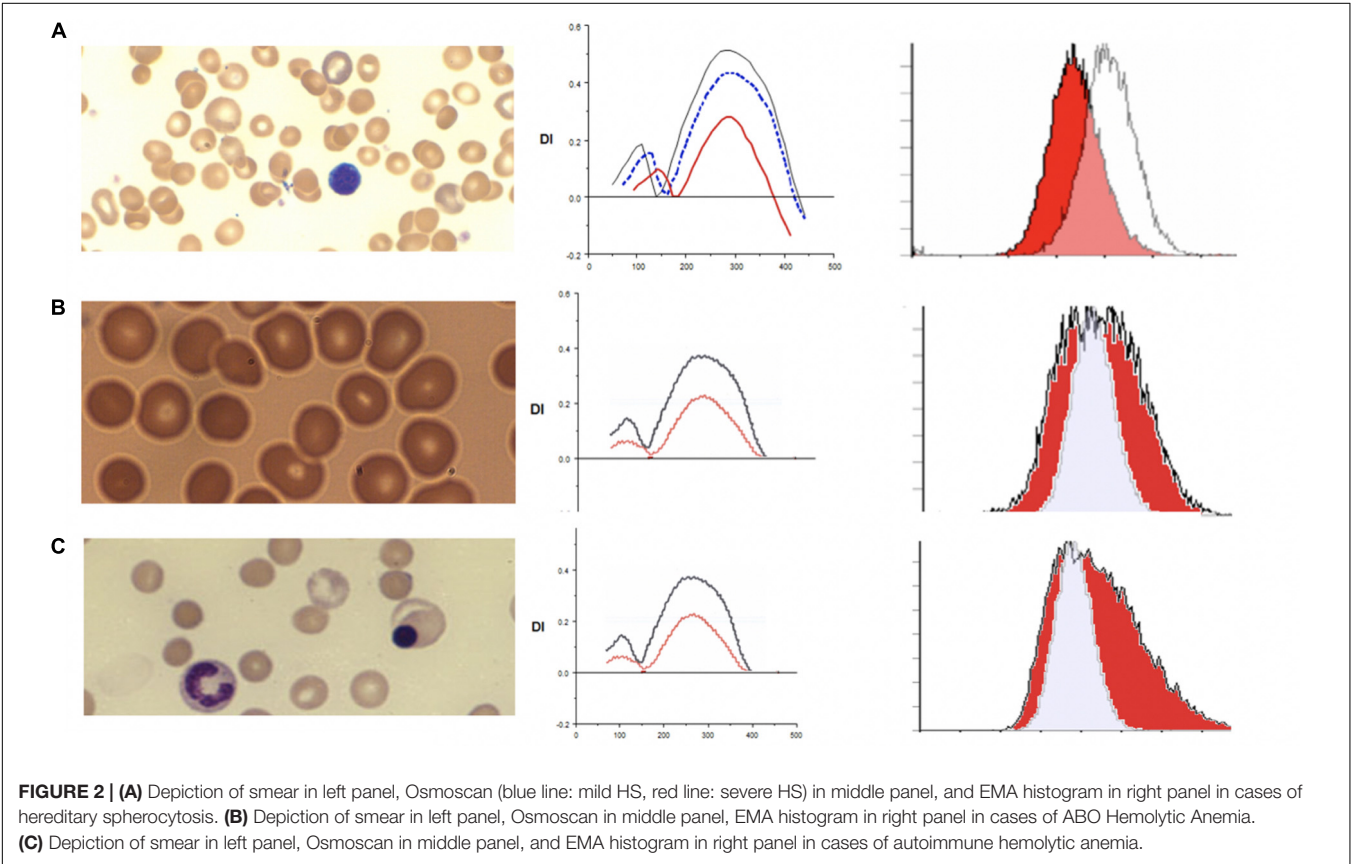


**TABLE 2 |** Hereditary spherocytosis.

| HS (n = 43)                |        |       | Normal controls (n = 76)   |        |       |
|----------------------------|--------|-------|----------------------------|--------|-------|
|                            | Mean   | SD    |                            | Mean   | SD    |
| MCF                        | 395.69 | 53.48 | MCF                        | 514.50 | 15.25 |
| O <sub>min</sub> (X-axis)  | 166.11 | 14.65 | O <sub>min</sub> (X-axis)  | 147.67 | 6.90  |
| DI <sub>MAX</sub> (Y-axis) | 0.34   | 0.08  | DI <sub>MAX</sub> (Y-axis) | 0.49   | 0.05  |

response are critical additive determinants of clinical severity. Molecular testing was done only in a few cases and thus we cannot make sweeping comments, but the reader is referred to a recent publication by the Dutch group (Huisjes et al., 2019). Lowest MCF values in HS cases were seen in a teenager with band 3 mutation (SLC4A1; NM\_000342.3; c.2423G > T, p.Arg808Leu) and in a child with ankyrin mutation (ANK1 NM\_000037.3; c.2023dup;pVal675Glyfs\*118). Arginine mutations appear to cause severe band 3 deficiency because of decreased incorporation of band 3 protein in to the lipid bilayer (Palek and Lux, 1983; Gallagher, 2013). However, the teenager (status post splenectomy) with SLC4A1 Arg808Leu had a hemoglobin of 17.8 g/dL, MCF 301.1 (ratio 59% when compared to mean control values) when tested at age 15.5 years. A young girl with ANK1 mutation had hemoglobin 6.5 g/dL at age 6 weeks and 8.5 g/dL at age 12 months with no interventions. Her brother had a hemoglobin of 10.3 g/dL at 18 months, and their father at age 26 had a hemoglobin of 13.6 g/dL; neither were transfused nor had splenectomy, and had the same mutation as the index patient. The EI<sub>MAX</sub> on the osmoscan was reduced to an equal degree in all three patients (51, 55, 56% of control).

Neither the osmoscans nor the EMA histograms can distinguish dominant HS from recessive HS. In the only child with recessive HS we have evaluated, the EMA MCF was 348 with MCF ratio of 0.87; the child had two alpha spectrin mutations (SPTA1 c.3267A > T, p.Y1089X and alpha-LEPRA [c.4339-99C > T]), in trans; the case was included in two recent publications on recessive HS (Chonat et al., 2015; Gallagher et al., 2019).

Heterozygotes with EPB42 mutations exhibit milder changes from our limited experience (2 cases) consistent with published data (Kalfa et al., 1993). Thus, in general, our findings are in agreement with the detailed structure-function correlations reported by the von Wijk laboratory (Huisjes et al., 2019).

## Spherocytes in Immune (Allo/Auto) Hemolytic Anemias

Immune hemolytic anemia is the result of antibody mediated destruction of red cells. It can be caused by maternally transferred alloantibodies as in neonates with Rh sensitization and A/B blood group infants born to type O mothers. In older children and adults acquired autoantibodies can cause hemolytic anemia. Variable numbers of spherocytes are present on smears. The osmoscan by itself cannot distinguish acquired from congenital spherocytosis, as is evident from the patterns shown in **Figure 2**. In ABO hemolytic disease, on the ektacytometer, the O<sub>min</sub> and DI<sub>max</sub> (Y axis) may appear similar to normal adult controls;

**TABLE 3 |** ABO hemolytic disease.

| ABO (n = 3)                |        |       | Normal controls (n = 76)   |        |       |
|----------------------------|--------|-------|----------------------------|--------|-------|
|                            | Mean   | SD    |                            | Mean   | SD    |
| MCF                        | 554.40 | 42.97 | MCF                        | 514.50 | 15.25 |
| O <sub>min</sub> (x-axis)  | 175.39 | 25.34 | O <sub>min</sub> (x-axis)  | 147.67 | 6.90  |
| DI <sub>MAX</sub> (y-axis) | 0.31   | 0.02  | DI <sub>MAX</sub> (y-axis) | 0.49   | 0.05  |

**TABLE 4 |** Autoimmune hemolytic anemia.

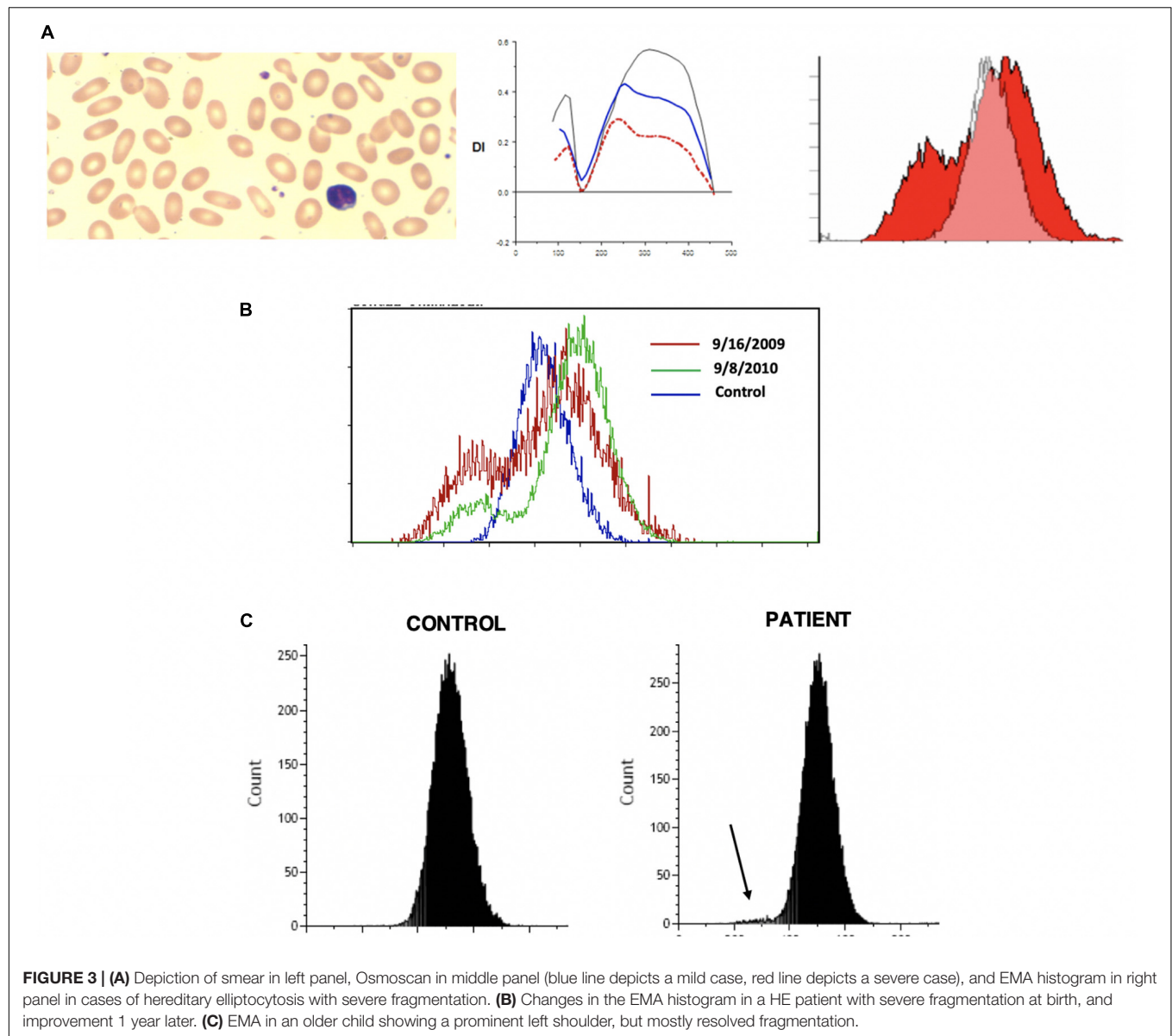
| AIHA (n = 4)               |        |       | Normal controls (n = 76)   |        |       |
|----------------------------|--------|-------|----------------------------|--------|-------|
|                            | Mean   | SD    |                            | Mean   | SD    |
| MCF                        | 497.63 | 66.84 | MCF                        | 514.50 | 15.25 |
| O <sub>min</sub> (x-axis)  | 169.24 | 6.53  | O <sub>min</sub> (x-axis)  | 147.67 | 6.90  |
| DI <sub>MAX</sub> (y-axis) | 0.35   | 0.06  | DI <sub>MAX</sub> (y-axis) | 0.49   | 0.05  |

neonatal red cells typically have high osmoscans (Johnson et al., 1999) and age matched neonatal controls usually are not available concurrently and thus a “normal” scan may actually indicate underlying spherocytosis (congenital or caused by antibody due to blood group incompatibility). An additional confounding variable is the high reticulocyte count. Evaluation of the slope of the curve on EMA test is frequently informative with leftward leaning curve indicating a gradual loss of membrane due to the antibody as opposed to the rapid loss caused by structural defects in HS where the whole curve is shifted left. This is consistent with the reported data on this topic (Johnson et al., 1999). Diagnosis of neonatal HS and distinction from spherocytosis associated with ABO incompatibility remains a challenge; family history is helpful and repeat testing 8–10 weeks postnatally should clarify the diagnosis in *de novo* congenital HS cases (see **Figures 2B,C** and **Tables 3, 4**).

## Hereditary Elliptocytosis (HE) and Hereditary Pyropoikilocytosis (HPP)

Hereditary elliptocytosis (HE) is clinically heterogeneous disorder. The presence of elliptically shaped red cells on the peripheral blood smear is the characteristic feature of HE. HE patients can have a diverse spectrum of clinical findings ranging from life threatening anemias to asymptomatic carrier state (Lazarova et al., 2017). The inheritance of HE is autosomal dominant, with rare reports of recessive mutations. Homozygous and compound heterozygous HE variants present with moderate anemia and hemolysis (Delaunay, 2007; An and Mohandas, 2008). Weakened lateral linkages in membrane skeletons due to either defective spectrin dimer-dimer interaction or weakened spectrin-actin-protein 4.1R junctional complex results in the decrease of mechanical stability in these patients (Gallagher, 2004). Significant fragmentation of red blood cells in addition to the classic elliptocytes are a feature of the disease (see **Figure 3**). Newborn infants may show high level of red cell fragmentation, so called hemolytic HE (as seen in **Figure 3A**), which improves by age 1–2 years (as seen in **Figure 3B**; Palek and Lux, 1983; Mentzer et al., 1987; An and Mohandas, 2008). In the family





with 4.1 deficiency, homozygotes had more severe disease than heterozygotes.

Hereditary elliptocytosis cases show distinctive indented plateau on osmoscans pattern (Tchernia et al., 1981; Johnson and Ravindranath, 1996; Silveira et al., 1997). HE cells generate a trapezoidal profile in an osmoscan, with a normally positioned  $O_{min}$  and  $O_{hyper}$  but diminished  $EI_{Max}$ . The truncated curve reflects the inability of the already elliptical cells to deform further under shear stress. These findings were conformed in more recent work (Suemori et al., 2015) and has been re-appraised with the use of the new generation ektacytometers (Da Costa et al., 2016).

On EMA scans a bimodal pattern comprised of distinct population of cells with decreased MCF (representing fragmented cells) and a population with normal to high MCF may be present, especially in neonates. The EMA histograms reflect the level of fragmentation seen on smears. In infants who show

high numbers of fragmented cells (“hemolytic HE”) two distinct populations one with low MCF and another with high MCF) can be identified (**Figure 3A**). Often in such cases the level of fragmentation decreases as the infant gets older and the EMA histograms reflect this with a decrease in the size of the red cell population with low MCF (**Figure 3B**). This feature also distinguishes hemolytic HE cases from cases of HPP where the extreme fragmentation gives a single population of cells with low MCF (**Figure 4**). In older children and adults the curve may overlap the control or shifted slightly to right but a trailing population of fragment cells can identified on the left shoulder of the curve (**Figure 3C**). This is an important finding as, it expands the value of the EMA test beyond the diagnosis of HS. In a recently reported work, heterogeneity in the ovalization of the HE patients had no association with EMA binding (Suemori et al., 2015).

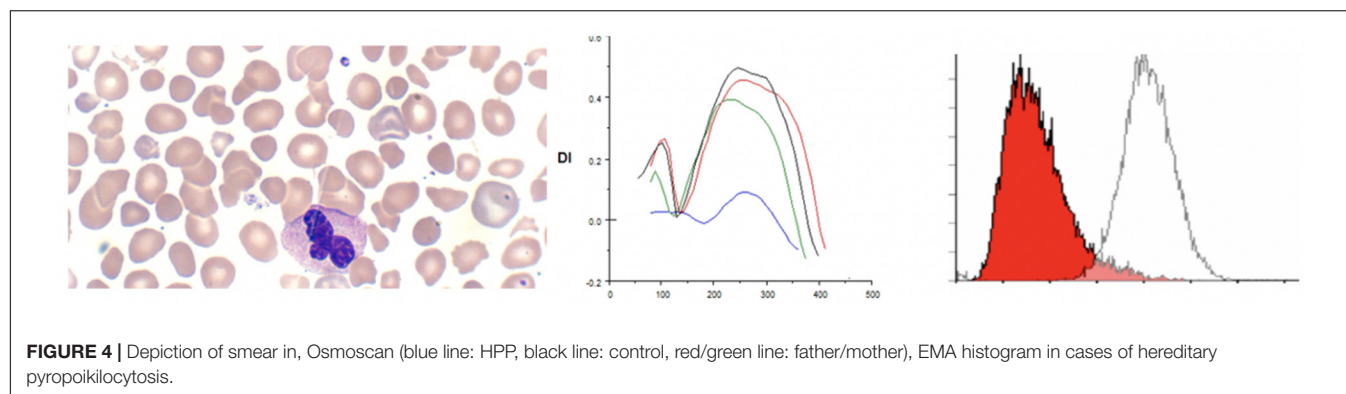


**FIGURE 4** | Depiction of smear in, Osmoscan (blue line: HPP, black line: control, red/green line: father/mother), EMA histogram in cases of hereditary pyropoikilocytosis.

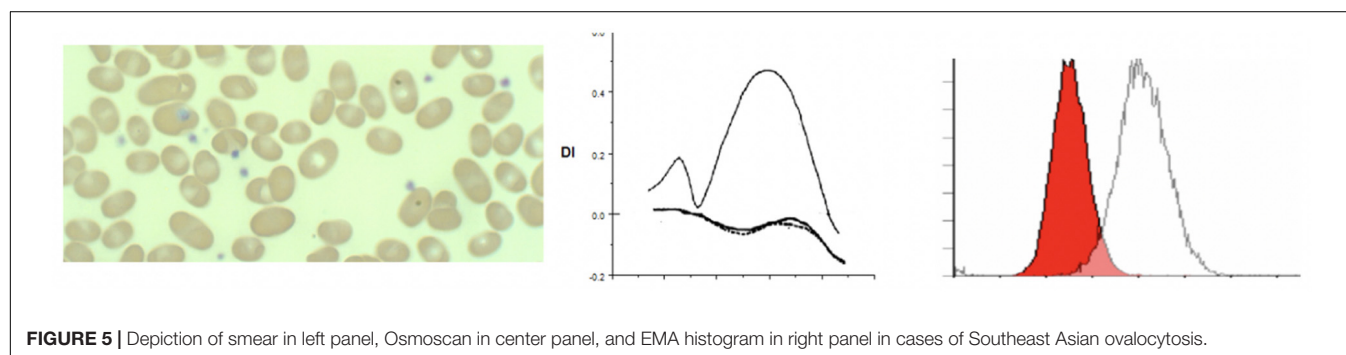


**FIGURE 5** | Depiction of smear in left panel, Osmoscan in center panel, and EMA histogram in right panel in cases of Southeast Asian ovalocytosis.

Hereditary pyropoikilocytosis (HPP), originally thought to be a unique and separate disease process, has been reclassified as a subset of HE due to double heterozygosity of mutations in the alpha-spectrin gene (Gallagher, 2004). This severe subset of HE-type disorders, in which red blood cells appear like those seen in thermal burn patients (Zarkowsky et al., 1975), is characterized by neonatal jaundice and transfusion dependent hemolytic anemia that persists through life. A peripheral smear shows microspherocytosis or micropoikilocytes more than elliptocytes. A protein analysis of the phospholipid bilayer of HPP reveals a mild spectrin reduction but a greater increase in spectrin dimer content than in common HE (Zarkowsky et al., 1975). We have seen 3 families with HPP phenotype. In one family despite the name of the disorder we were unable to show heat instability by morphology or circular dichroism studies in purified spectrin (Ravindranath and Johnson, 1985). Molecular studies (courtesy of Bernard Forget, Yale University) showed double heterozygosity for mutations near the dimer-dimer association site in alpha spectrin (Alpha1 74 c.28 CGT to CAT p.Arg > His and Alpha1 50a at c.209 CTG > CCG, Leu to Pro). There was significant reduction in alpha spectrin. In these patients ( $n = 3$ ) there was extreme cellular fragmentation and transfusion requirements abated only after splenectomy. We noted the lowest MCF values, with MCF  $213.9 \pm 52$  in these cases, consistent with the MCV values of  $<50$  fl. There is also a very clear change in the  $O_{min}$  and the deformability index was severely decreased (see Figure 5). The red cells in HPP appear to have a significantly decreased ability to maintain deformability in the face of hypotonicity, evidenced by their critical hemolytic value occurring at an osmolality much higher than normal controls and

**TABLE 5** | Hereditary elliptocytosis.

|                     | Hereditary elliptocytosis ( $n = 8$ ) |       | Normal controls ( $n = 76$ ) |              |
|---------------------|---------------------------------------|-------|------------------------------|--------------|
|                     | Mean                                  | SD    | Mean                         | SD           |
| MCF                 | 478.69                                | 28.42 | MCF                          | 514.50 15.25 |
| $O_{min}$ (x-axis)  | 147.59                                | 21.06 | $O_{min}$ (x-axis)           | 147.67 6.90  |
| $DI_{MAX}$ (y-axis) | 0.22                                  | 0.05  | $DI_{MAX}$ (y-axis)          | 0.49 0.05    |

**TABLE 6** | Hereditary pyropoikilocytosis.

|                     | Hereditary pyropoikilocytosis ( $n = 3$ ) |       | Normal controls ( $n = 76$ ) |              |
|---------------------|---|-------|------------------------------|--------------|
|                     | Mean                                      | SD    | Mean                         | SD           |
| MCF                 | 213.85                                    | 52.26 | MCF                          | 514.50 15.25 |
| $O_{min}$ (x-axis)  | 175.75                                    | 13.44 | $O_{min}$ (x-axis)           | 147.67 6.90  |
| $DI_{MAX}$ (y-axis) | 0.11                                      | 0.14  | $DI_{MAX}$ (y-axis)          | 0.49 0.05    |

HS cases. These parameters distinguish HPP cases from common hemolytic HE especially in infants where the fragmentation could be mistaken for HPP. Both osmoscans and EMA test separate the two entities (see Tables 5, 6).

## Southeast Asian Ovalocytosis (SAO)

The first report of Southeast Asian Ovalocytosis (SAO) was over five decades ago (Eng, 1965) in malaria endemic regions of Papua New Guinea and Laos. It has now been described in other South East Asian populations and in African Americans (Ravindranath et al., 1994). The condition is inherited in

**TABLE 7 |** Southeast Asian ovalocytosis.

| Southeast Asian ovalocytosis (n = 3) |        |       | Normal controls (n = 76)   |        |       |
|--------------------------------------|--------|-------|----------------------------|--------|-------|
|                                      | Mean   | SD    |                            | Mean   | SD    |
| MCF                                  | 334.13 | 22.01 | MCF                        | 514.50 | 15.25 |
| O <sub>min</sub> (x-axis)            | NA     | NA    | O <sub>min</sub> (x-axis)  | 147.67 | 6.90  |
| DI <sub>MAX</sub> (y-axis)           | -7.33  | 6.43  | DI <sub>MAX</sub> (y-axis) | 0.49   | 0.05  |

a dominant fashion and genetic studies generally reveal heterozygotes. Subsequently, the genetic lesion has been found to be related to a mutation in band 3 (anion exchanger 1; SLC4A1) (Tse and Lux, 1999). The mutation results in the deletion of eight amino acid residues in band 3, that result in misfolding of the first transmembrane domain (Tanner et al., 1991). Most patients present with minimal hemolysis, though neonatal hyperbilirubinemia is described. Patients will have stomatocytic elliptocytes, that are pathognomonic to SAO (Liu et al., 1990; Tanner et al., 1991; Cheung et al., 2005). Ektacytometry studies show completely non-deformable red blood cells, with no discernable deformability across a wide osmotic gradient, resulting in a characteristic near flat curve (Mohandas et al., 1984; Ravindranath et al., 1994). EMA testing presents a unique signature as the 8 amino acid deletion in the first *trans* membrane loop of AE1 renders lysine 430 inaccessible to binding with EMA, band 3 content itself is not decreased (Moriyama et al., 1992). The reduction of MCF in our three patients (one Philippino, two African Americans) with SAO from normal controls was approximately 35% of control MCF value,

and approximately 16% lower from HS patients. This indicates the EMA can be used as a screening method for SAO, although ektacytometry is more specific (see Figure 5 and Table 7).

## Erythrocyte Volume Disorders

Erythrocyte volume disorders include hereditary xerocytosis (now referred to as dehydrated stomatocytosis) and stomatocytosis (overhydrated stomatocytosis) (Mohandas and Gallagher, 2008; Andolfo et al., 2016). A recent major discovery is the linkage of xerocytosis cases with mutation in the mechanosensitive calcium transporter PIEZO1 (Zarychanski et al., 2012). Other genes implicated in EVDs are the Gardos channel KCNN4 and potassium channel ABCB6. Anemia may be mild or in some cases mild erythrocytosis has been reported. The morphology is not always distinct with a variable mixture of xerocytes and stomatocytes. In three patients with erythrocyte volume disorders associated with PIEZO1 mutations we observed mixed patterns on osmoscans, similar to mild HS or a right shift of the curve suggesting increased cellular hydration (Knight et al., 2019). Classical xerocytosis with cellular dehydration results in a left shifted curve. In our experience the most common cause for a left shifted curve on osmoscans is in patients with hemoglobin C by itself or in combination with sickle hemoglobin (HbSC), consistent with the known effect of hemoglobin C on the Gardos channel (Hannemann et al., 2015). In our three patients with PIEZO1 mutations (c.4766 C > T p.Thr1589Ile, c.5182 C > T p.Arg1728Cys, c.6835C > T p.Arg2279Cys) EMA MCF scans were not diagnostic while Osmoscans were abnormal (Johnson and Ravindranath, 1996;

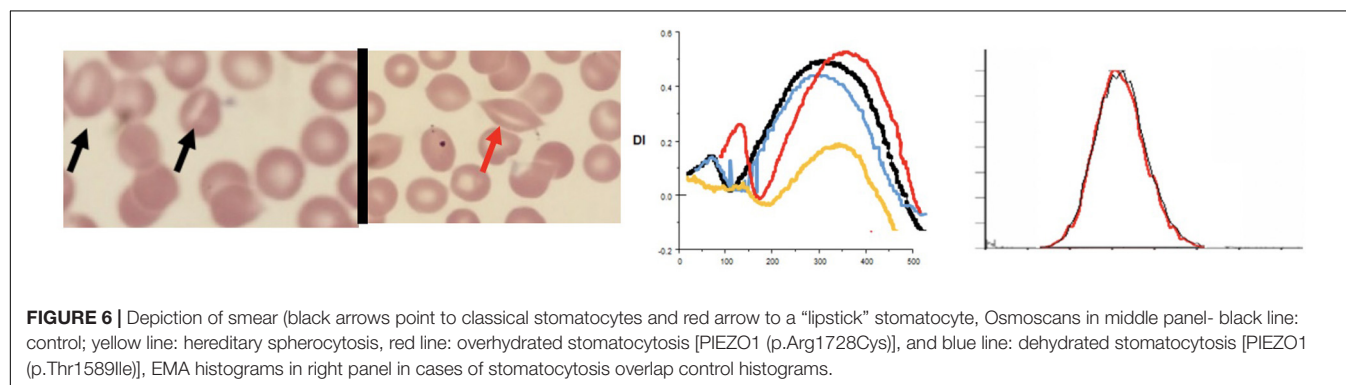


**FIGURE 6 |** Depiction of smear (black arrows point to classical stomatocytes and red arrow to a “lipstick” stomatocyte, Osmoscans in middle panel- black line: control; yellow line: hereditary spherocytosis, red line: overhydrated stomatocytosis [PIEZO1 (p.Arg1728Cys)], and blue line: dehydrated stomatocytosis [PIEZO1 (p.Thr1589Ile)], EMA histograms in right panel in cases of stomatocytosis overlap control histograms.

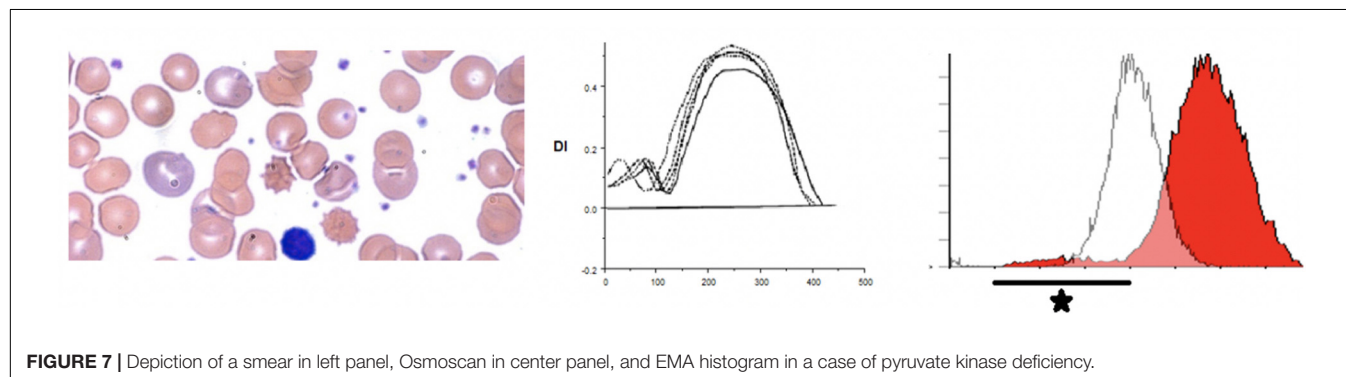
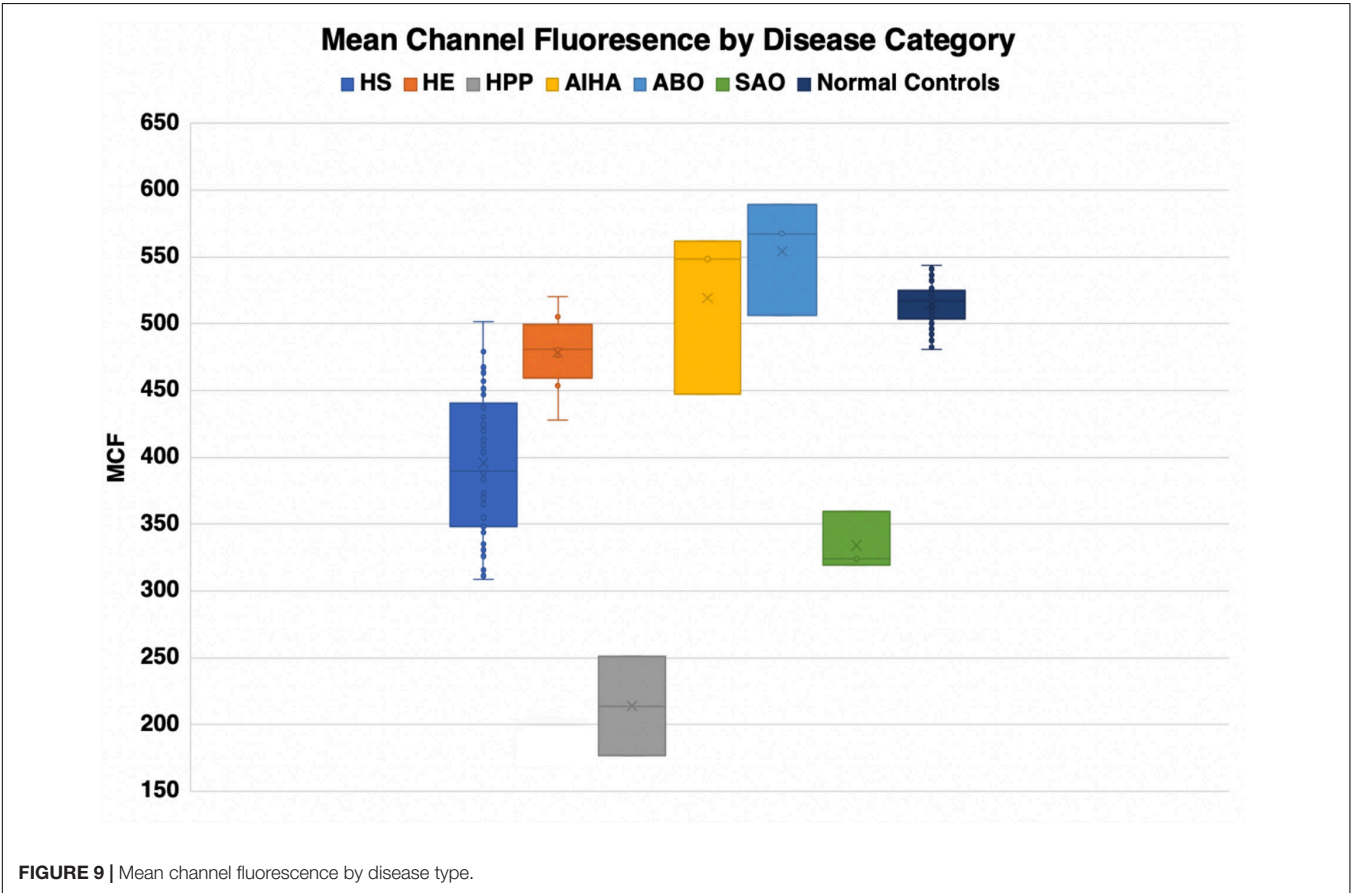
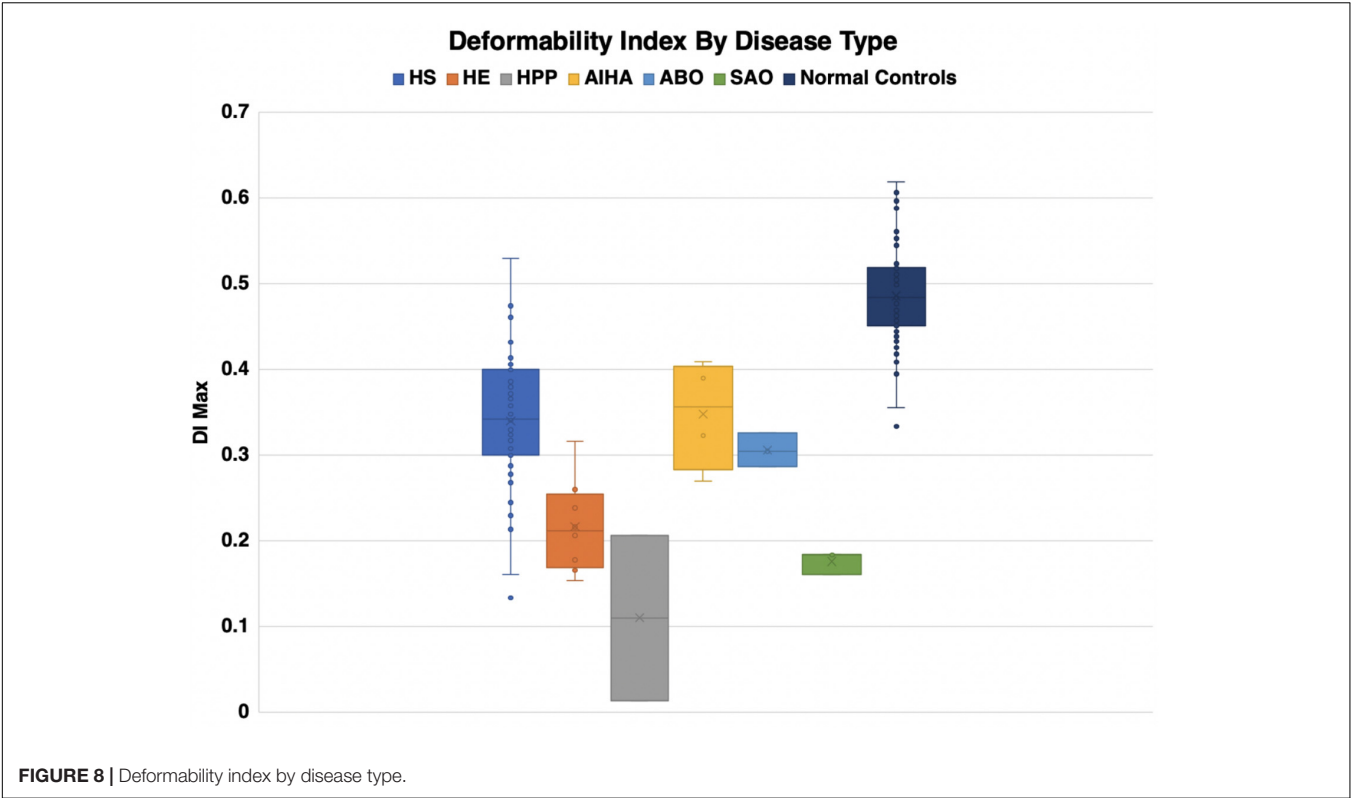


**FIGURE 7 |** Depiction of a smear in left panel, Osmoscan in center panel, and EMA histogram in a case of pyruvate kinase deficiency.





Da Costa et al., 2013; Andolfo et al., 2016; Knight et al., 2019). The clinical findings of xerocytes (dense spherocytes) and stomatocytes coupled with left or right shifted osmoscan curves should raise the suspicion of erythrocyte volume disorders; mutation testing is necessary for confirmation. The variable Osmoscan pattern may reflect the diverse mutations in PIEZO1 and their impact on the calcium and cation fluxes (Knight et al., 2019; see Figure 6).

## Other Disorders With Low MCF Values on EMA Test

Red cells from individuals with iron deficiency anemia and thalassemias show low MCF values on EMA scan but can be distinguished from HS cases because of a left shoulder of smaller cells indicating the anisopoikilocytosis in these disorders. A left shoulder may also be seen in cases with hemolytic uremic syndrome and other thrombotic microangiopathies indicating the level of circulating fragmented red cells.

## RBC Enzyme Deficiency

In G6PD deficiency and glycolytic enzyme disorders ektacytometry shows high osmoscans indicating greater deformability of red cells (Johnson and Ravindranath, 1996). EMA test in patients with glycolytic enzyme deficiencies, in this case phosphoglycerate kinase 1, show higher MCF with right shifted curves reflecting the high MCV noted in these cases (low mean cell age) (Zaidi et al., 2019). In addition our review of patients with glycolytic enzyme deficiency (in 3 cases of pyruvate kinase (PK) deficiency (post splenectomy) and a new case of phosphoglycerate kinase (PGK1) deficiency) revealed a previously unsuspected signature -on scatter plots and histograms there is a distinctive tail of small cells - presumably the ATP depleted dense spiculated cells (Zaidi et al., 2019; see Figure 7).

## CONCLUSION

Eosin-5-maleimide testing and osmoscans are complementary and the combined information can lead to better diagnosis of red cell membrane disorders. There are very salient and key differences in the diagnostic ability of the EMA test and ektacytometry. The EMA provides a static, quantifiable measurement of the amount of band 3 protein, while the ektacytometer provides a fluid, physiologically simulated test that assesses red blood cell deformability in an active fashion (Figures 8, 9). In interpreting the EMA test, attention should be paid to not only the MCF value, but also the slope of the curve

on either side, which together reflect the heterogeneity of cell size (Figure 2). The lowest MCF values were seen in HPP cases; SAO cases had MCF values intermediate between HPP and HS cases (Figure 9). In erythrocyte volume disorders EMA tests may be normal, but changes in cell hydration can be suspected better on the osmoscan. At present, the use of the Osmoscan is limited by the availability of the instrument, and the need for specialized staff. The EMA is user-friendly, with quick turnaround time of testing, and flow cytometers are readily available in most institutions. These tests can provide very different results, and should be used in combination with morphology on blood smears and blood counts including the red cell indices. Molecular testing is needed for confirmation of erythrocyte volume disorders.

## DATA AVAILABILITY STATEMENT

All datasets generated for this study are included in the article/supplementary material.

## ETHICS STATEMENT

This review was approved by the Wayne State University Human Investigation Committee.

## AUTHOR CONTRIBUTIONS

AM set up the EMA test. MH-M, SBa, and KJ digitized the osmoscans and determined the  $O_{min}$ ,  $DI_{max}$ , and  $O_{hyper}$  values. Ektacytometry testing was done under supervision of RJ. AZ wrote the manuscript. RJ gifted the ektacytometer to YR. YR supervises the red cell and flow cytometry laboratories. All authors contributed to the article and approved the submitted version.

## ACKNOWLEDGMENTS

Gerard Goyette, now deceased, performed the osmoscans for several decades and we gratefully acknowledge his many contributions to our work over the past 3 decades.

## FUNDING

YR was funded by the Georgie Ginopolis Endowed chair in Pediatric Cancer and Hematology, WSU School of Medicine.

## REFERENCES

- An, X., and Mohandas, N. (2008). Disorders of red cell membrane. *Br. J. Haematol.* 141, 367–375. doi: 10.1111/j.1365-2141.2008.07091.x
- Andolfo, I., Russo, R., Gambale, A., and Iolascon, A. (2016). New insights on hereditary erythrocyte membrane defects. *Haematologica* 101, 1284–1294. doi: 10.3324/haematol.2016.142463
- Bessis, M., Mohandas, N., and Feo, C. (1980). Automated ektacytometry: a new method of measuring red cell deformability and red cell indices. *Blood Cells* 6, 315–327.
- Bianconi, E., Piovesan, A., Facchin, F., Beraudi, A., Casadei, R., Frabetti, F., et al. (2013). An estimation of the number of cells in the human body. *Ann. Hum. Biol.* 40, 463–471. doi: 10.3109/03014460.2013.807878

- Bolton-Maggs, P. H. B., Langer, J. C., Iolascon, A., Tittensor, P., and King, M. J. (2012). Guidelines for the diagnosis and management of hereditary spherocytosis - 2011 update. *Br. J. Haematol.* 156, 37–49. doi: 10.1111/j.1365-2141.2011.08921.x
- Cheung, J. C., Cordat, E., and Reithmeier, R. A. F. (2005). Trafficking defects of the Southeast Asian ovalocytosis deletion mutant of anion exchanger 1 membrane proteins. *Biochem. J.* 392, 425–434. doi: 10.1042/BJ20051076
- Chonat, S., Risinger, M., Dagaonkar, N., Maghathe, T., Rothman, J., Connor, J., et al. (2015). The spectrum of alpha-spectrin associated hereditary spherocytosis. *Blood* 126:941. doi: 10.1182/blood.v126.23.941.941
- Clark, M. R., Mohandas, N., and Shohet, S. B. (1983). Osmotic gradient ektacytometry: comprehensive characterization of red cell volume and surface maintenance. *Blood* 61, 899–910. doi: 10.1182/blood.v61.5.899.bloodjournal615899
- Cobb, C. E., and Beth, A. H. (1990). Identification of the eosinyl-5-maleimide reaction site on the human erythrocyte anion-exchange protein: overlap with the reaction sites of other chemical probes. *Biochemistry* 29, 8283–8290. doi: 10.1021/bi00488a012
- Crisp, R. L., Solari, L., Gammella, D., Schwartzman, G. A., Rapetti, M. C., and Donato, H. (2012). Use of capillary blood to diagnose hereditary spherocytosis. *Pediatr. Blood Cancer* 59, 1299–1301. doi: 10.1002/pbc.24157
- Da Costa, L., Galimand, J., Fenneteau, O., and Mohandas, N. (2013). Hereditary spherocytosis, elliptocytosis, and other red cell membrane disorders. *Blood Rev.* 27, 16–178. doi: 10.1016/j.blre.2013.04.003
- Da Costa, L., Suner, L., Galimand, J., Bonnel, A., Pascreau, T., Couque, N., et al. (2016). Diagnostic tool for red blood cell membrane disorders: assessment of a new generation ektacytometer. *Blood Cells, Mol. Dis.* 56, 9–22. doi: 10.1016/j.bcmd.2015.09.001
- Delaunay, J. (2007). The molecular basis of hereditary red cell membrane disorders. *Blood Rev.* 21, 1–20. doi: 10.1016/j.blre.2006.03.005
- Eng, L. I. (1965). Hereditary ovalocytosis and haemoglobin E-ovalocytosis in Malayan aborigines. *Nature* 208:1329. doi: 10.1038/2081329a0
- Gallagher, P. G. (2004). Hereditary Elliptocytosis: spectrin and Protein 4.1R. *Semin. Hematol.* 41, 142–164. doi: 10.1053/j.seminhematol.2004.01.003
- Gallagher, P. G. (2013). Abnormalities of the erythrocyte membrane. *Pediatr. Clin. North Am.* 60, 1349–1362. doi: 10.1016/j.pcl.2013.09.001
- Gallagher, P. G., Maksimova, Y., Lezon-Geyda, K., Newburger, P. E., Medeiros, D., Hanson, R. D., et al. (2019). Aberrant splicing contributes to severe  $\alpha$ -spectrin-linked congenital hemolytic anemia. *J. Clin. Invest.* 129, 2878–2887. doi: 10.1172/JCI127195
- Gallagher, P. G., Weed, S. A., Tse, W. T., Benoit, L., Morrow, J. S., Marchesi, S. L., et al. (1995). Recurrent fatal hydrops fetalis associated with a nucleotide substitution in the erythrocyte  $\beta$ -spectrin gene. *J. Clin. Invest.* 95, 1174–1182. doi: 10.1172/JCI117766
- Groner, W., Mohandas, N., and Bessis, M. (1980). New optical technique for measuring erythrocyte deformability with the ektacytometer. *Clin. Chem.* 26, 1435–1442. doi: 10.1093/clinchem/26.10.1435
- Hannemann, A., Rees, D. C., Tewari, S., and Gibson, J. S. (2015). Cation homeostasis in red cells from patients with sickle cell disease heterologous for HbS and HbC (HbSC Genotype). *EBiomedicine* 2, 1669–1676. doi: 10.1016/j.ebiom.2015.09.026
- Huisjes, R., Makhro, A., Llaudet-Planas, E., Hertz, L., Petkova-Kirova, P., Verhagen, L. P., et al. (2019). Density, heterogeneity and deformability of red cells as markers of clinical severity in hereditary spherocytosis. *Haematologica* 2018:188151. doi: 10.3324/haematol.2018.188151
- Hunter, F. T. (1940). A photoelectric method for the quantitative determination of erythrocyte fragility. *J. Clin. Invest.* 19, 691–694. doi: 10.1172/JCI101172
- Johnson, R. M., Panchoosingh, H., Goyette, G., and Ravindranath, Y. (1999). Increased erythrocyte deformability in fetal erythropoiesis and in erythrocytes deficient in glucose-6-phosphate dehydrogenase and other glycolytic enzymes. *Pediatr. Res.* 45, 106–113. doi: 10.1203/00006450-199901000-00018
- Johnson, R. M., and Ravindranath, Y. (1996). Osmotic scan ektacytometry in clinical diagnosis. *J. Pediatr. Hematol. Oncol.* 18, 122–129. doi: 10.1097/00043426-199605000-00005
- Kalfa, T. A., Connor, J. A., and Begtrup, A. H. (1993). *EPB42-Related Hereditary Spherocytosis*. Available online at: <http://www.ncbi.nlm.nih.gov/pubmed/24624460> (accessed January 7, 2019).
- King, M. J., Behrens, J., Rogers, C., Flynn, C., Greenwood, D., and Chambers, K. (2000). Rapid flow cytometric test for the diagnosis of membrane cytoskeleton-associated haemolytic anaemia. *Br. J. Haematol.* 111, 924–933. doi: 10.1111/j.1365-2141.2000.02416.x
- King, M.-J., Smythe, J. S., and Mushens, R. (2004). Eosin-5-maleimide binding to band 3 and Rh-related proteins forms the basis of a screening test for hereditary spherocytosis. *Br. J. Haematol.* 124, 106–113. doi: 10.1046/j.1365-2141.2003.04730.x
- Knight, T., Zaidi, A. U., Wu, S., Gadgeel, M., Buck, S., and Ravindranath, Y. (2019). Mild erythrocytosis as a presenting manifestation of PIEZO1 associated erythrocyte volume disorders. *Pediatr. Hematol. Oncol.* 36, 317–326. doi: 10.1080/08880018.2019.1637984
- Lazarova, E., Gulbis, B., van Oirschot, B., and van Wijk, R. (2017). Next-generation osmotic gradient ektacytometry for the diagnosis of hereditary spherocytosis: interlaboratory method validation and experience. *Clin. Chem. Lab. Med.* 55, 394–402. doi: 10.1515/cclm-2016-0290
- Liu, S.-C., Zhai, S., Palek, J., Golan, D. E., Amato, D., Hassan, K., et al. (1990). Molecular defect of the band 3 protein in southeast asian ovalocytosis. *N. Engl. J. Med.* 323, 1530–1538. doi: 10.1056/NEJM199011293232205
- Lux, S. E. (2014). *Chapter 15 - Red Cell Membrane*, 8th Edn. Amsterdam: Elsevier, doi: 10.1016/B978-1-4557-5414-4.00015-2
- Lux, S. E. (2016). Anatomy of the red cell membrane skeleton: unanswered questions. *Blood* 127, 187–199. doi: 10.1182/blood-2014-12
- Mentzer, W. C., Iarocci, T. A., Mohandas, N., Lane, P. A., Smith, B., Lazerson, J., et al. (1987). Modulation of erythrocyte membrane mechanical stability by 2,3-diphosphoglycerate in the neonatal poikilocytosis/elliptocytosis syndrome. *J. Clin. Invest.* 79, 943–949. doi: 10.1172/JCI112905
- Mohandas, N., Clark, M. R., Jacobs, M. S., and Shohet, S. B. (1980). Analysis of factors regulating erythrocyte deformability. *J. Clin. Invest.* 66, 563–573. doi: 10.1172/JCI109888
- Mohandas, N., and Gallagher, P. G. (2008). Red cell membrane: past, present, and future. *Blood* 112, 3939–3948. doi: 10.1182/blood-2008-07-161166
- Mohandas, N., Lie-Injo, L. E., Friedman, M., and Mak, J. W. (1984). Rigid membranes of Malayan ovalocytes: a likely genetic barrier against malaria. *Blood* 63, 1385–1392. doi: 10.1182/blood.v63.6.1385.bloodjournal6361385
- Moriyama, R., Ideguchi, H., Lombardo, C. R., Van Dort, H. M., and Low, P. S. (1992). Structural and functional characterization of band 3 from Southeast Asian ovalocytes. *J. Biol. Chem.* 267, 25792–25797.
- Nussenzweig, R. H., Christensen, R. D., Prchal, J. T., Yaish, H. M., and Agarwal, A. M. (2014). Novel  $\alpha$ -spectrin mutation in trans with  $\alpha$ -spectrin causing severe neonatal jaundice from hereditary spherocytosis. *Neonatology* 106, 355–357. doi: 10.1159/000365586
- Palek, J., and Lux, S. E. (1983). Red cell membrane skeletal defects in hereditary and acquired hemolytic anemias. *Semin. Hematol.* 20, 189–224.
- Perrotta, S., Gallagher, P. G., and Mohandas, N. (2008). Hereditary spherocytosis. *Lancet* 372, 1411–1426. doi: 10.1016/S0140-6736(08)61588-3
- Ravindranath, Y., Goyette, G., and Johnson, R. M. (1994). Southeast Asian ovalocytosis in an African-American family. *Blood* 84, 2823–2824. doi: 10.1182/blood.v84.8.2823.bloodjournal8482823
- Ravindranath, Y., and Johnson, R. M. (1985). Altered spectrin association and membrane fragility without abnormal spectrin heat sensitivity in a case of congenital hemolytic anemia. *Am. J. Hematol.* 20, 53–65. doi: 10.1002/ajh.2830200108
- Ribeiro, M. L., Alloisio, N., Almeida, H., Gomes, C., Texier, P., Lemos, C., et al. (2000). Severe hereditary spherocytosis and distal renal tubular acidosis associated with the total absence of band 3. *Blood* 96, 1602–1604.
- Silveira, P., Cynober, T., Dhermy, D., Mohandas, N., and Tchernia, G. (1997). Red Blood cell abnormalities in hereditary elliptocytosis and their relevance to variable clinical expression. *Am. J. Clin. Pathol.* 108, 391–399. doi: 10.1093/ajcp/108.4.391
- Suemori, S. I., Wada, H., Nakanishi, H., Tsujioka, T., Sugihara, T., and Tohyama, K. (2015). Analysis of hereditary elliptocytosis with decreased binding of eosin-5-maleimide to red blood cells. *Biomed Res. Int.* 2015:451861. doi: 10.1155/2015/451861

- Tanner, M. J., Bruce, L., Martin, P. G., Rearden, D. M., and Jones, G. L. (1991). Melanesian hereditary ovalocytes have a deletion in red cell band 3. *Blood* 78, 2785–2786. doi: 10.1182/blood.v78.10.2785.bloodjournal78102785
- Tchernia, G., Mohandas, N., and Shohet, S. B. (1981). Deficiency of skeletal membrane protein band 4.1 in homozygous hereditary elliptocytosis. Implications for erythrocyte membrane stability. *J. Clin. Invest.* 68, 454–460. doi: 10.1172/jci110275
- Tse, W. T., and Lux, S. E. (1999). Red blood cell membrane disorders. *Br. J. Haematol.* 104, 2–13. doi: 10.1111/j.1365-2141.1999.01130.x
- Won, D., and Suh, J. S. (2009). Flow cytometric detection of erythrocyte osmotic fragility. *Cytom. Part B Clin. Cytom.* 76B, 135–141. doi: 10.1002/cyto.b.20448
- Zaidi, A. U., Bagla, S., and Ravindranath, Y. (2019). Identification of a novel variant in phosphoglycerate kinase-1 (PGK1) in an African-American child (PGK1 Detroit). *Pediatr. Hematol. Oncol.* 36, 302–308. doi: 10.1080/08880018.2019.1639863
- Zaidi, A. U., Herrera-Martinez, M., Goyette, G. W., Buck, S., Gadgeel, M., Mohan, A., et al. (2015). Red Cell Band 3 Content Evaluation By Eosin Maleimide (EMA) Fluorescence: Beyond Diagnosis of Dominant Hereditary Spherocytosis (HS). *Blood* 126:3343. doi: 10.1182/blood.v126.23.3343.3343
- Zarkowsky, H. S., Mohandas, N., Speaker, C. B., and Shohet, S. B. (1975). A congenital haemolytic anaemia with thermal sensitivity of the erythrocyte membrane. *Br. J. Haematol.* 29, 537–543. doi: 10.1111/j.1365-2141.1975.tb02740.x
- Zarychanski, R., Schulz, V. P., Houston, B. L., Maksimova, Y., Houston, D. S., Smith, B., et al. (2012). Mutations in the mechanotransduction protein PIEZO1 are associated with hereditary xerocytosis. *Blood* 120, 1908–1915. doi: 10.1182/blood-2012-04-422253

**Conflict of Interest:** The authors declare that the research was conducted in the absence of any commercial or financial relationships that could be construed as a potential conflict of interest.

Copyright © 2020 Zaidi, Buck, Gadgeel, Herrera-Martinez, Mohan, Johnson, Bagla, Johnson and Ravindranath. This is an open-access article distributed under the terms of the Creative Commons Attribution License (CC BY). The use, distribution or reproduction in other forums is permitted, provided the original author(s) and the copyright owner(s) are credited and that the original publication in this journal is cited, in accordance with accepted academic practice. No use, distribution or reproduction is permitted which does not comply with these terms.

# Advantages of publishing in Frontiers



## OPEN ACCESS

Articles are free to read  
for greatest visibility  
and readership



## FAST PUBLICATION

Around 90 days  
from submission  
to decision



## HIGH QUALITY PEER-REVIEW

Rigorous, collaborative,  
and constructive  
peer-review



## TRANSPARENT PEER-REVIEW

Editors and reviewers  
acknowledged by name  
on published articles

## Frontiers

Avenue du Tribunal-Fédéral 34  
1005 Lausanne | Switzerland

Visit us: [www.frontiersin.org](http://www.frontiersin.org)

Contact us: [info@frontiersin.org](mailto:info@frontiersin.org) | +41 21 510 17 00



## REPRODUCIBILITY OF RESEARCH

Support open data  
and methods to enhance  
research reproducibility



## DIGITAL PUBLISHING

Articles designed  
for optimal readership  
across devices



## FOLLOW US

@frontiersin



## IMPACT METRICS

Advanced article metrics  
track visibility across  
digital media



## EXTENSIVE PROMOTION

Marketing  
and promotion  
of impactful research



## LOOP RESEARCH NETWORK

Our network  
increases your  
article's readership